Charles University in Prague
Faculty of Mathematics and Physics

DOCTORAL THESIS

Mgr. Markéta Pazderková

Raman optical activity of biomolecules: From simple models to complex systems

Institute of Physics of Charles University

Supervisor: Prof. RNDr. Vladimír Baumruk, DrSc.

Consultants: Ing. Petr Maloň, CSc.,
RNDr. Lucie Bednárová, CSc., Institute of Organic Chemistry and Biochemistry AS CR, v.v.i.

Study programme: Physics

Specialization: Biophysics, Chemical and Macromolecular Physics

Prague 2015

I would like to thank first and foremost my supervisor Professor Vladimír Baumruk. I am particularly grateful for his guidance, constant interest and encouragement. My thanks go also to my consultants Dr. Petr Maloň and Dr. Lucie Bednárová. They gave me the most valuable advice. Their suggestions and constructive criticism helped me to improve not only quality of my thesis and projects I was working on, but also the way of my scientific thinking. As part of my VCD experimental work was carried out at VCD spectroscopy laboratory (BioTools, Inc., FL, U.S.A.), I would like to acknowledge Prof. L. A. Nafie and Dr. Rina K. Dukor for helping me to acquire theoretical and practical skills needed for VCD spectroscopy, for providing me with the access to their VCD instrument and for the kind help with the measurements. I am especially grateful for their kindness and hospitality. I had a wonderful time working with them on our exciting collaborative projects and I very much look forward to our future cooperation.

My sincere thanks go to RNDr. Václav Profant who helped me with theoretical calculations and interpretation of the calculated results and also to Dr. Giuliano Siligardi who provided us the access to far UV ECD synchrotron facility (Harwell, U.K.). We acknowledge Diamond Light Source for time on Beamline B23 under Proposal SM7630.

Drs Martin Flegel and Zuzana Flegelová are greatly acknowledged for providing samples of neurohypophyseal hormones and antimicrobial peptides, while my sincere thanks go to Dr. Petr Maloň, Dr. Jaroslav Šebestík and Dr. Jana Hodačová for the synthesis and optical resolution of spirocyclic dilactams. I am also grateful to Prof. Marie Urbanová and Pavlína Novotná for the VCD measurements on neurohypophyseal hormones and dilactams.

The Charles University Grant Agency (project no. 578212) is acknowledged for providing me with financial support. I would also like to acknowledge Charles University Mobility Fund and The Fund of Karel Urbánek for financial support of my study stay at Biotools, FL and State University of New York at Albany.

Finally, I thank my family, especially my parents, my husband Tomáš and my parents-in-law for all their support and encouragement and for taking care of my little daughter Hana while I was writing.

I declare that I carried out this doctoral thesis independently, and only with the cited sources, literature and other professional sources.

I understand that my work relates to the rights and obligations under the Act No. 121/2000 Coll., the Copyright Act, as amended, in particular the fact that the Charles University in Prague has the right to conclude a license agreement on the use of this work as a school work pursuant to Section 60 paragraph 1 of the Copyright Act.

In Prague, June 25, 2015 Markéta Pazderková

Název práce: Ramanova optická aktivita biomolekul: Od jednoduchých modelů ke komplexním systémům

Autor: Mgr. Markéta Pazderková

Katedra / Ústav: Fyzikální ústav UK

Vedoucí doktorské práce: Prof. RNDr. Vladimír Baumruk, DrSc., Fyzikální ústav UK

Abstrakt:

Práce je zaměřena na studium specifických projevů disulfidové a neplanární amidové skupiny ve spektrech Ramanovy optické aktivity (ROA) s cílem ukázat, že ROA umožňuje získat informace o konformaci peptidů a proteinů, které je obtížné nebo dokonce nemožné získat pomocí jiných spektroskopických technik. Jako modelové systémy pro studium neplanární amidové vazby jsou použity speciálně navržené malé rigidní molekuly s dobře definovanou strukturou – tricyklické spirodilaktamy. Možnost detekce disulfidové skupiny je studována v ROA spektrech modelových peptidů s jednou až dvěma disulfidovými skupinami, z nichž některé jsou biologicky aktivní (neurohypofyzární hormony a jejich agonistické a antagonistické analogy, antimikrobiální peptid lasiocepsin a jeho analogy s různým disulfidovým přemostěním). Kromě ROA jsou tyto systémy studovány také pomocí komplementárních chiroptických metod – vibračního (VCD) a elektronového (ECD) cirkulárního dichroismu, a to v rozšířeném spektrálním oboru (pod 180 nm) s využitím synchrotronového zdroje (SRCD). Současné využití těchto technik umožňuje získat komplexní informaci o struktuře studovaných molekul. Experimentální chiroptická data jsou dále srovnána s teoretickými ab initio výpočty. V chiroptických spektrech se nám podařilo identifikovat a interpretovat signály odrážející neplanaritu amidové skupiny. Ve spektrech ROA se nám dále podařilo identifikovat signál příslušející valenčním vibracím disulfidové vazby, který pravděpodobně může odrážet smysl torze disulfidové skupiny.

Klíčová slova: Ramanova optická aktivita, peptidy a proteiny, disulfidové můstky, neplanární amidová vazba

Title: Raman optical activity of biomolecules: From simple models to complex systems

Author: Mgr. Markéta Pazderková

Department / Institute: Institute of Physics of Charles University

Supervisor of the doctoral thesis: Prof. RNDr. Vladimír Baumruk, DrSc., Institute of Physics of Charles University

Abstract:

The aim of the thesis is to utilize Raman optical activity (ROA) to get unique information on peptide/protein conformation, which is otherwise difficult or even impossible to obtain. We have focused on investigation of amide and disulfide groups. Utilizing tailor-made model structures (rigid tricyclic spirodilactams with two interacting nonplanar amide groups), special model peptides and even biologically active molecules (neurohypophyseal hormones and their agonistic and antagonistic analogs, antimicrobial peptide lasiocepsin and its analogs having different disulfide pattern) we have traced specific spectral manifestation of nonplanar amides and disulfides. ROA results were supplemented by data obtained by complementary chiroptical methods – electronic (including vacuum UV – SRCD) and vibrational circular dichroism. When used in a concerted fashion, these techniques provide complex information on peptide/protein secondary structure. Where possible, experimental chiroptical data were compared to ab initio calculations. In chiroptical spectra we have found and interpreted signals reflecting nonplanarity of the amide group. Moreover, in ROA spectra we have identified signals due to S–S stretching vibrations which seem to reflect sense of the disulfide group torsion.

Keywords: Raman optical activity, peptides and proteins, disulfide bridges, nonplanar amide group

Contents

Preface

Raman optical activity (ROA) is a spectroscopic phenomenon arising from differences in Raman scattering of chiral systems when alternatively left- and right-circularly polarized light is involved.[1] It formally represents an almost straightforward extension of the previously known chiroptical methods, optical rotatory dispersion (ORD) and electronic circular dichroism (ECD) from merely electronic absorption spectroscopy towards molecular vibrations and Raman scattering. The difference derives from the fact that in contrast to absorption phenomena Raman scattering is a two photon process related to molecular polarizability, not the dipole moment. Therefore it stands on a different theoretical basis and follows different selection rules.[2] Similarly to its absorption counterpart (vibrational circular dichroism - VCD), ROA promises to combine the enormous sensitivity of chiroptical methods to even small details of spatial arrangement of molecules with a sizable richness and structural detail of vibrational spectra, knowledge of which has been collected over the years.[3] In addition, Raman spectroscopy unlike absorption and VCD utilizes water as its most natural solvent which makes it attractive for biomolecular applications. This and yet other specific advantages of ROA logically spawned interest and the technique has been successfully demonstrated as early as in the beginning of 1970s.[4] However, ROA proved to be a rather difficult technique both theoretically and experimentally, and as a consequence it took a long time to develop it into a useful analytical tool. Recent progress in ROA instrumentation, introduction of commercial ROA spectrometers and significant improvements in computational methodology (implementation of ROA tensors with analytic derivatives in Gaussian 09, resulting in a rapid increase of computational speed)[5] made the ROA technique accessible to broader range of users. Although ROA is still not as widely used as other chiroptical spectroscopies (particularly electronic circular dichroism – ECD), it is already well established as one of important spectroscopic methods and its applications to biomolecules, particularly peptides and proteins, are becoming increasingly frequent.[6–8] At present, it is well established as the analytical tool which can provide (a) absolute configuration assignment when combined with theoretical calculations[1,9,10] – particularly useful for natural products and pharmaceutical research;[11] (b) which can

supplement chiroptical data of biopolymers collected by other procedures (ECD, VCD) with particular emphasis on short-range details.[8] However, despite these successful contributions, ROA is still considered a somewhat "exotic" kind of chiroptical spectroscopy, mainly because this technique has been largely used to supplement information provided by other spectroscopies, while not enough attention has been paid to developing ROA as a self-contained tool providing exclusive information. It is true that solitary application of ROA might probably bring only a limited view of the studied systems. However, when combined together with results obtained by other chiroptical spectroscopies, it can provide a rather detailed view on the studied molecules and enable deep understanding of their structure. We will explore possibilities of ROA to provide information not accessible by other means, especially on biomolecules. For this purpose we will study simple models and try to extrapolate the knowledge thus obtained to more complex biomolecular systems. We will try to learn whether ROA can be used as a unique technique allowing us to directly investigate amide and disulfide bonds when they are hardly accessible by other experimental techniques, i.e. when they are embedded into complicated peptide/protein structures.

The thesis is organized into four chapters. Chapter 1 brings a brief overview of ROA, VCD and ECD. It also describes utilization of these methods for the studies of biomolecules, particularly peptides and proteins. The objectives of the thesis are summarized in Chapter 2. Chapter 3 concentrates on a description of samples, experimental methods and procedures used for the interpretation of experimental data. The results achieved within this work are discussed in Chapter 4, which is divided into two parts involving: (a) a discussion of the results achieved on model spirocyclic dilactams containing nonplanar amide groups; (b) the investigation of disulfide group conformation in model peptides including neurohypophyseal hormone analogs and antimicrobial peptides from Lasiocepsin family.

1 Introduction

1.1 Fundamentals of Raman Optical Activity

ROA is defined as a difference in Raman scattering intensity from chiral molecular systems for right I^R and left I^L circularly polarized light (incident, scattered or both – depending on the arrangement of ROA experiment):[1]

$$\Delta I(\nu) = I^R(\nu) - I^L(\nu), \qquad (1)$$

where ν is the frequency.

Because ROA is a two photon process, the actual technique is more complex (both experimentally and theoretically) than the complementary absorption-based method of VCD, despite the fact that both techniques deal with identical vibrational transitions.[12] While there is only one setup of VCD experiment (one-photon differential absorption form – see **Figure 2** below), for ROA there are four distinct forms, varying in modulation of incident and scattered light[13] (energy-level diagrams illustrating their definition are shown in **Figure 1**). These involve (**a**) the original form – incident circular polarization (ICP) ROA,[14] consisting in modulation of incident laser beam between RCP and LCP states and Raman measurement at a fixed linear or unpolarized radiation state; (**b**) scattered circular polarization (SCP) ROA,[15] using linear or unpolarized incident light and measuring the difference in RCP and LCP Raman scattered light; (**c**) in-phase dual circular polarization (DCP_I) ROA, where polarization states of both incident and scattered light are modified synchronously between RCP and LCP states; and (**d**) out-of-phase dual circular polarization (DCP_{II}) ROA, where polarization states of both incident and scattered light are switched between RCP and LCP states with opposite phases.[16,17] Besides that, ROA can be defined using distinct scattering geometries (including forward (0°), right-angle (90°) or backward (180°) configuration) and frequencies of incident radiation.[12]

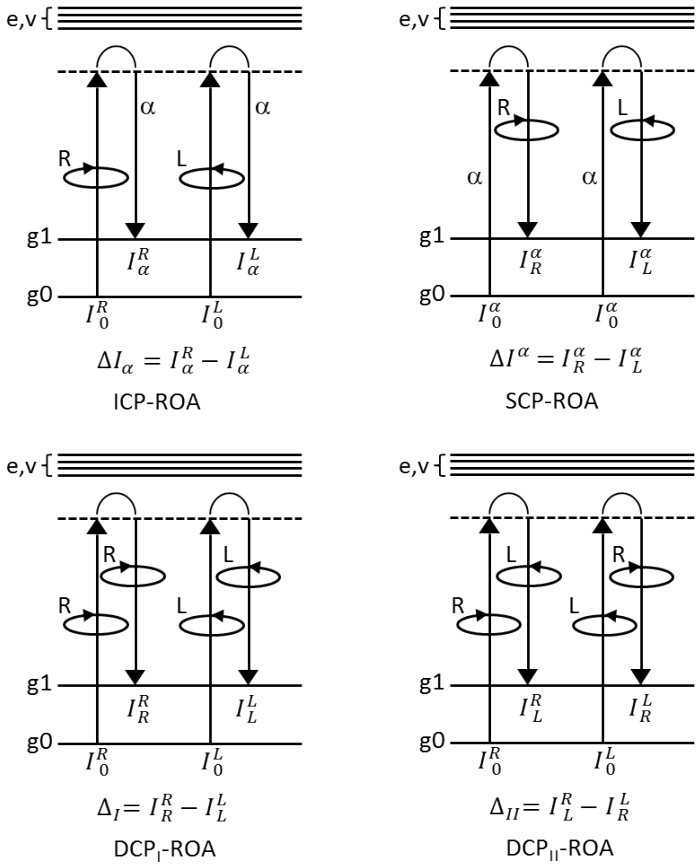

Figure 1: Energy-level diagrams illustrating definition of four distinct forms of ROA for the molecule undergoing transition from the zeroth (g0) to the first (g1) vibrational level of the ground electronic state (e,v – electronic-vibrational levels of the excited intermediate state; redrawn from ref. 12).

As the appropriate experimental quantity, a dimensionless circular intensity difference (CID)[4] is typically used for the description of ROA experiment. It is defined as a ratio between ROA and Raman signals:

$$\Delta = (I^R - I^L)/(I^R + I^L), \qquad (2)$$

where I^R and I^L are the intensities in RCP and LCP light. The CID values are different for forward (0°), backward (180°) and right-angle (90°) experimental geometries (see equations (5–(8 in Chapter 1.2).

This overview documents that arrangement of ROA experiment offers several possibilities, all of which are not exactly equivalent.[12] However, at the time being most of the practical experiments are done in backscattering geometry and use either ICP (mainly laboratory-built instruments)[18–21] or SCP (commercial equipment) modulation scheme.[15] It has been shown that ICP and SCP instruments provide equivalent information (within the far-from-resonance approximation).[22] The

backscattering geometry is currently considered the best experimental strategy for most of the ROA studies. The main advantage of such ROA arrangement consists in higher intensities and lower artifact level.[1]

Compared to the above complex possibilities how to arrange the ROA experiment, the related absorption-based experiments (which were elaborated earlier into practical use) are simpler. Circular dichroism (either electronic or vibrational) simply corresponds to a difference in absorption ΔA of left A_L and right A_R circularly polarized light:

$$\Delta A(\nu) = A_L(\nu) - A_R(\nu), \qquad (3)$$

The photon absorption processes giving rise to electronic and vibrational CD are illustrated on an energy-level polarization diagram in **Figure 2**.

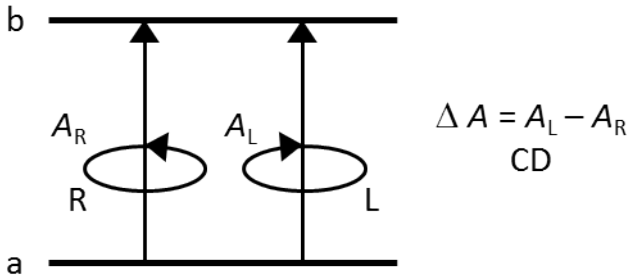

Figure 2: Energy-level polarization diagram illustrating the photon transitions associated with CD. The a and b denote for the respective ground and electronic state for ECD, while for VCD a and b correspond to two vibrational levels of the ground electronic state (redrawn from ref. 23).

While ECD refers to absorption processes between two electronic states, VCD deals with transitions between two vibrational sublevels of the same electronic state. To exhibit electronic circular dichroism spectrum, the molecule has to contain at least one chromophore which absorbs radiation in an accessible spectral region and is either chiral itself (inherent chirality), or is situated in an optically active environment.[24,25] In VCD the concept of chromophores is not that easy to follow. Molecular vibrations are often localized along chemical bonds, implying that elementary contributions are small and linear. It is not intuitive to deduce rotational components within molecular vibrations, although attempts to visualize them have been made.[12]

1.2 Theoretical Basis of Optical Activity

The ultimate goal in structural interpretation of chiroptical data is to construct a theoretical spectrum that compares favorably with the experimental data. The procedure for theoretical spectra calculation involves several steps.[26] It is first necessary to determine the molecular structure. Nowadays, the calculations are usually carried out at the density functional theory (DFT) level using a sufficient quality polarized basis set (such as 6-311++G**). Molecular geometry has to be optimized (to fulfill the condition that energy gradient is zero, i.e. the molecular geometry has to correspond to a stationary point on the energy hypersurface). Within the harmonic approximation (assuming quadratic form of the potential), it is then possible to calculate a set of quadratic force constants d^2E/dx^2 (a symmetrical matrix). It is often also very important to model chemical environment of the molecule, especially if the experiments are carried out in polar solvents (e.g. water). It is often sufficient to employ continuum solvent models where the solvent is represented as a continuous medium (e.g. Conductor-like Screening Model – COSMO).[27] Such methods are computationally much less demanding than utilization of discrete solvent models, which operate with individual solvent molecules and usually also require combining ab initio calculations with molecular dynamics (MD) simulations.[28] For flexible molecules, the procedure should also reflect conformational equilibria. It is usually implemented by simple conformational averaging, where discrete local energetic minima are included with respect to their Boltzmann distribution.[26]

It is then possible to calculate quantities related to chiroptical intensities – either rotational strengths for calculation of ECD/VCD spectra or ROA tensors for calculation of ROA spectra. For the calculation of chiroptical intensities, it is necessary to go beyond the dipole approximation. With advantage, circular dichroism related to both electronic and vibrational spectroscopy utilizes identical basic relations. Rotational strength for a transition from a molecular state *a* to a molecular state *b* is given by:

$$R_{ab} = Im(\langle a|\boldsymbol{\mu}|b\rangle \cdot \langle b|\boldsymbol{m}|a\rangle) \qquad (4)$$

(Rosenfeld equation[29]), where $\langle a|\boldsymbol{\mu}|b\rangle$ is the electric dipole transition moment (real quantity), $\langle b|\boldsymbol{m}|a\rangle$ is the magnetic dipole transition moment (imaginary quantity)

and *Im* denotes for 'imaginary part'. The cosine function involved in the above dot product is the main source of particular sensitivity of circular dichroism towards stereochemistry of chiral molecules. The underlying properties of chiral molecules involve that both components in the product must be non-zero and not perpendicular to each other. Although the actual calculation of rotational strengths, which follows the force field calculation, is conceptually straightforward, it is still a complex procedure which involves calculations of atomic polar and axial tensors. Calculation of the latter brought the problem of origin choice,[30] which has been solved lately by implementation of gauge-independent atomic orbitals (GIAO).[31] We describe calculations of vibrational transitions, which occur in the well-defined electronic ground state.

For the calculations of magnetic dipole transition moments, it is necessary to introduce corrections to Born-Oppenheimer (B-O) approximation, as the use of B-O approximation leads to a physically unrealistic result where the electronic contribution to magnetic dipole transition moment vanishes.[32] Several theoretical approaches have been developed over the years which deal with the problem differently. Apart from approximate methods (like localized molecular orbital (LMO) method, which is based on localization of molecular orbitals into bonding orbitals and lone pairs and subsequent determination of VCD intensities from the motion of nuclei and centroids of the LMOs,[33–35]) there are three main a priori methods for VCD calculations, which enable deriving expressions for the electronic contributions to atomic polar and axial tensors. These methods are formally equivalent and can be derived from perturbation theory.[36] They include magnetic field perturbation (MFP),[32] the sum-over-states (SOS) vibronic coupling theory (VCT)[37] and nuclear velocity perturbation (NVP).[38] Current VCD calculations mainly involve use of the MFP method[32] developed by Stephens and co-workers. The method is based on the VCT[39] and consists in perturbation of the ground electronic state wavefunction by a magnetic field. The MFP formalism has been implemented into Gaussian software already in 1998[40] and is now a standard method for VCD calculations.[5,31] An alternative – formally equivalent approach to the MFP method – the SOS VCT, where the electronic contribution to the atomic axial tensor is expressed as a sum over excited electronic states, was implemented for practical calculations of VCD by Rauk and co-workers[37] several years after the MFP method was implemented. Although these two procedures provide results of a comparable

accuracy (when the same level of approximation is used), the MFP theory prevails. Recently the first implementation NVP theory, which is based on nuclear velocity perturbation of the ground electronic state wavefunction and was theoretically proposed in 1992 by Nafie,[38] has been reported.[41] The reformulated NVP theory within DFT (using linear order density perturbation theory) appears to provide theoretical data of the same quality as the MFP approach, and offers a possibility to incorporate anharmonic effects into VCD calculations.[41]

Current VCD calculations mainly involve use of MFP formalism and DFT,[31] with hybrid functionals like B3LYP or B3PW91 and a GIAO basis set at the minimal level of 6-31G(d). For similar ab initio calculations of electronic rotatory strengths (i.e. ECD) it is necessary to calculate transitions into electronically excited states. It became possible in recent years by means of the time-dependent density functional theory (TDDFT).[42]

Compared to ECD and VCD, theory of ROA is more complex and the quantities needed for the ROA calculation can be estimated with sufficient precision only when employing higher-level ab initio calculations.[43] Apart from induced electric dipole (which is sufficient for the description of Raman scattering), it is necessary to include into calculations also the magnetic dipole and electric quadrupole. In the far-from resonance (FFR) approximation (where the lowest excited electronic state is much higher in energy than the incident and scattered photon energies),[12] ROA intensities depend on normal mode derivatives of three polarizability tensors: electric dipole-electric dipole molecular polarizability tensor $\alpha_{\alpha\beta}$, electric dipole-magnetic dipole polarizability tensor $G'_{\alpha\beta}$ and electric dipole-electric quadrupole polarizability tensor $A_{\alpha\beta\gamma}$. The derivatives are used for formation of five tensor invariants (two Raman tensor invariants and three ROA tensor invariants) from which the Raman intensities and ROA intensity differences can be derived.[6] For an isotropic sample (within the FFR approximation), the dimensionless CID can be then expressed in terms of $\alpha_{\alpha\beta}$, $G'_{\alpha\beta}$ and $A_{\alpha\beta\gamma}$ as follows:[6]

$$\Delta(0°) = \frac{4[45\alpha G' + \beta(G') - \beta(A)^2]}{c[45\alpha^2 + 7\beta(\alpha)^2]} \quad (5)$$

$$\Delta(180°) = \frac{24[\beta(G')^2 + 1/3\beta(A)^2]}{c[45\alpha^2 + 7\beta(\alpha)^2]} \quad (6)$$

$$\Delta_x(90°) = \frac{2[45\alpha G' + 7\beta(G')^2 + \beta(A)^2]}{c[45\alpha^2 + 7\beta(\alpha)^2]} \quad (7)$$

$$\Delta_z(90°) = \frac{12[\beta(G')^2 - 1/3\beta(A)^2]}{6c\beta(\alpha)^2} \quad (8)$$

where α and G' are the isotropic invariants defined as:

$$\alpha = \frac{1}{3}\alpha_{\alpha\alpha},\ G' = \frac{1}{3}G'_{\alpha\alpha}$$

and $\beta(\alpha)^2$, $\beta(G')^2$ and $\beta(A)^2$ are anisotropic invariants defined as:

$$\beta(\alpha)^2 = \frac{1}{2}\left(3\alpha_{\alpha\beta}\alpha_{\alpha\beta} - \alpha_{\alpha\alpha}\alpha_{\beta\beta}\right),\ \beta(G')^2 = \frac{1}{2}\left(3\alpha_{\alpha\beta}G'_{\alpha\beta} - \alpha_{\alpha\alpha}G'_{\beta\beta}\right),$$

$$\beta(A)^2 = \frac{1}{2}\omega\alpha_{\alpha\beta}\varepsilon_{\alpha\gamma\delta}A_{\gamma\delta\beta}.$$

The above equations allow for the numerical comparison of theoretical and experimental ROA data. Their practical implementation has been incorporated most thoroughly into the Gaussian software package.[5] The application to ROA has been recently critically analyzed[44] and it has been found that calculation of Raman and ROA tensors has its specific requirements, which appear somewhat more stringent than the preceding geometry optimization and force field calculation. Raman and ROA calculations typically require inclusion of diffuse functions (such as aug-cc-pVTZ[45–48] or reduced diffuse polarization shell – rDPS[49]). Of these the rDPS basis set (being derived from Pople's 3-21G) is possibly applicable also to larger molecules. The analysis also indicates that the inclusion of electric dipole-electric quadrupole polarizabilities may not be absolutely necessary for ROA calculations, but this finding still needs to be verified. In light of this, it appears advantageous to use two theoretical levels within one calculation: one, somewhat less sophisticated, for geometry optimization and force field calculation, and the other, augmented with diffuse functions, for Raman/ROA tensors. However, it has to be noted that such an internally inconsistent calculation requires additional quantities and the time saving may be not that efficient.[44]

Ab initio calculations lead to total numerical interpretation which, in a successful case, approaches the accuracy of experimental data. This is of course a favorable situation, but it would often suffice to gain an approximate interpretation providing basic understanding of the decisive effects. Quite often, the computational

interpretation is too detailed and it is therefore difficult to obtain basic understanding. In ECD spectroscopy, such understanding is often provided by the so called sector rules,[28] which are sometimes totally empirical, but can be also theory-based (see J.A. Schellman[50]). This concept has been perfected by G. Snatzke in his qualitative molecular orbital theory of optical rotatory strengths.[51] It is difficult to construct a counterpart to these studies for vibrational optical activity (VOA), because the concept of chromophores is not so universally valid here. In VOA, the chromophores are often small (mainly single bonds) and their vibrations typically do not simultaneously contribute to electric and magnetic transition moments. It is typically necessary to combine several such contributions together. This is valid for both VCD and ROA and it implicitly means that it is difficult to consider inherent chirality in VOA.

Out of the conceptually simple approaches, only the so called coupled oscillator mechanism (dipole-dipole coupling)[52,53] is universally extendable over dichroism spectra (ECD, VCD). This model can be used for optically active systems containing equivalent, separated achiral oscillators which are mutually chirally oriented – i.e. they form a virtual helix-like arrangement. The approach is particularly suitable for simple chiral systems such as dimer-like structures, but its use can be extended also to several coupled oscillators (e.g. for polymers). The coupled oscillator model allows calculating rotational strengths and component splitting from the known molecular geometries and measured absorption intensities. For the dimer consisting of monomeric subunits *a* and *b*, which couple energetically and oscillate coherently either in-phase (+) or out-of-phase (–), the rotational strengths are:

$$R^{\pm} = \mp \frac{\pi \nu}{2c} \boldsymbol{R}_{ab} \cdot (\boldsymbol{\mu}_a \times \boldsymbol{\mu}_b), \qquad (9)$$

where ν corresponds to the frequency of the monomer transition, μ_a and μ_b are electric transition dipole moments of the monomers *a* and *b* and $\boldsymbol{R}_{ab}$ is the vector pointing from the center of mass of the monomer *a* to the center of mass of the monomer *b*. The relative shift in transition energies of in-phase and out-of-phase modes is given by:

$$E^{\pm} = \frac{\boldsymbol{\mu}_a \cdot \boldsymbol{\mu}_b}{R_{12}^3} - \frac{3(\boldsymbol{\mu}_a \cdot \boldsymbol{R}_{12})(\boldsymbol{\mu}_b \cdot \boldsymbol{R}_{12})}{R_{12}^5} \qquad (10)$$

L.D. Barron constructed analogous model for ROA. Similarly to the coupled oscillator model, the so called two-group model[54,55] is also applicable to the molecules containing two achiral groups in a chiral environment. According to this model, ROA signals can be generated by interference between waves independently scattered from the two groups. Although the two group model is conceptually similar to coupled oscillator model of circular dichroism, there is a significant difference between the two mechanisms – while the generation of CD signals requires dynamic coupling of the two groups, no interaction of these groups is needed for the ROA signal generation. For VCD the attempt to enhance understanding the VCD origin has been done by Nafie et al. using visualization of transition current density (TCD).[56] In summary, it seems that nowadays it is even somewhat easier to computationally interpret VOA than ECD, although even in this field there is lately a significant progress – TDDFT.

Simplifying computational models enable simulating VOA spectra even for larger molecules (e.g. peptides/proteins). As follows from the calculation on the model dipeptide unit – acetyl-L-alanine methylamide,[57] VOA is largely influenced by short range interactions. The study demonstrates that even such a short model peptide when folded according to segments of basic secondary structures can simulate (although somewhat crudely) basic VCD features even of proteins. Nowadays it is possible to perform analogous ab initio calculations of VOA on even slightly larger molecules using more sophisticated level of theory (DFT, with modern functionals and flexible basis sets). For biopolymers, when the structure involves a regular repetition of building blocks it is possible to simulate their spectra by employing the Cartesian tensor transfer method by Bouř et al,[58] which utilizes ab initio calculations on small fragment subunits and later combines them into spectra of large molecules under the inter-group interaction potential. Complete ab initio calculations of ROA on a diamide unit (AcAlaNHMe) have been also already done.[57]

1.3 Chiroptical Spectroscopy of Biomolecules

1.3.1 Chirality of Biological Molecules

Chirality is an important phenomenon. The word 'chiral,' derived from the Greek word 'cheir' meaning hand, refers to a specific type of asymmetry, which is uniquely defined on the basis of group theory (see e.g. Bishop: Group Theory and Chemistry)[59] by the absence of symmetry plane, center and rotation-reflection axis. It is frequently illustrated on the example of human hands: although right and left hands are mirror images of each other, they are not identical (i.e. it is not possible to position the right hand in a way that it becomes the left hand and vice versa). In other words, an object is called chiral if it cannot be superimposed on its mirror image (enantiomer). For biomolecules, chirality often plays a critical role, as most such molecules are chiral and usually only one of the possible forms (enantiomeric or diastereoisomeric) is biologically active.

One of the most frequent topological chirality concepts consists in chiral stereocenters (i.e. the asymmetric carbon atom, which is by definition bonded to four different substituents). For example, the well-known proteolytic enzyme chymotrypsin contains 251 stereocenters in the molecule with 2^{251} possible stereoisomers, but only one of them is synthesized and utilized in living organisms.[60] Within relatively small molecules with or without biological significance the central chirality (described by the general R,S system)[61] often represents a complete description. In biopolymers (peptides/proteins, nucleic acids (DNA, RNA)), the more or less regular repetition of their chiral subunits (mostly L-amino acid residues in peptides/proteins, D-sugars in nucleic acids, etc.) gives rise to segments of chiral secondary structures (helices, sheets) often displaying intense chiroptical spectra. The frequently implied helical motif is closely related to a definition ($\mathbf{\mu}\cdot\mathbf{m}$) of optical rotatory strength (Rosenfeld equation[29]), which further confirms the very close relationship between chiroptical properties and three-dimensional structure of molecular systems. Chirality of biomolecules and its relation to biologically important processes is currently being thoroughly investigated and it represents the leading direction in applications of chiroptical spectroscopies.[28]

1.3.2 Chiroptical Spectroscopy of Biomolecules

For structural studies of biomolecules, chiroptical spectroscopy represents a collection of complementary techniques, which allow us to either obtain quickly the basic statistical-like view of three-dimensional structure or to fill in voids in much more detailed and sophisticated picture provided by alternative higher resolution methods like the X-ray, NMR or electron microscopy. Although these methods provide very detailed information on biomolecular structure often at atomic resolution, they have also several limitations. The main limitation of otherwise very powerful X-ray analysis is a necessity to crystallize the studied molecule. This may be often rather problematic (especially for short peptides, membrane proteins etc.); moreover, even if the peptide/protein crystallization is successful, one cannot be sure whether the form in which the structure crystallizes is biologically relevant. NMR spectroscopy, although capable of studying peptides/proteins in solution, suffers a size limit of studied biopolymers. It is typically used for molecules not larger than ~100 kDa[62] and, moreover, often requires isotopic labelling. Electron microscopy provides electron density images of overall shape of the molecule (resolution about 5 Å).[63] All these methods suffer problems when they are applied to flexible biomolecules. Such molecules are far more difficult to study, since their electron density is smeared over a large space.

Consequently, it often appears advantageous to apply suitable alternative methods of chiroptical spectroscopy. Although these methods do not provide us with high-resolution data at atomic level, they are a valuable source of information on structure and dynamical behavior of biomolecules and they can be routinely applied to a wide range of biological systems. Another important advantage is the extra sensitivity towards even small changes in spatial arrangement of biomolecules.[64] Low-resolution analysis of peptide/protein secondary structure by application of chiroptical methods is well established and rather easy to setup and execute.[3,28,65–69] Chiroptical experiments are versatile and can adopt a variety of experimental conditions including pH, temperature, concentration and/or chemical environment and it is therefore possible to study not only static-averaged in time structure of biomolecules, but also to unravel dynamics of conformational changes. It is particularly this feature that makes chiroptical methods a useful tool for studying various biomolecular processes including folding,[70,71] denaturation[72] or even

interaction with ligands.[36,73] In the following text we focus our attention to application of these methods to structural studies of peptides and proteins as this is the primary subject of this work.

1.3.3 Chiroptical Spectroscopy of Peptides and Proteins

Protein conformational analyses are based on evaluation of the changes in secondary structure content, because different secondary structure elements (such as α-helices, β-sheets or β-turns) typically give rise to unique, characteristic spectral features. The fastest and easiest secondary structure evaluation is usually provided by ECD spectroscopy.[66] ECD bands characteristic for particular types of secondary structures can be found in the spectral region of amide group absorption (far-UV CD, below 250 nm). In this region, a typical protein spectrum shows the π–π* (~190 nm and ~140 nm) and n–π* transitions (~220 nm). The region below ~180 nm is not accessible by commercial ECD instruments. However, this limitation can be overcome by employing synchrotron radiation circular dichroism (SRCD) which uses an intense synchrotron light beam and allows ECD measurements down to the vacuum-UV (VUV) region.[74]

There are several analytical programs (e.g. Dichroweb,[75] Protein Circular Dichroism Data Bank[76] or CDPro[77]) which can provide an approximate estimation of secondary structure fractions based on experimental ECD spectra. Such methods are suitable mainly for identification of well-defined structures with an intense ECD signals, such as α-helices. On the other hand, ECD usually gives only an approximate view on β-sheet or β-turn structures, because their ECD signals are often unambiguous. Identification of structures exhibiting low-intensity ECD bands might be rather problematic, particularly in the presence of α-helical structures whose signals often dominate the ECD spectra. ECD spectroscopy can also contribute to tertiary structure assessment. Information on the tertiary structure can be found in the absorption region of aromatic residues (phenylalanine, tyrosine and tryptophan) in the spectral range 250–290 nm and/or disulfide bonds (near UV CD, above ~250 nm).[28]

Since ECD deals with electronic transitions, it hints on the overall three dimensional arrangement of the molecules, but usually lacks enough structural detail. For the more detailed peptide/protein conformational analysis, it is often beneficial to

supplement the electronic CD data with information obtained by the methods of VOA (ROA and VCD) in combination with their non-chiral variants. Particularly infrared (IR) absorption can provide a rapid estimation of β-structure content. Although VOA methods are experimentally more demanding than ECD (as they require higher sample concentrations, longer accumulation times and, in the case of ROA, also high-purity samples), they have also significant advantages. VOA spectroscopies are generally more sensitive to local structural details and can provide more specific information on particular parts of the molecules. In VOA spectra, signals corresponding to distinct parts of the molecule are usually well separated. Therefore it is possible to follow independently spectral changes caused by changing structural arrangement of amide groups, aromatic residues or disulfide groups.[12] VOA methods can be used for discrimination of β-sheets, β-turns or various types of helices[69,78] (including e.g. left-handed polyproline II (PPII) helices, which are considered to be important structural elements of so called random coil structures).[79–81] VCD and ROA obey different selection rules and, consequently, they have different sensitivities towards distinct parts of biomolecular structures. It is therefore beneficial to use both techniques simultaneously for studying the same problem. However, this approach is still quite rare.[12]

In VCD spectra, secondary structure information can be mostly derived from the patterns of VCD bands in amide I and amide II regions. Based on analyses of VCD spectra of proteins of known secondary structures, spectral patterns characteristic for particular secondary structure elements could be determined.[69,82,83] A characteristic VCD pattern of α-helical structure involves a negative/positive couplet at ~1660 and 1640 cm^{-1} in the amide I region and a negative band at ~1515 cm^{-1} in the amide II region. An oppositely signed couplet in the amide I region together with a VCD negative band in the amide II region is typical for VCD spectra of 'random coil' proteins (probably composed of short segments having a left-handed helicity – PPII-like[80]). VCD can be also used for determination of β-sheet and β-turn structure. However, amide I VCD signals due to β-structures are of a rather low intensity and it can be difficult to separate them from other, more prominent VCD signals (especially in molecules with prevailing α-helical or PPII structure). In such cases it is very advantageous to combine VCD with classical IR spectroscopy. Recently it has been shown that VCD spectroscopy is particularly sensitive to supramolecular chiral structures such as protein fibrils.[84] As has been

demonstrated for various peptide/protein samples,[85,86] formation of fibrils leads to an enormous enhancement of VCD intensity, giving rise to a characteristic five-band spectral curve with either the (+,+,–,+,+), or the opposite (–,–,+,–,–) spectral pattern corresponding respectively to the left or right-handed supramolecular chirality of the fibrils.

Unlike VCD, ROA spectroscopy enables recording protein spectra in a wide range of vibrational frequencies (while the VCD low-frequency limit is ~800 cm^{-1}, the ROA spectra can be measured from ~150 cm^{-1}). ROA spectra are thus very rich in structural information. Vibrations of polypeptide backbone can be found in three main ROA spectral regions: backbone skeletal stretch region (~870–1150 cm^{-1}), extended amide III region (~1230–1350 cm^{-1}) and amide I region (~1600–1700 cm^{-1}). For the interpretation of protein ROA spectra, the most informative seems to be the extended amide III region, particularly due to high sensitivity of the coupling between N–H and C_α–H deformations to protein geometry.[1] In the ROA spectra it is possible to detect bands which can be assigned to particular types of secondary structure such as α-helices (a positive band at ~1340–1345 cm^{-1} in the extended amide III region, a negative/positive couplet at ~1640 and 1660 cm^{-1} in amide I region and a positive ROA signal in the range ~870–950 cm^{-1}), β-sheets (a negative band at ~1245 cm^{-1} for hydrophobic and ~1220 cm^{-1} for hydrophilic environment in amide III region, a negative/positive couplet at ~1650 and 1680 cm^{-1} in amide I region) or PPII helix (a positive band at ~1320 cm^{-1} in the extended amide III region and a positive band at ~1630 cm^{-1} in amide I region).[3] Moreover, ROA can provide information on protein structural motif or fold[87] due to the presence of well resolved signals of loops and turns, and is able to distinguish between hydrated and unhydrated forms of α-helices.[3,88] Particularly the signals corresponding to β-turns (positive band at ~1295 cm^{-1} and negative band at ~1345 and 1375 cm^{-1}) are a valuable source of information, as they help distinguishing between α+β and α/β structures.[87] Unlike VCD, ROA can also provide additional information on aromatic side chains (particularly tryptophan and phenylalanine)[8] and disulfide bridges.[3] It also proved to be sensitive to the polyproline ring puckering.[89–91] ROA signals associated with aromatic side chain vibrations can be found in several spectral regions, such as ~1545–1560 cm^{-1} and ~1400–1480 cm^{-1} (tryptophan) or ~1600–1630 cm^{-1} (phenylalanine and tyrosine).[3,78] Among these signals, particularly useful seems to be the tryptophan band at ~1545–

1560 cm^{-1}, which can give information on its absolute stereochemistry.[3,92] Signals related to disulfide group vibrations can be found in the low-wavenumber region (below ~600 cm^{-1})[3,93] and will be discussed in more detail in the following section.

1.4 Optical Activity of Amide and Disulfide Groups

1.4.1 Optical Activity of the Amide Group

Understanding spectroscopic properties of amide group is of fundamental importance because it acts as the basic building block of peptides and proteins. It connects particular amino acid residues in peptides and proteins together, forming a chain – peptide/protein backbone. Besides its role in peptides and proteins, amide groups are present in many other molecules, often of considerable importance in biologically relevant materials (amide-containing drugs, alkaloids, etc.). Amide group itself involves just 6 atoms including the two C_α atoms, but despite that it is of amazing complexity. These 6 atoms involve three lone electron pairs, each of a different nature, and a three-centric π-system spanning over atoms with different electronegativities. As shown already in 1950s by Linus Pauling,[94] the central C'–N bond in the amide group is of partially double bond character (**Figure 3**).

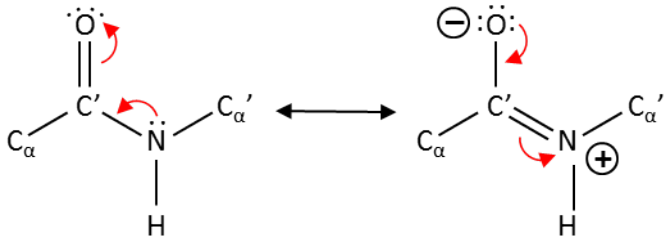

Figure 3: Amide group resonance.

In simple terms, while hybridization (sp^3) of its constituent N atom drives the molecule into nonplanar geometry, conjugation within the three-centric π–system favors planar arrangement with sp^2 nitrogen. It is to be noted that the basic question whether the amide group is a slightly nonplanar or planar entity is still not solved with certainty. It is only clear that minor deviations from planarity ($|\Delta\omega| \leq 10–15°$ – see **Figure 4**) are easy to achieve.[95] This metastable character of amide group increases its stability at physiological pH and temperature. It also affects its polarity, leading to high dipole moment. Amide groups often participate in hydrogen bonding,

which is particularly important in protein folding. The ability to form hydrogen bonds varies for primary, secondary and tertiary amides (for which the amide nitrogen atom is alternatively attached to two, one or no hydrogen atoms). While tertiary amides (containing the C'=O bonds) can act just as H-bond acceptors, primary and secondary amides (containing additionally one or two N–H bonds) can act as both H-bond donors and acceptors. This affects geometry and acido-basic properties. There is also an effect on solubility and vapor tension.

Amide group exhibits specific and characteristic manifestation in molecular spectra, both electronic and vibrational. In electronic spectra, amide group acts as a very distinct chromophore. Signals due to n–π* and π–π* electronic transitions of amides, peptides and proteins dominate ECD spectra in the UV region and give rise to spectral curves characteristic for the particular types of conformation (secondary structure). Amide signals in vibrational spectra are also characteristic and informative. It is possible to recognize up to 9 specific amide bands (amide A, B, I–VII). Particularly amide I (~1620–1700 cm^{-1}, mainly C'=O stretching vibration with small contributions of out-of-phase C'–N stretching, C_α–C'–N deformation and N–H in-plane bending), amide II (~1550 cm^{-1}, mainly C'–N stretching and N–H in-plane bending) and amide III (~1200–1400 cm^{-1}, mainly N–H bending and C'–N stretching) vibrations are usually well separated from other molecular motions. They are typically used for peptide/protein secondary structure elucidation as amide I and amide II vibrations are active in IR/VCD, while amide I and amide III are active in Raman/ROA).

Primary analysis of peptide/protein secondary structure (see previous chapter) is usually based on chiroptical signals of amide groups. There are numerous experimental and theoretical studies regarding this subject (see e.g. ref.[3,12,65,66,68]) as these procedures derive from rather extensive knowledge. Yet, it seems that the amide bands carry even more information and might reflect additional details of molecular structure. One of the promising applications appears to be a detection of possible amide nonplanarity. Although the amide linkage in peptides and proteins is usually considered to be planar with the dihedral angle ω (C_α–C'–N– C_α) either *trans* (180°) or *cis* (0°, occurring usually in Pro residues only), significant deviations from planarity (|Δω| up to 15–20°) have been revealed in many peptide and protein structures.[96,97] Nonplanarity is usually represented as pyramidalization ($sp^2 \rightarrow sp^3$ partial hybridization change) at amide nitrogen which is characterized by the angle

$\chi_N = -2\Delta\omega$[98] for the regular pyramidal arrangement[95] (see **Figure 4** for graphic definition of conformational angles and chirality specifications). Such an arrangement affects basicity of amide nitrogen and may be important for e.g. protein folding or enzymatic reactions. It also adds an additional degree of conformational freedom to the polypeptide main chain (the conformational angle ω in addition to the known conformational angles φ – rotation around the N–C_α bond, and ψ – rotation around the C_α–C' bond).

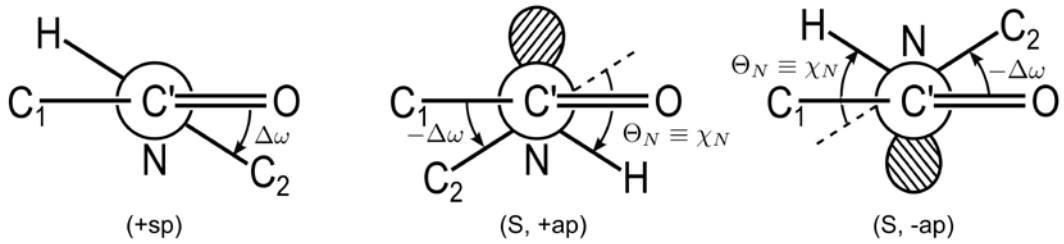

Figure 4: Graphic definition of conformational angles describing amide nonplanarity and specifications of its chirality. The Cahn-Ingold-Prelog RS nomenclature is used for specification of the pyramid on the N-atom (with the following substituent preference: C', C_2^α, H, N-lone pair) while the Klyne-Prelog system is used for the description of torsion around the C'–N bond (using the angle O=C'–N–C_2^α). Redrawn from ref. 99.

In the past years properties of nonplanar amides have been investigated by many means. While early studies were mostly based on experimental data (X-ray, electron diffraction and IR spectroscopy) and semiempirical calculations on simple models such as formamide,[100] N-methylformamide or N-methylacetamide,[101,102] it soon became obvious that nonplanar amide group is an inherently chiral chromophore (unlike planar amides, nonplanar amides lack the plane of symmetry) and therefore its spectral properties can be separately investigated by chiroptical spectroscopy. First such studies were based on ECD of models such as monolactams[103–111] or dilactams[112–114] with rigid, well defined geometries that allowed embedding amide groups into fixed environment. Dilactams also allowed studying amide group interactions. Depending on the polycyclic ring arrangement and size, these models also enabled inducing various degree of amide nonplanarity. The simplified interpretation of experimental ECD curves allowed establishing basic rules describing spectral manifestation of amide nonplanarity. A relation was found between handedness (absolute conformation) of amide nonplanarity and the corresponding sign pattern of the amide ECD bands:[99] While the right-handed arrangement leads to a positive-negative pair of the respective n–π* and π–π* ECD

bands, the left-handed arrangement gives rise to a pair of the bands with opposite sign pattern (**Figure 5**).

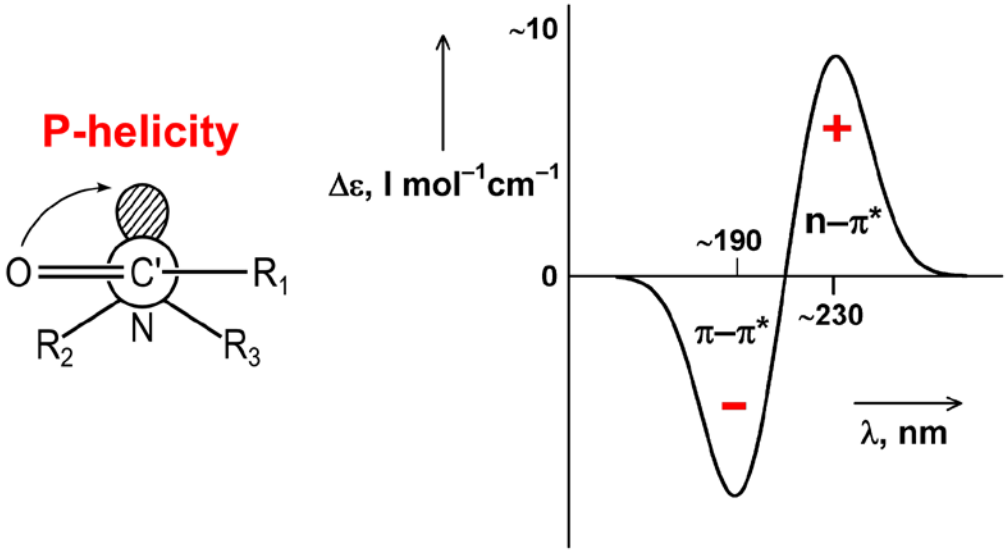

Figure 5: A relation between sense of amide nonplanarity and ECD amide signals.

Preliminary attempts have been also made to study the amide nonplanarity by VOA. The methods of VOA appear particularly promising as vibrational spectra are rich in structural detail and provide more local geometry-oriented information than the more commonly used ECD. They might be therefore more sensitive to local details including amide nonplanarity – especially if it is possible to separate its spectral manifestation from other features. For this purpose the most promising seem to be the amide I and II regions in VCD spectra and amide I, III and possibly also IV–VI spectral regions in the spectra of ROA. Rather surprisingly, vibrational data on nonplanar amides also bring some parallels to ECD, such as a bathochromic shift of amide I band, which was first observed for nonplanar amides by Smolíková et al. in the IR absorption spectra.[115] First successful VCD measurements of nonplanar amide-containing molecules were performed on model dilactams containing two tertiary nonplanar amides fixed in a three-ring system[116] (the attempts to measure VCD of monolactams containing secondary amides in *cis* configuration were also done; however, the molecules did not exhibit any amide-related VCD signals).[117] Promising amide-related signals were found in both amide I and II spectral regions; however, at that time a thorough theoretical interpretation was not possible.

Nowadays, advances in ab initio computational methods allow more detailed interpretation of ECD spectra (mainly due to the implementation of TDDFT

procedures) and also offer a possibility to interpret in detail VOA data (including computationally demanding ROA). Preliminary DFT calculations of chiroptical manifestation of nonplanar amides have been attempted for N-methylacetamide containing a single amide group.[118] The study involved simulations of ECD, VCD and ROA spectra and indicated that combined use of all three techniques should provide enough markers for nonplanarity detection, even in the case of more complex systems. Particularly promising appears to be the utilization of ROA spectroscopy. The potential amide nonplanarity manifestation should be possible to detect particularly in amide I and amide III region, and because of a relatively weak coupling with other molecular vibrations, bands due to amide nonplanarity should not be obscured by other molecular signals.

1.4.2 Optical Activity of Disulfide Group

Apart from the peptide bond itself, the disulfide (S–S) is the only covalent linkage connecting amino acids in peptides and proteins. Although disulfide groups are not as frequent in polypeptide chains as amide groups, they significantly influence peptide/protein structure and properties. Disulfide bonds affect protein stability, folding and function, because they limit polypeptide chain flexibility and can even control access to important sites of the structure.[119] S–S bonds are also the only covalent bonds which can connect or disconnect loops within one polypeptide chain (intramolecular S–S bridges)[120] or between distinct separate polypeptide chains (intermolecular S–S bridges).[121]

Disulfide groups are rather flexible and can adopt a wide scale of conformations. In peptides/proteins, geometries of disulfide bridges are determined by five torsion angles (see **Figure 6**): χ_1 (N_1–$C_{\alpha1}$–$C_{\beta1}$–S_1), χ_2 (or χ_{C-S}, $C_{\alpha1}$–$C_{\beta1}$–S_1–S_2), χ_3 (or χ_{S-S}, $C_{\beta1}$–S_1–S_2–$C_{\beta2}$), χ_2' (or χ'_{C-S}, S_1–S_2–$C_{\beta2}$–$C_{\alpha2}$) and χ_3' (S_2–$C_{\beta2}$–$C_{\alpha2}$–N_2).

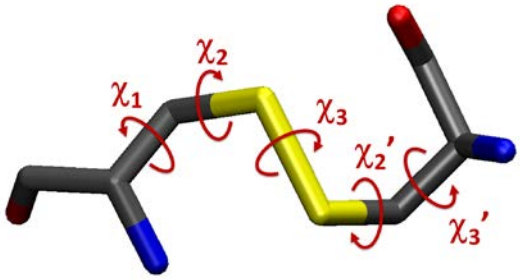

Figure 6: Disulfide group torsion angle definitions.

Experimental and theoretical conformational analyses of disulfide bridge patterns in more than 130 proteins of known structure[122,123] allowed summarizing features which appear common to most protein molecules: (**a**) The dihedral angle $\chi_{S\text{-}S}$ (χ_3 – see **Figure 6**) is usually close to 90°. The C–S–S–C group can possess two enantiomorphous chiral conformations with the $\chi_{S\text{–}S}$ either right- (+90°) or left-handed (–90°) (**Figure 7**). Both these conformations occur with approximately the

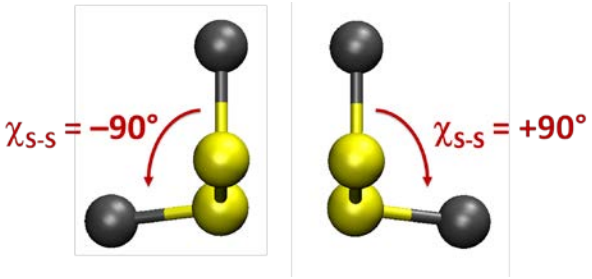

Figure 7: Disulfide group chirality.

same probability and the energy barrier between them is low. (**b**) For $\chi_{S\text{–}S} < 0$, the most probable $\chi_{C\text{–}S}$ and $\chi'_{C\text{–}S}$ (χ_2 and χ_2' – see **Figure 6**) value is ~ –60°, followed by ~180°. The most frequent conformation of the C_α–C_β–S–S–C_β–C_α fragment is the so called left-handed spiral (see **Figure 8** for graphical representation of the most populated disulfide group rotamers) with the $\chi_{S\text{–}S}$ = ~ –90° and $\chi_{C\text{–}S}$, $\chi'_{C\text{–}S}$ = ~ –60°. Using the alternative *gauche* (g) and *trans* (t) notation for a description of $\chi_{S\text{–}S}$ and $\chi_{C\text{–}S}$ torsion angles, such conformation is denoted as g'g'g' (where the initial and terminal letters describe the respective $\chi_{C\text{–}S}$ and $\chi'_{C\text{–}S}$ conformations and the central letter describes the $\chi_{S\text{–}S}$ conformation; the apostrophes denote negative torsion angle values). (**c**) Conformational flexibility of disulfide bridges is further given by the rotation around the $C_{\beta 2}$–$C_{\alpha 2}$ bonds. The most probable χ_1 and χ_1' conformation is ~ -60°, followed by ~ +60° and ~180°.

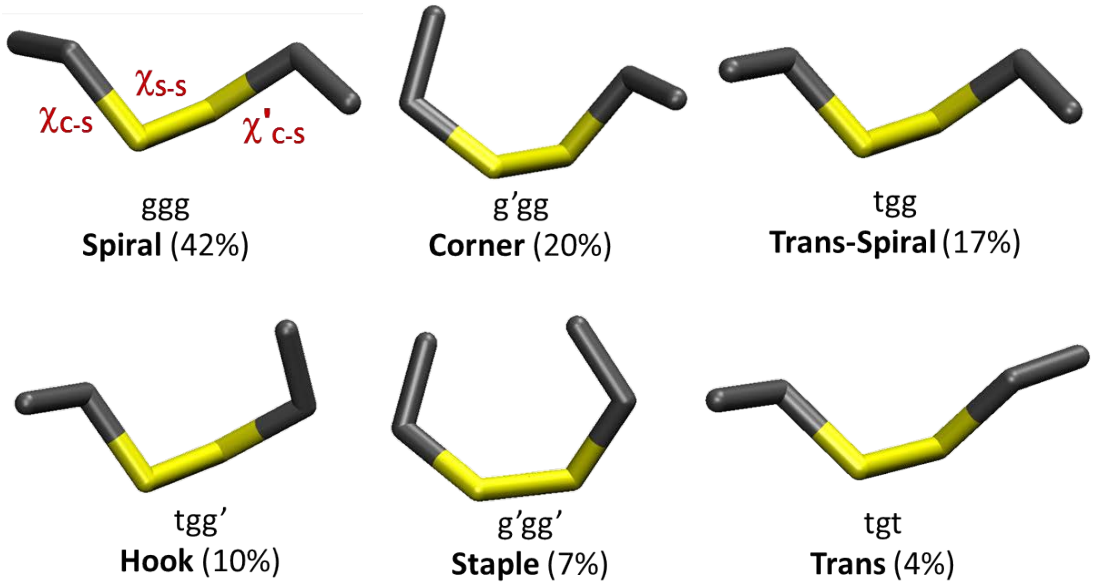

Figure 8: The most populated disulfide group conformations in proteins.[123] $|\chi_{S-S}| \approx 90°$, where $\chi_{S-S} > 0$ and $\chi_{S-S} < 0$ appear with equal probabilities. For the right-handed form (shown in the picture), $\chi_{S-S} \in (0, 180)$ and $\chi_{C-S} \in (0, 120)$ are denoted g, and $\chi_{C-S} \in (-120, 0)$ are denoted g').

Despite the important role of disulfide groups in peptides and proteins, their thorough investigations are rather scarce. It is difficult to apply crystallographic methods due to disulfide flexibility and, similarly, the use of NMR spectroscopy is limited by the lack of a suitable coupling constant. Among other techniques, Raman spectroscopy appears more promising. In Raman spectra, signals corresponding to disulfide stretching vibrations (ν_{S-S} and ν_{C-S}) are usually rather intense and well discernible from other vibrational modes. Moreover, unlike IR absorption, the spectral region in which the ν_{S-S} (~490–550 cm^{-1}) and ν_{C-S} (600–760 cm^{-1}) vibrations occur is easily accessible. Based on the frequencies of signals corresponding to S–S stretching vibrations, it is possible to distinguish between three basic conformations of the C_α–C_β–S–S–C_β–C_α fragment[124–126] (**Figure 9**): while the ggg conformation gives rise to a Raman signal at ~510 cm^{-1}, signals corresponding to tgg conformation can be found at ~525 cm^{-1} and signals due to tgt conformation at ~540 cm^{-1}. C–S Stretching vibrations can be then used for the estimation of S–C_β–C_α–C fragment conformation: the ν_{C-S} vibrations occurring at 630–670 cm^{-1} correspond to the P_H conformation of the S–C_β–C_α–C fragment (i.e. H atom in *trans*

position with respect to the S atom), while the signals at 700–745 cm^{-1} correspond to either P_C, or P_N conformation (i.e. C or N atom in *trans* position with respect to the S atom).[124,126]

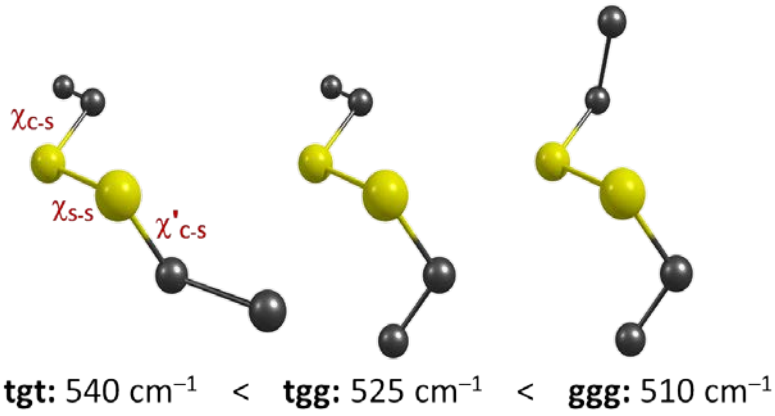

Figure 9: Correlation between disulfide conformation and S–S stretching frequency.

Nonplanar disulfide group (χ_{S-S} different from 0 or 180°) is a chiral entity, and therefore it appears promising to investigate its chiroptical properties. Unlike conventional spectroscopies, chiroptical techniques may give information on the sense of disulfide group torsion and might be used for the estimation of its absolute conformation. Yet, applicability of electronic CD is rather limited. The transitions into the lowest excited electronic state of disulfides (n_A–σ*, n_B–σ*) give rise to two bands of mutually opposite signs, which become strictly degenerate at the topologically most chiral conformation (χ_{S-S}= ±90°) and therefore cancel each other. For the χ_{S-S} close to 90°, this effect results in bands of low intensity, which are dominated by the environmental effects from the disulfide group surroundings.[127] Interpretation and assignment of disulfide ECD signals is therefore difficult and typically requires additional information, such as approximate magnitude of the χ_{S-S} angle (a relation between the sign of the long-wavelength disulfide band and chirality of the χ_{S-S} angle follows the so-called quadrant rule: while the positive sign of the band corresponds to χ_{S-S} in the range between 0 to +90° or –90 to –180°, the negative sign arises from χ_{S-S} in the range 0 to –90° or +90 to +180° – see **Figure 10**).[127–130] It is also helpful to supplement experimental data by theoretical calculations.[131] Investigation of disulfide group conformation is even more complicated in case of peptides and proteins, because the relatively weak disulfide bands are often obscured by stronger signals of more populated amide (~190–250 nm) and aromatic (~250–290 nm) chromophores.[28]

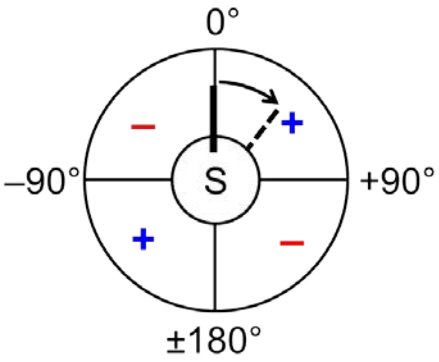

Figure 10: Quadrant rule describing a relation between chirality of the χ_{S-S} torsion angle and the sign of the n-σ* disulfide ECD band.

Preliminary theoretical studies of model disulfides[131] indicated that application of VOA methods might be more straightforward. Particularly VCD and ROA signals in the S–S stretching region might provide useful information on disulfide conformation. Experimentally, the use of ROA technique appears more promising because unlike in VCD, the region of S–S and C–S stretching vibrations (450–800 cm^{-1}) is easily accessible. Moreover, ROA spectra can be easily measured in aqueous solutions. Despite these potential advantages, ROA studies of disulfide group signals are still rather scarce. Weak experimental signals in the S–S stretching region were first mentioned several years ago in the work of Zhu and coworkers.[3] Signals in C–S stretching region were then reported in the ROA spectra of the hinge peptide containing two disulfide groups.[132,133] However, signals due to S–S stretching vibrations were not unambiguously assigned. The assignment of the S–S stretching signals was reported later by us in the ROA spectra of model cyclodextrin-based compounds containing one, two or three disulfide groups[93,134] and also of the neurohypophyseal hormone oxytocin.[134] Our experimental data were compared to calculations on simple model disulfides (H_2S_2, $(CH_3)_2S_2$, and $(CH_3CH_2)_2S_2$)[93,131] and, where available, also to known X-ray structures of the molecules. The results indicated that ROA might be capable of distinguishing between right- and left-handed chirality of the disulfide group: the right-handed disulfide group seems to give rise to a positive ROA S–S stretching signal and vice versa. However, this relation has to be further tested using more sophisticated theoretical procedures and also by employing other disulfide group containing model molecules.

2 Objectives

The aim of this work is to look for the specific and possibly unique applications of ROA in structural and conformational studies of biomolecules. The method itself has been already proven to be a useful tool for characterization of biomolecular structure and dynamics.[78] Up to now, most experimental and theoretical ROA studies have focused on structural interpretation of protein spectra.[12] Thanks to the extensive knowledge acquired over the past twenty years, ROA can be nowadays used rather routinely for the estimation of peptide/protein secondary structure content. Due to the enhanced sensitivity to structural details and local chirality and also due to wide accessible spectral range and possibility to measure routinely in aqueous solutions, ROA can extend the information obtained by other chiroptical spectroscopies.

For protein structure analysis, ROA has several advantages over other spectroscopies.[3] In peptide/protein spectra, particularly informative seems to be the amide III region, which cannot be utilized in VCD spectroscopy due to different selection rules. This spectral region provides information e.g. on loops and turns, hydration state of α-helices or polyproline ring puckering. Unlike VCD ROA can also provide useful information on aromatic side chains (see Chapter 1.3.3). As current ROA spectrometers enable measurements down to ~200 cm^{-1}, it is now possible to acquire ROA data also in the low-wavenumber region (which is not experimentally accessible by the complementary VCD spectroscopy). This region may be also very informative, because it includes signals of e.g. low-frequency amide modes (amide IV–VII), helix breathing, torsions, and skeletal deformations[135] or disulfide group stretching vibrations.[3] However, ROA studies utilizing this region and providing detailed interpretation of the low-frequency experimental data are still rather limited.

We focus on spectroscopic characterization of two important structural elements of peptides and proteins: (**a**) the amide and (**b**) the disulfide group.

(**a**) We intend to demonstrate that ROA spectroscopy is capable of detecting possible nonplanarity of amide groups, which may naturally occur in various biological systems. In this context ROA should provide data parallel to the previous ECD-based findings and put the amide nonplanarity detection on the firm basis given by chiroptical spectroscopy. For this purpose we utilize specially designed molecules

(spirodilactams) containing two amide groups exhibiting varying degree of amide nonplanarity.

(**b**) ROA investigation of disulfide group conformation (following the results of Master's thesis of the author)[134] represents a very different application. As follows from the previous symmetry considerations and semiempirical calculations, ECD cannot be applied here because it does not provide unequivocal results. On the other hand, we have already demonstrated the ability of ROA to detect conformation-related signals corresponding to S–S stretching vibrations (at ~500 cm^{-1}) in the spectra of simple cyclodextrin-based models containing one, two or three disulfide groups[93] and a neurohypophyseal hormon oxytocin.[134] Here we extend the analysis to a set of oxytocin analogs exhibiting different pharmacological properties and to even more complex antimicrobial peptides from Lasiocepsin family (containing two, one or no disulfide). We will investigate the possibilities of conformation determination with respect to disulfide group torsion.

3 Materials and Experimental Methods

The measurements of IR absorption and Raman/ROA spectra were performed at Charles University in Prague, Faculty of Mathematics and Physics, Institute of Physics, and at the Institute of Organic Chemistry and Biochemistry AS CR, v.v.i., Prague (IOCB). ECD spectra were measured at the IOCB. The far-UV ECD spectra of dilactams were measured at Diamond Light Source, Harwell, UK in collaboration with Dr. Giuliano Siligardi. VCD measurements of neurohypophyseal hormones and spirocyclic dilactams were performed by Prof. Marie Urbanová at the Institute of Chemical Technology in Prague. VCD spectra of antimicrobial peptides were measured at BioTools, Inc. facility (FL, U.S.A.) under the supervision of Prof. Laurence A. Nafie and Dr. Rina K. Dukor.

3.1 Samples

3.1.1 Spirodilactams I and II

Samples designed for studies of amide nonplanarity included both enantiomers of tricyclic spirodilactams 5,8-diazatricyclo[6,3,0,$0^{1,5}$]undecane-4,9-dione (dilactam I) and its 6,6,7,7-tetradeuterioderivative (dilactam II) (**Figure 11**). The molecules contain two tertiary amide groups fixed in a spirocyclic system and possess nonplanar amide groups.

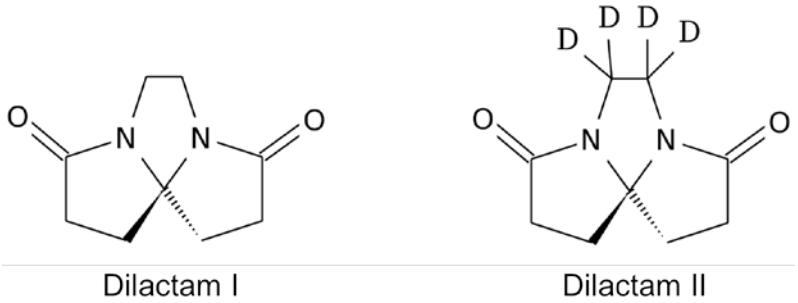

Figure 11: (1R)-(–) enantiomers of dilactams I and II.

Racemic dilactams were prepared by a condensation of 4-oxopimelic diethylester with ethylenediamine or its tetradeuterioisotopomer.[136] The racemic mixtures were resolved into pure enantiomers by high-performance liquid

chromatography (HPLC) on the commercial enantioselective chromatographic column. Details of the procedure are described in ref. 137.

3.1.2 Neurohypophyseal hormones

Neurohypophyseal hormones (NHH) oxytocin (I), arginine and lysine vasopressin (II, III) and their analogs methyloxytocin (IV), atosiban (V), desmopressin (VI) and terlipressin (VII) were produced as bulk pharmaceutical chemicals under Current Good Manufacturing Practice at Polypeptide Laboratories in Prague. The synthesis was based on the valid documents (master batch production records) and all peptides were fully analytically characterized as required for these pharmaceuticals and already described in the pharmacopeia chapters. They were all used for further work without additional purification. The inhibitor VIII was kindly provided by Prof. Maurice Manning (Medical College of Ohio, U.S.A.) and used as received. The simplified ring model IX was prepared using standard procedures of solid phase peptide synthesis employing Fmoc/tert-butyl strategy and trifluoroacetic acid (TFA) cleavage from the resin. Oxidation of the S–H groups was carried out at the concentration 0.5 mg/mL by oxygen. The crude product was isolated by lyophilisation and purified by commonly used HPLC method on reverse phase column C18 using UV detector and a mobile phase containing 0.04 % TFA for ion suppression and acetonitrile as organic modifier. The peptide was at least 95 % pure (based on HPLC).

3.1.3 Antimicrobial peptides from Lasiocepsin family

The antimicrobial peptide Lasiocepsin (LAS) containing two disulfide bridges and its three analogs having either only one (LAS 2, LAS 3) or none at all disulfide groups (LAS 4) were prepared using standard methods of solid-phase peptide synthesis as described in ref. 138. Sample purities and identities were checked using HPLC and mass spectrometry (MS). Presence of the correct disulfide bridge pattern was verified by digesting the peptides by trypsin followed by identification of the resulting fragments by mass spectrometry.[138] The synthesis was carried out at Spyder Institute Praha, s.r.o. and the samples thus obtained were used for spectroscopic studies without further purification.

3.2 Experimental methods

3.2.1 Raman Optical Activity

Raman and ROA spectra were measured on a commercial ROA spectrometer Chiral*RAMAN-2X*™ (BioTools, Inc., U.S.A.; SCP-P) and on a home-built ROA instrument (Institute of Physics, Charles University in Prague; ICP-P). These two spectrometers are conceptually different. Details of the home-built instrument, which is based on the original concept of ROA instrumentation as introduced first by Barron's group,[14] are described in ref. 20,139. The spectrometer uses incident circular polarization (ICP) modulation scheme, consisting in polarization modulation of incident laser radiation (see – **Figure 1** in Chapter 1.1). ROA spectra are then measured as a difference between Raman scattering from the sample illuminated by the right- (RCP) and left- (LCP) circularly polarized light. Polarization of the incident beam is modulated between RCP and LCP states using electro-optic modulator (EOM) – in this case a longitudinal Pockels cell based on a potassium dideuteriophosphate crystal. The main drawback of this ICP approach consists in the presence of the so called "flicker noise" – a random noise which might be caused by e.g. instabilities in laser beam, presence of randomly moving dust particles in the light path, density fluctuations in the sample etc.[64] This type of noise can be partially suppressed by extending time of the measurement or by increasing sample concentration. The home-built instrument currently uses argon laser (Coherent, Innova 305, excitation 514.5 nm), a fast stigmatic spectrograph HoloSpec HS-f/1.4 (Kaiser Optical Systems), and reaches the spectral resolution of 6.5 cm^{-1}. The spectrograph is equipped with three interchangeable holographic transmission gratings which allow covering the whole range of fundamental vibrations: HSG-514.5-LF (–250–2370 cm^{-1}), HSG-532-LF (580–3070 cm^{-1}) and HSG-514.5-HF (2270–4510 cm^{-1}). A neon-lamp standard is used for the calibration of wavenumber scale.

The other, commercial Chiral*RAMAN-2X*™ instrument follows the concept of W. Hug.[15] It uses scattered circular polarization (SCP) configuration (modulation of the light scattered by the sample – see **Figure 1** in Chapter 1.1). The RCP and LCP scattered components are measured simultaneously, which enables to eliminate flicker noise and effectively speeds up the experiment. The instrument uses 2W green diode laser OPUS 532 (532 nm laser excitation) and technically enables

recording data in the range of ~ –10–2430 cm^{-1}. The recent replacement of the originally implemented notch filter (SuperNotch-Plus™, Kaiser Optical Systems, Inc.) to edge filter (532-nm RazorEdge, LP03-532RE-25, Semrock, Inc.; SCP-P B) enabled blocking Rayleigh line more efficiently and allows reliable Raman/ROA measurements down to ~100 cm^{-1}. Toluene spectra are used for the calibration of the wavenumber scale.

Both instruments work in backscattering geometry, which is currently considered the best experimental strategy. The main advantage of the backscattering ROA setup is the highest possible intensity.[1] Within our experiments, we tested spirodilactam samples measured on both instruments (see **Figure 12**). The spectra were found nearly identical. The commercial spectrometer allows faster data collection, while spectra measured on the home-built instrument achieve slightly better resolution.

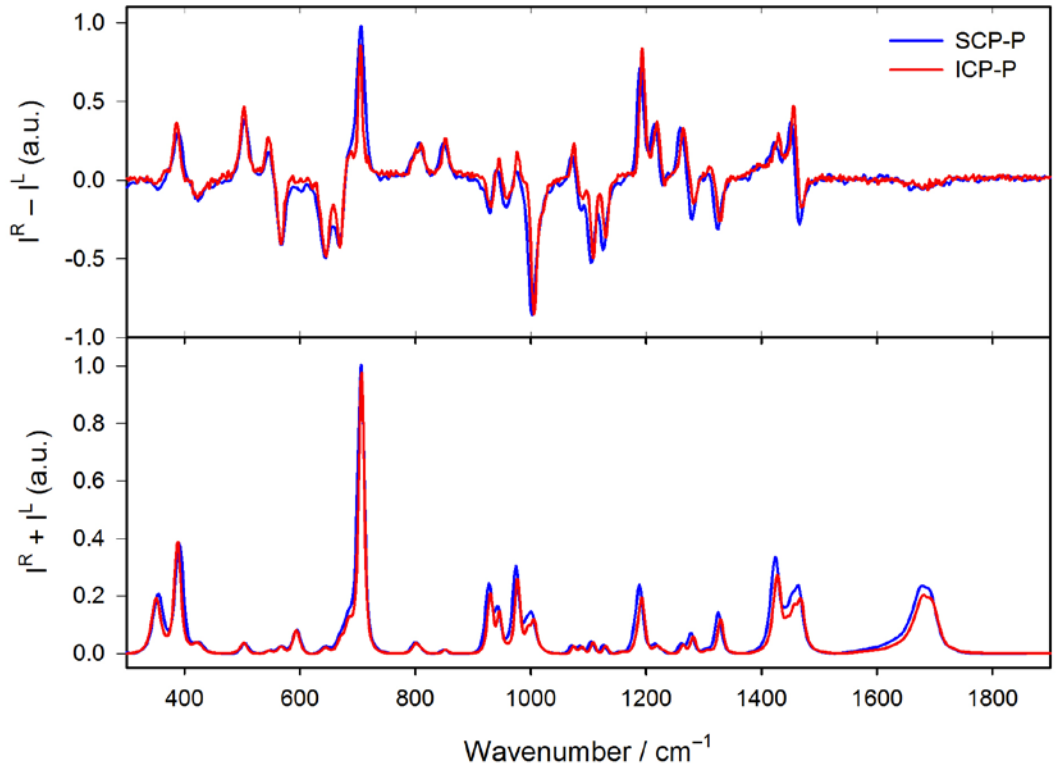

Figure 12: ROA (top) and Raman (bottom) spectra of the 1R-enantiomer of dilactam I measured on two different instruments (a commercial ROA spectrometer ChiralRAMAN-2X™ – SCP-P and a home-built ROA instrument – ICP-P).

The samples were measured in distilled water at room temperature in quartz thin-wall microcells (~60 µl, 4 × 3 mm; Starna Scientific Ltd.) with antireflectively coated windows. Experimental conditions varied depending on the sample,

instrument and experimental setup, and were as follows. Acquisition time: 20–40 h (model dilactams), 3–4 days (NHH analogs), 6–8 days (LAS peptides); sample concentrations: 0.5–0.7 M (model dilactams), 6–10 × 10^{-2} M (NHH analogs), 4 × 10^{-2} M (LAS peptides); power at the sample: 550−650 mW (model dilactams), 250–300 mW (NHH analogs I, II, IV–VII, IX – measured on Chiral*RAMAN-2X*™), 650 mW (NHH analog III – measured on a home-built instrument), 350−500 mW (LAS peptides).

The post-processing of experimental data was done using GRAMS/AI software (Thermo Electron Corporation) and typically involved solvent signal subtraction (Raman spectra) and a linear baseline correction (Raman/ROA spectra). Higher-order polynomials were used for correction of Raman spectra exhibiting fluorescence background. For the molecules with both enantiomers available (dilactams), ROA spectra were further processed by subtracting spectra of one enantiomer from those of the other one followed by dividing the result by two in order to improve quality of experimental data and to suppress possible experimental artifacts. In order to compare Raman/ROA spectra measured using different experimental setups (e.g. different gratings – see above) and instruments, the spectra were normalized to identical spectral intensities (in Raman spectra) within the overlapping spectral regions; identical scaling factors were then used for the normalization of the corresponding ROA spectra.

3.2.2 Electronic Circular Dichroism

UV absorption and ECD measurements in the spectral range of 180–400 nm were performed on a commercial spectropolarimeter Jasco J-815 (Tokyo, Japan), using a 150 W Xe lamp as a light source and a piezoelastic modulator for modulation of the incident light polarization. The samples were measured at room temperature in quartz cells (Hellma) with a 1–0.05 cm pathlength, depending on the used spectral range and sample concentration. The solvents included water (NHHs, LAS peptides, dilactams), pH 7.5 phosphate buffer (NHHs), acetonitrile (ACN, dilactams) and 2,2,2-trifluoroethanol (TFE, LAS peptides). Spectral range of ~185–300 nm, scanning speed of 50 nm/min, 4 s response time and 1 mm pathlength were typically used for the measurements in amide absorption region and the 1 cm pathlength was used for the measurements in disulfide region (~250–400 nm). The final UV

absorption and ECD data of dilactams and peptides in disulfide region were expressed as the respective ε and Δε values (L mol^{-1} cm^{-1}). For the spectra of peptides in amide region, the data were expressed in terms of molar elipticity [θ] per residue (deg cm^2 mol^{-1}). Sample concentrations were 2−3 × 10^{-2} M for model dilactams, 5–20 × 10^{-4} mol L^{-1} for NHH samples, 4 × 10^{-5} (amide region) and 4 × 10^{-3} (disulfide region) for the LAS peptides.

In addition to ECD experiments in the traditionally utilized spectral range, the dilactam samples were measured also in the far UV (VUV) region (170−200 nm), using the dedicated B23 beamline on synchrotron radiation circular dichroism (SRCD) instrument at Diamond Light Source, Ltd. (Harwell, UK).[140] The samples were measured as solutions (in TFE and distilled water, concentration 2−3 × 10^{-2} M) in CaF_2 cells with 0.1 mm pathlength. The final UV absorption and ECD data were expressed in the respective terms of ε and Δε values (L mol^{-1} cm^{-1}).

3.2.3 Vibrational Circular Dichroism

VCD spectra were measured using three different commercial instruments. While spectra of NHHs and model spirodilactams I and II were recorded at the Institute of Chemical Technology on non-specialized FTIR spectrometers supplemented with VCD attachments (Bruker, Germany), VCD spectra of Las-related peptides were measured on a dedicated ChiralIR-2X™ instrument at the BioTools facility.

Measurements of NHHs and spirodilactams I and II in the mid-IR (1800–1000 cm^{-1}) spectral region were performed using a general FTIR spectrometer IFS-66/S equipped with VCD/IRRAS module PMA 37 (Bruker, Germany). The setup included BaF_2 polarizer, ZnSe photoelastic modulator (PEM, Hinds Instruments, Inc.), HgCdTe (MCT) detector (InfraRed Associates, Inc.) and a lock-in amplifier SR830 (Stanford Research Systems, Inc.). NHH samples were measured in D_2O (50 mg/ml) in a demountable sample cell with CaF_2 windows (25 μm pathlength), while the dilactams were measured in $CDCl_3$ (50 mg/ml) in a cell with KBr windows with a 210 μm spacer. The data of NHHs were collected for 2 hours (4 blocks of 30 min scans) at 8 cm^{-1} spectral resolution, while the dilactam spectra were measured for ~2–3 h (7–10 blocks of 20 min scans) with 4 cm^{-1} spectral resolution.

VCD spectra of the spirodilactam samples were further measured in the region of C–D and C–H stretching vibrations (2000–3800 cm^{-1}). These

measurements utilized the Tensor 27 FTIR spectrometer equipped with VCD/IRRAS module PMA 50 (Bruker, Germany). The setup involved BaF_2 polarizer, ZnSe PEM (Hinds Instruments, Inc.), LN-InSb detector D4143/6 (InfraRed Associates, Inc.) and a lock-in amplifier SR830 (Stanford Research Systems, Inc.). The spectra in C–D stretching region (2000–2350 cm^{-1}) we measured in $CHCl_3$ (20 mg/ml) and those in C–H stretching region (2600–3200 cm^{-1}) in $CDCl_3$ (20 mg/ml) using a demountable sample cell (210 μm pathlength) with windows from either CaF_2 (C–D region) or infrasil quartz (C–H region). The data were collected for either ~10 hours (C–D region, 25–30 blocks of 20 min scans) or ~5 h (C–H region, 9–18 blocks of 20 min scans). Solvent scans were subtracted as background for all the measured samples and a correction for zero line was made.

VCD spectra of Lasiocepsin peptides were measured together with low resolution (8 cm^{-1}) IR absorption at the BioTools facility (Jupiter, FL, U.S.A.) on a commercial dual source[141] dual PEM[142] VCD spectrometer Chiral*IR-2X*™ (BioTools, Inc., U.S.A.) equipped with two SiC sources, two photoelastic modulators (ZnSe 36.996 and 37.02 kHz, Hinds Instruments, Inc.) - one before and the other after the sample, and a liquid nitrogen-cooled MCT detector. The patented dual-PEM strategy represents one of the major improvements of VCD measurement methodology and leads to a substantial suppression of absorption artifacts.[142] The lasiocepsin samples were measured in distilled H_2O (100 mg/ml) using CaF_2 cell (Biocell™, 6 μm pathlength, volume ~8 μl). The data were collected for ~12 hours at room temperature (25 °C, 8 cm^{-1} resolution, 12 blocks of 6000 scans, total absorbance of ~0.9 at ~1650 cm^{-1}). Solvent scans were subtracted as background. The data processing was done using GRAMS/AI software (Thermo Electron Corporation) and included a linear baseline correction and smoothing using second-order Savitzky-Golay filter with a 9-point window.

3.3 Interpretation

Several approaches were utilized for the interpretation of chiroptical data. These involve empirical analyses, semiempirical procedures and advanced ab initio calculations. Details of the procedures involved therein are described in the following chapter.

3.3.1 Ab Initio Calculations

The ab initio calculations of ECD, VCD and ROA spectra of model tricyclic dilactams were performed using Gaussian 09 software (revision A.02).[5] Geometry optimization and calculation of chiroptical spectra was always done at the same level of approximation. Various methods, basis sets and functionals were tested to check stability of the results towards particular computational procedure (for the details see Materials and Methods sections in Appendices 1 and 2 (ref. 137,143). For the detailed analysis of experimental data, theoretical procedures which consistently provided good agreement with the experiment were employed. This involved the use of DFT procedure,[144] B3LYP functional[145–147] and 6-311G** basis set[148] for the calculation of VCD and ROA spectra. TDDFT procedure,[149,150] PBE0 functional[151] and aug-cc-pVTZ basis set[45–48] were used for the calculation of ECD spectra. 70 singlet excited states were included in the calculations. The spectral bandwidths of 20 nm (10 cm^{-1}) and Gaussian band shapes were used for the simulation of theoretical ECD (VCD/ROA) curves. The effect of solvent was included in all the calculations and involved the use of implicit solvation model COSMO.[27] Facio 14.3.2 computational chemistry environment[152] was used for visualization of molecular orbitals (ECD calculations) and normal modes of vibrations (VCD and ROA calculations).

In order to get detailed description of vibrational motions of model tricyclic spirodilactams, the theoretical data were interpreted in terms of potential energy distribution (PED). For this purpose, a set of non-redundant internal coordinates was defined following the procedure described in ref. 153. This step cannot be done automatically, because the choice of internal coordinates depends on the particular molecular situation. In case of model tricyclic spirodilactams, the coordinates have to be chosen with particular caution, as there are several redundancy-related problems – the situation is complicated by C_2 symmetry of the molecules and by the presence of three annelated rings. The procedure specific for our dilactams I and II is described in detail in ref. 137. Atom numbering and ring definitions are specified in Figure 3, Appendix 2. The final set of internal coordinates is mostly based on recommended definitions[153] and includes: (**a**) all the bond stretching coordinates (C–C, C–N, C–H and C=O) except for the C_6–$C_{6'}$ stretching mode, which is included only implicitly as a contribution to in-plane and out-of-plane deformations of the N_2–C_6 and $N_{2'}$–$C_{6'}$

groups, to avoid redundancy; (**b**) scissoring, rocking, wagging and torsions deformations of all the CH_2 groups; (**c**) in-plane and out-of-plane deformations of the C_3=O_7, $C_{3'}$=$O_{7'}$, N_2–C_6 and $N_{2'}$–$C_{6'}$ groups; (**d**) deformations and torsions of the five-membered rings A and B (the rings are treated separately, utilizing specific definitions for five-membered rings described again in the ref. 153). Torsions and deformations of the ring C are not described explicitly as they are already included in the deformation modes around atoms N_2, $N_{2'}$, C_6, $C_{6'}$ and the attached H atoms. Again their explicit inclusion would introduce redundancies. **(e**) The tetra-substituted spiro-atom C_1 is treated specifically and description of its deformation motion is modelled after the formally analogous CH_2 group description. The corresponding internal coordinates include rocking, wagging and torsion deformations on the C_1 atom (scissoring deformations are included implicitly). These modes then describe motions of the ring A with respect to the ring B. For clarity this coordinate system is depicted in **Figure 13**.

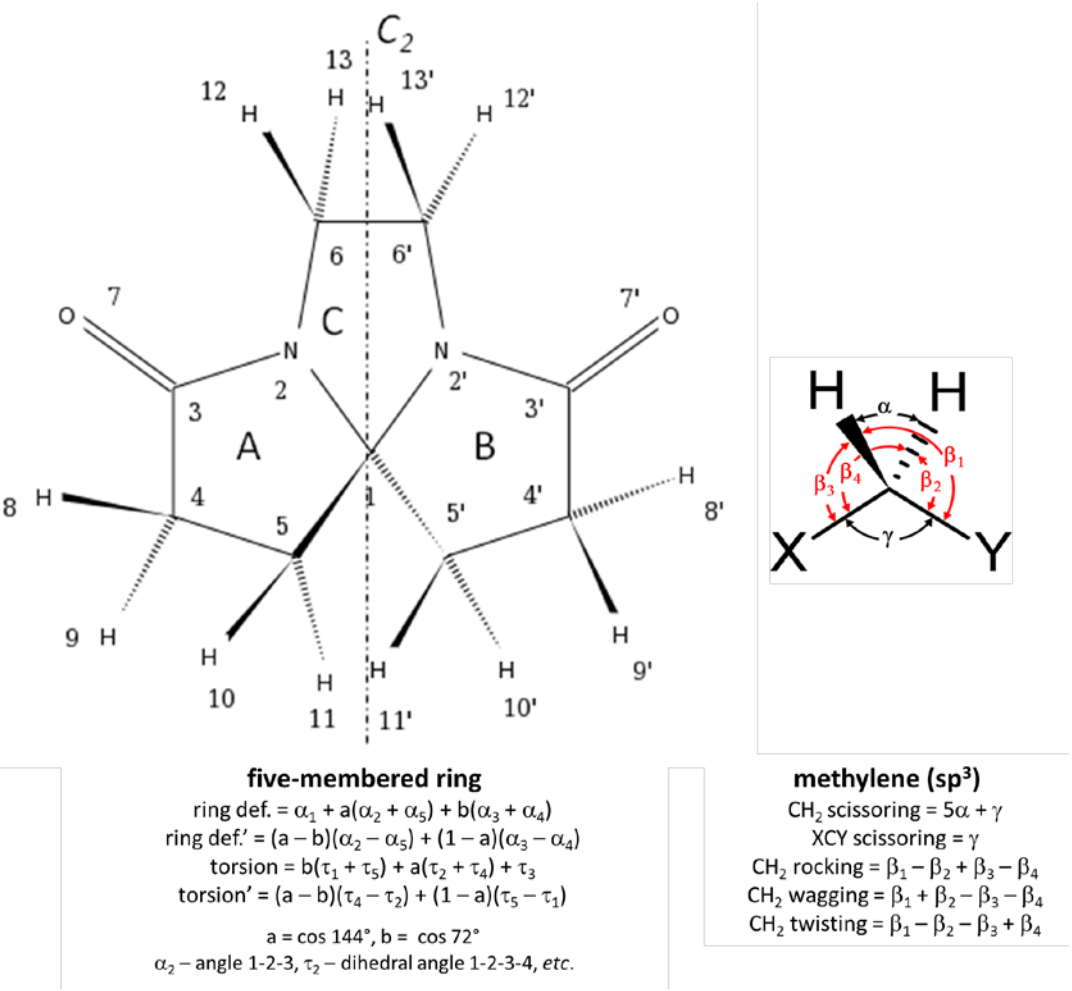

Figure 13: Internal coordinates used for vibrational analysis of dilactams I and II.

3.3.2 Empirical and Semiempirical Procedures

For the interpretation of the VCD spectra of model dilactam I and II, we have attempted to use also a simple coupled oscillator approach in order to evaluate and, if possible, to explain the proportion of inter-amide coupling in the VCD of amide I and amide II bands. A coupled oscillator model represents the only simple and effective procedure that can be used for VOA interpretation if the dipole-dipole coupling between originally mostly achiral but mutually chirally oriented groups is the decisive mechanism of VOA origin. Here we have applied the procedure to mutual coupling of nonplanar amide chromophores in order to compare directly the effects of amide nonplanarity vs. the amide-amide coupling. We have used this approach for basic evaluation of the effect of dipole-dipole coupling between C'=O stretching vibrations and also between C'–N stretching vibrations on the respective amide I and amide II bands in VCD spectra of dilactam I. Rotational strengths and component splittings were calculated from the equation 9 and 10 (Chapter 1.2), while the corresponding geometry factors were taken from the optimized geometry of dilactam I. The results were compared to full DFT calculation (see below).

4 Results and Discussions

Here we present a brief summary and generalized overview of the results which were achieved within this work. They were either already published in primary scientific journals (4 papers) or are being prepared for submission (1 manuscript). Full texts of printed papers are attached to the thesis as Appendices 1–4. The results are arranged in two, separately shown parts. The Chapter 4.1 summarizes results obtained with model polycyclic dilactams, which are suitable models allowing us to extract spectroscopic and chiroptical properties that are typical for nonplanar amide groups (Appendices 1 and 2). In relation to this investigation, it appeared possible to expand the ROA experimental technique by intensity calibration and wavenumber extension (Appendix 3). The separate study of chiroptical properties of a disulfide group in peptides is given in Chapter 4.2. It utilizes model peptides including a set of neurohypophyseal hormone analogs (Appendix 4) and antimicrobial peptides from Lasiocepsin family (manuscript in preparation).

Both these projects continue further on. Recently we have succeeded in preparing additional model compounds possessing varying degree of amide nonplanarity and having varying stiffness, such as a bicyclic molecule 1,6-diazaspiro[4,4]nonan-2,7-dione (dilactam III) which is less rigid and contains almost planar (but secondary) amide groups, or a tetracyclic molecule 2,6-diazatetracyclo[2,2,2,3]tetradecan-3,7-dione (dilactam IV) exhibiting extreme rigidity and extreme amide nonplanarity (**Figure 14**). Their investigation including

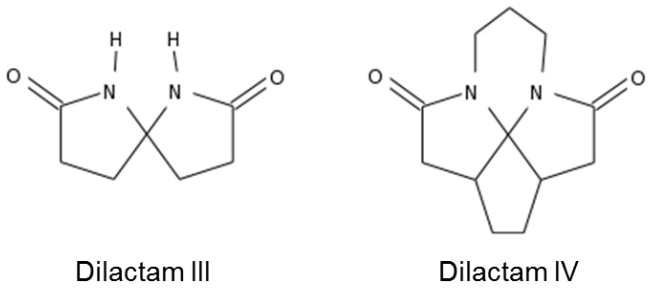

Figure 14: Model dilactams III and IV.

deep UV ECD (SRCD), VCD, ROA and calculations will be a subject of future studies and should help us to quantify a relation between amide nonplanarity (a merely local effect) and amide-amide coupling (a longer distance, between amide

groups effect). Similarly, we will continue investigation of S–S group conformation in antimicrobial peptides especially by ROA in the environment containing SDS-generated micelles. Most of these data were already collected.

4.1 Optical activity of nonplanar amide group

Studies of nonplanar amides in solution are not very frequent, despite the fact that amide nonplanarity is an important phenomenon influencing chemical properties of peptides, proteins and other amide-containing molecules (e.g. alkaloids, antibiotics, etc.). It is advantageous to utilize in these studies chiroptical spectroscopy of suitable, well-defined model molecules containing amide groups with some defined degree of nonplanarity. Such systems could allow us to identify specific features in chiroptical spectra which might reflect amide nonplanarity and provide means of its detection. Of various possibilities it appears particularly promising to investigate polycyclic lactams and dilactams. These systems offer several important advantages: (**a**) The amide groups are fixed in a rigid, well-defined polycyclic environment, and their crystal structures are mostly already known.[154–156] Therefore the calculations of molecular geometries are easier to perform as they generally do not require conformational search. (**b**) In dilactams, presence of two amides in one molecule enables us to simulate more closely the situation in more complex systems such as peptides and proteins. (**c**) The molecules (particularly tertiary amides) are well soluble in water and organic solvents. (**d**) The availability of these model compounds in the form of both pure enantiomers in multi-milligram quantities allows us to record more complete sets of chiroptical data (ECD, VCD and ROA) with confidence and to eliminate a potential danger of experimental artifacts. On the other hand, these systems also possess several disadvantages, such as the improper (head-to-head) connection of the interacting amide groups, which does not correspond to their ordering in peptides and proteins. But at least this mutual arrangement of amide groups is fixed in space. In addition, these models contain tertiary amide groups, which are not very common in peptides/proteins. A direct comparison is possible with proline-containing peptides, while other amino acids are connected by secondary amide groups.

The family of model polycyclic spirodilactams which follows from the above more general concept comprises about a dozen molecular systems varying in ring pattern, molecular symmetry, rigidity and substitution (**Figure 15**). If we wish to extract completely and quantitatively their spectroscopic properties it would be justified to investigate all of them, but for extracting fundamental characteristics, especially those pertaining to the embedded amide groups it is sufficient to select several representative examples. The tri- and tetracyclic compounds belonging to this series definitely contain nonplanar amide groups and their molecules are nearly completely rigid. Together with chirality and $\boldsymbol{C_2}$ symmetry of most of these molecules this makes them advantageous models for investigating properties of nonplanar amide groups mutually interacting within the well-defined geometrical arrangement.

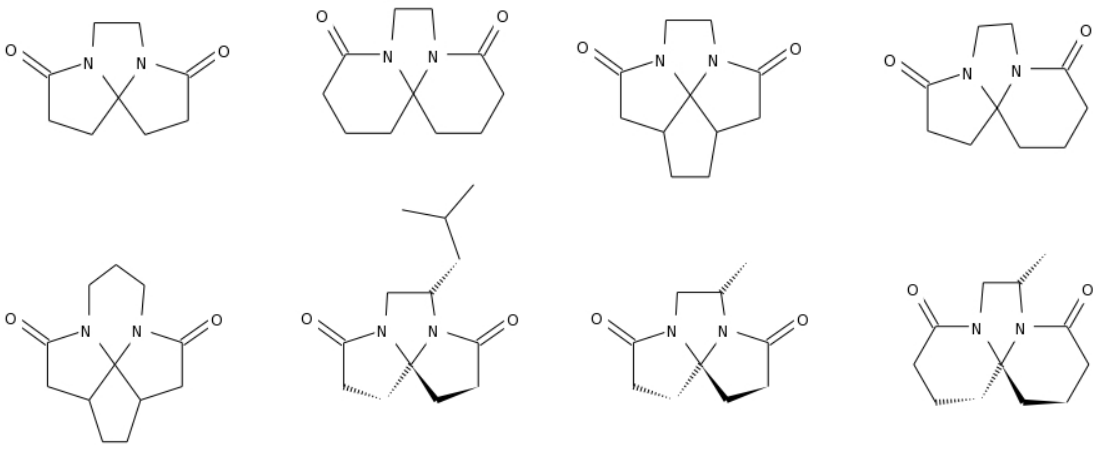

Figure 15: Model polycyclic spirodilactams.

To comply with these requirements, we have used for this work the tailor-made model systems belonging to the twisted dilactam class – the optically active tricyclic dilactam I (5,8-diazatricyclo[6,3,0,$0^{1,5}$]undecan-4,9-dione) and its very closely analogous 6,6,7,7-tetradeuterioderivative – the dilactam II (**Figure 11**). The deuterated derivative II was included in order to help detailed assignment of vibrational spectra and, particularly, because it offered the rare opportunity to record signals due to VOA (particularly ROA) within C–D stretching vibrations. The dilactams I and II exhibit pyramidal arrangements of bonds to the amide nitrogen atoms ($|\chi_N| \approx 42°$) and nearly planar arrangements at carbonyl carbon atoms ($|\chi_C| \approx 0.3°$) (**Figure 16**). Amide nonplanarity parameters are based on known X-ray data[154] (molecular geometries of dilactams I and II are considered identical - isotopomers). For angular parameters describing amide nonplanarity see Table 1 in Appendix 2.

We took advantage of recent advances in chromatographic enantioselective separations which provided these compounds in milligram quantities chemically as well as enantiomerically pure.[137] We studied the dilactams by both electronic and vibrational optical activity. ECD study is described in the ref. 143 (see Appendix 1) and is oriented predominantly towards understanding amide nonplanarity (n–π* transitions) and amide-amide interactions (π–π* transitions). VOA (ref. 137, see Appendix 2) possesses a more detailed view due to its sensitivity to short-range interactions. In the ref. 157 (see Appendix 3) we provide details on the new procedure of rigorous assembling of the wide (panoramic), extended spectral range ROA spectra from the shorter components measured in limited sub-regions (including C–D and C–H stretching vibrations).

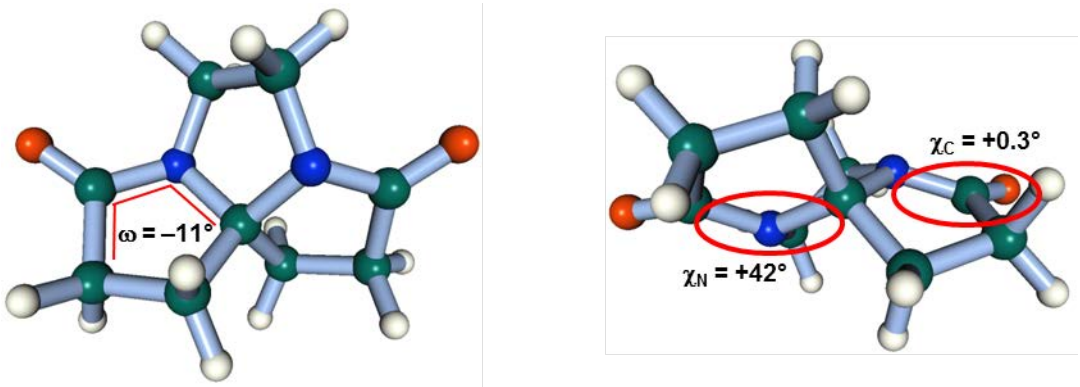

Figure 16: Three dimensional geometry of the (1R)-(–)-enantiomer of dilactam I.

4.1.1 ECD spectra of the dilactam I

Preliminary ECD studies of partially optically active dilactam I have been recorded previously.[112,113] For the R-enantiomer, the data (measured in water) showed a negative shoulder at ~225 nm which was superimposed over an intense negative dichroic band at ~205 nm. Towards even shorter wavelengths this band was evidently followed by an additional high intensity dichroic component of opposite (positive) sign manifesting itself as a tail of another unreached short-wavelength ECD band. The negative shoulder at ~225 nm was assigned to a sum band describing the amide n–π* transition, while the following pair of oppositely signed intense bands (a band at ~205 nm and a tail extending below 185 nm) to a couplet of π–π* transitions. A correlation connecting sign of the 225 nm (n–π*) band with the sense of amide nonplanarity follows the previously established rule (the right-handed

chirality leads to a positive (n–π*) CD signal, see **Figure 5** in Chapter 1.4.1). However, these preliminary correlations were based just on a comparison of experimental ECD data with those of the substituted dilactam derivatives and semiempirical calculations of model mono-amides[100–102,111,118,158–161] (operating only with n–π* and π–π* amide group configurations). On the contrary, proper interpretation of ECD due to amide nonplanarity requires a detailed direct quantum chemical calculation, because it is a case of inherently chiral chromophore. Moreover, the accuracy of preliminary experimental data was limited by low enantiomeric purity (~25 %) of available samples.

We have extended results achieved by these early ECD investigations of dilactam I along three lines: (**a**) We have further confirmed absolute configuration of optically active dilactam I by comparing experimental ECD with ab initio calculations of rotational strengths; (**b**) We have increased substantially numerical accuracy of experimental ECD by utilizing both enantiomers (each of them moreover 100 % enantiomerically pure) in our experiments; (**c**) Using synchrotron radiation circular dichroism (SRCD) we obtained unique far UV (down to ~170 nm) ECD data, which allowed us to record ECD bands below 185 nm, which were previously detected only as a tailing dichroic absorption. Our new data (see **Figure 17**) confirmed presence of the ECD bands identified in preliminary studies, but also revealed several additional features. Taking the R-enantiomer for reference, the complete set of observed experimental ECD features includes the previously detected negative shoulder at ~215–240 nm (depending on the solvent - acetonitrile, water and trifluoroethanol) and an intense negative band at ~203−208 nm. Besides these earlier observed features there is an additional negative shoulder at ~192 nm, and an intense positive band at ~178 nm (which cannot be revealed completely without employing SRCD).

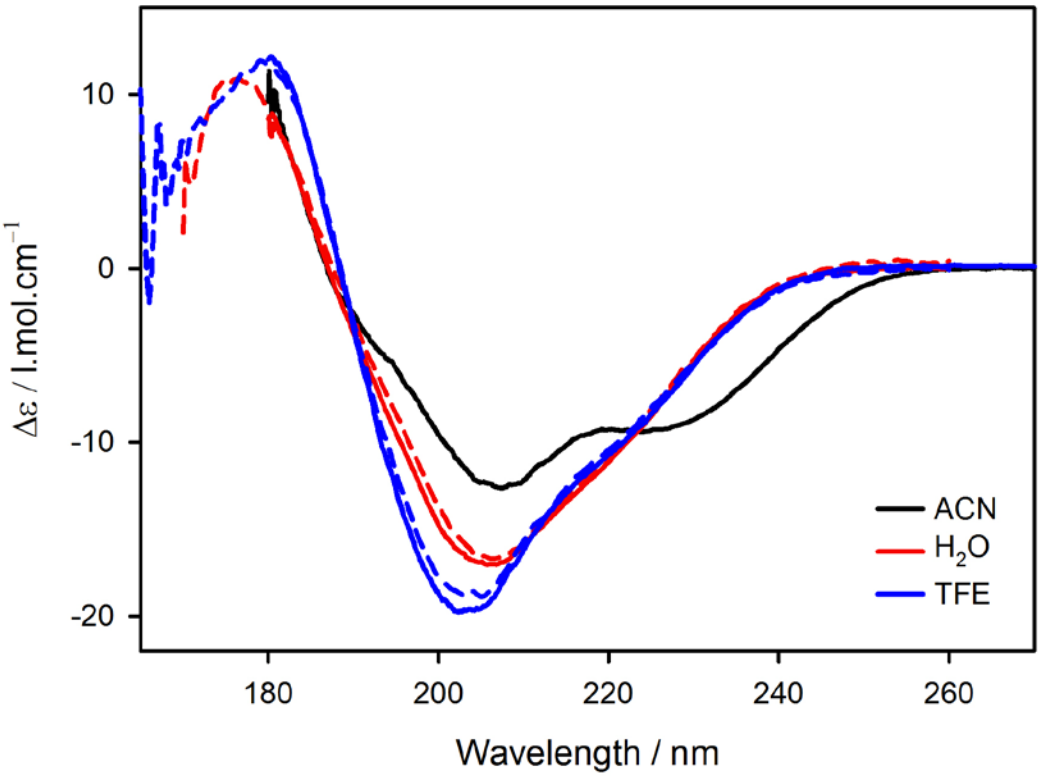

Figure 17: Experimental ECD spectra of (1R)-(–) enantiomer of dilactam I measured in acetonitrile (ACN), H_2O and 2,2,2-trifluoroethanol (TFE) using a stand-alone ECD spectrometer (solid line) and a SRCD instrument (dashed line).

For the assignment and interpretation of these more complete data we used advanced ab initio (TDDFT) calculations. The final band assignment was done using PBE0 functional, aug-cc-pVTZ basis set, CPCM solvation model and 70 singlet transition states; see Figure 2 and Table 2 in Appendix 1. Although the calculated ECD features lead to theoretical spectra which are apparently ~20 nm blue-shifted when compared to experimental curves, the overall shapes of theoretical ECD curves approximate the experiment rather well, including the less resolved features such as the shoulder at ~192 nm. Unlike early simple semiempirical interpretation which predicted only a presence of two n–π* and two π–π* transitions, ab initio calculations indicate that the situation is more complex. There are at least 11 distinct calculated electronic transitions (with the calculated rotational strengths |R| larger than 1×10^{-39} esu^2cm^2, see Table 2 in Appendix 1) which contribute significantly to the overall spectral shape of the calculated ECD curves above 170 nm. Although transitions above 180 nm are mainly contributed by valence-shell n–π* and π–π* configurations, additional contributions of configurations involving unoccupied σ*

and Rydberg-type orbitals become also important for transitions calculated at higher energies (below 180 nm).

According to calculations, the shoulder observed as the lowest energy ECD feature at ~220 nm is directly related to amide nonplanarity. Calculations show that this ECD band arises from a superposition of two components (being themselves two distinct electronic transitions) having mutually opposite signs and lying nearly at the same position (calculated at 218.4 and 218.1 nm, respectively). The sign of the resulting sum ECD band is then determined by the prevailing in magnitude, lower in energy component exhibiting antisymmetric (B) behavior with respect to the $\boldsymbol{C}_2$ axis of the molecule. Rotational strength of this component is almost three times higher than for the higher-energy component and its electric transition dipole moment is perpendicular to $\boldsymbol{C}_2$ axis due to the B symmetry. Calculations further reveal that these two components are contributed mainly by the n–π* (>50 %) configurations, as has been already predicted using simple interpretation – see above. Also in accord with this simple analysis, there is an additional significant contribution (~30 %) of π–π* configurations, which results from configurational perturbation conditioned by the inherent chirality of nonplanar amide groups. This finding is in agreement with previous ab initio analyses of model molecules containing single nonplanar amide groups.[118] As for the monolactams, the sign of the lowest energy band can be correlated with amide group chirality (i.e. the positive sign of the ECD band corresponds to right-handed helicity of the amide group and vice versa, as depicted in **Figure 5,** Chapter 1.4.1). In addition, as a consequence of amide nonplanarity, this band is shifted towards longer wavelengths (by up to ~15 nm).

It is more difficult to reveal and isolate amide nonplanarity manifestation in higher-energy spectral region. Although for the R enantiomer the experimental ECD spectra exhibit only a negative-positive couplet (previously ascribed to dipole-coupled π–π* transitions) and a negative shoulder, the theoretical analysis reveals significant contributions of at least ten bands of different origins. While the negative band at ~205 nm and the negative shoulder at 192 nm seem to be contributed mainly by two nearly pure π–π* (90 %) configurations, the positive high-energy band is contributed by several bands of different composition, mostly with significant contributions of π–π*, n–π* and n–σ* transitions. Based on our theoretical analysis, it seems that the general course of ECD curve is in this spectral region mostly given

by inter-amide coupling, while the amide nonplanarity contribution affects these spectra only moderately.

ECD spectra of the dilactam I reaching farther into UV region (~170–200 nm) provide qualitatively more complete information. Our detailed theoretical TDDFT study of these data confirms that ECD spectroscopy can be utilized for amide nonplanarity detection. The results indicate that nonplanarity can be sensitively and separately observed particularly in the long wavelength (n–π*) region and that the relation between the sense of amide nonplanarity and sign of the amide n–π* band remains valid even for dilactams. Although the inter-amide coupling is a dominating effect in the π–π* region, calculations show not a simple π–π* couplet, but also the components with π–π*, n–π* and n–σ* contributions.

4.1.2 Vibrational Optical Activity of Dilactams I and II

We performed VOA investigation of the dilactam I and its tetradeuterioderivative II (Appendix 2). Such a detailed study was made possible by a combination of several favorable factors. Besides using the recent state-of-the-art experimental (ROA, VCD) and theoretical (including recent developments of DFT) techniques we took advantage of the rigidity of dilactams I and II (which helped to simplify all calculations) and of their availability in both enantiomeric forms. Particularly the recent successful preparation of enantiomerically pure dilactam I and II in sufficient quantities enabled us to obtain high-quality experimental data, in which even weak spectral features could be detected and interpreted with confidence. Both VCD and ROA data have been collected in broader than usual spectral ranges (~1000–3200 cm^{-1} for VCD, ~200–3100 cm^{-1} for ROA), i.e. covering also the regions of C–H and C–D stretching vibrations and, additionally, in ROA even the low-wavenumber region. It is to be noted that signals due to C–D stretching vibrations were observed in our ROA spectra for the first time at all.

Quantum chemical (DFT) calculation reproduced overall pattern of experimental spectra rather well, and, consequently, we were able to assign unambiguously most experimental VCD and ROA bands. The band assignment was less certain only for features in higher-frequency region (above 2000 cm^{-1}), which involves the anharmonic C–H and C–D stretching vibrations. Our harmonic-level-only calculations were not sufficient for their detailed description. Nevertheless, our

experimental data provide high-quality material for our intended future analysis of C–H and C–D stretching signals including anharmonic corrections, which is beyond the scope of our current study. Despite the lack of anharmonic corrections the overall spectral shape of theoretical curves resembles experimental data even in this region rather well. It is therefore possible to get at least basic understanding of spectral features in this region. Moreover, additional use of the deuterated compound II helps us with the assignment and allows us to analyze different types of CH_2 groups. Although a few discrepancies between theoretical and experimental data remain, particularly in the high-frequency region, we have achieved an overall very good agreement between calculated and experimental spectra for both VCD and ROA. Therefore we attempted a transformation into chemically meaningful non-redundant internal coordinates followed by a detailed band-to-band assignment. In this way particular assignments were further supported by potential energy distribution (PED) values. For this purpose we designed a set of internal valence coordinates (see Chapter 3.3.1 and also Appendix 2). This coordinate system can be used with little modification for bicyclic, tricyclic and even tetracyclic spirodilactams and still the corresponding force constants refer to comparable bases. Consequently, it should then be possible to construct a more general model of VOA due to amide nonplanarity, which might be simultaneously based on several such compounds while maintaining internal consistency of data treatment. In this way it is possible to evaluate numerically the relative contributions of particular internal coordinates to total potential energy associated with each of the 69 fundamental vibrational modes (see Tables S2 and S3 in Appendix 2). The resulting PEDs of selected amide-related vibrational modes of dilactam I and the corresponding assignments are shown in **Table 1** and **Figure 18**.

Amide-related vibrations contribute significantly to VOA signals in several spectral regions. Our study indicates that some of these signals might be promising for possible amide nonplanarity detection. R-enantiomers of dilactams I and II show an asymmetrical rather broad single-signed band in the amide I spectral region (at ~1700 cm^{-1}) which exhibits a positive sign in VCD and a negative one in ROA spectra. This feature is very well reproduced by theoretical calculations in VCD. For ROA the calculations of dilactam I indicate a couplet; however, it is strongly biased towards negative values and the final curve resembles a negative single-signed feature as shown in experiment.

Table 1: Potential energy distribution (PED) of selected amide-related vibrational modes (A) of the dilactam I.

A	S	Freq. (cm^{-1})				Assignment (PED %)
		ROA (H_2O)		VCD ($CHCl_3$)		
		calc.	exp.	calc.	exp.	
1	A	+1719		+1735	+1718	νC=O (75%), νC'-N, νC'-C (12%)
2	B	–1707	–1681	+1725	+1699	νC=O (76%), νC'-N, νC'-C (11%)
3	A	+1419	+1425	–1414	–1399	νC'-N, νC-N, νC'-C (50%)
4	B	–1374		+1371	+1357	νC'-N, νC-N (46%)
5	B	–1240	–1233	+1240	+1224	νC-N, δ_{ip}N-C (29%)
6	B	+1159		+1159	+1146	νC-N, δ_{ip}N-C (53%)
7	A	–1139	–1130	–1139	–1126	νC-N, δ_{ip}N-C, δ_{oop}N-C (30%)
8	B	–1021	–1019	+1021		νC-N, δ_{ip}N-C (41%)
9	A	–1006	–1005	+1005		νC-N, δ_{ip}N-C (28%)
10	A	–919	–929	+919		νC-N, δ_{oop}N-C (59%)
11	A	+703	+707	+702		νC-N, δ_{oop}C'=O (24%)
12	A	+683		+684		δ_{oop}N-C, δ_{oop}C'=O, νC-N, νC'-N (53%)
13	B	–649	–644	–650		δ_{oop}N-C, δ_{oop}C'=O, νC'-C (73%)
14	A	+595		–594		δ_{ip}N-C, δ_{oop}C'=O, δ_{oop}N-C, νC'-C (52%)
15	B	+593		–594		δ_{oop}N-C, δ_{ip}N-C (58%)
16	A	–562	–568	–562		δ_{oop}N-C, δ_{oop}C'=O (54%)
17	B	+541	+547	+540		δ_{oop}N-C, νC-N, δ_{ip}N-C (37%)
18	B	+498	+501	+497		δ_{oop}N-C, δ_{oop}C'=O, δ_{ip}C'=O (30%)
19	A	–419	–423	–420		δ_{oop}N-C, δ_{ip}C'=O (61%)

S – symmetry; Freq. – frequency

According to PED, the amide I band arises mostly (~75 %) from the two (in-phase and out-of-phase stretching) C'=O modes (see modes 1 and 2 in **Table 1** and **Figure 18**). In VCD spectra, manifestation of the amide I band as the single-signed feature instead of a couplet, which is typical for VCD of larger molecules containing multiple interacting amide groups (like peptides and proteins), might be surprising. It indicates that other effects besides the typical amide-amide coupling might be important as well. We tried to estimate the relative effect of dipole-dipole coupling between C'=O stretching vibrations on amide I VCD of the dilactam I using the simple coupled oscillator calculation (see Appendix 2). Our calculations indicate that dipole-dipole coupling within the amide I vibration should give rise to a couplet comparable in intensity to other bands in VCD spectra of dilactam I. However, manifestation of the single-signed band indicates that the effect of amide-amide coupling is overridden by another effect of a different origin. The most probable

candidate appears to be again the amide nonplanarity. Similarly to VCD, a single-signed amide I band is observed even in ROA spectra. We can only speculate that even in this case the amide I band may reflect predominantly nonplanar amide chirality. To analyze further such an assumption, it would be beneficial to perform additional studies on other model molecules (like e.g. dilactams III or IV, see **Figure 14**) possessing varying degree of amide nonplanarity.

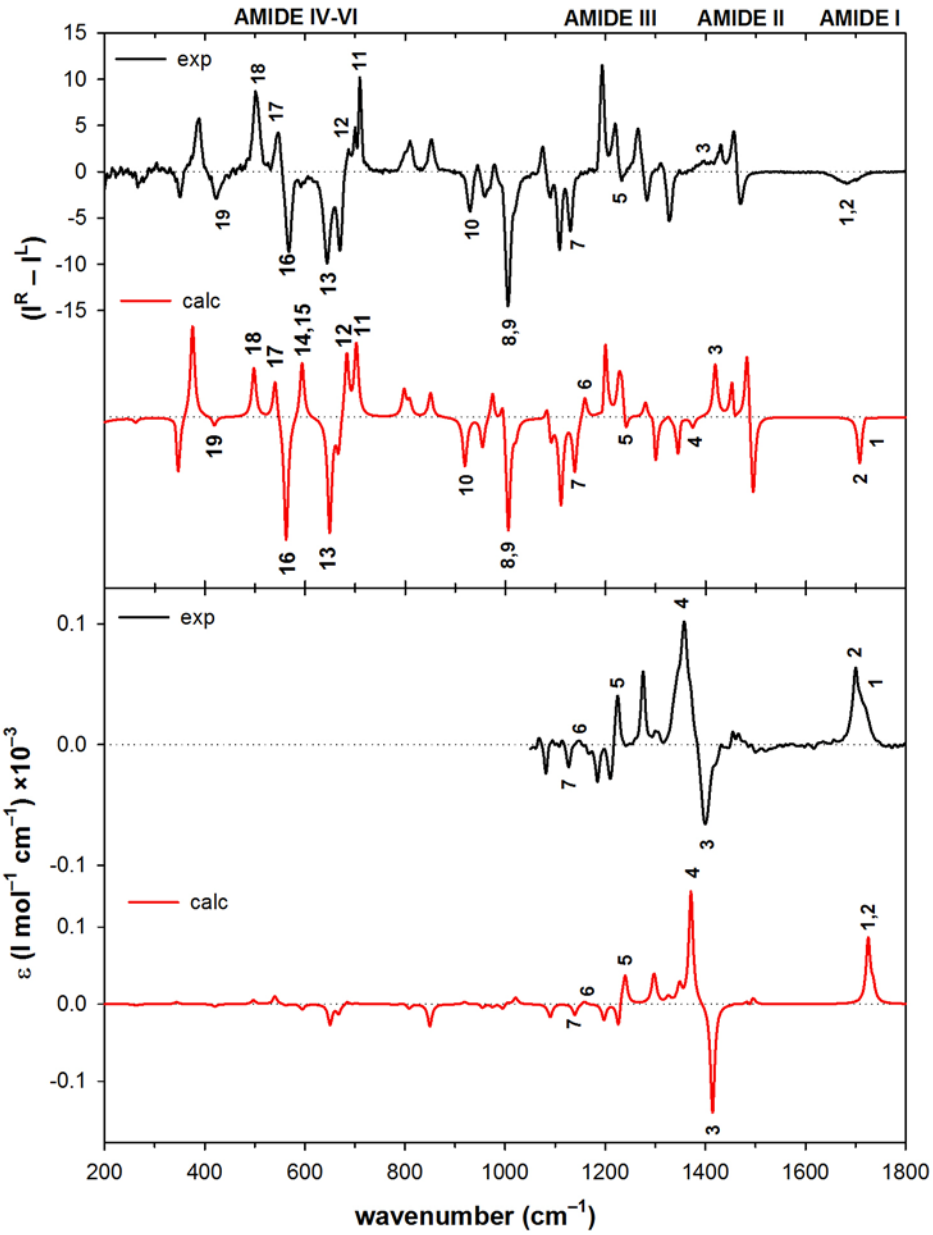

Figure 18: Assignment of the selected amide-related vibrations in ROA (top) and VCD (bottom) spectra of the R enantiomer of dilactam I.

Amide II vibrations of dilactams I and II are red-shifted to about 1380 cm^{-1}, because of the tertiary amide groups. In VCD we observe a very strong couplet (centered at ~1380 cm^{-1}), which dominates the whole spectrum. According to calculations, the two components (symmetric and antisymmetric with respect to C_2 axis) arise from the C'−N stretching vibrations (~35 %) mixed with skeletal N–C and C'–C stretches, ring deformations, and the in-plane skeletal and C'=O deformations (modes 3 and 4 in **Table 1** and **Figure 18**). These signals describe the modified amide II vibrations, where the non-existing contributions of N–H in-plane deformations (which are typical for amide II vibrations in primary and secondary amides) are replaced by motions of other skeletal atoms. The relative contributions of C'−N stretching modes are comparable to those in secondary amides. The observed VCD couplet is further confirmed by our coupled oscillator calculations including the sign pattern. This result indicates that in amide II region the amide-amide coupling overrides the effect of amide nonplanarity. However, here the amide II signals seem to be seriously affected by the specific geometry of our molecules, and the strong couplet is probably a consequence of unusual mutual orientation of interacting amide groups (the coupling is probably favored because of the close proximity of amide nitrogen atoms). For the generalization to peptide structures, different model systems (containing amide groups oriented in the usual head-to-tail manner) should be employed.

In Raman/ROA spectra of peptides and proteins, amide II vibrations are usually not observed, but valuable information can be derived from signals in the amide III region (~1200–1400 cm^{-1}). In secondary amides, amide III vibrations are also mostly given by a combination of N–H in-plane bending and C'–N stretching vibrations (just a different combination, active in Raman/ROA, not active in IR absorption/VCD). However, there are no N–H bonds present in our molecules and, consequently, there are no significant contributions of amide related signals around ~1300 cm^{-1}. Stretching and deformation vibrations involving amide nitrogen significantly contribute (~30–50 %) to ~6 vibrational modes between ~1250–900 cm^{-1} (modes 5–10 in **Table 1** and **Figure 18**). These bands are again reproduced well by ab initio calculations. However, it is rather difficult to deduce some general conclusions, as the amide-related vibrations mix extensively with other molecular

motions (predominantly CH_2 deformations, but also other skeletal vibrations). Yet, we can expect that for secondary amides the amide III bands may be observed and should even possess an analytical potential.

Unlike VCD, ROA enables recording experimental signals below 1000 cm^{-1}. Vibrations in this region usually involve skeletal motions, but contributions of low-frequency amide group motions can be also observed (e.g. amide IV – mainly C'–N and C'–C stretching vibrations together with in-plane N-involving and C'-involving deformations, amide V – mainly out-of-plane N-involving deformations and amide IV – mainly out-of-plane C'-involving deformations). In the spectra of our dilactams we can find several characteristic bands which are significantly contributed by amide-related motions, mainly involving in-plane and out-of-plane deformations at amide nitrogen atoms, but also deformations at the C' atom (for the dilactam I, these involve modes 11–13, 16–19 in **Table 1** and **Figure 18**). These bands are again described well by theoretical spectra, with the exception of the positive band calculated at 594 cm^{-1} (contributed by two overlapping bands corresponding to the modes 14, 15 – not visible in the experimental spectrum), and the positive band calculated at 683 cm^{-1} (mode 12 – obscured in the experimental spectrum due to presence of strongly polarized band in the parent Raman spectrum). For the potential amide nonplanarity detection, particularly promising seem to be spectral bands which are contributed mainly by the out-of-plane deformations at amide nitrogen, such as a negative ROA feature at ~568 cm^{-1} (mode 16, contributed by δ_{oop}(N–C) by ~50 %). It is possible that these features might be used in future for the evaluation of amide nonplanarity including sign and magnitude of amide group distortion.

4.1.3 ROA Measurement of Dilactam I and II in the Extended Spectral Range

ROA spectra of model dilactams I and II were recorded in the extended spectral range, including the high frequency region covering signals of C–D and C–H stretching vibrations (see above). So far, the attempts to record experimental data in the high-frequency region have been scarce despite the fact that such data might be a valuable source of information. First measurements in the extended spectral range were realized by Hug in 1975 on a dispersive ROA instrument.[162] Since then, the only reported ROA measurements in high-frequency region were performed in our

laboratory[134,163] on the home-built ICP-ROA spectrometer.[139] This instrument is equipped with three interchangeable gratings covering three partially overlapping spectral regions, and enables recording ROA data in the whole range of fundamental vibrations (~150–4000 cm^{-1}).

Correct assembling of complete ROA spectra from the sub-parts collected with different gratings requires a correction procedure eliminating the effects of varying experimental conditions. Such a procedure should allow us not only to assemble ROA data measured on the same instrument at different sub-ranges, but also to correlate ROA data measured on several distinct instruments. We have tested reproducibility of ROA signals measured on a single instrument but utilizing varying experimental setups. Moreover, we have compared ROA data measured on non-identical ROA instruments. As reference molecules we used α-pinene and the dilactam II. While α-pinene is commonly used for quality testing of experimental and theoretical ROA data, dilactam II seems to be a very suitable model, as it possesses well-defined ROA signals over the whole range of fundamental vibrations, including the C–D and C–H stretching regions.

The effect of varying experimental setup (different gratings) on ROA spectra of dilactam II is illustrated in **Figure 19A**, while **Figure 20A** shows a comparison of its ROA spectra measured on two different instruments (the home-built ICP-ROA instrument (ICP-P) and the commercial SCP-ROA instrument (SCP-P)). The results indicate that, although the ROA spectral patterns remain nearly identical independently on the setup/instrument used, the intensities of particular ROA bands vary rather significantly, particularly in the border regions of the spectra. This is a consequence of different response functions of particular setups/instruments.

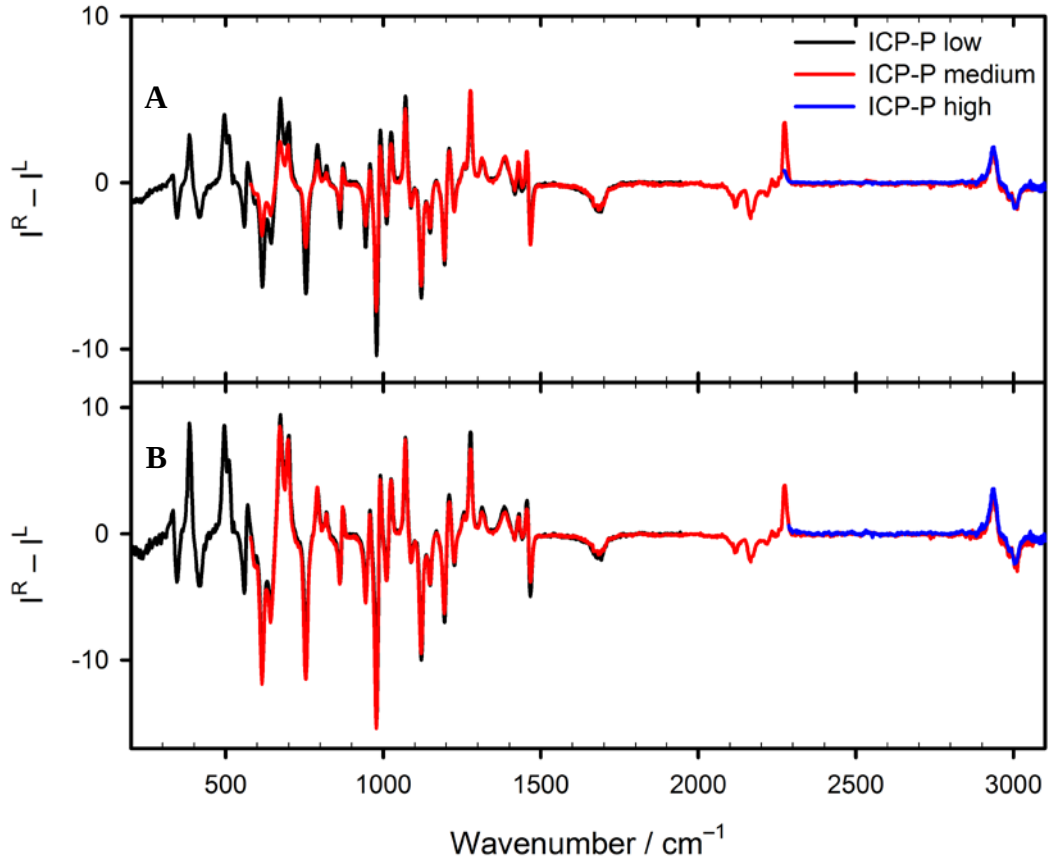

Figure 19: Experimental uncorrected (A) and corrected (B) spectra of (1R)-(–)-enantiomer of dilactam II measured in the extended spectral range using three different gratings.

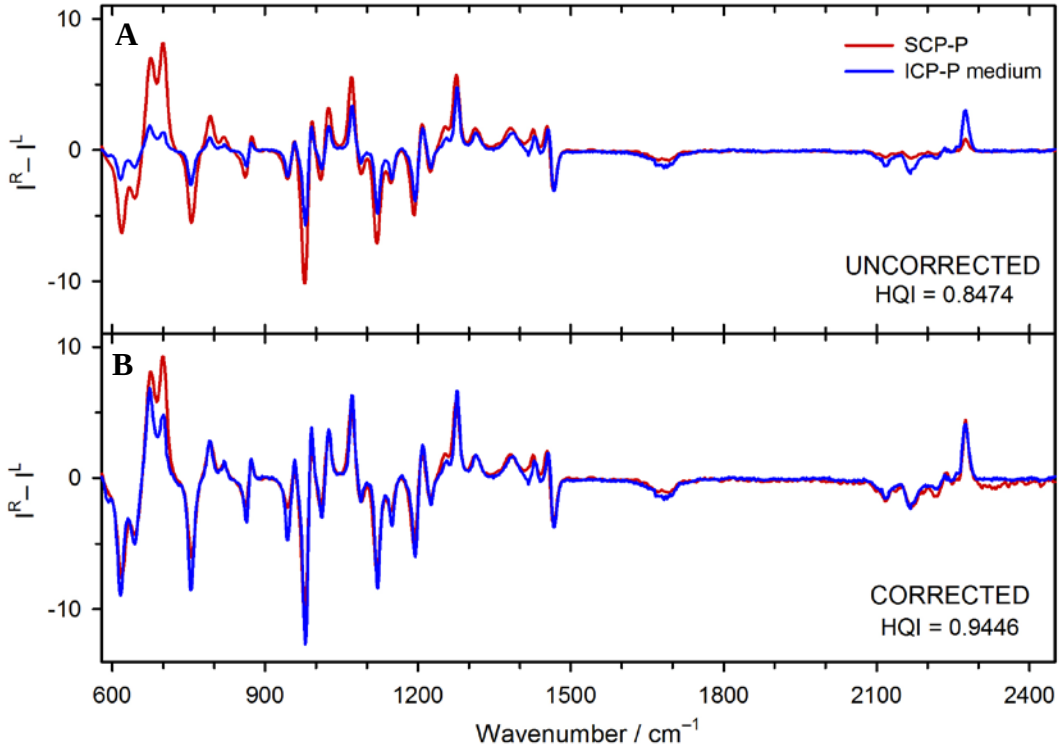

Figure 20: Experimental uncorrected (A) and corrected (B) ROA spectra of (1R)-(–)-enantiomer of dilactam II measured on two different instruments.

To determine the corresponding intensity response functions and to eliminate their effects on ROA spectra of our molecules, we have utilized the procedure which is nowadays used rather commonly for the correction of relative intensities of Raman spectra.[164–166] The procedure is based on the use of certified luminescence standards of the known relative spectral irradiance. Based on a comparison of the certified vs. experimentally obtained luminescence curves it is possible to establish instrument response function $S_{SRM}(\Delta\nu)$ of particular experimental setup/instrument. Subsequently, the experimental data can be corrected using this function. The resulting correction curve $C(\Delta\nu)$ is obtained by dividing the polynomial describing the shape of the standard luminescence spectrum $P_{SRM}(\Delta\nu)$ by the corresponding instrument response function (measured glass luminescence spectrum) $S_{SRM}(\Delta\nu)$. The correction curves for the particular experimental setups and instruments (used for the measurement of ROA spectra of dilactam II) are shown in **Figure 21**. The shapes of these curves indicate that a correction is needed particularly towards the edges of each spectral range, (the $C(\Delta\nu)$ values exceed 2). For each setup/instrument there is only a ~800 cm^{-1} interval in which the effect of a correction is almost negligible (i.e. the corresponding multiplication factor is close to 1).

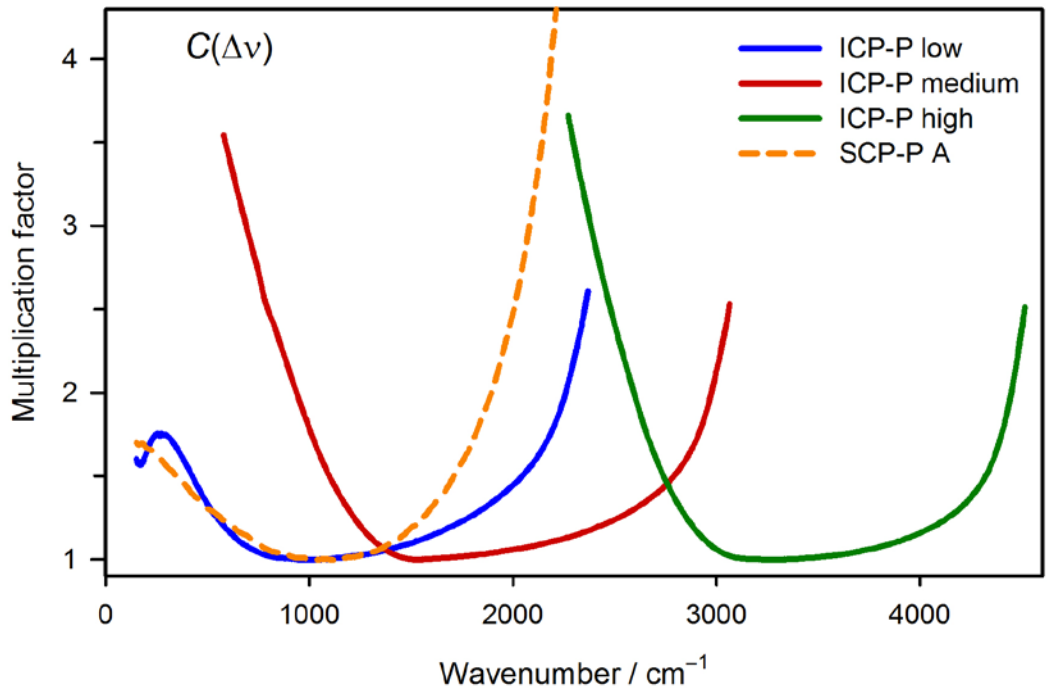

Figure 21: Correction curves $C(\Delta\nu)$ for different instruments and experimental setups. The low-wavenumber cut off at 150 cm^{-1} is given by the lower limit of certified luminescence spectrum.

As demonstrated in **Figure 19B** and **Figure 20B**, a correction of experimental ROA spectra by C(Δν) significantly improves the agreement between ROA data measured with different setups. The corrected spectra become comparable not only qualitatively, but also quantitatively. We can observe significant improvement in the agreement between integral intensities of particular ROA bands and also an improvement in hit quality index[167] (HQI – see equation 2 in Appendix 3 for its definition) (which is, however, less sensitive to overall spectral changes as it is just a single number). Application of the corrective procedure improves data reliability over a wide spectral range and enables common utilization of spectra recorded at different conditions or using different instruments.

4.2 Chiroptical properties of the disulfide group in model peptides

The study on chiroptical manifestation of disulfide group in model peptides follows our previous work.[93,134] Our results obtained on cyclodextrin-based models containing one, two or three disulfides[93,134] and on the neurohypophyseal hormone (NHH) oxytocin[134] have indicated that particularly ROA can give us valuable information on stereochemistry of disulfide bridges. Comparison of our experimental data with ab initio calculations on simple models hinted on a possible correlation of the sign of ROA bands due to S–S stretching vibrations with chirality of the disulfide group: while positive twist of the disulfide group appears to give rise to a positive ROA band in the S–S stretching region, a negative band in the same region might arise from the negative disulfide twist. To further analyze this relation, we extended our study to other model compounds including (**a**) a set of NHH analogs having just slightly modified sequence but differing widely in their pharmacological properties and (**b**) AMP Lasiocepsin and its analogs differing in disulfide bridge pattern and possessing various degrees of biological activity. These molecules represent suitable models due to their relatively small size and a presence of one or two disulfide groups in the molecule. Moreover, both groups of molecules are biologically active and they allow us to look for possible correlation between disulfide group conformation and biological properties of the peptides. Three-dimensional structures

of our molecules are analyzed using both electronic (ECD) and vibrational (VCD and ROA) optical activity. ECD provides us with basic secondary structure. For the more detailed analysis we employ VOA, as it is more sensitive to smaller-scale structural detail. Luckily, besides ROA probing the S–S group stereochemistry VOA can help us to identify structural motifs which are not easy to determine by ECD such as left-handed PPII helix, β-sheet or β-turn.

Chiroptical studies of disulfide group in NHHs (oxytocin, arginine vasopressin, lysine vasopressin and six of their analogs) (described in ref. 168 – see Appendix 4) are summarized in Chapter 4.2.1, while the analogous investigation of disulfide bridges in AMPs (Lasiocepsin and its three analogs differing in disulfide bridge pattern) is given in Chapter 4.2.2. The manuscript covering these models is in preparation.

4.2.1 Investigation of disulfide group conformation in neurohypophyseal hormones oxytocin, arginine vasopressin, lysine vasopressin and their several analogs

Disulfide group is a characteristic and important element of NHHs and a determination of its conformation represents further step in understanding a relation between NHH's biological activity and three-dimensional structure. NHHs belong to an evolutionary old class of peptides whose derivatives can be found in nearly all vertebrate species.[169] All NHHs are short peptides composed of ~9 amino acids. They comprise a heterodetic ring (with an aromatic amino acid residue at the position 2) composed of 6 residues, which is closed by the disulfide bridge connecting Cys^1 and Cys^6. The sequence is terminated by a flexible C-terminal part involving 3 residues. At the C-terminus the NHH sequence is terminated by primary amide (see **Figure 22**). Based on the amino acid residue at the position 8, NHHs are classified into oxytocin (neutral amino acid at the position 8) and vasopressin family (basic Arg or Lys residues at the position 8).[170] These peptidic hormones have a wide range of biological functions. While oxytocin is mostly known for its uterotonic and milk-ejecting activity, vasopressin is involved in a regulation of water retention in the body (antidiuretic activity) and a maintenance of blood pressure (pressoric activity).[170]

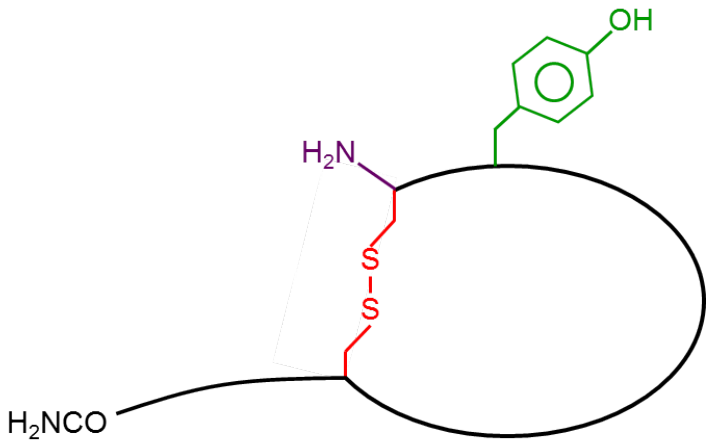

Figure 22: Schematic representation of basic structural elements of neurohypophyseal hormones.

Even minor changes in the sequence often lead to significant changes in biological activities of NHHs. Over the years hundreds of oxytocin and vasopressin analogs, often having only minor structural modifications but differing widely in their pharmacological effects, were synthesized. Many of these molecules were utilized as drugs and are now commonly used in pharmaceutical industry. Structural studies of these molecules have shown that although the analogs display such diverse activities, they are considerably consistent in their three-dimensional arrangement.[171] To get deeper understanding of the relation between NHH's structure and activity, it is therefore important to look even for minor differences in spatial arrangement of these molecules. Particular attention should be paid to conformation of the aromatic amino acid at the position 2, to primary amide at the C-terminus and to the arrangement of the disulfide group, as modifications to these motifs typically result in notable changes of biological activities but do not cause their complete loss.[171] However, it is not easy to get detailed information on NHH's structure at the atomic level. The molecules are rather difficult to crystallize and X-ray data are mostly available only for the complexes with carrier proteins.[172,173] Most structural studies of NHHs in solution are based on NMR, CD, fluorescence and Raman studies.[174] The data indicate presence of a β-turn (OT, AVP) in the ring part of these molecules (between residues 2, 3 or 3, 4) and an exposition of the Tyr residue at the position 2 to the solvent. Disulfide group has been investigated mainly by Raman spectroscopy, which indicated the prevailing ggg conformation.[174] However, conventional Raman spectroscopy provides us only with partial information, as it is not capable of distinguishing between the disulfide group right- and left-handedness. As discussed

above, such information should be best approachable by chiroptical methods, particularly by ROA.

In order to get this missing detail and to clarify the possible effect of disulfide group conformation on NHH's biological activity, we have collected a more complete set of chiroptical data (ECD, VCD and ROA) of neurohypophyseal hormones oxytocin (I), arginine vasopressin (II) and lysine vasopressin (III) and six of their analogs having agonistic (methyloxytocin – IV, desmopressin – VI, terlipressin – VII), antagonistic (atosiban – V, NHH inhibitor – VII) or no biological activities (inactive model – IX) (see **Table 2**). These peptides represent a suitable set of model systems, as the differences in their biological activities are mostly achieved by minor changes in their primary (and probably also secondary) structure. As an additional advantage, most of these molecules are used as therapeutics and are therefore accessible in sufficient quantities and high purity. While ECD data of the compounds are already partially known (see ECD studies on compounds I–III, VI, IX),[175–178] VOA data, which might provide us with the still missing structural details, have been collected by us for the first time.

Table 2: A set of the studied NHH samples

Neurohypophyseal hormones		
I	**Cys**-Tyr-Ile-Gln-Asn-**Cys**-Pro-Leu-Gly-NH_2	Oxytocin
II	**Cys**-Tyr-Phe-Gln-Asn-**Cys**-Pro-Arg-Gly-NH_2	Arginine Vasopressin
III	**Cys**-Tyr-Phe-Gln-Asn-**Cys**-Pro-Lys-Gly-NH_2	Lysine Vasopressin
Analogs used as drugs		
IV	**Cys**-Tyr(OMe)-Ile-Gln-Asn-**Cys**-Pro-Leu-Gly-NH_2	Methyloxytocin
V	**Mpr**-D-Tyr(OEt)-Ile-Thr-Asn-**Cys**-Pro-Orn-Gly-NH_2	Atosiban
VI	**Mpr**-Tyr-Phe-Gln-Asn-**Cys**-Pro-D-Arg-Gly-NH_2	Desmopressin
VII	$(Gly)_3$-**Cys**-Tyr-Phe-Gln-Asn-**Cys**-Pro-Lys-Gly-NH_2	Terlipressin
Inhibitors and inactive models		
VIII	cpm**Cys** D-Tyr Ile Thr Asn **Cys** Pro Orn-NH_2	NHH Inhibitor
IX	**Cys** Gly Gly Gly Asn **Cys**-NH_2	Inactive Ring Model

Mpr – mercaptopropionic acid; cmpCys – β-cyclopentamethylene cysteine
Cys (or Mpr) residues are connected by disulfide bridges and are written in bold

A complete set of ECD spectra of I–IX measured in the disulfide transition region (250–380 nm) is shown in Figure 2 in Appendix 4. These data demonstrate that identification of the S–S group based on ECD signals is rather complicated, because the corresponding bands partially overlap with signals of aromatic chromophores (Tyr, Phe; 250–350 nm) which are present in all structures except for

the inactive model of the oxytocin ring (IX). The analyses are therefore limited to longer-wavelength parts of spectra above ~290 nm. As it is not possible to correlate sign of experimental ECD bands with the sense of disulfide group torsion without having a rather precise information on the sense and magnitude of the S–S group dihedral angle (see quadrant rule in Chapter 1.4.2), we may only hypothesize that the mutually similar course of our ECD curves might correspond to similar disulfide group conformation. In this way, we can classify our molecules into three groups based on similarities in the shape of the long-wavelength tail of the ECD curve. The group (**a**) includes molecules exhibiting a negative low-intensity band. There are 6 molecules falling into this category: the NHHs oxytocin (I), arginine vasopressin (II) and lysine vasopressin (III), oxytocin agonistic analog methyloxytocin (IV) and two vasopressin agonistic analogs desmopressin (VI) and terlipressin (VII). The group (**b**) includes the vasopressin/oxytocin antagonistic analog atosiban (V), which exhibits an intense negative ECD band of rather high intensity. The inactive model (IX), exhibiting a negative ECD band of a medium intensity, can be categorized either into group (**a**) or (**b**). The group (**c**) then involves the NHH inhibitor (VII) exhibiting an intense positive ECD band. Although any generalization is hardly possible, it is worth noticing that all agonistic NHH analogs exhibit similar disulfide bands and fall into the group (**a**), while the antagonistic analogs or inhibitors exhibit different ECD curves and fall into groups (**b**) or (**c**).

VCD spectroscopy cannot be applied directly to the investigation of disulfide group conformation, because the corresponding spectral region is not experimentally accessible. However, our data demonstrate that it can provide us with additional details on conformation of the peptide backbone. VCD spectra of our molecules in the mid-IR region are shown in Figure 3 in Appendix 4. For all these molecules, the spectra are remarkably consistent, exhibiting a negative couplet in amide I' region (consisting of a positive band at ~1670 cm^{-1} and a negative band at ~1630 cm^{-1}, which is slightly shifted to higher wavenumbers for the compound IX) and a negative band in amide II' region (at ~1440 cm^{-1}). This specific spectral pattern indicates a left-handed PPII-type helix.[80] On the basis of its intensity we can deduce that for molecules I–VIII such type of structure probably involves only two to three amino acid residues (the $\Delta\varepsilon/\varepsilon$ ratio is approximately three times lower than for polyproline peptides). There seems to be only a minor portion of PPII structure in the most

flexible compound IX (a model of the oxytocin ring) with the Δε/ε ratio about two times lower than for other compounds.

Similarly to VCD, ROA provides us with useful details on peptide backbone conformation (signals in the amide I and extended amide III region). Furthermore, it enables us to investigate manifestation of the disulfide group using signals due to C–S and S–S stretching vibrations below ~800 cm^{-1}. Raman/ROA spectra of the compounds I–VII and IX are shown in **Figure 23**. ROA spectrum of VIII could not be obtained as the sample quantity was not sufficient for ROA experiment. The ROA spectra of all our samples are dominated by a positive band in the extended amide III region at ~1320 cm^{-1}. Together with a positive band in amide I region (at ~1650–1680 cm^{-1}), this feature is a well-established marker of PPII structure.[3] This finding is consistent with VCD data. In addition signals in the extended amide III region further indicate presence of β-turns (a positive band or shoulder at ~1295–1300 cm^{-1}; compounds I–VI) and an antiparallel β-sheet structure (a negative band at ~1245–1250 cm^{-1}; compounds I–VII). As already indicated by NMR data and molecular dynamics simulations for compound I–III),[174] the presence of such structures in NHH molecules is quite probable. Apart from the prominent bands in amide I and extended amide III region reflecting sensitively peptide backbone conformation, ROA spectra exhibit promising signals in the S–S stretching region. For all our samples the conventional Raman spectra consistently indicate the prevailing ggg conformation of the disulfide bridge (band at ~510 cm^{-1}). The corresponding ROA signals at ~510 cm^{-1} can be found in the spectra of all the measured samples except for VI. Interestingly, the observed ROA signal is positive for the NHH agonists (oxytocin I, arginine vasopressin II and lysine vasopressin III, methyloxytocin IV and terlipressin VII), and negative for the inactive (ring model IX) and inhibitory analogs (atosiban V). Based on previous calculations on simple disulfide models,[131] these data may indicate that the agonistic analogs seem to favor right-handed disulfide orientation, while the inhibitors or inactive compounds might tend to the opposite (left-handed) disulfide arrangement. As there is no distinguishable signal in the ROA spectrum of desmopressin, we may assume that disulfide group is in this case probably more flexible, allowing both right- and left-handed disulfide arrangements.

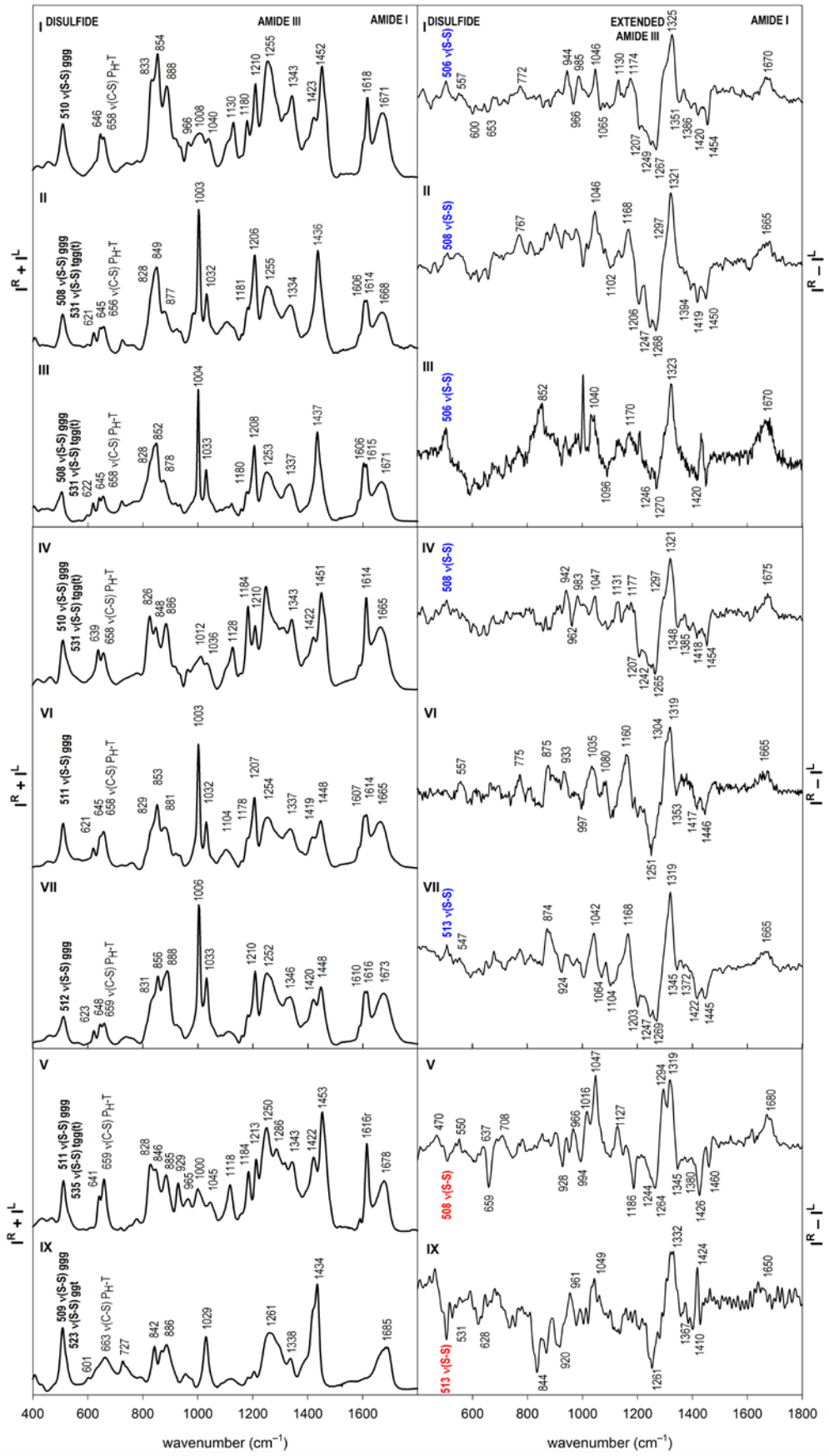

Figure 23: Raman (left) and ROA (right) spectra of compounds I–VII and IX measured in H_2O. Bands assigned to S–S stretching vibrations of the disulfide group are in bold (positive ROA signals are in blue, negative ROA bands in red).

Our chiroptical study of NHHs and their analogs demonstrates that VOA can extend the existing knowledge of NHH conformation, which has been, up to now, mainly based on NMR and ECD data. VCD confirms that the main chain conformation is consistent within all these analogs and does not depend on their biological function. Within our studied model compounds, VOA indicates a left-handed chain reversal of the cyclic part. According to our data, the structural differences seem to concentrate into the region of the disulfide bond. The most valuable information on NHH disulfide group conformation appears to be provided by ROA spectroscopy, which indicates mutually reversed sense of the S–S torsion for NHH agonistic and inhibitory or inactive analogs. However, such relation should be further tested using additional models, particularly NHH inhibitory analogs. This will be a subject of our future investigation.

4.2.2 Structural role of disulfide bridges in the antimicrobial peptide Lasiocepsin and its three analogs

In order to further analyze the possibilities of determining disulfide group conformation by chiroptical methods, we have extended our study to even more complex molecules – peptides from the Laciosepsin family having two, one or no disulfide group in the molecule. The natural peptide Lasiocepsin (LAS), isolated from the venom of the eusocial bee *Lasioglossum laticeps*,[138] belongs to a unique, structurally diverse group of molecules – antimicrobial peptides (AMPs). AMPs are evolutionary old peptides acting probably as a first line of organism defense against microbial infections. These peptides have considerable therapeutic potential because, compared to common antibiotics, they typically have broader range of activities against pathogens and usually do not cause microbial resistance.[179,180] Instead of targeting specific receptors, AMPs mostly interact with microbial cell membranes (particularly negatively charged phospholipids), causing membrane perturbation and/or disruption of membrane-associated processes.[179] Although AMPs differ widely in their amino acid sequence and structure, they have several common features. They typically consist of 10 to 50 amino acid residues, have a positive net charge (due to the presence of positively charged residues such as lysine or arginine) and contain approximately 50% of hydrophobic residues.[181] Upon interaction with microbial membranes, AMPs usually adopt amphipathic structure (often α-helical)

with hydrophobic and polar residues arranged into separate regions. Amphipathicity then enables AMPs to penetrate into membrane lipid bilayer.

LAS is a medium-sized AMP containing 27 amino acid residues and two disulfide bridges (Cys^{8}–Cys^{25}, Cys^{17}–Cys^{27}). The set of these related compounds further includes three analogs having different disulfide patterns: two analogs containing one native disulfide group while having the two remaining cysteine residues replaced by alanine residues – LAS 2 ($Ala^{8,25}$, Cys^{17}–Cys^{27}) and LAS 3 (Cys^{8}–Cys^{25}, $Ala^{17,27}$), and a completely linear (therefore very flexible) analog with all cysteine residues replaced by alanines – LAS 4 ($Ala^{8,17,25,27}$) (see **Table 3**). In accord with results presented earlier,[138] differences in disulfide pattern significantly influence biological properties of these peptides. While natural LAS possesses substantial antibacterial and antifungal activities, its disulfide-modified analogs exhibit either reduced activity (LAS 3) or are almost inactive (LAS 2, LAS 4).

Table 3: Primary structures and antimicrobial activities of LAS and its analogs

LAS analogs		**Antimicrobial activity** MIC (μM)				
		B.s.	*S.a.*	*E.c.*	*P.a.*	*C.a.*
LAS	GLPRKILCAIAKKKGKCKGPLKLVCKC	0.4	93	8.6	15	3.6
LAS 2	GLPRKILAAIAKKKGKCKGPLKLVAKC	4.2	>100	>100	>100	50
LAS 3	GLPRKILCAIAKKKGKAKGPLKLVCKA	0.5	>100	55	65	70
LAS 4	GLPRKILAAIAKKKGKAKGPLKLVAKA	12	>100	>100	>100	>100

MIC – Minimum inhibitory concentration; *B.s. – Bacillus subtilis, S.a. – Staphylococcus aureus, E.c. – Escherichia coli, P.a. – Pseudomonas aeruginosa, C.a. – Candida albicans*.
Disulfide bridges connecting the cysteine residues Cys^{8}–Cys^{25} and Cys^{17}–Cys^{27} are indicated in blue and red, respectively. Sequence modifications are indicated in yellow.
The compounds do not show any haemolytic activity.[138]

As follows from preliminary ECD data of LAS and its analogs 2-4,[138] and also from the recent NMR study of LAS,[182] disulfide bridges play important role in stabilization of LAS conformation. In water, natural LAS possesses well-defined secondary structure (see **Figure 24**), consisting of two α-helices (Arg^{4}–Lys^{13}, Pro^{20}–Val^{24}) connected by a structured six-residue loop (Lys^{14}–Gly^{19}) and stabilized in a mutually nearly orthogonal position by the disulfide bridge Cys^{8}–Cys^{25}. An additional disulfide bond (Cys^{17}–Cys^{27}) which connects the C-terminal Cys^{27} with the structured loop, stabilizes C-terminal part of the molecule.[182] According to NMR data, the α-helical segments of LAS are not amphipathic, yet the whole peptide adopts an amphipathic structure due to the presence of two distinct positively

charged domains (Arg^4, Lys^5 and $Lys^{12,13,14,16,18,22,26}$) and connecting hydrophobic patches. As follows from ECD data, the absence of one or both disulfides results in a significant decrease of α-helical content and an increase of random coil and/or PPII content. Interestingly, even the analogs lacking one or both disulfide groups show the ability to form α-helical structure upon addition of a helix-inducing agent, like trifluoroethanol (TFE). A significant increase of α-helical content is observed even for the inactive analogs, indicating that presence of α-helical structure is not the only requirement for the antimicrobial action.[138] Consequently, LAS's antimicrobial activity seems to be influenced by additional factors such as length and position of particular α-helical segments and/or their mutual orientation (nearly perpendicular in LAS itself – see **Figure 24**).

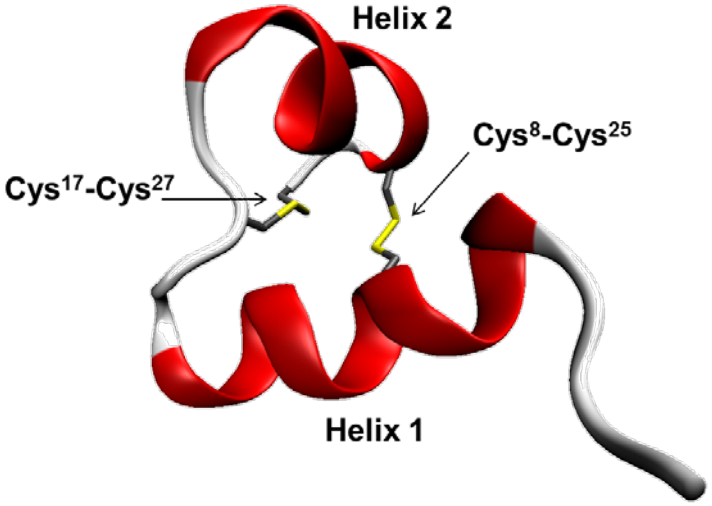

Figure 24: NMR structure of antimicrobial peptide lasiocepsin (PDB ID: 2mbd).[182]

In this study we supplement the existing spectroscopic data on LAS and its analogs 2–4 in order to get better understanding of the mutual relation between LAS spatial arrangement, role of disulfide groups and antimicrobial mode of action. Utilizing both electronic and vibrational optical activity, we investigate the effect of varying disulfide ring closure on LAS conformation, including geometry of the disulfide groups. Our ECD experiments follow the preliminary ECD study of LAS peptides (which included measurements in water and TFE in amide region) and involve, in addition, investigation of conformational changes of these peptides as caused by presence of SDS micelles (representing simplified membrane-mimicking models – these supplementary results require additional ROA experiments and will be yet added) and measurements in the disulfide region. In addition, we utilize the

methods of VCD and ROA, which can aid with the secondary structure assignment (as they are more sensitive to secondary structure elements such as left-handed PPII helix, β-sheet or β-turn) and enable deeper studies of disulfide bridges (see above). The following text includes a detailed description of experimental data together with their preliminary interpretation. These results might further benefit from additional ECD and ROA spectra measured in the presence of SDS micelles. We plan to include these in the final version of the manuscript.

As shown in the previous study,[138] ECD of LAS in water (**Figure 25**) exhibits a positive band at 190 nm and negative bands at 206 nm and 222 nm. Such spectral pattern is typical for the peptides/proteins with prevailing α-helical conformation.

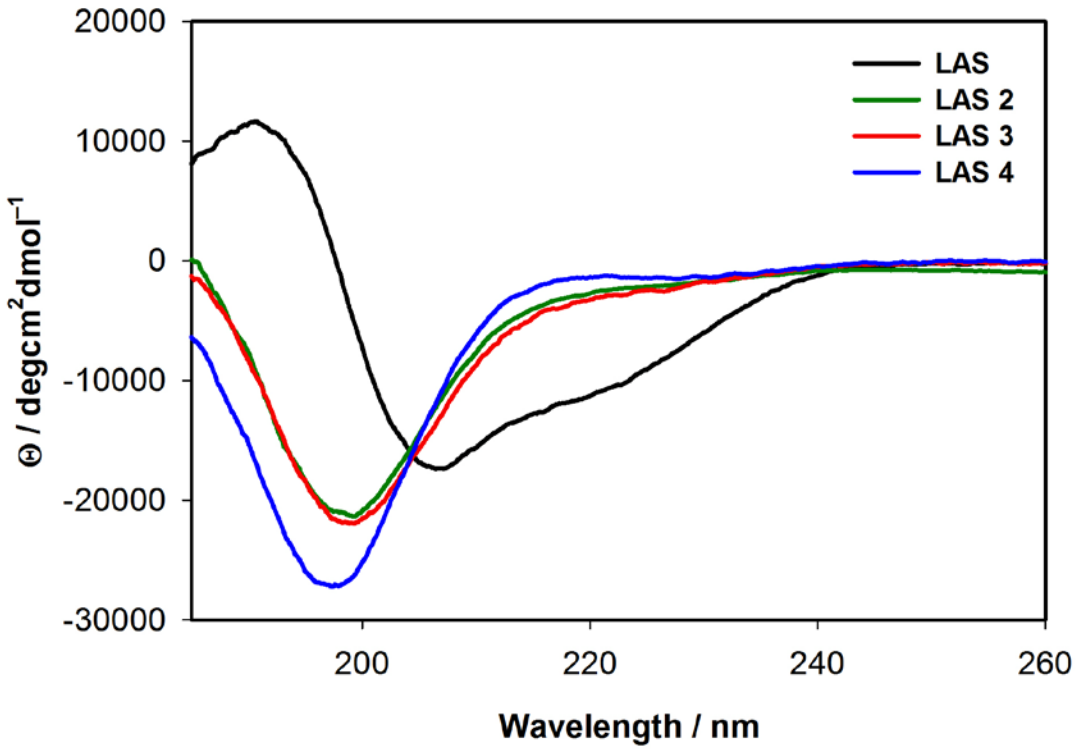

Figure 25: ECD spectra of LAS and its analogs measured in H_2O in amide region.

However, relatively low intensity of the bands (~1–1.5×10^4 deg cm^2 $dmol^{-1}$) which is about two times smaller than for α-helical peptides indicates presence of additional secondary structures. According to numerical analysis,[75] the α-helical fraction (~35%) appears complemented by unordered (and/or PPII), β-sheet and β-turn fractions (each of which comprises approximately 20 %). The presence of α-helical and PPII structures is further supported by IR/VCD (**Figure 26**) and Raman/ROA data (**Figure 27**). VCD spectra of LAS indicate prevailing α-helical conformation by

a strong negative band at 1661 cm^{-1} (amide I region) and by a negative band at 1519 cm^{-1} (amide II region).[82] The absence of a positive component of the amide I VCD couplet (~1640 cm^{-1} – typical for α-helical conformation) is probably caused by the presence of another, negative band at ~1625 cm^{-1} (band due to PPII structure).[69] This result indicates that α-helical and PPII conformations are present

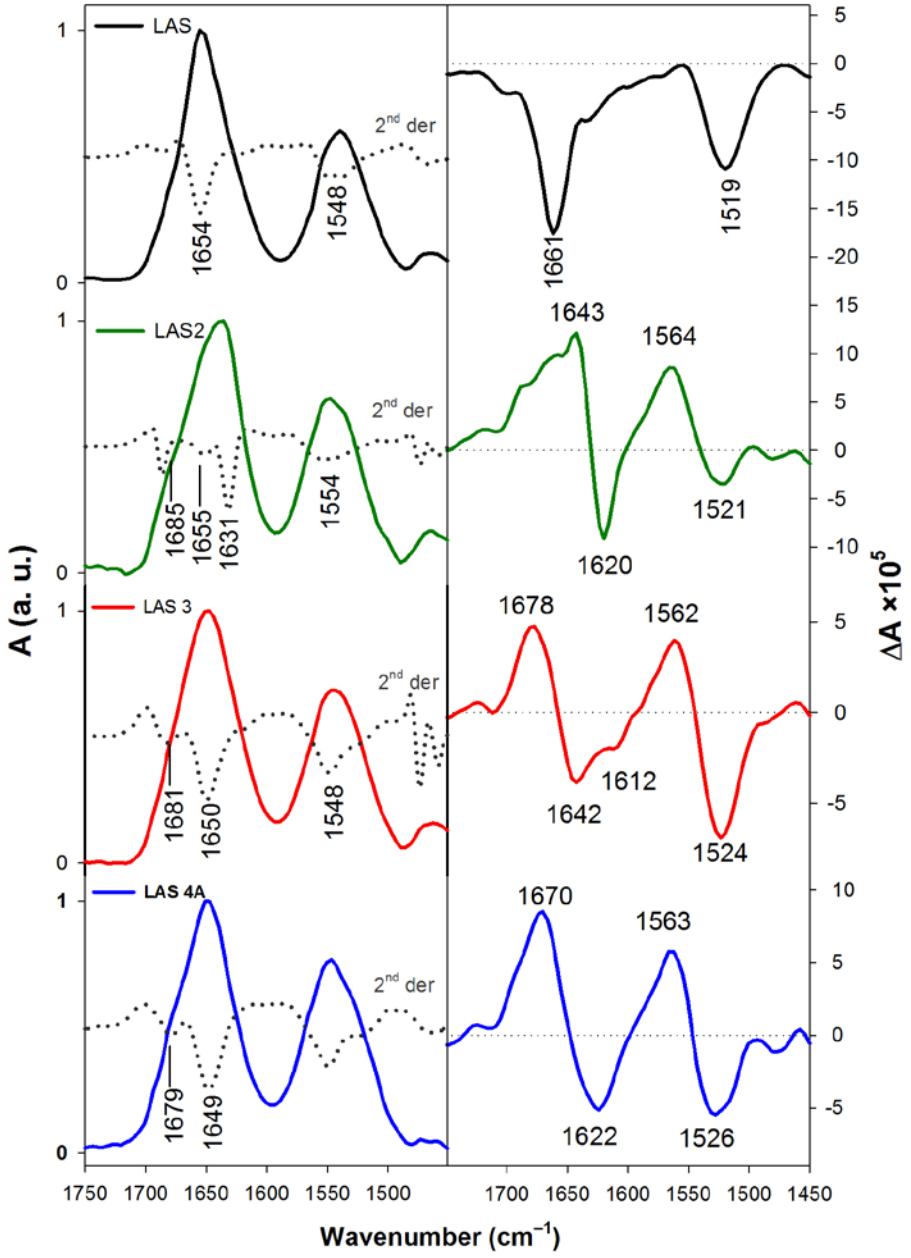

Figure 26: IR absorption (left) and VCD (right) spectra of LAS and its analogs measured in H_2O. The second derivatives of IR spectra are depicted as dotted lines.

simultaneously, which is further supported by ROA data (**Figure 27**). In ROA spectra we can clearly distinguish bands due to α-helices (in amide I region a negative/positive couplet at 1638 and 1660 cm^{-1} and an additional positive band at 1345 cm^{-1} in extended amide III region) and PPII conformations (a positive band in the extended amide III region at 1316 cm^{-1}).[3] On the other hand, the amount of β-sheet structure as predicted by ECD seems to be overestimated, as neither IR/VCD

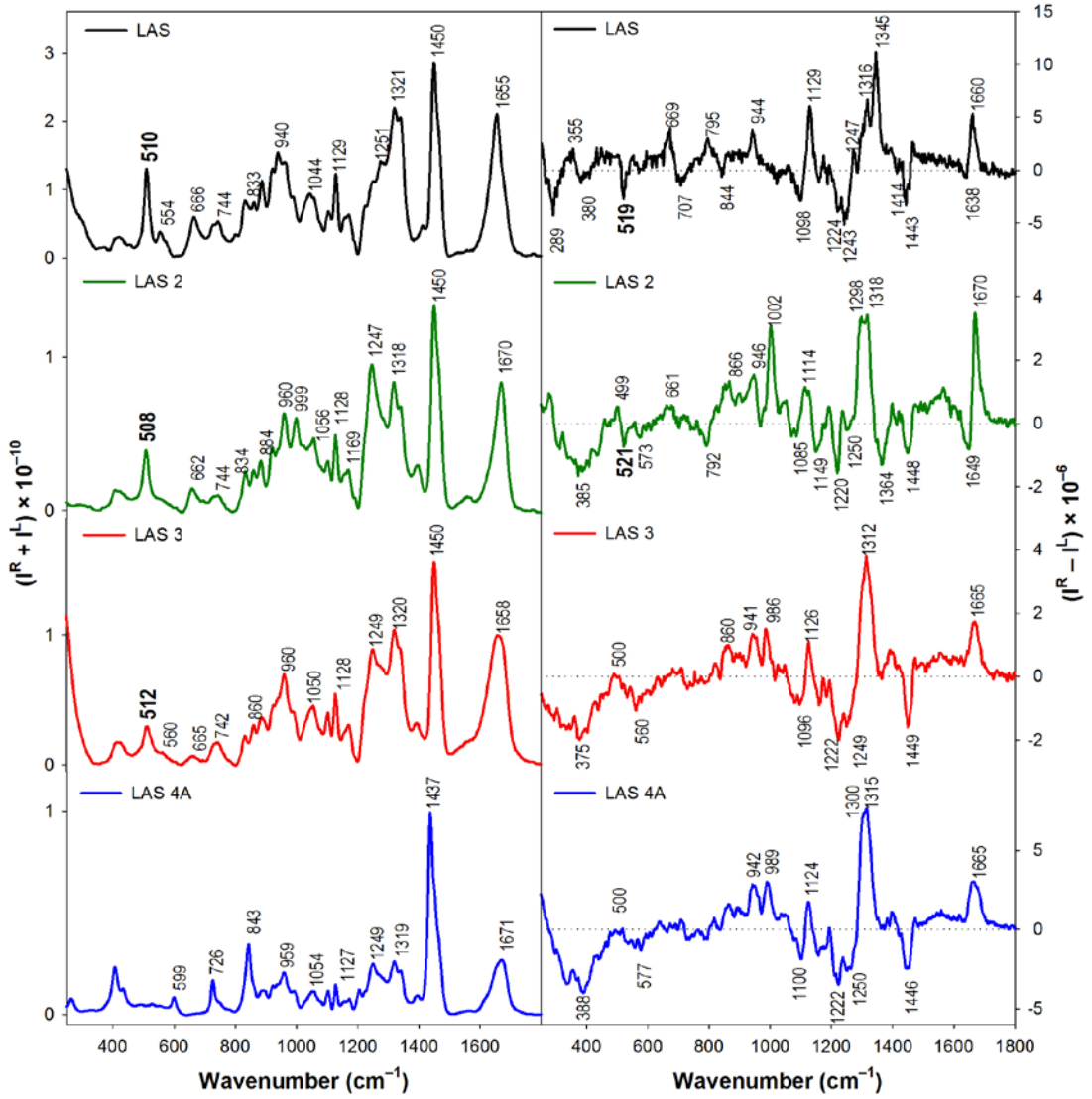

Figure 27: Raman (left) and ROA (right) spectra of LAS and its analogs measured in H_2O.

nor Raman/ROA show distinctive β-structure contribution (besides minima at 1639 cm^{-1} and 1678 cm^{-1} evident in 2nd derivation of IR spectra, indicating that some minor portion of β-structure is present[183]). The results of our secondary structure analysis are in a good agreement with NMR (see above and ref. 182). Although the

amount of α-helical structure as predicted by NMR (~55 %) appears some 20 % higher when compared to results of ECD analysis, this discrepancy can be explained by the fact that terminal residues contribute to CD manifestation of α-helices to a lesser extent. Consequently, we estimate that α-helical content as found by ECD is underestimated by ~15 % (if we assume that contributions of two terminal residues of each of the two α-helices are excluded).

ECD spectra of the analogs LAS 2 and LAS 3 in amide region (**Figure 25**) exhibit similar features. Unlike for native LAS, we observe one negative minimum at 198 nm of a rather low intensity (~-2×10^4 deg cm^2 dmol^{-1}) and no positive maxima, indicating prevailing unordered and β-sheet conformations (numerical data[184] show ~50 % β-sheets, ~20 % β-turns, ~20 % unordered (and/or PPII) structure and only ~10 % α-helical conformation). For LAS 2, the supplementing IR data (**Figure 26**) confirm prevailing β-sheet structure (bands at 1631 and 1685 cm^{-1}) together with a small portion of (unresolved in IR) unordered and/or α-helical conformation (the band at 1655 cm^{-1}). High β-sheet content is also suggested by VCD (**Figure 26**) (a negative band at ~1620 cm^{-1} in amide I region and a positive/negative couplet at ~1564 and 1521 cm^{-1} in amide II region). Two additional positive amide I VCD bands of LAS 2 at ~1662 and 1643 cm^{-1} together with a rather high intensity of the negative amide I band at ~1620 cm^{-1} hint on a presence of an additional secondary structure, probably a left-handed PPII helix, characterized by a positive/negative couplet at ~1662 and 1620 cm^{-1}.[69] Presence of β-sheet, β-turn and PPII structures is further supported by ROA (**Figure 27**), particularly by a strong negative/positive couplet at ~1650 and 1670 cm^{-1} in amide I region and by a positive band at ~1298 cm^{-1} in amide III region, which indicate presence of β-structure,[87] and also by a sharp positive band at ~1318 cm^{-1} in the extended amide III region, which is a marker band of PPII conformation.[3,185] Although ECD spectra of LAS 2 and LAS 3 are nearly identical, considerable differences can be found in IR/VCD (**Figure 26**) and Raman/ROA spectra (**Figure 27**). For LAS 3, IR spectrum exhibits a strong maximum at ~1650 cm^{-1} which can be ascribed to unordered/PPII or α-helical structures. An additional shoulder at ~1680 cm^{-1} indicates presence of a β-structure. VCD spectra exhibit a positive/negative couplet at ~1678 and 1642 cm^{-1} (amide I) and another positive/negative one at ~1562 and 1524 cm^{-1} (amide II). This indicates a possible combination of PPII and β-structures.[69] As follows from ROA data of LAS 3, PPII structure seems to be a dominant feature, based on both amide I (a

single-signed band centered at ~1665 cm^{-1}) and extended amide III (a strong positive maximum at ~1315 cm^{-1}) manifestations.[3] The negative band at ~1247 cm^{-1} further confirms the assumed presence of β-sheet structure.[87]

ECD spectrum of the peptide LAS 4 containing no disulfide bridges (**Figure 25**) is slightly different from the spectra of LAS 2 and LAS 3. It exhibits an intense negative band at 197 nm and the overall spectral shape indicates a possible presence of yet another weak positive feature with the maximum at about 215 nm. It might be caused by a somewhat higher portion of PPII structure.[185,186] IR absorption data showing a strong maximum at ~1650 cm^{-1} (either unordered-PPII or α-helical structure), a shoulder at ~1680 cm^{-1} (β-structure) and a maximum at ~1550 cm^{-1} together with VCD spectra (**Figure 26**) with a positive/negative couplet at ~1670 and 1622 cm^{-1} and a positive/negative couplet at ~1563 and ~1525 cm^{-1} indicate a prevailing PPII conformation containing some portion of β-structures. Signals corresponding to PPII structure are dominant even in ROA spectra (**Figure 27**) with a positive band at ~1315 cm^{-1} in the extended amide III region and a positive single-signed band centered at ~1665 cm^{-1} in amide I region. An additional contribution of β-structures is observed in the extended amide III region (a positive shoulder at ~1300 cm^{-1} due to β-turns and a negative band at ~1250 cm^{-1} due to the β-sheet structure).

Unlike peptides/proteins containing aromatic amino acid residues, ECD spectra of LAS and its analogs exhibit pure disulfide signals in the disulfide transition region (~250–350 nm, **Figure 28**). There is no overlap with long-wavelength π–π* bands of aromatic chromophores (below ~280 nm).[28] Yet, the analysis of disulfide-related signals is rather complicated, because a number of disulfide chromophores is different for native LAS (two disulfides), LAS 2 and 3 (one disulfide) and LAS 4 (no disulfide groups). In addition, even minor changes of disulfide conformation can cause changes in intensity and even sign of the disulfide bands (see above). Still there are several features that indicate differences between geometries of particular disulfides. Particularly while spectra of LAS 2 and LAS 3 show a single negative CD band with the maximum at ~272 nm, the spectrum of native LAS exhibits a negative shoulder with about half the dichroic absorption intensity. Moreover, in the spectra of LAS 2 and LAS 3 there appears to be an additional negative minimum at ~252 nm, i.e. just before the large negative ECD band due to amide n-π* transitions takes over. Based on the ECD data we can

therefore speculate that disulfide groups may adopt similar conformations in the molecules of LAS 2 and 3, while a conformation of disulfides in native LAS may be different.

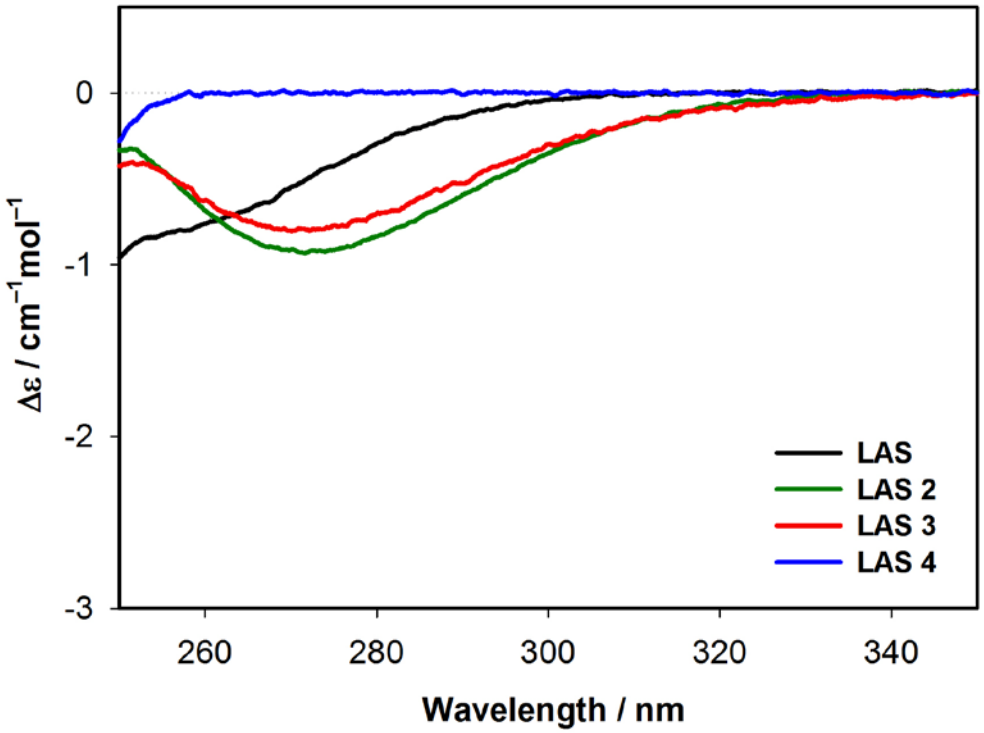

Figure 28: ECD spectra of LAS and its analogs measured in H_2O in disulfide region.

Additional information on disulfide group conformation can be found in Raman/ROA spectra (**Figure 27**). For the peptides containing disulfide groups (LAS, LAS 2, LAS 3), Raman spectra in the S–S stretching vibration region are dominated by an intense band at ~510 cm^{-1}, indicating a prevailing ggg conformation of the C_α–C_β–S–S–C_β–C_α fragment. An additional low-intensity band at ~554 cm^{-1} (LAS) or a shoulder at ~560 cm^{-1} (LAS 2, LAS 3) indicates also a minor portion of the ggt conformation. Based on Raman signals in the C–S stretching region, the S–C_β–C_α–C fragments of disulfide groups in LAS, LAS 2 and LAS 3 adopt both P_H (band at ~665 cm^{-1}) and P_C or P_N conformations (band at ~745 cm^{-1}).[126] Spectral intensities of the 665 and 745 cm^{-1} bands indicate presence of a slightly higher portion of P_H conformation in the native LAS and the analog LAS 2, while the P_C or P_N conformations seem to be dominant in the analog LAS 3. Signals in the S–S and C–S regions are discernible also in ROA spectra. However, as reported earlier[133] one should be careful with the interpretation of these signals. A positive feature at ~500 cm^{-1} (which can be found in the ROA spectra of analogs LAS 2 and LAS 3)

and a negative band at ~560 cm^{-1} (in the spectrum of LAS 3) cannot be ascribed to S–S stretching vibrations, because similar features are present also in the spectrum of LAS 4 containing no disulfides. On the contrary, an intense negative band at ~520 cm^{-1} in the spectrum of the native LAS and a band at the same position showing slightly lower intensity in the spectrum of LAS 2 cannot be found in the spectra of LAS 4. Therefore this feature probably rises from S–S stretching vibrations. According to previous calculations,[131] the negative sign of this band probably indicates a left-handed conformation of the disulfides. Its intensity is approximately two times higher for the native LAS (containing two disulfides) than for the analog LAS 2 (having only one disulfide group – Cys^{17}–Cys^{27}), which may indicate that in the molecule of the native LAS, a left-handed conformation is adopted by both disulfides. ROA spectra of the analog LAS 3 do not contain any discernible band due to S–S stretching vibrations, which may be caused by higher flexibility of the Cys^{8}–Cys^{25} disulfide group.

Summarizing results of the secondary structure analysis of LAS peptides, we come to the following conclusions. (**a**) In aqueous solution, the absence of one or both disulfide groups in the peptide results in significant decrease of α-helical content and an increase of PPII and/or β-sheet content. (**b**) While the increasing tendency to form α-helical structure does not seem to correlate with increasing biological activity of the peptides, there appears to be a correlation between decreasing biological activity and increasing tendency to form β-sheet structure. (**c**) In solution, disulfide groups in native LAS and its analog LAS 2 seems to adopt a left-handed conformation. Cys^{8}–Cys^{25} disulfide which is present in the molecule of LAS 3 appears to be more flexible.

In order to interpret more thoroughly the disulfide-related features in experimental ROA spectra of LAS peptides we are currently running more sophisticated ab initio calculations (employing better variants of DFT with respect to functionals and basis sets together with the more relevant optimization techniques compared to those used in the ref. 131). These calculations are being performed using molecular models resembling more closely situation in peptides/protein (such as N-acetyl-cystine-methylamide) and utilizing the recent NMR and MD simulations of the native LAS.[182] Results of this theoretical analysis of the experimental ROA spectra of LAS peptides will be included in the final version of the manuscript.

Conclusions

Utilizing model dilactams I and II, we succeeded in discerning and isolating chiroptical manifestation of nonplanar amide groups in rigid environment of well-defined known geometry. The sign of electronic n–π* transition relates to absolute conformation of nonplanar amide chromophore. ECD band related to electronic amide n–π* transition appears definitely to be a local phenomenon. In nonplanar situations it exhibits a significant bathochromic (red) shift and as such it can be used for amide nonplanarity detection. VOA (both VCD and ROA) in amide I region also exhibits single signed nonplanarity-related bands, not seriously influenced by amide-amide coupling. Chiroptical manifestation of amide nonplanarity was further analyzed by ab initio calculations of electronic (TDDFT) as well as vibrational (DFT) optical activity. The results confirmed and further explained experimental findings. The right-handed arrangement of the O=C–N–LP (lone electron pair on the amide nitrogen atom) corresponds to:

(**a**) a single strong positive ECD band due to n–π* amide transition

(**b**) a single negative VCD band due to amide I vibration (or at least a negative bias to whatever VCD is observed in this region)

(**c**) a single positive ROA feature due to amide I vibration (or at least a positive bias to whatever ROA is observed in this region).

These characteristic spectral features can be utilized for amide nonplanarity detection and absolute conformation assignment. It is even possible to estimate nonplanarity magnitude on the basis of bathochromic shift and dichroic bands magnitude evaluation.

ECD due to π–π* transitions (investigated deeper into the UV spectral range using SRCD) exhibits a couplet corresponding to amide-amide coupling. Its sign pattern was established using coupled oscillator theory. Therefore in model dilactams we can separately observe chiroptical manifestation of amide-amide coupling (a longer distance phenomenon conditioned and explainable by dipole-dipole interaction) and that of amide nonplanarity – inherent chirality (a local phenomenon within a single amide group). Similarly, dipole-dipole coupling controls VCD due to amide II vibrations. However, in this case the observed large couplet could be caused

by the special geometry (close mutual proximity of both amide nitrogen atoms) of our models.

Utilization of chiroptical spectroscopy for amide nonplanarity detection in more complex and/or flexible systems (such as peptides and proteins) will require further studies. Besides continuing detailed studies of small specially designed model compounds (like e.g. bicyclic and also tetracyclic analogs of dilactams I and II), in the next step one should attempt detecting and analyzing amide nonplanarity within larger systems, possibly including real peptides or proteins. It is logical to turn towards two possible directions: (**a**) to investigate spectroscopically several small cyclic peptides, e.g. cyclohexapeptides acting as β-turn models or even smaller cyclotripeptides, with strained rings, like e.g. cyclo(tri-L-prolyl) and (**b**) to try computing theoretical chiroptical spectra using the so-called independent systems approach.[64] The existing computer programs will require modifications enabling incorporation of amide nonplanarity.

We have demonstrated that dilactams (particularly the deuterated molecule – dilactam II) are suitable models for the investigation of ROA signals in the whole range of fundamental vibrations, including the high-wavenumber region (above ~2000 cm^{-1}) which involves C–H and C–D stretching vibrations. In ROA spectra, signals due to C–D stretching vibrations have been recorded for the first time. Measurement in the extended spectral range, which was made possible due to rather recent innovation of our home-built ROA instrument, requires utilization of different experimental setups (gratings). As follows from our study, ROA spectra collected with different setups exhibit nearly identical spectral patterns, but the varying experimental conditions affect rather significantly intensities of particular ROA bands (mainly in the border regions). In order to correct our experimental data for different instrument responses we have utilized a procedure for correcting relative intensities of ROA spectra based on the use of certified luminescence standards. Although this procedure is used rather commonly in standard Raman spectroscopy, its application to ROA data has not been reported yet. We have shown that application of such procedure improves rather significantly the agreement between experimental ROA data measured with different setups or even using different ROA instruments.

We have identified ROA signals corresponding to S–S stretching vibrations of disulfide bridges in the spectra of model peptides containing one or two disulfide

groups in the molecule (neurohypophyseal hormone (NHH) oxytocin, arginine vasopressin, lysine vasopressin and their analogs having different agonistic and antagonistic properties and antimicrobial peptides from Lasiocepsin family differing in disulfide bridge pattern). In ROA spectra of NHHs and their analogs we have found signals at ~510–515 cm^{-1}. The results indicate that there might be a correlation between sign of these ROA bands and biological activity of the peptides. While a positive ROA signal (which, according to calculations on model disulfides,[131] indicates right-handed chirality of the disulfide group) has been identified in the spectra of agonistic analogs, a negative signal (indicating left-handed disulfide group chirality)[131] was found in the spectra of inactive model and NHH inhibitory compound. Disulfide-related signals have been identified even in the spectra of more complex systems – antimicrobial peptides lasiocepsin (LAS, having two disulfide bridges) and one its analog (LAS 2, containing only one disulfide group). Negative sign of the bands probably indicates left-handed disulfide group orientation.[131]

Our results obtained on disulfide-containing models indicate that ROA may be the only spectroscopic technique capable of distinguishing sign of the disulfide group torsion. Such information is difficult or even impossible to obtain by other spectroscopic methods. However, to further analyze this relation it appears necessary to: (**a**) utilize additional model molecules, (**b**) employ more sophisticated theoretical procedures for the interpretation of experimental data (better variants of DFT with respect to functionals and basis sets together with the more relevant optimization techniques, taking into consideration also MD simulations and, where possible, also NMR data). For LAS-related peptides these calculations are currently in progress. Theoretical analysis of the experimental data will be discussed in the manuscript which is currently in preparation.

We have shown that concerted use of electronic and vibrational chiroptical spectroscopies brings the following advantages: (**a**) the enormous sensitivity of chiroptical methods towards even small changes in spatial arrangement of the studied systems. Although this phenomenon is particular to all chiroptical methods, it is especially manifested by electronic optical activity. The involved wave functions expand over large portions of molecules and even small changes can thus be experimentally detected. (**b**) On the other hand, richness and a response to detail of vibrational spectroscopy allow us to stress a particular structural feature like amide nonplanarity or disulfide group conformation. Together with the complementary

nature of VCD and ROA spectroscopies, which parallels closely that of the parent IR absorption and Raman scattering phenomena, the combination of electronic and vibrational chiroptical spectra represents a very efficient and powerful tool. Within this work the complementarity was demonstrated experimentally (successful use of very different solvents for VCD and ROA) and within the practical interpretation (amide II bands in VCD vs. amide III bands in ROA, S–S and C–S stretching vibrations in ROA).

Bibliography

(1) Barron, L. D.; Buckingham, A. D. Vibrational Optical Activity. *Chem. Phys. Lett.* **2010**, *492*, 199–213.

(2) *Infrared and Raman Spectroscopy*; Schrader, B., Ed.; Wiley-VCH Verlag GmbH: Weinheim, Germany, 1995.

(3) Zhu, F. J.; Isaacs, N. W.; Hecht, L.; Barron, L. D. Raman Optical Activity: A Tool for Protein Structure Analysis. *Structure* **2005**, *13*, 1409–1419.

(4) Barron, L. D.; Buckingham, A. D. Rayleigh and Raman Scattering from Optically Active Molecules. *Mol. Phys.* **1971**, *20*, 1111–1119.

(5) Frisch, M. J.; Trucks, G. W.; Schlegel, H. B.; Scuseria, G. E.; Robb, M. A.; Cheeseman, J. R.; Scalmani, G.; Barone, V.; Mennucci, B.; Petersson, G. A.; et al. Gaussian 09, Revision A.02, 2009.

(6) Barron, L. D. *Molecular Light Scattering and Optical Activity*; 2nd ed.; Cambridge University Press: Cambridge, 2004.

(7) Barron, L. D. Structure and Behaviour of Biomolecules from Raman Optical Activity. *Curr. Opin. Struct. Biol.* **2006**, *16*, 638–643.

(8) Barron, L. D.; Zhu, F.; Hecht, L.; Tranter, G. E.; Isaacs, N. W. Raman Optical Activity: An Incisive Probe of Molecular Chirality and Biomolecular Structure. *J. Mol. Struct.* **2007**, *834-836*, 7–16.

(9) Polavarapu, P. L.; Pickard, S. T.; Smith, H. E.; Black, T. M.; Barron, L. D.; Hecht, L. Determination of Absolute Configurations from Vibrational Raman Optical Activity: (trans)-2,3-Dimethylthiirane. *Talanta* **1993**, *40*, 545–549.

(10) Haesler, J.; Schindelholz, I.; Riguet, E.; Bochet, C. G.; Hug, W. Absolute Configuration of Chirally Deuterated Neopentane. *Nature* **2007**, *446*, 526–529.

(11) Spencer, K. M.; Edmonds, R. B.; Rauh, R. D. Analytical Chiral Purity Verification Using Raman Optical Activity. *Appl. Spectrosc.* **1996**, *50*, 681–685.

(12) Nafie, L. A. *Vibrational Optical Activity: Principles and Applications*; John Wiley & Sons: Chichester, U.K., 2011.

(13) Nafie, L. A. Infrared and Raman Vibrational Optical Activity: Theoretical and Experimental Aspects. *Annu. Rev. Phys. Chem.* **1997**, *48*, 357–386.

(14) Barron, L. D.; Bogaard, M. P.; Buckingham, A. D. Raman Scattering of Circularly Polarized Light by Optically Active Molecules. *J. Am. Chem. Soc.* **1973**, *95*, 603–605.

(15) Hug, W.; Hangartner, G. A Novel High-Throughput Raman Spectrometer for Polarization Difference Measurements. *J. Raman Spectrosc.* **1999**, *30*, 841–852.

(16) Che, D.; Hecht, L.; Nafie, L. A. Dual and Incident Circular Polarization Raman Optical Activity Backscattering of (—)-Trans-Pinane. *Chem. Phys. Lett.* **1991**, *180*, 182–190.

(17) Nafie, L. A.; Freedman, T. B. Dual Circular Polarization Raman Optical Activity. *Chem. Phys. Lett.* **1989**, *154*, 260–266.

(18) Hecht, L.; Barron, L. D.; Gargaro, A. R.; Wen, Z. Q.; Hug, W. Raman Optical Activity Instrument for Biochemical Studies. *J. Raman Spectrosc.* **1992**, *23*, 401–411.

(19) Hecht, L.; Blanch, E. W.; Bell, A. F.; Day, L. A. Raman Optical Activity Instrument for Studies of Biopolymer Structure and Dynamics. *J. Raman Spectrosc.* **1999**, *30*, 815–825.

(20) Hanzlíková, J.; Praus, P.; Baumruk, V. Raman Optical Activity Spectrometer for Peptide Studies. *J. Mol. Struct.* **1999**, *481*, 431–435.

(21) Yamamoto, S.; Watarai, H. Incident Circularly Polarized Raman Optical Activity Spectrometer Based on Circularity Conversion Method. *J. Raman Spectrosc.* **2010**, *41*, 1664–1669.

(22) Nafie, L. A. Theory of Raman Scattering and Raman Optical Activity: Near Resonance Theory and Levels of Approximation. *Theor. Chem. Acc.* **2007**, *119*, 39–55.

(23) Nafie, L. A. Circular Polarization Spectroscopy of Chiral Molecules. *J. Mol. Struct.* **1995**, *347*, 83–100.

(24) Moscowitz, A. Some Applications of the Kronig-Kramers Theorem to Optical Activity. *Tetrahedron* **1961**, *13*, 48–56.

(25) *Fundamental Aspects and Recent Developments in Optical Rotatory Dispersion and Circular Dichroism*; Ciardelli, F.; Salvadori, P., Eds.; Heyden & Son Ltd.: London, 1973.

(26) Autschbach, J. Computing Chiroptical Properties with First-Principles Theoretical Methods: Background and Illustrative Examples. *Chirality* **2009**, *21 Suppl 1*, E116–E152.

(27) Klamt, A. Cosmo and Cosmo-Rs. In *Encyclopedia of Computational Chemistry*; Schleyer, P. R.; Allinger, N. L., Eds.; John Wiley & Sons: Chichester, U.K., 1998; pp. 604–615.

(28) *Comprehensive Chiroptical Spectroscopy: Applications in Stereochemical Analysis of Synthetic Compounds, Natural Products, and Biomolecules, Volume 2*; Berova, N.; Polavarapu, P. L.; Nakanishi, K.; Woody, R. W., Eds.; John Wiley & Sons, Inc.: Hoboken, New Jersey, 2012.

(29) Rosenfeld, L. Quantenmechanische Theorie Der Natürlichen Optischen Aktivität von Flüssigkeiten Und Gasen. *Zeitschrift für Phys.* **1929**, *52*, 161–174.

(30) Stephens, P. J. Gauge Dependence of Vibrational Magnetic Dipole Transition Moments and Rotational Strengths. *J. Phys. Chem.* **1987**, *91*, 1712–1715.

(31) Cheeseman, J. R.; Frisch, M. J.; Devlin, F. J.; Stephens, P. J. Ab Initio Calculation of Atomic Axial Tensors and Vibrational Rotational Strengths Using Density Functional Theory. *Chem. Phys. Lett.* **1996**, *252*, 211–220.

(32) Stephens, P. J. Theory of Vibrational Circular Dichroism. *J. Phys. Chem.* **1985**, *89*, 748–752.

(33) Nafie, L. A.; Walnut, T. H. Vibrational Circular Dichroism Theory: A Localized Molecular Orbital Model. *Chem. Phys. Lett.* **1977**, *49*, 441–446.

(34) Walnut, T. H.; Nafie, L. A. Infrared Absorption and the Born–Oppenheimer Approximation. II. Vibrational Circular Dichroism. *J. Chem. Phys.* **1977**, *67*, 1501–1510.

(35) Nafie, L. A. Localized Molecular Orbital Calculations of Vibrational Circular Dichroism. I. General Theoretical Formalism and CNDO Results for the Carbon–deuterium Stretching Vibration in Neopentyl-1-D-Chloride. *J. Chem. Phys.* **1981**, *75*, 2935.

(36) *Circular Dichroism: Principles and Applications, 2nd Edition*; Berova, N.; Nakanishi, K.; Woody, R. W., Eds.; John Wiley & Sons, Inc., 2000.

(37) Dutler, R.; Rauk, A. Calculated Infrared Absorption and Vibrational Circular Dichroism Intensities of Oxirane and Its Deuterated Analogs. *J. Am. Chem. Soc.* **1989**, *111*, 6957–6966.

(38) Nafie, L. A. Velocity-Gauge Formalism in the Theory of Vibrational Circular Dichroism and Infrared Absorption. *J. Chem. Phys.* **1992**, *96*, 5687–5702.

(39) Nafie, L. A. Vibronic Coupling Theory of Infrared Vibrational Transitions. *J. Chem. Phys.* **1983**, *78*, 7108.

(40) Frisch, M. J.; Trucks, G. W.; Schlegel, H. B.; Scuseria, G. E.; Robb, M. A.; Cheeseman, J. R.; Zakrzewski, V. G.; Montgomery, J. A., J.; Stratmann, R. E.; Burant, J. C.; et al. Gaussian 98, 1998.

(41) Scherrer, A.; Vuilleumier, R.; Sebastiani, D. Nuclear Velocity Perturbation Theory of Vibrational Circular Dichroism. *J. Chem. Theory Comput.* **2013**, *9*, 5305–5312.

(42) Casida, M. E. Timedependent Density-Functional Response Theory for Molecules. In *Recent Advances in Density Functional Methods, Part I*; Chong, D. P., Ed.; World Scientific Publishing Co.: Singapore, 1995; pp. 155–192.

(43) Ruud, K.; Thorvaldsen, A. J. Theoretical Approaches to the Calculation of Raman Optical Activity Spectra. *Chirality* **2009**, *21 Suppl 1*, E54–E67.

(44) Cheeseman, J. R.; Frisch, M. J. Basis Set Dependence of Vibrational Raman and Raman Optical Activity Intensities. *J. Chem. Theory Comput.* **2011**, *7*, 3323–3334.

(45) Dunning, T. H. Gaussian Basis Sets for Use in Correlated Molecular Calculations. I. The Atoms Boron through Neon and Hydrogen. *J. Chem. Phys.* **1989**, *90*, 1007–1023.

(46) Kendall, R. A.; Dunning, T. H.; Harrison, R. J. Electron Affinities of the First-Row Atoms Revisited. Systematic Basis Sets and Wave Functions. *J. Chem. Phys.* **1992**, *96*, 6796–6806.

(47) Woon, D. E.; Dunning, T. H. Gaussian Basis Sets for Use in Correlated Molecular Calculations. III. The Atoms Aluminum through Argon. *J. Chem. Phys.* **1993**, *98*, 1358–1371.

(48) Peterson, K. A.; Woon, D. E.; Dunning, T. H. Benchmark Calculations with Correlated Molecular Wave Functions. IV. The Classical Barrier Height of the H+H2→H2+H Reaction. *J. Chem. Phys.* **1994**, *100*, 7410–7415.

(49) Zuber, G.; Hug, W. Rarefied Basis Sets for the Calculation of Optical Tensors. 1. The Importance of Gradients on Hydrogen Atoms for the Raman Scattering Tensor. *J. Phys. Chem. A* **2004**, *108*, 2108–2118.

(50) Schellman, J. A. Symmetry Rules for Optical Rotation. *Acc. Chem. Res.* **1968**, *1*, 144–151.

(51) Snatzke, G. Circular Dichroism and Absolute Conformation: Application of Qualitative MO Theory to Chiroptical Phenomena. *Angew. Chemie Int. Ed. English* **1979**, *18*, 363–377.

(52) Mason, S. F. *Molecular Optical Activity and the Chiral Discriminations*; Cambridge University Press: Cambridge, 1982.

(53) Holzwarth, G. Optical Activity of Vibrational Transitions: A Coupled Oscillator Model. *J. Chem. Phys.* **1972**, *57*, 1632.

(54) Barron, L. D.; Buckingham, A. D. Simple Two-Group Model for Rayleigh and Raman Optical Activity. *J. Am. Chem. Soc.* **1974**, *96*, 4769–4773.

(55) Barron, L. D.; Buckingham, A. D. Rayleigh and Raman Optical Activity. *Annu. Rev. Phys. Chem.* **1975**, *26*, 381–396.

(56) Nafie, L. A. Electron Transition Current Density in Molecules. 1. Non-Born−Oppenheimer Theory of Vibronic and Vibrational Transitions. *J. Phys. Chem. A* **1997**, *101*, 7826–7833.

(57) Bour, P.; Keiderling, T. A. Ab Initio Simulations of the Vibrational Circular Dichroism of Coupled Peptides. *J. Am. Chem. Soc.* **1993**, *115*, 9602–9607.

(58) Bouř, P.; Sopková, J.; Bednárová, L.; Maloň, P.; Keiderling, T. A. Transfer of Molecular Property Tensors in Cartesian Coordinates: A New Algorithm for Simulation of Vibrational Spectra. *J. Comput. Chem.* **1997**, *18*, 646–659.

(59) Bishop, D. M. *Group Theory and Chemistry*; Oxford University Press: New York-London, 1973.

(60) Bettelheim, F.; Brown, W.; Campbell, M.; Farrell, S.; Torres, O. *Introduction to Organic and Biochemistry*; Cengage Learning, 2012.

(61) IUPAC-IUB Commission on Biochemical Nomenclature. Abbreviations and Symbols for the Description of the Conformation of Polypeptide Chains. Tentative Rules (1969). *Biochemistry* **1970**, *9*, 3471–3479.

(62) Burmann, B. M.; Hiller, S. Chaperones and Chaperone–substrate Complexes: Dynamic Playgrounds for NMR Spectroscopists. *Prog. Nucl. Magn. Reson. Spectrosc.* **2015**, *86-87*, 41–64.

(63) Kühlbrandt, W. Cryo-EM Enters a New Era. *Elife* **2014**, *3*, e03678.

(64) *Comprehensive Chiroptical Spectroscopy, Instrumentation, Methodologies, and Theoretical Simulations, Volume 1*; Berova, N.; Polavarapu, P. L.; Nakanishi, K.; Woody, R. W., Eds.; John Wiley & Sons, Inc.: Hoboken, New Jersey, 2012.

(65) Kelly, S. M.; Price, N. C. The Use of Circular Dichroism in the Investigation of Protein Structure and Function. *Curr. Protein Pept. Sci.* **2000**, *1*, 349–384.

(66) Greenfield, N. J. Using Circular Dichroism Spectra to Estimate Protein Secondary Structure. *Nat. Protoc.* **2006**, *1*, 2876–2890.

(67) Bulheller, B. M.; Rodger, A.; Hirst, J. D. Circular and Linear Dichroism of Proteins. *Phys. Chem. Chem. Phys.* **2007**, *9*, 2020–2035.

(68) Keiderling, T. A. *Peptide and Protein Conformational Studies with Vibrational Circular Dichroism and Related Spectroscopies*; Berova, N.; Nakanishi, K.; Woody, R. W., Eds.; 2nd ed.; New York, 2000.

(69) Keiderling, T. A. Protein and Peptide Secondary Structure and Conformational Determination with Vibrational Circular Dichroism. *Curr. Opin. Chem. Biol.* **2002**, *6*, 682–688.

(70) Dobson, C. M. Experimental Investigation of Protein Folding and Misfolding. *Methods* **2004**, *34*, 4–14.

(71) Radford, S. Protein Folding: Progress Made and Promises Ahead. *Trends Biochem. Sci.* **2000**, *25*, 611–618.

(72) Venyaminov SYu; Baikalov, I. A.; Shen, Z. M.; Wu, C. S.; Yang, J. T. Circular Dichroic Analysis of Denatured Proteins: Inclusion of Denatured Proteins in the Reference Set. *Anal. Biochem.* **1993**, *214*, 17–24.

(73) Boxer, D. H.; Zhang, H.; Gourley, D. G.; Hunter, W. N.; Kelly, S. M.; Price, N. C. Sensing of Remote Oxyanion Binding at the DNA Binding Domain of the Molybdate-Dependent Transcriptional Regulator, ModE. *Org. Biomol. Chem.* **2004**, *2*, 2829–2837.

(74) Clark Sutherland, J.; Desmond, E. J.; Takacs, P. Z. Versatile Spectrometer for Experiments Using Synchrotron Radiation at Wave-Lengths Greater than 100 Nm. *Nucl. Instruments Methods* **1980**, *172*, 195–199.

(75) Whitmore, L.; Wallace, B. a. DICHROWEB, an Online Server for Protein Secondary Structure Analyses from Circular Dichroism Spectroscopic Data. *Nucleic Acids Res.* **2004**, *32*, 668–673.

(76) Whitmore, L.; Woollett, B.; Miles, A. J.; Klose, D. P.; Janes, R. W.; Wallace, B. A. PCDDB: The Protein Circular Dichroism Data Bank, a Repository for Circular Dichroism Spectral and Metadata. *Nucleic Acids Res.* **2011**, *39*, D480–D486.

(77) Sreerama, N.; Woody, R. W. Estimation of Protein Secondary Structure from Circular Dichroism Spectra: Comparison of CONTIN, SELCON, and CDSSTR Methods with an Expanded Reference Set. *Anal. Biochem.* **2000**, *287*, 252–260.

(78) Barron, L. D.; Hecht, L.; Blanch, E. W.; Bell, A. F. Solution Structure and Dynamics of Biomolecules from Raman Optical Activity. *Prog. Biophys. Mol. Biol.* **2000**, *73*, 1–49.

(79) Krimm, S.; Mark, J. E. Conformations of Polypeptides with Ionized Side Chains of Equal Length. *Proc. Natl. Acad. Sci. U. S. A.* **1968**, *60*, 1122–1129.

(80) Dukor, R. K.; Keiderling, T. A. Reassessment of the Random Coil Conformation: Vibrational CD Study of Proline Oligopeptides and Related Polypeptides. *Biopolymers* **1991**, *31*, 1747–1761.

(81) Tiffany, M. L.; Krimm, S. Effect of Temperature on the Circular Dichroism Spectra of Polypeptides in the Extended State. *Biopolymers* **1972**, *11*, 2309–2316.

(82) Ma, S.; Freedman, T. B.; Dukor, R. K.; Nafie, L. A. Near-Infrared and Mid-Infrared Fourier Transform Vibrational Circular Dichroism of Proteins in Aqueous Solution. *Appl. Spectrosc.* **2010**, *64*, 615–626.

(83) Baumruk, V.; Pancoska, P.; Keiderling, T. A. Predictions of Secondary Structure Using Statistical Analyses of Electronic and Vibrational Circular Dichroism and Fourier Transform Infrared Spectra of Proteins in H2O. *J. Mol. Biol.* **1996**, *259*, 774–791.

(84) Ma, S.; Cao, X.; Mak, M.; Sadik, A.; Walkner, C.; Freedman, T. B.; Lednev, I. K.; Dukor, R. K.; Nafie, L. a. Vibrational Circular Dichroism Shows Unusual Sensitivity to Protein Fibril Formation and Development in Solution. *J. Am. Chem. Soc.* **2007**, *129*, 12364–12365.

(85) Kurouski, D.; Lombardi, R. a; Dukor, R. K.; Lednev, I. K.; Nafie, L. a. Direct Observation and pH Control of Reversed Supramolecular Chirality in Insulin Fibrils by Vibrational Circular Dichroism. *Chem. Commun. (Camb).* **2010**, *46*, 7154–7156.

(86) Kurouski, D.; Lu, X.; Popova, L.; Wan, W.; Shanmugasundaram, M.; Stubbs, G.; Dukor, R. K.; Lednev, I. K.; Nafie, L. A. Is Supramolecular Filament Chirality the Underlying Cause of Major Morphology Differences in Amyloid Fibrils? *J. Am. Chem. Soc.* **2014**, *136*, 2302–2312.

(87) McColl, I. H.; Blanch, E. W.; Gill, A. C.; Rhie, A. G.; Ritchie, M. A.; Hecht, L.; Nielsen, K.; Barron, L. D. A New Perspective on Beta-Sheet Structures Using Vibrational Raman Optical Activity: From poly(L-Lysine) to the Prion Protein. *J. Am. Chem. Soc.* **2003**, *125*, 10019–10026.

(88) McColl, I. H.; Blanch, E. W.; Hecht, L.; Barron, L. D. A Study of Alpha-Helix Hydration in Polypeptides, Proteins, and Viruses Using Vibrational Raman Optical Activity. *J. Am. Chem. Soc.* **2004**, *126*, 8181–8188.

(89) Kapitán, J.; Baumruk, V.; Kopecký, V.; Pohl, R.; Bour, P. Proline Zwitterion Dynamics in Solution, Glass, and Crystalline State. *J. Am. Chem. Soc.* **2006**, *128*, 13451–13462.

(90) Kapitán, J.; Baumruk, V.; Bour, P. Demonstration of the Ring Conformation in Polyproline by the Raman Optical Activity. *J. Am. Chem. Soc.* **2006**, *128*, 2438–2443.

(91) Profant, V.; Baumruk, V.; Li, X.; Safařík, M.; Bouř, P. Tracking of the Polyproline Folding by Density Functional Computations and Raman Optical Activity Spectra. *J. Phys. Chem. B* **2011**, *115*, 15079–15089.

(92) Hudecová, J.; Horníček, J.; Buděšínský, M.; Šebestík, J.; Šafařík, M.; Zhang, G.; Keiderling, T. A.; Bouř, P. Three Types of Induced Tryptophan Optical Activity Compared in Model Dipeptides: Theory and Experiment. *Chemphyschem* **2012**, *13*, 2748–2760.

(93) Maloň, P.; Bednárová, L.; Straka, M.; Krejčí, L.; Kumprecht, L.; Kraus, T.; Kubáňová, M.; Baumruk, V. Disulfide Chromophore and Its Optical Activity. *Chirality* **2010**, *22*, E47–E55.

(94) Pauling, L.; Corey, R. B.; Branson, H. R. The Structure of Proteins; Two Hydrogen-Bonded Helical Configurations of the Polypeptide Chain. *Proc. Natl. Acad. Sci. U. S. A.* **1951**, *37*, 205–211.

(95) Ramachandran, G. N.; Lakshminarayanan, A. V; Kolaskar, A. S. Theory of the Non-Planar Peptide Unit. *Biochim. Biophys. Acta* **1973**, *303*, 8–13.

(96) Dasgupta, A. K.; Majumdar, R.; Bhattacharyya, D. Characterization of Non-Planar Peptide Groups in Protein Crystal Structures. *Indian J. Biochem. Biophys.* **2004**, *41*, 233–240.

(97) MacArthur, M. W.; Thornton, J. M. Deviations from Planarity of the Peptide Bond in Peptides and Proteins. *J. Mol. Biol.* **1996**, *264*, 1180–1195.

(98) Winkler, F. K.; Dunitz, J. D. The Non-Planar Amide Group. *J. Mol. Biol.* **1971**, *59*, 169–182.

(99) Maloň, P.; Bystrický, S.; Bláha, K. Non-Planar Amide Group and Its Chiroptical Manifestation. In *Peptides 1978, Proceedings of the 15th European Peptide Symposium*; Wroclaw University Press: Wroclaw, 1979; pp. 269–272.

(100) Maloň, P.; Bystrický, S.; Bláha, K. Semi-Empirical Calculation of Optical-Rotatory Strength of Non-Planar Conformations of Formamide. *Collect. Czechoslov. Chem. Commun.* **1978**, *43*, 781–790.

(101) Tvaroška, I.; Bystrický, S.; Maloň, P.; Bláha, K. Nonplanar Conformations of Methylacetamide - Solvent Effect and Chiroptical Properties. *Collect. Czechoslov. Chem. Commun.* **1982**, *47*, 17–28.

(102) Andrushchenko, V.; Matějka, P.; Anderson, D. T.; Kaminský, J.; Horníček, J.; Paulson, L. O.; Bouř, P. Solvent Dependence of the N-Methylacetamide Structure and Force Field. *J. Phys. Chem. A* **2009**, *113*, 9727–9736.

(103) Tichý, M.; Dušková, E.; Bláha, K. Optically Active 4-azatricyclo[4,4,0,$0^{3,8}$]decan-5-One: Model of a Non-Planar Amide Bond. *Tetrahedron Lett.* **1974**, *15*, 237–240.

(104) Frič, I.; Maloň, P.; Tichý, M.; Bláha, K. Chiroptical Properties of 4-azatricyclo[4,4,0,$0^{3,8}$]decan-5-One - A Lactam with a Non-Planar Cis-Amide Group. *Collect. Czechoslov. Chem. Commun.* **1977**, *42*, 678–686.

(105) Maloň, P.; Bláha, K. Quantum Chemical Calculations on 4-Azatricyclo[4,4,0,$0^{3,8}$]Decan-5-One - Lactam with a Non-Planar Cis-Amide Group. *Collect. Czechoslov. Chem. Commun.* **1977**, *42*, 687–696.

(106) Maloň, P.; Frič, I.; Tichý, M.; Bláha, K. Chiroptical Properties of (-)-4-Methyl-4-Azatricyclo[4,4,0,$0^{3,8}$]Decan-5-One - Lactam with a Non-Planar Tertiary Cis-Amide Group. *Collect. Czechoslov. Chem. Commun.* **1977**, *42*, 3104–3110.

(107) Bláha, K.; Maloň, P.; Tichý, M.; Frič, I.; Usha, R.; Ramakumar, S.; Venkatesan, K. Crystal Structure and Chiroptical Properties of (+)-(3S)-4-azatricyclo[4,3,1,$0^{3,7}$]decan-5-One. *Collect. Czechoslov. Chem. Commun.* **1978**, *43*, 3241–3251.

(108) Tichý, M.; Maloň, P.; Frič, I.; Bláha, K. Synthesis and Chiroptical Properties of (-)-(1R)-3-Azatricyclo[5,4,0,$0^{4,9}$]Undecan-2-One - Lactam with Non-Planar Cis-Amide Group. *Collect. Czechoslov. Chem. Commun.* **1979**, *44*, 2653–2659.

(109) Tichý, M.; Farag, A. M.; Maloň, P.; Kálal, P.; Bláha, K. (3R)-5-Azatricyclo[4.3.1.$0^{3,8}$]Decan-4-One, a Lactam with a Non-Planar Cis-Amide Group - Synthesis, Geometry and Chiroptical Properties. *Collect. Czechoslov. Chem. Commun.* **1984**, *49*, 834–839.

(110) Klyne, W.; Kirk, D. N.; Tilley, J.; Suginome, H. Chiroptical Studies-Part 99: The Circular Dichroism of Seven-Membered Lactams and Lactones. *Tetrahedron* **1980**, *36*, 543–553.

(111) Frelek, J.; Lysek, R.; Borsuk, K.; Jagodziński, J.; Furman, B.; Klimek, A.; Chmielewski, M. Structure-Chiroptical Properties Relationship in Oxabicyclic Beta-Lactam Derivatives. *Enantiomer* **2002**, *7*, 107–114.

(112) Bláha, K.; Buděšínský, M.; Frič, I.; Koblicová, Z.; Maloň, P.; Tichý, M. Polycyclic Dilactams with Inherently Chiral Amide Chromophores. *Tetrahedron Lett.* **1978**, *19*, 3949–3952.

(113) Bláha, K.; Buděšínský, M.; Koblicová, Z.; Maloň, P.; Tichý, M.; Baker, J. R.; Hossain, M. B.; Van der Helm, D. Optically Active Tricyclic Dilactams with Nonplanar Cis-Amide Groups - Synthesis, X-Ray, NMR and CD Studies. *Collect. Czechoslov. Chem. Commun.* **1982**, *47*, 1000–1019.

(114) Bláha, K.; Farag, A. M.; Van der Helm, D.; Hossain, M. B.; Buděšínský, M.; Maloň, P.; Smolíková, J.; Tichý, M. Stereoisomeric Chiral 2,9-diazabicyclo[4.4.0.]decane-3,10-Diones as Models of Dipeptide Grouping: Synthesis, X-Ray, IR, NMR and CD Studies. *Collect. Czechoslov. Chem. Commun.* **1984**, *49*, 712–742.

(115) Smolíková, J.; Koblicová, Z.; Bláha, K. Amino-Acids and Peptides .110. Infrared-Spectra of Polycyclic Spiro-Dilactams with Non-Planar Amide Bonds. *Collect. Czechoslov. Chem. Commun.* **1973**, *38*, 532–547.

(116) Maloň, P.; Barness, C. L.; Buděšínský, M.; Dukor, R. K.; Van der Helm, D.; Keiderling, T. A.; Koblicová, Z.; Pavlíková, F.; Tichý, M.; Bláha, K. (1S,7S)-7-Methyl-6,9-Diazatricyclo[6,3,0,$0^{1,6}$]Tridecane-5,10-Dione, a Tricyclic Spirodilactam Containing Non-Planar Amide Groups - Synthesis, NMR, CrystalStructure, Absolute-Configuration, Electronic and Vibrational Circular Dichroism. *Collect. Czechoslov. Chem. Commun.* **1988**, *53*, 2447–2472.

(117) Maloň, P. Unpublished Results. *Univ. Illinois Chicago* **1987**.

(118) Bednárová, L.; Maloň, P.; Bouř, P. Spectroscopic Properties of the Nonplanar Amide Group: A Computational Study. *Chirality* **2007**, *19*, 775–786.

(119) Wedemeyer, W. J.; Welker, E.; Narayan, M.; Scheraga, H. A. Disulfide Bonds and Protein Folding. *Biochemistry* **2000**, *39*, 4207–4216.

(120) Benham, C. J.; Jafri, M. S. Disulfide Bonding Patterns and Protein Topologies. *Protein Sci.* **1993**, *2*, 41–54.

(121) Garrett, R.; Grisham, C. M. *Biochemistry*; Granite Hill Publishers, 1995.

(122) Petersen, M. T.; Jonson, P. H.; Petersen, S. B. Amino Acid Neighbours and Detailed Conformational Analysis of Cysteines in Proteins. *Protein Eng.* **1999**, *12*, 535–548.

(123) Ozhogina, O. A.; Bominaar, E. L. Characterization of the Kringle Fold and Identification of a Ubiquitous New Class of Disulfide Rotamers. *J. Struct. Biol.* **2009**, *168*, 223–233.

(124) Sugeta, H.; Go, A. S-S and C-S Stretching Vibrations and Molecular Conformations of Dialkyl Disulfides and Cystine. *Chem. Lett.* **1972**, 83–86.

(125) Van Wart, H. E.; Scheraga, H. A. Agreement with the Disulfide Stretching Frequency-Conformation Correlation of Sugeta, Go, and Miyazawa. *Proc. Natl. Acad. Sci. U. S. A.* **1986**, *83*, 3064–3067.

(126) Havel, H. A. *Spectroscopic Methods for Determining Protein Structure in Solution*; VCH Publishers, Inc.: New York, 1996.

(127) Linderberg, J.; Michl, J. On the Inherent Optical Activity of Organic Disulfides. *J. Am. Chem. Soc.* **1970**, *92*, 2619–2625.

(128) Woody, R. W. Application of the Bergson Model to the Optical Properties of Chiral Disulfides. *Tetrahedron* **1973**, *29*, 1273–1283.

(129) Bergson, G. Molecular Orbital Treatment of the 3para-Alpha-Interaction in Five-Membered Cyclic Disulphides. *Ark. Kemi* **1958**, *12*, 233–237.

(130) Bergson, G. A Semi-Empirical Study of Interaction between Lone-Pair Electrons with Special Reference to Problem of Hybridization and Theory of Restricted Rotation About Single Bonds - Applications to Structure and Reactivity of Sulphur Chains. *Ark. Kemi* **1962**, *18*, 409–434.

(131) Bednárová, L.; Bouř, P.; Maloň, P. Vibrational and Electronic Optical Activity of the Chiral Disulphide Group: Implications for Disulphide Bridge Conformation. *Chirality* **2010**, *22*, 514–526.

(132) Kapitán, J.; Baumruk, V.; Gut, V.; Hlaváček, J.; Dlouhá, H.; Urbanová, M.; Wünsch, E.; Maloň, P. Raman Optical Activity of the Central Part of Hinge Peptide. *Collect. Czechoslov. Chem. Commun.* **2005**, *70*, 403–409.

(133) Kapitán, J.; Baumruk, V.; Hulačová, H.; Maloň, P. Raman Optical Activity of the Hinge Peptide. *Vib. Spectrosc.* **2006**, *42*, 88–92.

(134) Kubáňová, M. Raman Optical Activity and Conformation of Structurally Important Groups in Peptides and Proteins (MSc Thesis), Charles University in Prague, 2009.

(135) Tu, A. T. . In *Spectroscopy of Biological Systems (Advances in Spectroscopy)*; Clark, R. J. H.; Hester, R. E., Eds.; John Wiley & Sons: Chichester, U.K.; 1986; Vol. 13, pp. 47–112.

(136) Smolíková, J.; Koblicová, Z.; Bláha, K. Amino Acids and Peptides. CX. The Infrared Spectra of Polycyclic Spiro-Dilactams with Non-Planar Amide Bonds. *Collect. Czechoslov. Chem. Commun.* **1973**, *38*, 532–547.

(137) Pazderková, M.; Profant, V.; Hodačová, J.; Šebestík, J.; Pazderka, T.; Novotná, P.; Urbanová, M.; Šafařík, M.; Buděšínský, M.; Tichý, M.; et al. Nonplanar Tertiary Amides in Rigid Chiral Tricyclic Dilactams. Peptide Group Distortions and Vibrational Optical Activity. *J. Phys. Chem. B* **2013**, *117*, 9626–9642.

(138) Monincová, L.; Slaninová, J.; Fučík, V.; Hovorka, O.; Voburka, Z.; Bednárová, L.; Maloň, P.; Štokrová, J.; Čeřovský, V. Lasiocepsin, a Novel Cyclic Antimicrobial Peptide from the Venom of Eusocial Bee Lasioglossum Laticeps (Hymenoptera: Halictidae). *Amino Acids* **2012**, *43*, 751–761.

(139) Kapitán, J. Theoretical and Experimental Development of Raman Optical Activity as a Stereochemical Probe for Aqueous Environment (PhD Thesis), Charles University in Prague, 2006.

(140) Hussain, R.; Jávorfi, T.; Siligardi, G. Circular Dichroism Beamline B23 at the Diamond Light Source. *J. Synchrotron Radiat.* **2012**, *19*, 132–135.

(141) Nafie, L. A.; Buijs, H.; Rilling, A.; Cao, X.; Dukor, R. K. Dual Source Fourier Transform Polarization Modulation Spectroscopy: An Improved Method for the Measurement of Circular and Linear Dichroism. *Appl. Spectrosc.* **2004**, *58*, 647–654.

(142) Nafie, L. A. Dual Polarization Modulation: A Real-Time, Spectral-Multiplex Separation of Circular Dichroism from Linear Birefringence Spectral Intensities. *Appl. Spectrosc.* **2000**, *54*, 1634–1645.

(143) Pazderková, M.; Profant, V.; Seidlerová, B.; Dlouhá, H.; Hodačová, J.; Jávorfi, T.; Siligardi, G.; Baumruk, V.; Bednárová, L.; Maloň, P. Electronic Circular Dichroism of the Chiral Rigid Tricyclic Dilactam with Nonplanar Tertiary Amide Groups. *J. Phys. Chem. B* **2014**, *118*, 11100–11108.

(144) Parr, R. G.; Yang, W. *Density-Functional Theory of Atoms and Molecules*; Oxford University Press: New York, 1994.

(145) Becke, A. D. Density-Functional Thermochemistry. III. The Role of Exact Exchange. *J. Chem. Phys.* **1993**, *98*, 5648–5652.

(146) Kim, K.; Jordan, K. D. Comparison of Density Functional and MP2 Calculations on the Water Monomer and Dimer. *J. Phys. Chem.* **1994**, *98*, 10089–10094.

(147) Stephens, P. J.; Devlin, F. J.; Chabalowski, C. F.; Frisch, M. J. Ab Initio Calculation of Vibrational Absorption and Circular Dichroism Spectra Using Density Functional Force Fields. *J. Phys. Chem.* **1994**, *98*, 11623–11627.

(148) Ditchfield, R. Self-Consistent Molecular-Orbital Methods. IX. An Extended Gaussian-Type Basis for Molecular-Orbital Studies of Organic Molecules. *J. Chem. Phys.* **1971**, *54*, 724–728.

(149) Runge, E.; Gross, E. K. U. Density-Functional Theory for Time-Dependent Systems. *Phys. Rev. Lett.* **1984**, *52*, 997–1000.

(150) Ullrich, C. A. *Time-Dependent Density-Functional Theory: Concepts and Applications*; Oxford University Press: Oxford, UK, 2011; Vol. 569.

(151) Adamo, C.; Barone, V. Toward Reliable Density Functional Methods without Adjustable Parameters: The PBE0 Model. *J. Chem. Phys.* **1999**, *110*, 6158–6170.

(152) Suenaga, M. Facio: New Computational Chemistry Environment for PC GAMESS. *J. Comput. Chem. Japan* **2005**, *4*, 25–32.

(153) Fogarasi, G.; Pulay, P. Ab Initio Vibrational Force Fields and Vibrational Spectra. In *Vibrational Spectra and Structure*; Elsevier: Amsterdam, 1985; pp. 125–219.

(154) Ealick, S. E.; Van der Helm, D. The Crystal and Molecular Structure of 5,8-Diaza-4,9-dioxotricyclo[6,3,0,0,1,5]undecane, a Non-Planar Tertiary Amide. *Acta Crystallogr.* **1975**, 2676–2680.

(155) Ealick, S. E.; Washecheck, D. M.; Van der Helm, D. The Crystal Structures of Two Tetracyclic Spirodilactams Containing Non-Planar Amide Bonds. *Acta Crystallogr.* **1976**, *B32*, 895–900.

(156) Ealick, S. E.; Van der Helm, D. The Crystal and Molecular Structure of 6,9-Diaza-5,10-dioxotricyclo[7.3.0.$0^{1,6}$]dodecane, a Molecule Designed to Contain Non-Planar Amide Bonds. *Acta Crystallogr.* **1977**, *B33*, 76–80.

(157) Profant, V.; Pazderková, M.; Pazderka, T.; Maloň, P.; Baumruk, V. Relative Intensity Correction of Raman Optical Activity Spectra Facilitates Extending the Spectral Region. *J. Raman Spectrosc.* **2014**, *45*, 603–609.

(158) Renugopalakrishnan, V.; Rein, R. Energetics of Deformation of a Peptide Unit - Semiempirical Molecular-Orbital and Ab-Initio Study of N-Methyl Acetamide and N-Acetyl-L-Alanine N-Methyl Amide. *Biochim. Biophys. Acta* **1976**, *434*, 164–168.

(159) Boyd, D. B.; Riehl, J. P.; Richardson, F. S. Chiroptical Properties of 1-Carbapenam and Orbital Mixing in Nonplanar Amides. *Tetrahedron* **1979**, *35*, 1499–1508.

(160) Woody, R. W. A Simple Model for the Optical Properties of Chiral Amides. *Biopolymers* **1983**, *22*, 189–203.

(161) Chalupský, J.; Vondrášek, J.; Spirko, V. Quasiplanarity of the Peptide Bond. *J. Phys. Chem. A* **2008**, *112*, 693–699.

(162) Hug, W.; Kint, S.; Bailey, G. F.; Scherer, J. R. Raman Circular Intensity Differential Spectroscopy. Spectra of (-)-Alpha-Pinene and (+)-Alpha-Phenylethylamine. *J. Am. Chem. Soc.* **1975**, *97*, 5589–5590.

(163) Hudecová, J.; Profant, V.; Novotná, P.; Baumruk, V.; Urbanová, M.; Bouř, P. CH Stretching Region: Computational Modeling of Vibrational Optical Activity. *J. Chem. Theory Comput.* **2013**, *9*, 3096–3108.

(164) Etz, E. S.; Choquette, S. J.; Hurst, W. S. Development and Certification of NIST Standard Reference Materials for Relative Raman Intensity Calibration. *Microchim. Acta* **2005**, *149*, 175–184.

(165) McCreery, R. L. *Raman Spectroscopy for Chemical Analysis*; Winefordner, J. D., Ed.; Wiley-Interscience: New York, NY, 2000.

(166) McCreery, R. L. Photometric Standards for Raman Spectroscopy. In *Handbook of Vibrational Spectroscopy*; Chalmers, J. M.; Griffiths, P. R., Eds.; John Wiley & Sons, Ltd.: Chichester, U.K., 2002; pp. 920–932.

(167) Rodriguez, J. D.; Westenberger, B. J.; Buhse, L. F.; Kauffman, J. F. Quantitative Evaluation of the Sensitivity of Library-Based Raman Spectral Correlation Methods. *Anal. Chem.* **2011**, *83*, 4061–4067.

(168) Pazderková, M.; Bednárová, L.; Dlouhá, H.; Flegel, M.; Lebl, M.; Hlaváček, J.; Setnička, V.; Urbanová, M.; Hynie, S.; Klenerová, V.; et al. Electronic and Vibrational Optical Activity of Several Peptides Related to Neurohypophyseal Hormones: Disulfide Group Conformation. *Biopolymers* **2012**, *97*, 923–932.

(169) Sawyer, W. H. Evolution of Neurohypophyseal Hormones and Their Receptors. *Fed. Proc.* **1977**, *36*, 1842–1847.

(170) Gimpl, G.; Fahrenholz, F. The Oxytocin Receptor System: Structure, Function, and Regulation. *Physiol. Rev.* **2001**, *81*, 629–683.

(171) Jošt, K.; Lebl, M.; Brtnik, F. *CRC Handbook of Neurohypophyseal Hormone Analogs, Vol. 2*; CRC Press: Boca Raton, FL, 1987; Vol. 2.

(172) Rose, J. P.; Wu, C. K.; Hsiao, C. D.; Breslow, E.; Wang, B. C. Crystal Structure of the Neurophysin-Oxytocin Complex. *Nat. Struct. Biol.* **1996**, *3*, 163–169.

(173) Wu, C. K.; Hu, B.; Rose, J. P.; Liu, Z. J.; Nguyen, T. L.; Zheng, C.; Breslow, E.; Wang, B. C. Structures of an Unliganded Neurophysin and Its Vasopressin Complex: Implications for Binding and Allosteric Mechanisms. *Protein Sci.* **2001**, *10*, 1869–1880.

(174) Hruby, V. J.; Lebl, M. Conformational Properties of Neurohypophyseal Hormone Analogs in Solution as Determined by NMR and Laser Raman Spectroscopies. In *CRC Handbook of Neurohypophyseal Hormone Analogs*; Jost, K.; Lebl, M.; Brtnik, F., Eds.; CRC Press: Boca Raton, 1987; pp. 105–155.

(175) Urry, D. W.; Quadrifoglio, F.; Walter, R.; Schwartz, I. L. Conformational Studies on Neurohypophyseal Hormones: The Disulfide Bridge of Oxytocin. *Proc. Natl. Acad. Sci. U. S. A.* **1968**, *60*, 967–974.

(176) Tu, A. T.; Lee, J.; Deb, K. K.; Hruby, V. J. Laser Raman-Spectroscopy and Circular-Dichroism Studies of the Peptide-Hormones Mesotocin, Vasotocin, Lysine Vasopressin, and Arginine Vasopressin - Conformational-Analysis. *J. Biol. Chem.* **1979**, *254*, 3272–3278.

(177) Hlaváček, J.; Frič, I.; Maloň, P.; Jošt, K.; Bláha, K. Three Cyclohexapeptides Modelling the Oxytocin Ring Moiety: Synthesis and Circular Dichroism. *Collect. Czechoslov. Chem. Commun.* **1987**, *52*, 1841–1856.

(178) Frič, I.; Kodíček, M.; Flegel, M.; Zaoral, M. Circular-Dichroic Spectra of Vasopressin Analogues and Their Cyclic Fragments. *Eur. J. Biochem.* **1975**, *56*, 493–502.

(179) Fjell, C. D.; Hiss, J. a.; Hancock, R. E. W.; Schneider, G. Designing Antimicrobial Peptides: Form Follows Function. *Nat. Rev. Drug Discov.* **2012**, *11*.

(180) Zasloff, M. Antimicrobial Peptides of Multicellular Organisms. *Nature* **2002**, *415*, 389–395.

(181) Hancock, R. E. W.; Scott, M. G. The Role of Antimicrobial Peptides in Animal Defenses. *Proc. Natl. Acad. Sci.* **2000**, *97*, 8856–8861.

(182) Monincová, L.; Buděšínský, M.; Čujová, S.; Čeřovský, V.; Veverka, V. Structural Basis for Antimicrobial Activity of Lasiocepsin. *Chembiochem* **2014**, *15*, 301–308.

(183) Barth, A.; Zscherp, C. What Vibrations Tell Us about Proteins. *Q. Rev. Biophys.* **2002**, *35*, 369–430.

(184) Whitmore, L.; Wallace, B. a. Protein Secondary Structure Analyses from Circular Dichroism Spectroscopy: Methods and Reference Databases. *Biopolymers* **2008**, *89*, 392–400.

(185) Bochicchio, B.; Tamburro, A. M. Polyproline II Structure in Proteins: Identification by Chiroptical Spectroscopies, Stability, and Functions. *Chirality* **2002**, *14*, 782–792.

(186) Drake, A. F.; Siligardi, G.; Gibbons, W. A. Reassessment of the Electronic Circular Dichroism Criteria for Random Coil Conformations of poly(L-Lysine) and the Implications for Protein Folding and Denaturation Studies. *Biophys. Chem.* **1988**, *31*, 143–146.

List of Abbreviations

ACN	Acetonitrile
AMP	Antimicrobial peptide
AVP	Arginine vasopressin
B-O	Born-Oppenheimer
CD	Circular dichroism
CID	Circular intensity difference
COSMO	Conductor-like Screening Model
DFT	Density functional theory
DCP	Dual circular polarization
ECD	Electronic circular dichroism
EOM	Electro-optical modulator
FFR	Far-from resonance
FTIR	Fourier transform infrared (spectroscopy)
GIAO	Gauge-independent atomic orbitals
HPLC	High-performance liquid chromatography
HQI	Hit quality index
ICP	Incident circular polarization
IOCB	Institute of Organic Chemistry and Biochemistry
IR	Infrared
LAS	Lasiocepsin
LCP	Left circularly polarized
LMO	Localized molecular orbital
LVP	Lysine vasopressin
MCT	Mercury cadmium telluride
MD	Molecular dynamics
MFP	Magnetic field perturbation
MS	Mass spectrometry
NHH	Neurohypophyseal hormone
ORD	Optical rotatory dispersion
OT	Oxytocin
PED	Potential energy distribution
PEM	Photoelastic modulator
PPII	Polyproline II
RCP	Right circularly polarized
ROA	Raman optical activity
SCP	Scattered circular polarization
SOS	Sum-over-states
SRCD	Synchrotron radiation circular dichroism
TCD	Transition current density
TFA	Trifluoroacetic acid
TFE	2,2,2-trifluoroethanol
TDDFT	Time-dependent density functional theory
VCD	Vibrational circular dichroism
VCT	Vibronic coupling theory
VOA	Vibrational optical activity
VUV	Vacuum-UV

List of Publications

[I] **Pazderková, M.**; Profant, V.; Seidlerová, B.; Dlouhá, H.; Hodačová, J.; Jávorfi, T.; Siligardi, G.; Baumruk, V.; Bednarova, L.; Maloň, P. Electronic Circular Dichroism of the Chiral Rigid Tricyclic Dilactam with Nonplanar Tertiary Amide Groups. J. Phys. Chem. B 2014, 118, 11100-11108.

[II] Profant, V.; **Pazderková, M.**; Pazderka, T.; Maloň, P.; Baumruk, V. Relative Intensity Correction of Raman Optical Activity Spectra Facilitates Extending the Spectral Region. J. Raman Spectrosc. 2014, 45, 603–609.

[III] **Pazderková, M.**; Profant, V.; Hodačová, J.; Šebestík, J.; Pazderka, T.; Novotná, P.; Urbanová, M.; Šafařík, M.; Buděšínský, M.; Tichý, M.; Bednárová, L.; Baumruk, V.; Maloň, P. Nonplanar Tertiary Amides in Rigid Chiral Tricyclic Dilactams. Peptide Group Distortions and Vibrational Optical Activity. J. Phys. Chem. B 2013, 117, 9626–9642.

[IV] **Pazderková, M.**; Kočišová, E.; Pazderka, T.; Maloň, P.; Kopecký Jr., V.; Monincová, L.; Čeřovský, V.; Bednárová, L. Antimicrobial Peptide from the Eusocial Bee Halictus Sexcinctus Interacting with Model Membranes. In Advances in Biomedical Spectroscopy, Volume 7; Marques, M. P.; Batista de Carvalho, L. A. E.; Haris, P. I., Eds.; IOS Press, 2013; pp. 79–83.

[V] **Pazderková, M.**; Bednárová, L.; Dlouhá, H.; Flegel, M.; Lebl, M.; Hlaváček, J.; Setnička, V.; Urbanová, M.; Hynie, S.; Klenerová, V.; Baumruk, V.; Maloň, P. Electronic and Vibrational Optical Activity of Several Peptides Related to Neurohypophyseal Hormones: Disulfide Group Conformation. Biopolymers 2012, 97, 923–932.

[VI] **Pazderková, M.**; Kočišová, E.; Pazderka, T.; Maloň, P.; Kopecký Jr., V.; Monincová, L.; Čeřovský, V.; Bednárová, L. Antimicrobial Peptide from the Eusocial Bee HalictusSexcinctus Interacting with Model Membranes. Spectroscopy: An International Journal, 2012, 27, 497–502.

[VII] Maloň, P.; Bednárová, L.; Straka, M.; Krejčí, L.; Kumprecht, L.; Kraus, T.; **Kubáňová, M.**; Baumruk, V. Disulfide Chromophore and Its Optical Activity. Chirality 2010, 22 Suppl 1, E47–55.

Attachments

Appendix 1

Electronic Circular Dichroism of the Chiral Rigid Tricyclic Dilactam with Nonplanar Tertiary Amide Groups

J. Phys. Chem. B 2014, 118, 11100-11108

Pazderková, M.,[1,2] Profant, V.,[1] Seidlerová, B.,[2] Dlouhá, H.,[2] Hodačová, J.,[3] Jávorfi, T.,[4] Siligardi, G.,[4] Baumruk, V.,[1] Bednárova, L.,[2] Maloň, P.[1]

[1]*Charles University in Prague, Faculty of Mathematics and Physics, Ke Karlovu 5, 121 16 Prague 2, Czech Republic*
[2]*Institute of Organic Chemistry and Biochemistry, AS CR, Fleming square 2, 166 10 Prague 6, Czech Republic*
[3]*Institute of Chemical Technology, Technická 5, 166 28 Prague 6, Czech Republic*
[4]*Diamond Light Source, Chilton, Didcot, Oxfordshire, OX11 0DE, U.K.*

THE JOURNAL OF PHYSICAL CHEMISTRY B

Article

pubs.acs.org/JPCB

Electronic Circular Dichroism of the Chiral Rigid Tricyclic Dilactam with Nonplanar Tertiary Amide Groups

Markéta Pazderková,[†,‡] Václav Profant,[†] Beata Seidlerová,[‡] Helena Dlouhá,[‡] Jana Hodačová,[∥] Tamás Jávorfi,[§] Giuliano Siligardi,[§] Vladimír Baumruk,[†] Lucie Bednárová,[‡] and Petr Maloň*[,†]

[†]Faculty of Mathematics and Physics, Charles University in Prague, Ke Karlovu 5, 121 16 Prague 2, Czech Republic

[‡]Institute of Organic Chemistry and Biochemistry, AS CR, Fleming sq. 2, 166 10 Prague 6, Czech Republic

[∥]Institute of Chemical Technology, Technická 5, 166 28 Prague 6, Czech Republic

[§]Diamond Light Source, Chilton, Didcot, Oxfordshire, OX11 0DE, U.K.

Supporting Information

ABSTRACT: Electronic circular dichroism (ECD) of the spirocyclic dilactam 5,8-diazatricyclo[6,3,0,$0^{1,5}$]undecane-4,9-dione has been measured in the extended wavelength range (170−260 nm) utilizing far-UV CD instrumentation including synchrotron radiation light source. The data of this model of two nonplanar tertiary amide groups interacting within the rigid chiral environment provided new information particularly about the shorter wavelength $\pi-\pi^*$ transition region below 190 nm. The interpretation using TDDFT calculations confirmed that effects of amide nonplanarity follow our previous observations on *mono*lactams as far as amide n$-\pi^*$ transitions are concerned. ECD band in the n$-\pi^*$ transition region of the nonplanar *di*amide exhibits an identical bathochromic shift and its sign remains tied to the sense of nonplanar deformation in the same way. As far as n$-\pi^*$ transitions are concerned amide nonplanarity acts as a local phenomenon independently reflecting sum properties of single amide groups. On the other hand, CD bands associated with $\pi-\pi^*$ transitions (found between ∼170 to 210 nm) form an exciton-like couplet with the sign pattern determined by mutual orientation of the associated electric transition moments. This sign pattern follows predictions pertaining to a coupled oscillator. The influence of amide nonplanarity on $\pi-\pi^*$ transitions is only minor and concentrates into the shorter wavelength lobe of the $\pi-\pi^*$ couplet. The detailed analysis of experimental ECD with the aid of TDDFT calculations shows that there is only little interaction between effects of inherent chirality caused by nonplanarity of amide groups and amide−amide coupling. Consequently these two effects can be studied nearly independently using ECD. In addition, the calculations indicate that participation of other type of transitions (n$-\sigma^*$, $\pi-\sigma^*$ or Rydberg type transitions) is only minor and is concentrated below 180 nm.

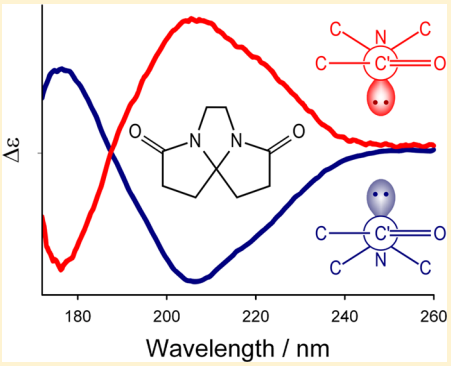

INTRODUCTION

It is well-known[1,2] that amide group can adopt a certain degree of nonplanarity. Nonplanar amide deformations have been found in crystal structures of peptides/proteins,[3−5] natural products often of pharmacological significance (e.g., alkaloids, antibiotics[6]) or polycyclic lactams.[7−12] The studies on various models (including the extreme case of 1-azabicyclo[2,2,2]-octane-2-one[13−15]) provided a finding that minor degree of amide nonplanarity is rather common and that it usually involves a partial $sp^2 \rightarrow sp^3$ hybridization change (the pyramidalization) of the amide nitrogen atom, not only a simple rotation around the C′−N bond. Amide group in the nonplanar arrangement loses its symmetry plane (C_s) and becomes an inherently chiral chromophore (C_1) as has been shown first by us[7,8] and confirmed by others.[6,16−18] Therefore, it can be studied with advantage using chiroptical properties. Knowledge of the circular dichroism spectra of rigid nonplanar amides may provide valuable information on their role in other, more flexible systems, including a connection to biologically relevant peptides and proteins. Investigation of model amides[19−21] provided basic data and suggested that the easiest way to detect and understand amide nonplanarity consists in application and detailed evaluation of electronic circular dichroism (ECD) spectra. Our studies were mainly based on rigid polycyclic monolactams derived from twistane skeleton. These compounds represent nearly ideal models, because they possess well-defined geometries and still do not introduce excessive angular strain. Their intense ECD spectra provide the following observations. Within a single amide group, nonplanarity leads to a relative enhancement of the ECD band due to amide n$-\pi^*$ transition and to its significant bathochromic shift up to 230−232 nm. This rather characteristic parameter is sensitive enough to serve as a nonplanarity marker. Similar results were achieved in later studies by others; however, most

Received: June 26, 2014
Revised: August 29, 2014
Published: September 2, 2014

dx.doi.org/10.1021/jp5063463 | J. Phys. Chem. B 2014, 118, 11100−11108

other models employ small ring systems having excessively strained bond angles.[16,22]

ECD due to amide nonplanarity seems to be a local phenomenon originating mainly by the perturbing interaction between n−π^* and π−π^* electronic configurations.[12,23] These interactions result in a pair of rather intense n−π^* and π−π^* ECD bands having mutually opposite signs. The absolute signs are determined by the relative orientation of the lone electron pair on the amide nitrogen atom (the axis of the pyramid of bonds to nitrogen) and the carbonyl C═O—see Figure 1 in ref 23. The finding that the amide n−π^* ECD band originates locally and, consequently, that nonplanarity manifestation within this ECD feature corresponds to a local phenomenon is not in contrast with the general experience. On the other hand, amide π−π^* transitions are known to reflect interactions between amide groups via, e.g., dipole−dipole coupling. Amide nonplanarity might interfere with the frequent use of ECD for the peptide/protein conformation determination and it is of interest to evaluate in detail its effect on the π−π^* region of ECD spectra of models having more than one nonplanar amide group in their molecules like the spirocyclic dilactams and similar compounds.

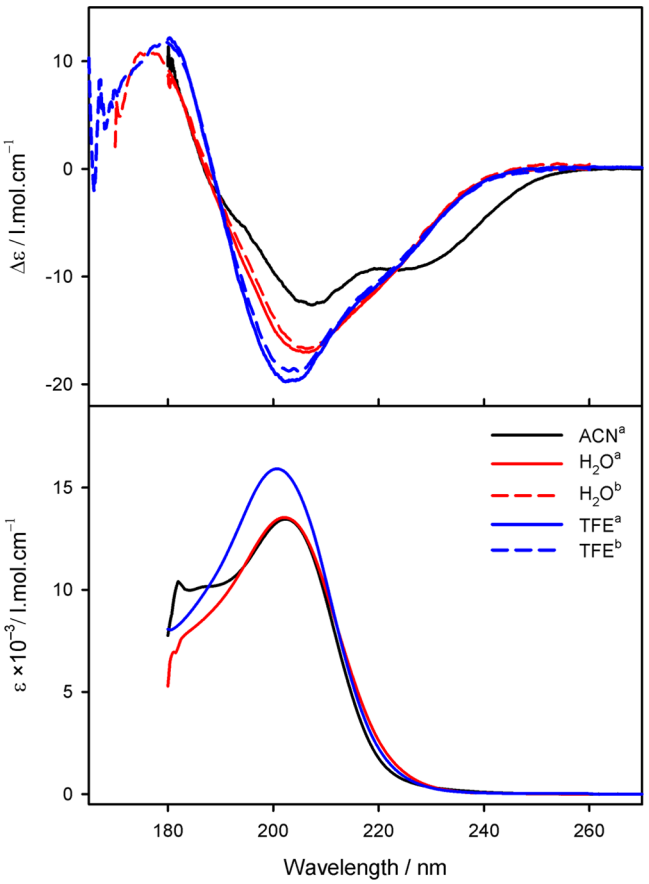

Figure 1. Experimental ECD and absorption spectra of *R*-(−)-**I** measured in ACN, TFE and H_2O (curve a, measured on stand-alone ECD spectrometer; curve b, measured on Diamond B23 circular dichroism beamline).

The spirocyclic dilactam 5,8-diazatricyclo[6,3,0,$0^{1,5}$]-undecane-4,9-dione (**I**, Scheme 1) belongs to the class of polycyclic dilactams representing convenient models for nonplanar tertiary amides in a rigid, well-defined and chiral environment.

Scheme 1. Spirocyclic Dilactam I

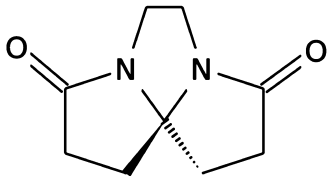

(−)-(1R)-I

As racemates, these compounds are known since the 1970s;[24] however, preparation of pure enantiomers in quantities sufficient for thorough physicochemical investigation succeeded only recently.[25] Nowadays the synthesis can be achieved in both enantiomeric forms by chromatographic resolution of the racemates using commercial columns and enantiomer separating instrumentation. As a further advantage the absolute configuration of the spirodilactam system is known on the basis of a correlation to corresponding 6-methyl[26] and 6-isobutylderivatives,[27] which were prepared from precursors of known absolute configurations (L-alanine and L-leucine). These derivatives introduce an additional chiral center at C_6, which is in the known diastereomeric relation (determined by both NMR and X-ray) with the spirodilactam moiety. Rigidity, knowledge of their geometries and availability in milligram quantities together with their established absolute configuration makes spirodilactams useful models for thorough investigation of spectroscopic properties of two interacting nonplanar amide groups.

In the preceding preliminary studies[27,28] we presented electronic optical activity in the n−π^* and partially π−π^* transition region (180−260 nm). However, the interpretation of these data was only empirical and operated with the classical electronic picture of the amide bond as composed of n−π^* and π−π^* configurations, while inherent chirality of the nonplanar amide chromophore requires the interpretation using quantum chemical methods. Preliminary TDDFT calculations[23] on single nonplanar amides have been already attempted, but a theoretical study of interacting nonplanar amides has yet to be done. Comparison of such a calculation to experiment requires more complete data because the existing ones (above 180 nm) do not show the π−π^* transitions completely. Therefore, we report ECD experiments below the usual threshold of 185−190 nm for the measurements in solution, which require special instrumental adaptations (synchrotron radiation light source). Measurements in the extended range should help us to reveal positions and intensities of shorter-wavelength dichroic bands and provide more detailed information on the mixing of n−π^* and π−π^* electronic configurations. A new more detailed calculation using wider selection of recent more advanced theoretical procedures (mainly based on TDDFT theory) should enable us to build a model of amide nonplanarity contributions to ECD spectra of properly oriented homoconjugated amide groups that occur in real peptides/proteins. Because of the unique nature of our dilactams (mainly the rigid geometry and sample availability) such a model might be built with more confidence using simultaneously a wider selection of spectroscopic techniques including vibrational optical activity (VOA). These vibrational

dx.doi.org/10.1021/jp5063463 | J. Phys. Chem. B 2014, 118, 11100−11108

Table 1. Experimental Absorption and ECD Data of *R*-(−)-I[a]

$\lambda_{max,ACN}$ ($\varepsilon_{max} \times 10^{-3}$; $\Delta\varepsilon_{max/min}$)	λ_{max,H_2O} ($\varepsilon_{max} \times 10^{-3}$; $\Delta\varepsilon_{max/min}$)	$\lambda_{max,TFE}$ ($\varepsilon_{max} \times 10^{-3}$; $\Delta\varepsilon_{max/min}$)
	$n-\pi^*$ Transition Region	
222 (−; −10, min)	220 (−; −10, sh)	215 (−; −15, sh)
	$\pi-\pi^*$ Transition Region	
208 (13.5, max; −12.5, min)	205 (14, max; −20, min)	207 (15, max; −17, min)
195 (−; −5, sh)	–	195 (−; −5, sh)
188 (−; z)	190 (−; z)	190 (−; z)
	180 (−; +11, max)	177 (n; +11, max)

[a]Key: ACN, acetonitrile; TFE, 2,2,2-trifluoroethanol; min, minimum; max, maximum; sh, shoulder; n, not measured; z, zero crossing.

chiroptical properties of the spirodilactam **I** have been already investigated[25] and provided interesting parallels to preliminary electronic CD,[27,28] like the bathochromic shift of the amide I vibration (first observed by Smolíková et al.[24]). Therefore, it appears important to find out whether detection of several inherently chiral nonplanar amide groups in one molecule can be achieved using experimentally simple electronic circular dichroism spectroscopy. A comparison should reveal whether ECD together with VOA can provide enough structural detail to recognize manifestation of amide nonplanarity in a more complex situation.

MATERIALS AND METHODS

The synthesis of both pure enantiomers of 5,8-diazatricyclo-[6,3,0,$0^{1,5}$]undecane-4,9-dione (**I**) was described in ref 25 together with the analytical data including absolute configuration. ECD and UV absorption measurements in the longer wavelength range (180−280 nm), in acetonitrile (ACN), 2,2,2-trifluoroethanol (TFE) and distilled water were performed using Jasco J-815 CD spectropolarimeter. For ECD measurements farther in the vacuum UV (VUV) region (165−200 nm)—in TFE and water—we used B23 beamline for synchrotron radiation circular dichroism (SRCD) (Diamond Light Source, Harwell, U.K.).[29] The measurements were performed in solutions (concentrations 2−3 × 10^{-2} M) using spectral grade solvents. We have also tried to record ECD in freely evaporated films, but these experiments were not successful due to the pronounced tendency of these dilactams to crystallize. We used sample cells with windows of either Suprasil quartz (far- and near-UV region, path length 1−0.1 mm) or calcium fluoride (VUV region, path length 0.1 mm). The assembled experimental UV and ECD spectra were plotted as the respective ε or $\Delta\varepsilon$ [L mol^{-1} cm^{-1}] values.

Theoretical transition energies, dipole and rotatory strengths were investigated using a rather extensive selection of computational methods utilizing Gaussian09 program suite.[30] The methods mostly involved TDDFT implementations using various pure and hybrid exchange correlation functionals, PBEPBE,[31,32] PBEhPBE,[33] PBE0 (PBE1PBE),[34] PBEh1PBE, HSE (wPBEhPBE), HSE03 (HSE2PBE), HSE06 (HSEh1PBE),[35−42] B3LYP,[43−45] and B3PW91,[46] and long-range corrected functionals CAM-B3LYP[47] and LC-wPBE.[48−50] For comparison we included also standard MP2[51] and Roothaan equations-based (HF) calculations. We have not employed the more advanced multireference perturbation methods (such as CASPT2[52]), which were used for, e.g., interpretation of amide electronic spectra—see, e.g., refs 53 and 54. Although these more advanced procedures undoubtedly produce better agreement with experiment, their time and cost demands are much higher. Furthermore, it has been shown that frequencies and spectral intensities calculated by CASPT2 and TDDFT do not differ excessively at least above 175 nm (see, e.g., ref 55). We checked the sensitivity of calculated results toward choice of the basis set by scanning through the Pople triple-ζ 6-311G**, 6-311++G**, 6-311++G** 6d 10f,[56] the Dunning/Huzinaga double-ζ D95++**,[57] the DGauss DGDZVP, DGTZVP,[58,59] the Dunning correlation consistent cc-pVDZ, cc-pVTZ, aug-cc-pVDZ, aug-cc-pVTZ[60−63] both without and with augmentation, and the Ahlrichs TZVP.[64,65] We also varied the number of singlet excited states included in TDDFT calculations (from 10 to 100) in order to determine their minimal number necessary for the successful simulation of absorption and ECD spectra down to 160 nm. The effect of solvent was included in all calculations using the implicit solvation model COSMO (conductor-like screening model)[66,67] for water, TFE, and acetonitrile. We did not include explicit solvent molecules into our calculation, because of the excessive computational demands and also due to the fact that other calculations including explicit water molecules (see, e.g., Figure 6 in ref 68) do not result in major improvements. Calculations always included two consecutive steps—geometry optimization and calculation of spectral properties (frequencies, intensities, and ECD). Both were consistently done at the same level of approximation. While the first step was necessary in order to enable internal consistency, the actual differences relating particular calculations of calculated and experimental values (based on X-ray studies) were small to negligible. For the comparison with experiment, theoretical spectra were simulated as sums of Gaussian bands with empirical bandwidths (fwhm) of 20 nm. As shown in the Results and Discussion, there are significant differences between theoretical spectra obtained using various procedures. Some of them (PBE0, PBEhPBE, HSE03, HSE06, B3LYP and B3PW91 combined with basis sets 6-311++G**, D95++**, aug-cc-pVDZ and aug-cc-pVTZ) give acceptable agreement with experiment (for further details see the Results and Discussion and the Supporting Information). The analysis shown further uses results obtained with PBE0/aug-cc-pVTZ and 70 singlet excited states which consistently provide good agreement with the experimental data.

RESULTS AND DISCUSSION

Experimental electronic absorption and CD spectra of the dilactam R-I are shown in Figure 1 and summarized in Table 1. Both enantiomers of **I** are compared in Figure S1 in the Supporting Information. One should take into account that measurements in solution below solvent cutoff limit at 175 nm do not give reliable data.[69]

A comparison of these ECD spectra with preliminary results obtained earlier for only partially resolved compound **I**[27,28] reveals that the older data, while identical in the overall shape (between 185−250 nm), exhibited four times weaker dichroic

dx.doi.org/10.1021/jp5063463 | J. Phys. Chem. B 2014, 118, 11100−11108

signals. Consequently, the previous preliminary ECD of *R*-(−)-**I** corresponded to a sample having only ∼25% e.e. On the other hand, our ECD data of **I** agree well with those of the closely related spirodilactam derivatives substituted with either methyl or isobutyl group in the 6-position of the tricyclic system (see ref 27, compounds **II** and **III**). This finding confirms that the course of ECD spectra of these dilactams is predominantly determined by the ring system chirality and rigid mutual orientation of the two nonplanar amide groups. On the other hand, additional substitution at C_6 causes only minor if any effect, although such substitution brings an additional chiral center into the molecule. In addition, numerical agreement between ECD intensities of **I** and of its substituted derivatives further confirms that our samples of optically active *R*-(−)- and *S*-(+)-I are indeed 100% enantiomerically pure.[27]

Absorption data of **I** (Table 1 and Figure 1) show consistently a single prominent ($\varepsilon \sim 10^4$ l mol^{-1} cm^{-1}) feature at about 205−208 nm, which is accompanied by shoulders on both sides. The course of ECD spectra is more complex. It is possible to observe at least three dichroic bands between 180−250 nm. At long wavelengths (215−240 nm, depending on the solvent) there is an evident trace of a broad (fwhm ∼20 nm) dichroic band. Although this band (negative for the *R*-(−)-enantiomer) is rather prominent, it shows a visible extremum only in acetonitrile. In more polar solvents it is detectable only as a shoulder. The corresponding absorption trace does not reveal this band at all—it remains detectable only in ECD spectra. The visible ECD band exhibits a bathochromic shift with decreasing solvent polarity between 220−250 nm. In accord with the previous observations and theoretical analyses,[26,27] all these characteristics point to the association of this band with the n−π^* transition of the nonplanar amide group. The spectra show a resolution which is typical for solution samples (15−20 nm) and limits somewhat the possibility to assign observed bands to particular electronic transitions. This problem might be partially solved using less polar solvents cyclohexane or iso-octane. Unfortunately, compound **I** is not soluble in saturated hydrocarbons.

Within the intense absorption band at 203−208 nm there is another ECD feature (a negative shoulder for the *R*-(−)-enantiomer) at ∼192 nm, which is followed at even lower wavelength by a band of the opposite sign (i.e., positive for the *R*-(−)-isomer). The latter ECD band is not completely observable on conventional instrumentation, as its extremum lies below the measurement threshold (∼178 nm). Previous interpretation based on empirical analogueies[26,27] resulted in the assignment of this dominant pair (at the respective 178 and 203−208 nm) to oppositely signed dichroic components of the split π−π^* transition of the dilactam. However, there are several contradictions: (a) the absorption maximum (found at 205−208 nm) is not positioned between the two dichroic components as expected, in fact it nearly corresponds to the dichroic component lying at lower wavelength (it is blue-shifted by only 3−4 nm); (b) the lower-wavelength dichroic component is found below 180 nm, i.e., it may be of a different origin; (c) there are more dichroic bands within this region as evidenced by a shoulder at ∼192 nm (most clearly detectable in acetonitrile). Evidently, the spectra below 200 nm are more complex than described by the original analogue interpretation and it seems necessary to utilize an advanced computational model. It is necessary to balance the effects of amide inherent chirality and the amide−amide interaction. Experimental position of the component at ∼178 nm exhibits only minor dependence on solvent polarity. Its magnitude is nearly constant and just slightly smaller than that of the dichroic band at ∼205 nm. The absorption curve indicates a shoulder in this region (at ∼185 nm). The long-wavelength ECD band due to n−π^* transition (220 nm and above) of the compound **I** follows the relationship introduced earlier for compounds with one nonplanar amide group:[23] it exhibits a positive sign when the amide grouping O=C−N−LP (LP − lone electron pair on nitrogen atom) arrangement is right-handed ($0 < \chi_{O=C-N-LP} < \pi$, in real situations generally not very different from $\pi/2$) and vice versa. However, this simple rule does not apply to bands at shorter wavelengths which are possibly associated with π−π^* transitions and a more thorough analysis is evidently needed.

Nonplanar amide group represents the inherently chiral chromophore. The detailed interpretation of its experimental circular dichroism requires quantum chemical calculations. We tested 11 variants of ab initio procedures all based on 6-311++G**/CPCM(water)/50 n-states. These mainly included variants of TDDFT which were supplemented by the earlier HF and MP2 methods (see Materials and Methods). The results (see Figure S2 in Supporting Information) revealed that the non-DFT procedures MP2 and HF provided seriously blue-shifted (∼40 nm) bands, while the DFT based procedures exhibit more realistic results. However, there are still discernible differences between particular DFT functionals. The spectra simulated by HSE (wPBEhPBE), PBEPBE, and PBEhPBE functionals give wrong ECD sign pattern even for n−π^* transitions and consequently they appear rather poorly designed for calculations of rotational strengths. On the other hand, the hybrid functionals PBE0 (PBE1PBE), PBEh1PBE, HSE03 (HSE2PBE), HSE06 (HSEh1PBE), B3LYP, and B3PW91 give results consistently matching the experiment more closely.

To investigate the effect of charge transfer between particular amide chromophores within the dilactam molecule we tested also the long-range corrected (LC) hybrid functionals CAM-B3LYP and LC-wPBE (Figure S3 in Supporting Information). Both these LC methods exhibit nearly identical results for the short wavelength region. However, a similar pattern can be obtained also without the LC, indicating thus that in this case either a sufficient description of charge transfer can be achieved even without LC or that the influence of charge transfer is negligible. In addition, LC functionals provide calculated ECD spectra with unrealistically separated n−π^* and π−π^* transitions (∼40 nm for LC methods compared to ∼20 nm with uncorrected functionals). For the above reasons we use functionals which do not include corrections for the long-range interactions.

The analysis of further computational variables−basis set and number of singlet transitions−was performed using standard B3LYP hybrid functional and CPCM(water). From the 11 basis sets only D95++**, 6-311++G**, aug-cc-pVDZ, and aug-cc-pVTZ were chosen for the next calculation. As shown in Figure S4 (Supporting Information), calculations with other basis sets provide spectra which are notably more shifted toward lower wavelengths. The agreement of calculated and experimental data is substantially improved by inclusion of diffuse functions (i.e., aug, ++), while the absence of polarization functions (DGDZVP, DGDTZVP) results in inaccuracies in the lower wavelength region. On the other hand, the addition of extra d and f orbitals to 6-311++G** basis set does not have any effect on the calculated spectra. Dependence on the number of

dx.doi.org/10.1021/jp5063463 | J. Phys. Chem. B 2014, 118, 11100−11108

included singlet transitions is shown in Figure S5 (Supporting Information). Evidently, increase of their number is connected with gradual improvement of the both absorption and ECD spectra toward lower wavelengths. When simulations are compared to the experimental spectra measured down to 180 nm, it is sufficient to use 50 singlet transitions. However, when we deal with farther UV ECD spectra, 70 singlet transitions seem to be the minimum. The methods and basis sets giving the best correspondence with experiment were finally used in combination. All these combinations describe the shape of experimental absorption and ECD spectra relatively well; however, the calculated band maxima are still blue-shifted by about 10−20 nm.

It is probable that at least part of the residual mismatch is caused by the effect of solvent. For solubility reasons the experimental values were taken in rather polar solvents (acetonitrile is our least polar environment) and they exhibit relatively serious band broadening which effectively limits the achievable resolution. As a consequence, some spectral components present themselves only as shoulders. In addition, the calculations include only a simple implicit solvent model (COSMO-PCM) causing the ECD spectra calculated in different solvents to be nearly identical (data not shown). Better calculation would evidently require an explicit solvent model enabling inclusion of the important solute−solvent interactions (perhaps hydrogen bonding of solvent molecules with amide carbonyls). Among the used and tested computational procedures, the PBE0 method in combination with the aug-cc-pVTZ basis set with 70 singlet transitions provides the best match between calculated and experimental data. This combination is then used for the final presentation of computational results (Figure 2 and Table 2).

The calculation reveals that between ∼220−160 nm the spectra of compound **I** are rich in electronic transitions (see Table 2). Instead of the four (two n−π^* plus two π−π^*) bands which for such a dilactam result from a semiempirical calculation, the ab initio theory predicts 24 distinct electronic transitions above 165 nm. Even if we limit our attention to stronger bands visibly contributing to the shape of ECD ($|R| > 1 \times 10^{-39}$ cgs) curves (see again Figure 2 and Table 2), the calculation reveals 11 electronic transitions manifesting themselves in non-negligible manner. Still, the most significant contributions to high intensity bands (mainly in ECD but also in absorption) are due to n−π^* and π−π^* configurations. However, toward higher energies (below ∼185 nm) nearly all transitions contain contributions involving higher unoccupied orbitals of σ^* or Rydberg types which influence the detailed shape of calculated spectra. Contribution of these higher in energy configurations is negligible only for the low-energy transitions. The Rydberg transitions calculated by our procedures below 180 nm might represent computational artifacts probably related to our limited treatment of solvent effects. However, experimental data do not provide in this region a sufficient material for comparison.

Within the spectra of **I** there is a pair of bands calculated at the absolutely lowest energy (transitions 1 and 2 in Table 2) at about 218 nm. The pair exhibits low absorption but considerable ECD intensity. Both its components belong to different symmetry species with respect to molecular C_2 axis (Table 2) and their rotational strengths are mutually opposite in sign. The lower in energy (B-symmetry) component with the transition electric dipole oriented perpendicularly toward the C_2 axis possesses stronger ECD. On the basis of the calculation

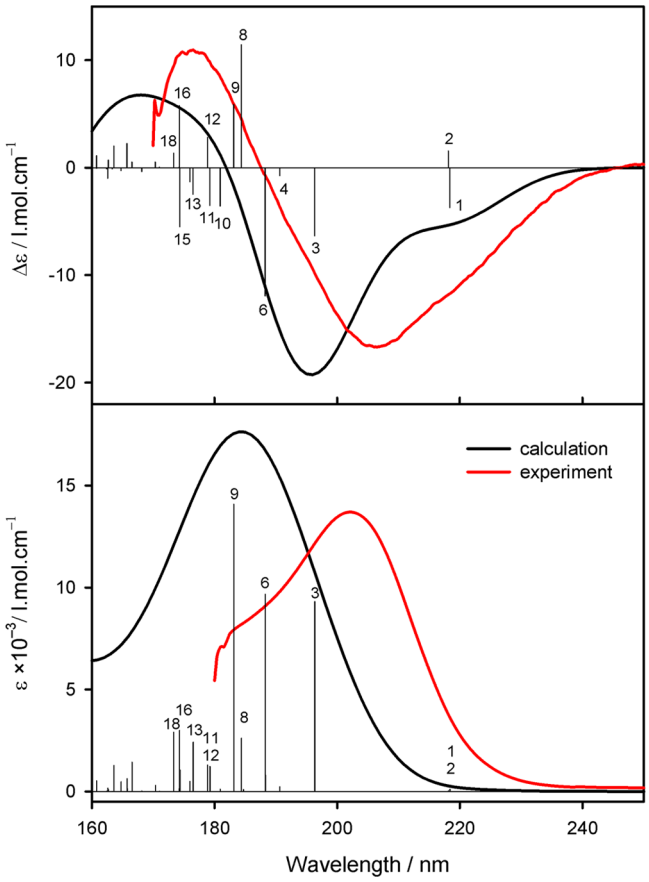

Figure 2. Experimental and calculated (PBE0/aug-cc-pVTZ/CPCM/70 n-states) ECD and absorption spectra of *R*-(−)-**I** in H_2O.

(Table 2), we assign these bands to n−π^* transitions of nonplanar amide groups. Further analysis of computed data reveals that these bands are contributed by >50% of n−π^* configurations. As a manifestation of inherent amide chirality there is an additional contribution (∼30%) of π−π^* configurations in accord with our results achieved earlier with model monoamides.[23] The calculated separation of n−π^* components is very small (<0.4 nm) and, consequently, the corresponding bands cannot be experimentally resolved. Instead, even in dilactams we observe a single CD band (as the truly separated distinct band only in solvents of lower polarity), the sign of which follows the sense of amide group nonplanarity. The ab initio TDDFT calculation of the dilactam **I** confirms the nonplanarity-conditioned interaction of n−π^* and π−π^* configurations which leads to the observed ECD band in the n−π^* transition region. The nonplanarity effect further leads to a bathochromic shift (up to ∼10 nm) of the n−π^* transition which has been already observed in nonplanar monolactams.[7−10,70,71]

Compared to the above simple description of bands due to n−π^* transitions, the pattern of calculated electronic transitions between 170−210 nm which concerns mainly π−π^* electronic configurations is considerably more complex. Calculations indicate 11 electronic transitions between 173−196 nm, whose rotational strengths are large enough ($|R| > 1 \times 10^{-39}$ cgs) to discernibly influence the resulting sum curve. These transitions are listed in Table 2 (no. 3, 6, 8−13, 15, 16 and 18). While most of them exhibit antisymmetric (B) behavior with respect to molecular C_2 axis (3, 6, 8, 9, 12, 13, 16, 18), there are

dx.doi.org/10.1021/jp5063463 | J. Phys. Chem. B 2014, 118, 11100−11108

Table 2. Calculated Absorption and ECD Bands of *R*-(−)-I[a]

n	sym	λ (nm)	D (debye^2)	R (cgs $\times 10^{40}$)	assignment
1	B	218.4	0.06	−18.6	n−π^*(54), π−π^*(28), n−σ^*(5)
2	A	218.1	0.02	7.7	n−π^*(52), π−π^*(29)
3	B	196.3	4.65	−31.7	π−π^*(87)
4	A	190.6	0.12	−3.7	π−π^*(93)
5	A	188.3	0.40	0.0	π−π^*(85)
6	B	188.3	4.83	−59.7	π−π^*(87)
7	A	184.7	0.05	−0.1	π−π^*(61), n−π^*(30)
8	B	184.4	1.31	57.2	n−π^*(58), π−π^*(18), π−Ry*(13)
9	B	183.1	7.04	29.4	π−π^*(65), n−π^*(28)
10	A	180.9	0.1	−17.9	π−Ry*(63), n−π^*(18), π−π^*(11)
11	A	179.3	0.61	−17.6	π−π^*(48), π−Ry*(26), n−π^*(8), π−σ^*(5), n−Ry*(5)
12	B	178.9	0.65	14.1	π−σ^*(92)
13	B	176.5	1.21	−12.4	π−Ry*(65), π−π^*(23)
14	A	176.0	0.25	−6.6	π−π^*(34), π−σ^*(26), n−π^*(20), n−Ry*(9)
15	A	174.4	0.53	−27.5	n−π^*(70), π−σ^*(14)
16	B	174.3	1.50	28.8	n−π^*(75), n−σ^*(11)
17	A	174.2	0.07	0.2	π−σ^*(43), n−π^*(31), n−Ry*(10)
18	B	173.4	1.45	6.8	π−π^*(55), n−π^*(21), π−Ry*(13)
19	A	171.0	0.01	0.2	n−π^*(46), n−Ry*(44)
20	B	170.4	0.15	2.6	n−σ^*(64), n−π^*(20), π−Ry*(7)

[a]Key: n, state; sym, symmetry; D, dipole strength; R, rotational strength.

yet two tight symmetry-related (A−B) couples (11−12, 15−16). However, the dichroic intensities of their components nearly cancel each other (Figure 2). The most important contributions to both ECD and absorption intensities are provided by transitions having B symmetry, which are oriented perpendicularly to C_2 axis. In polypeptides the dominant ECD couplet at 170−210 nm is usually ascribed to dipole-coupled π−π^* transitions. However, in compound **I**, this assignment remains valid only in part. In the calculated spectra, the couplet is defined mainly by transitions 3, 6, 8, and 9. The transitions 10−18 form a wide tail of dichroic absorption at its shorter wavelength side. The transitions 3 and 6 are nearly pure π−π^* (∼90%) states, while the other ones are either nearly pure π−σ^* (12) or exhibit significant proportions of n−π^* configurations (8, 9, 10, 15, 16, 18). This is particularly valid for the transitions 8, 15, and 16 for which the respective n−π^* contributions (58, 70 and 75%) are even dominant. In more general terms, the calculation-aided assignment confirms mutual mixing of n−π^* and π−π^* configurations as the leading mechanism through which the amide nonplanarity manifests itself in chiroptical spectra. While in the n−π^* transition region the chiroptical manifestation follows sense of amide nonplanarity and can be deduced rather simply, in the π−π^* transition region the amide nonplanarity competes with interamide coupling and the result depends on mutual balance of these two effects. The coupling follows the simple exciton chirality rule as described in, e.g., ref 72, and its magnitude depends on mutual orientation of the two interacting oscillators. For the R-enantiomer of **I**, the pseudodihedral angle O(7)···N(2)···N′(2′)···O′(7′) (see Figure 3 in ref 25 for atom numbering) amounts to ∼−150°, i.e., the system is left-handed (and not linear—the pseudobond angles O(7)···N(2)···N′(2′), O′(7′)···N′(2′)···N(2) amount to ∼150°) and the exciton mechanism predicts a couplet having a negative lobe at the longer wavelength. This qualitative estimate is confirmed by our ab initio calculations (Figure 2, Table 2). According to experimental data and the above calculations, the prevailing effect controlling the ECD spectra in the π−π^* transition region consists in the interamide coupling while the contribution of amide nonplanarity has only a minor effect.

The above analysis describes basic features of experimental absorption and ECD data, but there is still a need for more accurate positions of calculated bands (which are systematically blue-shifted ∼10 nm) and for more accurate band widths. Estimation of the latter is complicated by the fact that the observed experimental spectra represent sum curves of several components. Therefore, the band widths estimated directly from experimental data may be inaccurate. Circular dichroism curves may also indicate presence of features not yet accounted for. At about 192 nm, there is a shoulder indicating an additional ECD band. A similar band which appears more pronounced in small molecules having simpler electronic structure, has been observed even earlier in the spectra of small chiral model monolactams between the n−π^* and π−π^* CD bands. At the time of its original observation its tentative interpretation involved three possibilities: (a) vibronic structure of the electronic bands; (b) possible dimer formation; (c) extra valence shell transitions. Some of these possibilities are less probable. Vibronic structure is hard to observe in molecules of low symmetry like **I**. At the same time, the spectra of **I** are not dependent on concentration within the applied range. Hence we do not assume a dimer formation. Our calculations indicate that Rydberg-type transitions actively participate, but their contribution is mainly limited to transitions below 185 nm (transitions 10, 11, 13, 19). Our calculation did not find any participation of the second, lower-in-energy, lone electron pair orbital on the amide oxygen atom. But the observed pattern including additional shoulders can be explained just on the basis of valence-shell-only configurations (the calculations predict that the observed π−π^* couplet actually involves four overlapping transitions—see Table 2 and Figure 2). The observed irregularities and shoulders could then arise from mutual overlap of ECD bands corresponding to these individual components. The additional spectral features are usually observed within spectra of smaller model amides, not in the spectra of peptides/proteins with many overlapping amide

dx.doi.org/10.1021/jp5063463 | J. Phys. Chem. B 2014, 118, 11100−11108

related bands. In the latter case their complex overlap then leads to apparently simple smooth and wide spectral bands. This alternative explanation would imply that particular spectral components are significantly narrower than the often estimated value of 15−20 nm. In our future work we plan to examine this phenomenon in more detail.

In contrast to monolactams investigated earlier, the dilactam **I** contains two nonplanar amide groups having identical geometries. These are embedded in the rigid chiral environment and further constrained by molecular C_2 symmetry. ECD investigation of **I** offers an opportunity to critically evaluate the relative importance of local contributions caused by either inherent chirality of nonplanar amide chromophores (or of minor local effects within environments of single amide groups) with that of the over-the-longer-distance acting amide−amide interaction which is known to control circular dichroism of peptides and proteins, at least in the $\pi-\pi^*$ transition region. Our ECD study of **I** in the extended spectral region (≥170 nm) reveals that nonplanarity can be detected even when more than one amide group is present in the molecule. Amide nonplanarity could be evaluated and related to absolute sense of amide deformation (i.e., absolute configuration) using manifestation of amide $n-\pi^*$ transitions. These ECD bands do not show any coupling-related splitting, and they display the nonplanarity-related bathochromic shift already observed for monolactams. The relation between sign of the $n-\pi^*$ ECD band and the absolute amide geometry follows the earlier established rule,[23] which is based on a somewhat simplistic but explanatory semiempirical description of nonplanar amide ECD. This picture operates with the mixing of $n-\pi^*$ and $\pi-\pi^*$ configurations caused by the asymmetrically acting pyramidal arrangements of bonds to the amide nitrogen.[23] The mixing of occupied N_O and π orbitals causes the $n-\pi^*$ transition to gather partially $\pi-\pi^*$ character and vice versa. According to our calculations the loss of local amide symmetry plane causes some mixing of transitions related to σ framework into shorter wavelength components of $\pi-\pi^*$ states. However, this mixing does not appear too significant similarly to the participation of Rydberg type transitions. The nonplanarity conditioned interaction between $n-\pi^*$ and $\pi-\pi^*$ transitions in our case directly influences the transitions 8 and 9. Nonplanarity seems to influence the $\pi-\pi^*$ couplet in a relatively minor way (enlarging the apparent band widths) and may influence absolute ECD magnitudes. On the other hand, we cannot exclude that these phenomena are influenced by special geometry of the compound **I** (head-to-head connection of the two amide groups in contrast to the more usual head-to-tail connection which exists in peptides/proteins). Therefore, additional studies of planar and nonplanar lactams and detailed calculations in relation to peptide/protein structures would be beneficial.

The compound **I** together with its tetradeuterioderivative has been already investigated by the methods of vibrational optical activity including vibrational circular dichroism (VCD) and Raman optical activity (ROA) spectroscopy and analyzed in detail by ab initio DFT calculations.[25] The amide I vibration which usually describes amide−amide coupling in larger peptides/proteins, provides in **I** single-signed VCD and ROA signals. It seems therefore that the amide I VOA reflects predominantly nonplanar amide chirality, similarly to the above-reported ECD manifestation in the $n-\pi^*$ region. On the other hand, the amide−amide coupling scales down its significance. VCD of the pseudoamide **II** (tertiary amide) vibration shows a dominant couplet which describes amide−amide coupling within the special geometry of **I** (both amide nitrogen atoms are very close to one another and their coupling is therefore very efficient). It seems that some spectral characteristics of ECD and VOA describe very similar properties in parallel. This is particularly valid for the manifestation of amide nonplanarity via $n-\pi^*$ band in ECD and the same effect observed in amide I VOA (VCD and also ROA). Nevertheless, having in mind the known different sensitivity of electronic and vibrational spectroscopy toward longer distance effects, it seems necessary to analyze these observations in more detail. A dramatic example of the effect of differing interchromophoric distance on the eventual existence or nonexistence of the couplet like spectrum can be seen in VCD of pseudoamide **II**. This band usually describes just the local environment of amide bond, not the effects acting over the longer distance. However, in **I** the very short distance between the two amide nitrogen atoms induces a very efficient interchromophoric coupling which results in a strong couplet-like spectrum in this region, in fact this couplet dominates the whole spectrum.

Both electronic and vibrational optical activity confirm the basic fact that amide groups of compound **I** are seriously nonplanar. In extracting the nonplanar amide group properties both methods confirm a bathochromic shift of the very relevant bands ($n-\pi^*$ transition in ECD, amide I vibration in VCD and ROA). These characteristic bands manifest themselves as single chiroptical features, not couplets. In both electronic and vibrational spectroscopy, these bands therefore with high probability reflect the amide nonplanarity as a local phenomenon. Amide-amide coupling is not that easy to discern in detail. It can be detected in ECD as a $\pi-\pi^*$ couplet and also in manifestation of amide II vibration in VCD. However, in latter case our finding is limited to the special geometry of the spirodilactam **I**. The follow up research might utilize the universal nature of ECD and the ease of measuring e.g. temperature dependencies while VOA can perhaps benefit from isotopic substitution. In order to obtain yet more detailed information from ECD it might be helpful to perform experiments at higher wavelength resolution, i.e. in less polar solvents, perhaps using alternative, more soluble compounds.

■ CONCLUSIONS

Experimental studies of the dilactam **I** confirmed that chiroptical spectroscopy can detect nonplanarity of amide groups even in dilactams and that the relation between sense of a nonplanar deformation and signs of observable amide $n-\pi^*$ and $\pi-\pi^*$ bands is not limited to monolactams. In dilactams as well as in monolactams the left handed arrangement of the amide O═C−N−lone electron pair on N pattern leads to a negative sign of CD band corresponding amide $n-\pi^*$ transition (like in *R*-(−)-**I**). Amide nonplanarity causes bathochromic shift of the $n-\pi^*$ transition in dilactams the same way as in model monolactams and this characteristic feature can be utilized for detection purposes. CD bands in the $\pi-\pi^*$ transition region exhibit simultaneous manifestation of amide−amide interaction (leading to a couplet of CD bands) and nonplanarity-induced $n-\pi^*$ $\pi-\pi^*$ mixing analogous to that observed for monolactams (acting mainly on the short wavelength lobe of the couplet). Overall, the $\pi-\pi^*$ transition region involves several perhaps contradictory effects and therefore the amide nonplanarity detection is best based on bands due to amide $n-\pi^*$ transitions.

■ ASSOCIATED CONTENT

Supporting Information

(a) Comparison of ECD spectra of both enantiomers of **I**, (b) effect of ab initio procedure selection on absorption and ECD spectra of **I**, (c) effect of basis set selection on absorption and ECD spectra of **I**, and (d) effect of the number of included singlet transitions on the ECD and absorption spectra of **I**. This material is available free of charge via the Internet at http://pubs.acs.org.

■ AUTHOR INFORMATION

Corresponding Author

*(P.M.) Telephone: 00420-221-911-346. E-mail: malonp@karlov.mff.cuni.cz.

Notes

The authors declare no competing financial interests.

■ ACKNOWLEDGMENTS

This work has been supported by Grant Agency of the Czech Republic (P205-10-1276).

■ REFERENCES

(1) Pauling, L.; Coreu, R. B.; Branson, H. R. The Structure of Proteins; Two Hydrogen-Bonded Helical Configurations of the Polypeptide Chain. *Proc. Natl. Acad. Sci. U.S.A.* **1951**, *37*, 205−211.

(2) Edison, A. S. Linus Pauling and the Planar Peptide Bond. *Nat. Struct. Biol.* **2001**, *8*, 201−202.

(3) Ramachandran, G. N.; Kolaskar, A. S. The Non-Planar Peptide Unit. II. Comparison of Theory with Crystal Structure Data. *Biochim. Biophys. Acta* **1973**, *303*, 385−388.

(4) MacArthur, M. W.; Thornton, J. M. Deviations from Planarity of the Peptide Bond in Peptides and Proteins. *J. Mol. Biol.* **1996**, *264*, 1180−1195.

(5) Dasgupta, A. K.; Majumdar, R.; Bhattacharyya, D. Characterization of Non-Planar Peptide Groups in Protein Crystal Structures. *Indian J. Biochem. Biophys.* **2004**, *41*, 233−240.

(6) Klyne, W.; Kirk, D. N.; Tilley, J.; Suginome, H. Chiroptical Studies-Part 99: The Circular Dichroism of Seven-Membered Lactams and Lactones. *Tetrahedron* **1980**, *36*, 543−553.

(7) Tichý, M.; Dušková, E.; Bláha, K. Optically Active 4-azatricyclo[4,4,0,$0^{3,8}$]decan-5-One: Model of a Non-Planar Amide Bond. *Tetrahedron Lett.* **1974**, *15*, 237−240.

(8) Frič, I.; Maloň, P.; Tichý, M.; Bláha, K. Chiroptical Properties of 4-azatricyclo[4,4,0,$0^{3,8}$]decan-5-One - A Lactam with a Non-Planar Cis-Amide Group. *Collect. Czech. Chem. Commun.* **1977**, *42*, 678−686.

(9) Maloň, P.; Frič, I.; Tichý, M.; Bláha, K. Chiroptical Properties of (−)-4-Methyl-4-azatricyclo[4,4,0,$0^{3,8}$]decan-5-One - A Lactam with a Non-Planar Tertiary Cis-Amide Group. *Collect. Czech. Chem. Commun.* **1977**, *42*, 3104−3110.

(10) Tichý, M.; Farag, A. M.; Maloň, P.; Kálal, P.; Bláha, K. (3*R*)-5-Azatricyclo[4.3.1.$0^{3,8}$]decan-4-One, a Lactam with a Non-Planar *cis*-Amide Group: Synthesis, Geometry and Chiroptical Properties. *Collect. Czech. Chem. Commun.* **1984**, *49*, 834−839.

(11) Maloň, P.; Bystrický, S.; Bláha, K. Non-Planar Amide Group and Its Chiroptical Manifestation. In *Peptides 1978, Proceedings of the 15th European Peptide Symposium*; Wroclaw University Press: Wroclaw, Poland, 1979; pp 269−272.

(12) Bláha, K.; Maloň, P. Non-Planarity of the Amide Group and Its Manifestation. *Acta Univ. Palacki. Olomuc.* **1980**, *93*, 81−96.

(13) Pracejus, von H. 2.2-Dimethyl-Chinuclidon-(6), Ein Mesomeriefreies Saureamid. *Chem. Ber.—Recl.* **1959**, *92*, 988−998.

(14) Pracejus, von H.; Kehlen, M.; Kehlen, H.; Matschiner, H. Neues Zur Sterischen Mesomeriehinderung Bei Lactamen Vom Typ Des A-Chinuclidons. *Tetrahedron* **1965**, *21*, 2257−2270.

(15) Pracejus, von H. Bicyclische Basen Mit Einem Asymmetrischen N-Atom. IV: Die Stereoisomeren 2.2.6-Trimethyl-Chinuclidine Und -Chinuclidone-(7). *Chem. Ber.—Recl.* **1965**, *98*, 2897.

(16) Boyd, D. B.; Riehl, J. P.; Richardson, F. S. Chiroptical Properties of 1-Carbapenam and Orbital Mixing in Nonplanar Amides. *Tetrahedron* **1979**, *35*, 1499−1508.

(17) Shustov, G. V.; Kadorkina, G. K.; Varlamov, S. V.; Kachanov, A. V.; Kostyanovskii, R. G.; Rauk, A. The Nonplanar Amide Group in N-Acylaziridines: Conformational Behavior and Chiroptical Properties. *J. Am. Chem. Soc.* **1992**, *114*, 1616−1623.

(18) Shustov, G. V.; Kachanov, A. V.; Chervin, I. I.; Kostyanovsky, R. G.; Rauk, A. Stereochemistry and Chiroptical Properties of 1,3-Dialkylaziridinones (α-Lactams). Chiral Rules for the Nonplanar Amide Chromophore. *Can. J. Chem.* **1994**, *72*, 279−286.

(19) Maloň, P.; Bystrický, S.; Bláha, K. Semiempirical Calculation of Optical Rotatory Strength of Non-Planar Conformations of Formamide. *Collect. Czech. Chem. Commun.* **1978**, *43*, 781−790.

(20) Tvaroška, I.; Bystrický, S.; Maloň, P.; Bláha, K. Non-Planar Conformations of Methylacetamide: Solvent Effect and Chiroptical Properties. *Collect. Czech. Chem. Commun.* **1982**, *47*, 17−28.

(21) Maloň, P.; Bláha, K. Quantum Chemical Calculations on 4-azatricyclo[4,4,0,03,8]decan-5-One - A Lactam with a Non-Planar Cis-Amide Group. *Collect. Czech. Chem. Commun.* **1977**, *42*, 687−696.

(22) Frelek, J.; Lysek, R.; Borsuk, K.; Jagodziński, J.; Furman, B.; Klimek, A.; Chmielewski, M. Structure-Chiroptical Properties Relationship in Oxabicyclic Beta-Lactam Derivatives. *Enantiomer* **2002**, *7*, 107−114.

(23) Bednárová, L.; Malon, P.; Bour, P. Spectroscopic Properties of the Nonplanar Amide Group: A Computational Study. *Chirality* **2007**, *19*, 775−786.

(24) Smolíková, J.; Koblicová, Z.; Bláha, K. Amino Acids and Peptides. CX. The Infrared Spectra of Polycyclic Spiro-Dilactams with Non-Planar Amide Bonds. *Collect. Czech. Chem. Commun.* **1973**, *38*, 532−547.

(25) Pazderková, M.; Profant, V.; Hodačová, J.; Sebestík, J.; Pazderka, T.; Novotná, P.; Urbanová, M.; Safařík, M.; Buděšínský, M.; Tichý, M.; et al. Nonplanar Tertiary Amides in Rigid Chiral Tricyclic Dilactams. Peptide Group Distortions and Vibrational Optical Activity. *J. Phys. Chem. B* **2013**, *117*, 9626−9642.

(26) Maloň, P.; Barness, C. L.; Buděšínský, M.; Dukor, R. K.; Van der Helm, D.; Keiderling, T. A.; Koblicová, Z.; Pavlíková, F.; Tichý, M.; Bláha, K. (1S,7S)-7-Methyl-6,9-diazatricyclo[6,3,0,01,6]tridecane-5,10-Dione, a Tricyclic Spirodilactam Containing Non-Planar Amide Groups: Synthesis, NMR, Crystal Structure, Absolute Configuration, Electronic and Vibrational Circular Dichroism. *Collect. Czech. Chem. Commun.* **1988**, *53*, 2447−2472.

(27) Bláha, K.; Buděšínský, M.; Koblicová, Z.; Maloň, P.; Tichý, M.; Baker, J. R.; Hossain, M. B.; Van der Helm, D. Optically Active Tricyclic Dilactams with Non-Planar Cis-Amide Groups: Synthesis, X-Ray, NMR and CD Studies. *Collect. Czech. Chem. Commun.* **1982**, *47*, 1000−1019.

(28) Bláha, K.; Buděšinský, M.; Frič, I.; Koblicová, Z.; Maloň, P.; Tichý, M. Polycyclic Dilactams with Inherently Chiral Amide Chromophores. *Tetrahedron Lett.* **1978**, *19*, 3949−3952.

(29) Hussain, R.; Jávorfi, T.; Siligardi, G. Circular Dichroism Beamline B23 at the Diamond Light Source. *J. Synchrotron Radiat.* **2012**, *19*, 132−135.

(30) Frisch, M. J.; Trucks, G. W.; Schlegel, H. B.; Scuseria, G. E.; Robb, M. A.; Cheeseman, J. R.; Scalmani, G.; Barone, V.; Mennucci, B.; Petersson, G. A.; et al. *Gaussian 09*, Revision B.01, Gaussian, Pittsburgh, PA, 2009.

(31) Perdew, J. P.; Burke, K.; Ernzerhof, M. Generalized Gradient Approximation Made Simple. *Phys. Rev. Lett.* **1996**, *77*, 3865−3868.

(32) Perdew, J. P.; Burke, K.; Ernzerhof, M. Generalized Gradient Approximation Made Simple. *Phys. Rev. Lett.* **1996**, *77*, 3865; *Phys. Rev. Lett.* **1997**, *78*, 1396−1396.

(33) Ernzerhof, M.; Perdew, J. P. Generalized Gradient Approximation to the Angle- and System-Averaged Exchange Hole. *J. Chem. Phys.* **1998**, *109*, 3313−3320.

(34) Adamo, C.; Barone, V. Toward Reliable Density Functional Methods without Adjustable Parameters: The PBE0Model. *J. Chem. Phys.* **1999**, *110*, 6158−6170.
(35) Heyd, J.; Scuseria, G. E.; Ernzerhof, M. Hybrid Functionals Based on a Screened Coulomb Potential. *J. Chem. Phys.* **2003**, *118*, 8207−8215.
(36) Heyd, J.; Scuseria, G. E. Efficient Hybrid Density Functional Calculations in Solids: Assessment of the Heyd-Scuseria-Ernzerhof Screened Coulomb Hybrid Functional. *J. Chem. Phys.* **2004**, *121*, 1187−1192.
(37) Heyd, J.; Scuseria, G. E. Assessment and Validation of a Screened Coulomb Hybrid Density Functional. *J. Chem. Phys.* **2004**, *120*, 7274−7280.
(38) Heyd, J.; Peralta, J. E.; Scuseria, G. E.; Martin, R. L. Energy Band Gaps and Lattice Parameters Evaluated with the Heyd-Scuseria-Ernzerhof Screened Hybrid Functional. *J. Chem. Phys.* **2005**, *123*, 174101.
(39) Heyd, J.; Scuseria, G. E.; Ernzerhof, M. Erratum: "Hybrid Functionals Based on a Screened Coulomb Potential. *J. Chem. Phys.* **2003**, *118*, 8207; *J. Chem. Phys.* **2006**, *124*, 219906.
(40) Izmaylov, A. F.; Scuseria, G. E.; Frisch, M. J. Efficient Evaluation of Short-Range Hartree-Fock Exchange in Large Molecules and Periodic Systems. *J. Chem. Phys.* **2006**, *125*, 104103.
(41) Krukau, A. V.; Vydrov, O. A.; Izmaylov, A. F.; Scuseria, G. E. Influence of the Exchange Screening Parameter on the Performance of Screened Hybrid Functionals. *J. Chem. Phys.* **2006**, *125*, 224106.
(42) Henderson, T. M.; Izmaylov, A. F.; Scalmani, G.; Scuseria, G. E. Can Short-Range Hybrids Describe Long-Range-Dependent Properties? *J. Chem. Phys.* **2009**, *131*, 044108.
(43) Becke, A. D. Density-Functional Thermochemistry. III. The Role of Exact Exchange. *J. Chem. Phys.* **1993**, *98*, 5648−5652.
(44) Kim, K.; Jordan, K. D. Comparison of Density Functional and MP2 Calculations on the Water Monomer and Dimer. *J. Phys. Chem.* **1994**, *98*, 10089−10094.
(45) Stephens, P. J.; Devlin, F. J.; Chabalowski, C. F.; Frisch, M. J. Ab Initio Calculation of Vibrational Absorption and Circular Dichroism Spectra Using Density Functional Force Fields. *J. Phys. Chem.* **1994**, *98*, 11623−11627.
(46) Perdew, J.; Burke, K.; Wang, Y. Generalized Gradient Approximation for the Exchange-Correlation Hole of a Many-Electron System. *Phys. Rev. B* **1996**, *54*, 16533−16539.
(47) Yanai, T.; Tew, D. P.; Handy, N. C. A New Hybrid Exchange−correlation Functional Using the Coulomb-Attenuating Method (CAM-B3LYP). *Chem. Phys. Lett.* **2004**, *393*, 51−57.
(48) Vydrov, O. A.; Scuseria, G. E. Assessment of a Long-Range Corrected Hybrid Functional. *J. Chem. Phys.* **2006**, *125*, 234109.
(49) Vydrov, O. A.; Heyd, J.; Krukau, A. V.; Scuseria, G. E. Importance of Short-Range versus Long-Range Hartree-Fock Exchange for the Performance of Hybrid Density Functionals. *J. Chem. Phys.* **2006**, *125*, 074106.
(50) Vydrov, O. A.; Scuseria, G. E.; Perdew, J. P. Tests of Functionals for Systems with Fractional Electron Number. *J. Chem. Phys.* **2007**, *126*, 154109.
(51) Møller, C.; Plesset, M. S. Note on an Approximation Treatment for Many-Electron Systems. *Phys. Rev.* **1934**, *46*, 618−622.
(52) Andersson, K.; Malmqvist, P.-A.; Roos, B. O. Second-Order Perturbation Theory with a Complete Active Space Self-Consistent Field Reference Function. *J. Chem. Phys.* **1992**, *96*, 1218.
(53) Besley, N. A.; Brienne, M.-J.; Hirst, J. D. Electronic Structure of a Rigid Cyclic Diamide. *J. Phys. Chem. B* **2000**, *104*, 12371−12377.
(54) Hirst, J. D.; Hirst, D. M.; Brooks, C. L. Multireference Configuration Interaction Calculations of Electronic States of N -Methylformamide, Acetamide, and N -Methylacetamide. *J. Phys. Chem. A* **1997**, *101*, 4821−4827.
(55) Šebek, J.; Kejík, Z.; Bouř, P. Geometry and Solvent Dependence of the Electronic Spectra of the Amide Group and Consequences for Peptide Circular Dichroism. *J. Phys. Chem. A* **2006**, *110*, 4702−4711.
(56) Ditchfield, R. Self-Consistent Molecular-Orbital Methods. IX. An Extended Gaussian-Type Basis for Molecular-Orbital Studies of Organic Molecules. *J. Chem. Phys.* **1971**, *54*, 724−728.
(57) Dunning, T. H.; Hay, P. J. . In *Modern Theoretical Chemistry*; Shaefer, H. F., Ed.; Plenum: New York, 1976; pp 1−28.
(58) Godbout, N.; Salahub, D. R.; Andzelm, J.; Wimmer, E. Optimization of Gaussian-Type Basis Sets for Local Spin Density Functional Calculations. Part I. Boron through Neon, Optimization Technique and Validation. *Can. J. Chem.* **1992**, *70*, 560−571.
(59) Sosa, C.; Andzelm, J.; Elkin, B. C.; Wimmer, E.; Dobbs, K. D.; Dixon, D. A. A Local Density Functional Study of the Structure and Vibrational Frequencies of Molecular Transition-Metal Compounds. *J. Phys. Chem.* **1992**, *96*, 6630−6636.
(60) Dunning, T. H. Gaussian Basis Sets for Use in Correlated Molecular Calculations. I. The Atoms Boron through Neon and Hydrogen. *J. Chem. Phys.* **1989**, *90*, 1007−1023.
(61) Kendall, R. A.; Dunning, T. H.; Harrison, R. J. Electron Affinities of the First-Row Atoms Revisited. Systematic Basis Sets and Wave Functions. *J. Chem. Phys.* **1992**, *96*, 6796−6806.
(62) Woon, D. E.; Dunning, T. H. Gaussian Basis Sets for Use in Correlated Molecular Calculations. III. The Atoms Aluminum through Argon. *J. Chem. Phys.* **1993**, *98*, 1358−1371.
(63) Peterson, K. A.; Woon, D. E.; Dunning, T. H. Benchmark Calculations with Correlated Molecular Wave Functions. IV. The Classical Barrier Height of the H+H2→H2+H Reaction. *J. Chem. Phys.* **1994**, *100*, 7410−7415.
(64) Schafer, A.; Horn, H.; Ahlrichs, R. Fully Optimized Contracted Gaussian-Basis Sets for Atoms Li to Kr. *J. Chem. Phys.* **1992**, *97*, 2571−2577.
(65) Schafer, A.; Huber, C.; Ahlrichs, R. Fully Optimized Contracted Gaussian-Basis Sets of Triple Zeta Valence Quality for Atoms Li to Kr. *J. Chem. Phys.* **1994**, *100*, 5829−5835.
(66) Klamt, A.; Schuurmann, G. COSMO: A New Approach to Dielectric Screening in Solvents with Explicit Expressions for the Screening Energy and Its Gradient. *J. Chem. Soc. Perkin Trans. 2* **1993**, 799−805.
(67) Klamt, A. C.; Cosmo, R. In *Encyclopedia of Computational Chemistry*; Schleyer, P. R., Allinger, N. L., Eds.; John Wiley & Sons: Chichester, U.K., 1998; pp 604−615.
(68) Gaigeot, M.-P.; Besley, N. A.; Hirst, J. D. Modeling the Infrared and Circular Dichroism Spectroscopy of a Bridged Cyclic Diamide. *J. Phys. Chem. B* **2011**, *115*, 5526−5535.
(69) Hussain, R.; Jávorfi, T.; Siligardi, G. *Comprehensive Chirality*; Elsevier: Amsterdam, 2012; pp 438−448.
(70) Bláha, K.; Maloň, P.; Tichý, M.; Frič, I.; Usha, R.; Ramakumar, S.; Venkatesan, K. Crystal Structure and Chiroptical Properties of (+)-(3S)-4-azatricyclo[4,3,1,03,7]decan-5-One. *Collect. Czech. Chem. Commun.* **1978**, *43*, 3241−3251.
(71) Tichý, M.; Maloň, P.; Frič, I.; Bláha, K. Synthesis and Chiroptical Properties of (−)-(1R)-3-azatricyclo[5,4,0,04,9]undecan-2-One - A Lactam with Non-Planar Cis-Amide Group. *Collect. Czech. Chem. Commun.* **1979**, *44*, 2653−2659.
(72) *Comprehensive Chiroptical Spectroscopy*; Berova, N., Polavarapu, P. L., Nakanishi, K., Woody, R. W., Eds.; John Wiley & Sons: Hoboken, NJ, 2012; Vol. 2.

Electronic Circular Dichroism of the Chiral Rigid Tricyclic Dilactam with Nonplanar Tertiary Amide Groups

Markéta Pazderková,[†,‡] Václav Profant,[†] Beata Seidlerová,[‡] Helena Dlouhá,[‡] Jana Hodačová,[§] Tamas Javorfi,[Δ] Giuliano Siligardi,[Δ] Vladimír Baumruk,[†] Lucie Bednárová,[‡] and Petr Maloň*[,†]

[†]Faculty of Mathematics and Physics, Charles University in Prague, Ke Karlovu 5, 121 16 Prague 2, Czech Republic
[‡]Institute of Organic Chemistry and Biochemistry, Academy of Sciences of the Czech Republic, Fleming sq. 2, 166 10 Prague 6, Czech Republic
[§]Institute of Chemical Technology, Technická 5, 166 28 Prague 6, Czech Republic
[Δ]Diamond Light Source, Chilton, Didcot, Oxfordshire, OX11 0DE, UK

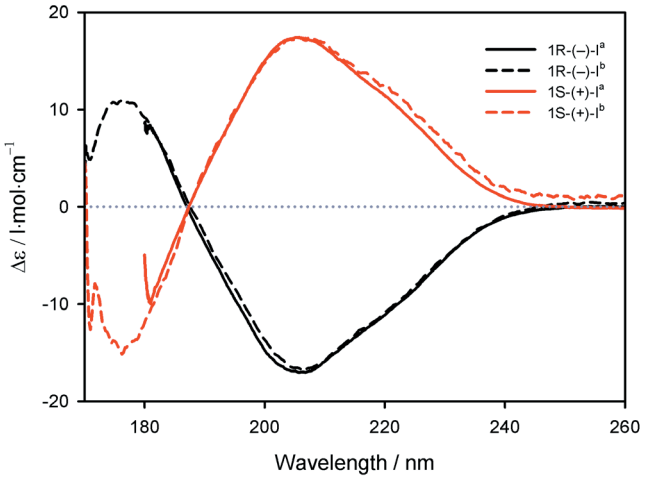

Figure S1. ECD spectra of both enantiomers of I measured in H_2O ([a]measured on stand-alone ECD spectrometer, [b]measured on Diamond B23 circular dichroism beamline).

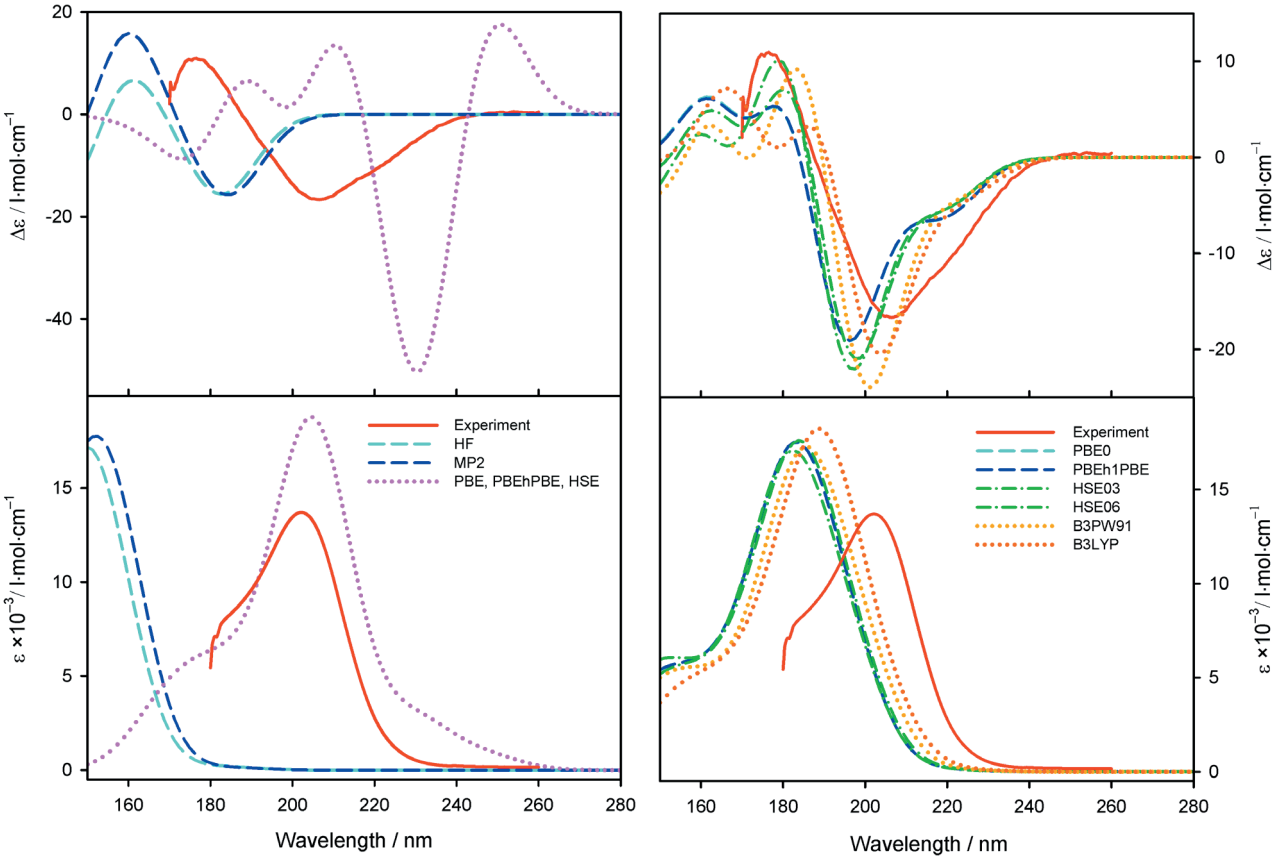

Figure S2. The effect of ab initio procedure selection on the ECD and absorption spectra of *R*-(–)-I (6-311++G**/CPCM (water)/50 *n*-states). Procedures providing better agreement with the experiment are shown on the right side.

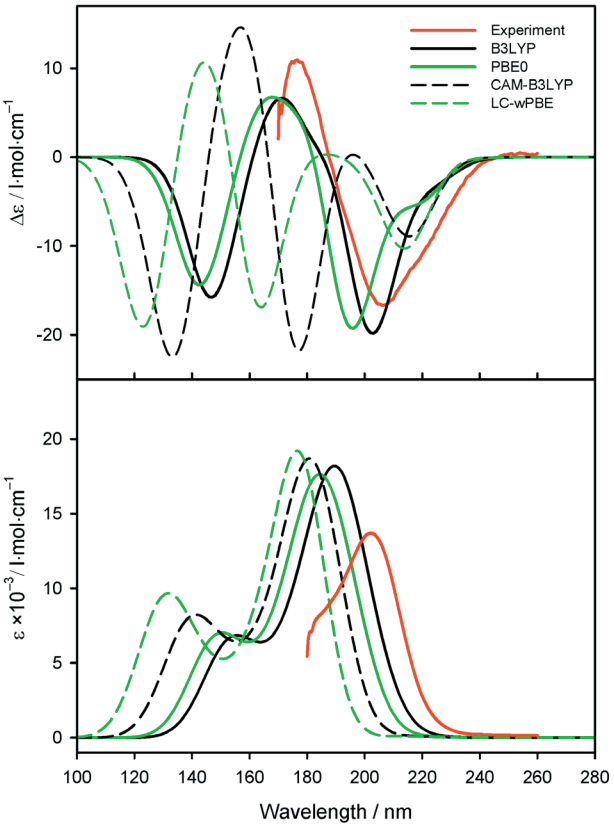

Figure S3. The effect of long-range interaction corrections (CAM-B3-LYP, LC-wPBE) on the calculated ECD and absorption spectra of *R*-(–)-I (aug-cc-pVTZ / CPCM(water) / 70 *n*-states.

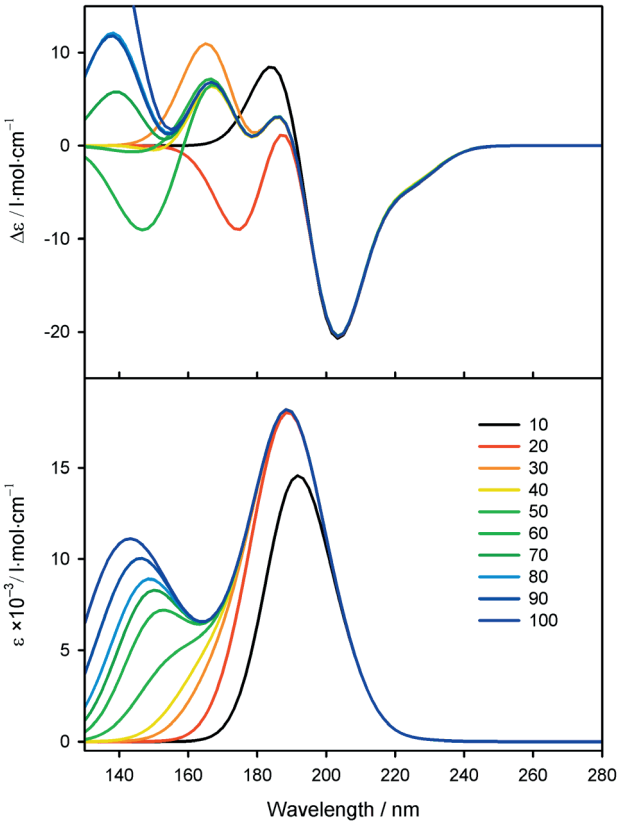

Figure S5. The effect of the number of included singlet transitions on the calculated ECD and absorption spectra of *R*-(–)-I (B3LYP / 6-311++G** / CPCM (water)).

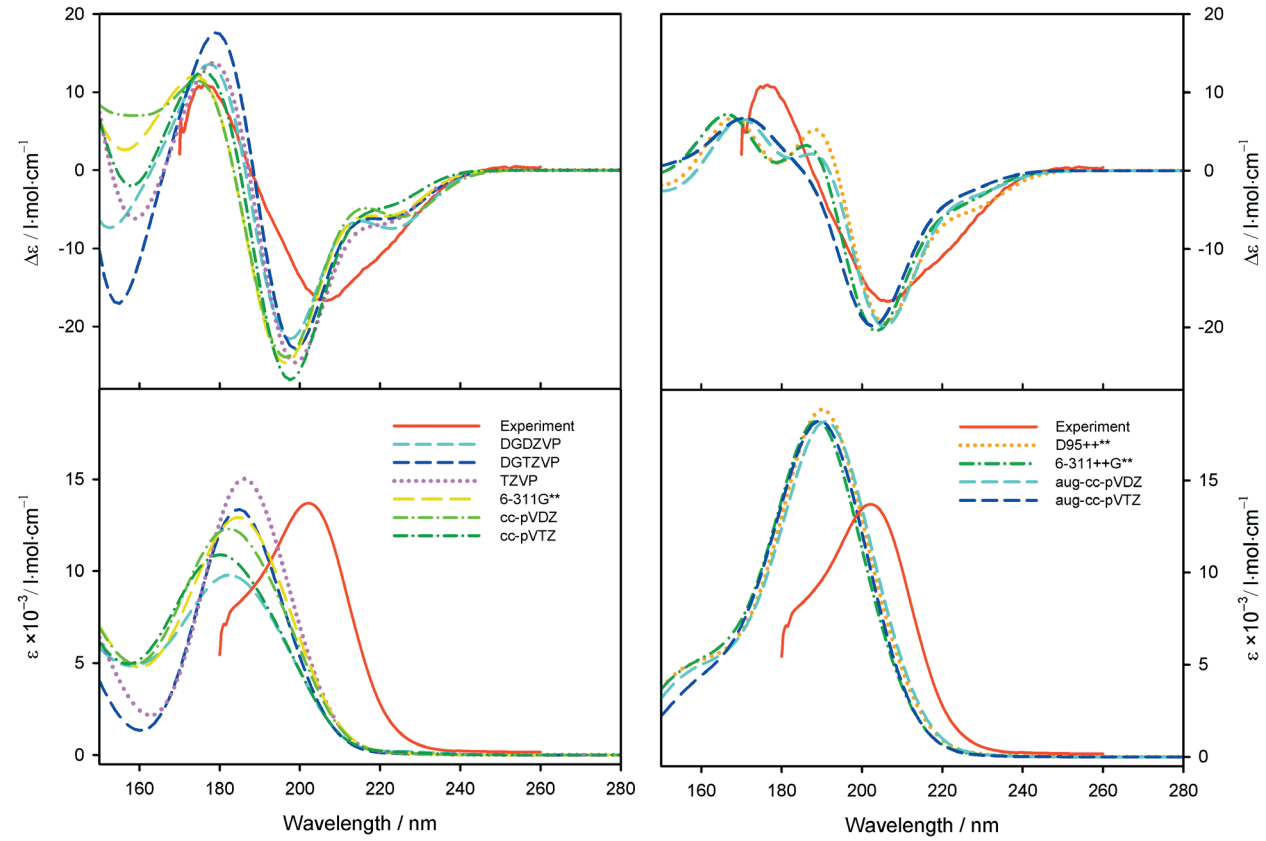

Figure S4. The effect of basis set selection on the ECD and absorption spectra of *R*-(–)-I (B3LYP / CPCM (water) / 50 *n*-states). Basis sets providing better agreement with the experiment are shown on the right side.

Appendix 2

Nonplanar Tertiary Amides in Rigid Chiral Tricyclic Dilactams. Peptide Group Distortions and Vibrational Optical Activity

J. Phys. Chem. B 2013, 117, 9626–9642

Pazderková, M.,[1,2] Profant, V.,[2] Hodačová, J.,[3] Šebestík, J.,[1] Pazderka, T.,[2] Novotná, P.,[3] Urbanová, M.,[3] Šafařík, M.,[1] Buděšínský, M.,[1] Tichý, M.,[1] Bednárová, L.,[1] Baumruk, V.,[2] Maloň, P.,[1,2]

[1]*Institute of Organic Chemistry and Biochemistry, AS CR, Fleming square 2, 166 10 Prague 6, Czech Republic*
[2]*Charles University in Prague, Faculty of Mathematics and Physics, Ke Karlovu 5, 121 16 Prague 2, Czech Republic*
[3]*Institute of Chemical Technology, Technická 5, 166 28 Prague 6, Czech Republic*

THE JOURNAL OF PHYSICAL CHEMISTRY B

Article

pubs.acs.org/JPCB

Nonplanar Tertiary Amides in Rigid Chiral Tricyclic Dilactams. Peptide Group Distortions and Vibrational Optical Activity

Markéta Pazderková,[†,‡] Václav Profant,[‡] Jana Hodačová,[§] Jaroslav Šebestík,[†] Tomáš Pazderka,[‡] Pavlína Novotná,[§] Marie Urbanová,[§] Martin Šafařík,[†] Miloš Buděšínský,[†] Miloš Tichý,[†] Lucie Bednárová,[†] Vladimír Baumruk,[‡] and Petr Maloň*[,†,‡]

[†]Institute of Organic Chemistry and Biochemistry AS CR, 166 10 Prague 6, Czech Republic

[‡]Charles University in Prague, 121 16 Prague 2, Czech Republic

[§]Institute of Chemical Technology, 166 28 Prague 6, Czech Republic

Supporting Information

ABSTRACT: We investigate amide nonplanarity in vibrational optical activity (VOA) spectra of tricyclic spirodilactams 5,8-diazatricyclo[6,3,0,0^{1,5}]undecan-4,9-dione (I) and its 6,6′,7,7′-tetradeuterio derivative (II). These rigid molecules constrain amide groups to nonplanar geometries with twisted pyramidal arrangements of bonds to amide nitrogen atoms. We have collected a full range vibrational circular dichroism (VCD) and Raman optical activity (ROA) spectra including signals of C−H and C−D stretching vibrations. We report normal-mode analysis and a comparison of calculated to experimental VCD and ROA. The data provide band-to-band assignment and offer a possibility to evaluate roles of constrained nonplanar tertiary amide groups and rigid chiral skeletons. Nonplanarity shows as single-signed VCD and ROA amide I signals, prevailing the couplets expected to arise from the amide−amide interaction. Amide−amide coupling dominates amide II (mainly C′−N stretching, modified in tertiary amides by the absence of a N−H bond) transitions (strong couplet in VCD, no significant ROA) probably due to the close proximity of amide nitrogen atoms. At lower wavenumbers, ROA spectra exhibit another likely manifestation of amide nonplanarity, showing signals of amide V (δ_{oop}(N−C) at ∼570 cm^{-1}) and amide VI (δ_{oop}(C′═O) at ∼700 cm^{-1} and ∼650 cm^{-1}) vibrations.

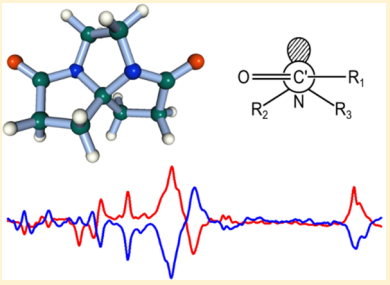

INTRODUCTION

An amide group can easily adopt a minor degree of nonplanarity as has been shown quite decisively on the basis of X-ray studies.[1,2] However, indication that this important group may be nonplanar dates back to its original formulation as a planar unit some 60 years ago.[3] Even Pauling's concept included a notion that the amide is somewhat flexible and small but distinct (and maybe important) deviations from the ideally planar trans or cis arrangements are possible.[4] The original view assumed a partial double bond character of the C′−N bond (about 40%) and counted with feasible modest angular deviations from planarity of 10−20° (causing an energy increase of a few kcal/mol). For peptides and proteins the potential amide nonplanarity can have important consequences. It may alter geometries, increase basicity of the amide nitrogen and influence important biochemical processes. It introduces an additional degree of conformational freedom for each amino acid residue in the form of the angle ω besides the angles Φ and Ψ. This has been analyzed first by Ramachandran et al.,[5] who examined structures of small model amides (like *N*-methylacetamide)[6,7] and X-ray data of small peptide molecules,[5,6,8] which have been known at the time with sufficient accuracy. They established that amide deformations are not just simple rotations around the C′−N bond (as given by the angle ω and easily obtainable from X-ray data), but they involve an improper rotation giving rise to a pyramidal arrangement of bonds to the amide nitrogen (χ_N). It leads to a partial change of nitrogen hybridization ($sp^2 \rightarrow sp^3$). Amide nonplanarity has been quantitatively characterized using angular parameters $\Delta\omega$, Θ_N, $\Theta_{C'}$[5] or alternatively ω, χ_N, $\chi_{C'}$, τ, τ'[9] (see Table 1 and Figure 1 for definitions). The least energy path toward pyramidal amide nitrogen follows at each point the approximate equation $\Theta_N \approx -2\Delta\omega$.[6] In this way the axis of the nitrogen lone electron pair remains approximately coplanar with the carbonyl π system, and the stabilizing $\pi-\pi$ type interaction between them remains maximized.

High accuracy X-ray data allowed to assemble several statistical analyses of critically selected protein structures.[1,2,10,11] Evaluation of amide nonplanarity showed that it occurs quite frequently. However, the attempts to correlate its abundance with particular structural features within a protein sequence remain inconclusive. These include occurrence of nonplanar amides within regular peptide conformations or a preference for particular handedness (chiral form) of the nonplanar amide in peptide/protein sequence. The suggested association of nonplanar amides with active sites of enzymes was shown not

Received: May 27, 2013
Revised: July 16, 2013
Published: July 18, 2013

dx.doi.org/10.1021/jp405226k | *J. Phys. Chem. B* 2013, 117, 9626−9642

Table 1. Angular Parameters Describing Nonplanarity of the Amide Group[9]

basic conformational angles
$\omega_1 = \omega(C_1^{\alpha}-C'-N-C_2^{\alpha})$
$\omega_2 = \omega(O=C'-N-H)$
$\omega_3 = \omega(O=C'-N-C_2^{\alpha})$
$\omega_4 = \omega(C_1^{\alpha}-C'-N-H)$
interrelated by:
$(\omega_1 + \omega_2) - (\omega_2 + \omega_3 + \omega_4) = 0 \pmod{2\pi}$
$\lvert\omega_1 - \omega_2\rvert < \pi$
amide nonplanarity parameters
$\chi_{C'} \equiv \Theta_{C'} = \omega_1 - \omega_3 + \pi = -(\omega_2 - \omega_4) + \pi \pmod{2\pi}$
$\chi_N \equiv -\Theta_N = \omega_2 - \omega_3 + \pi = -(\omega_1 - \omega_4) + \pi \pmod{2\pi}$
$\tau = 0.5(\omega_1 + \omega_2)$
$\tau' = 2\tau$
$\Delta\omega = \omega_1 \{-\pi/2 \le \omega_1 \le \pi/2\}; \pi - \omega_1 \{-\pi \le \omega_1 \le \pi/2; \pi/2 < \omega_1 \le \pi\}$

to be valid.[10] Moreover, nonplanarities of secondary amides (i.e., all amide groups within peptides/proteins excepting those in X-Pro bonds) are not fully specified on the sole basis of X-ray data. The positions of hydrogen atoms are quite inaccurate, if given at all, and consequently, the angles Θ_N, respectively χ_N, τ, τ' are not experimentally accessible. In addition, N−H bonds in amides are polarized and the positions of centroids of H-electron cloud (where the diffraction occurs) do not correspond to nuclear positions. The positions of amide hydrogens are influenced by hydrogen bonding within the crystal. Thus there is a need for a procedure which would enable studies in solution. Unfortunately, the conformational angles of interest are not accessible by NMR. Therefore it seems necessary to utilize other methods like molecular spectroscopy that, despite its lower resolution, offers a distinct advantage of experimental simplicity and selective sensitivity toward, e.g., amide nonplanarity. A nonplanar amide group is a locally nonsymmetrical structure and represents an inherently chiral chromophore (at least in electronic spectra), which makes it approachable by chiroptical techniques. Chiroptical manifestation of such inherently chiral nonplanar amide chromophores has been observed first by Tichy et al.[12] and subsequently analyzed by us in a series of papers using rigid chiral monolactams derived from twistane skeleton[13−18] and other spectroscopic studies.[19−21] Later, other groups utilized 7-membered ring lactams[22] and small ring systems containing chiral aziridinones[22−24] and azetidinones[23−25] or models derived from penicillamine.[26,27] The latter compounds suffer a disadvantage of having bond angles on the amide nitrogen severely distorted by their incorporation into angularly strained three- or four-membered rings. Electronic circular dichroism (ECD) studies including experiments on model lactams and even early semiempirical calculations (at the time mostly CNDO, but later also ab initio and DFT) on models like formamide[26−30] or *N*-methylacetamide[7,31−33] exhibited observable effects of nonplanar deformations on amide electronic transitions. It was also possible to establish basic relations between sense (i.e., handedness) of nonplanarity and signs of amide dichroic bands. It is evident that the observed effects in electronic spectra are conditioned by interactions between the two most prominent n−π^* and $\pi-\pi^*$ electronic configurations of the amide chromophore, which take place only under the condition of amide nonplanarity.[19,20,28] These interactions lead to a significant bathochromic shift of the n−π^* absorption/dichroic band (up to ∼10 nm depending on magnitude of nonplanar deviation) and to a pair of prominent dichroic bands with mutually opposite signs and nearly equal intensities, which are due to n−π^* and $\pi-\pi^*$ transitions.[28] In ECD spectra these bands resemble a couplet; however, the two components are of different electronic origins. The signs of these bands are related to handedness of the O=C′−N−LP (LP, lone electron pair) grouping as depicted in Figure 2. The right-handed arrangement (P-helicity) leads to a positive-negative combination of signs for the respective n−π^* and $\pi-\pi^*$ bands (Figure 2). In electronic absorption and CD spectra we cannot distinguish between cis- or trans-like amides since the corresponding O=C′−N−LP arrangements are equivalent.[28] These results were achieved with model monolactams and it is still unproven but quite probable that even in systems with many amide groups the dichroic manifestation of amide nonplanarity would be found close to the red end of n-π^* transition region. Even small (but consistently repeating) nonplanar deviations can be spectroscopically observable if they exist in segments of regular spatial structures.[34] On the basis of ECD spectroscopy, the findings on amide nonplanarity are indicative and useful, but yet hardly a final proof of particular three-dimensional arrangement. Further support can be obtained from vibrational spectroscopy including chiral variants, vibrational circular

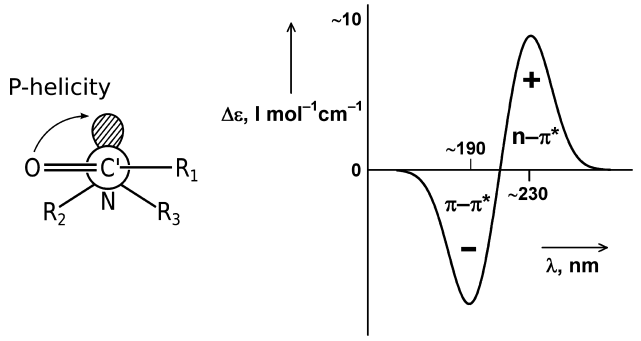

Figure 2. Relation between handedness of nonplanar amide and predicted signs of ECD bands.

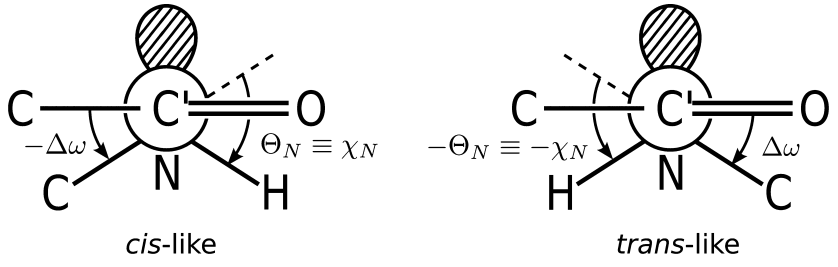

Figure 1. Nonplanar amide group, symbol definitions.

dx.doi.org/10.1021/jp405226k | J. Phys. Chem. B 2013, 117, 9626−9642

dichroism (VCD), and Raman optical activity (ROA; see refs 35−37 and references therein). Chiral vibrational spectroscopy combines sensitivity of chiroptical methods to spatial arrangement of molecules with the bonding detail, which is discernible from vibrational spectra. The observed molecular vibrations occur mostly in the well-defined electronic ground state while the spectrum itself is influenced by internal forces in addition to molecular geometries and charge distributions.[36] It is therefore rich in structural information if particular effects can be separated from one another. Compared to electronic spectra, molecular vibrations represent a more localized phenomenon, and we can expect that local effects including manifestation of amide nonplanarity might be relatively enhanced when compared to global couplings involving large parts of the molecule. Unlike ECD, vibrational spectroscopy can also distinguish between trans- and cis-like amide groups because local vibrational couplings are different. However, our initial attempts to record *cis*-amide VCD of monolactams derived from twistane were not successful. These models did not exhibit any amide-related VCD that would be larger than experimental noise despite the fact that they showed strong VCD signals in C−H stretching and C−H deformation regions. The internal couplings between N−H and N−C stretching and deformation motions in cis-like configurations probably do not represent efficient sources of vibrational circular dichroism. Starting with this assumption and considering the difficulty of preparing model compounds having well-defined trans-like nonplanar amide groups we turned our attention toward models involving tertiary amides. Within these compounds the interactions of N−C bonds with the carbonyl are maintained in both trans- and cis-like arrangements and allow evaluating their relative significance for the induction of vibrational optical activity. It is easier to design suitable models containing potentially nonplanar tertiary amides. These can include peptides with X-Pro connections or structures containing non-natural 2-azetidinecarboxylic (Aze) or pipecolic (Pip) acid residues. More rigid environments defining geometries of embedded functional groups can be realized on the basis of terpene-like structures. These polycyclic chiral compounds (like camphor or α-pinene) often serve as standards for development of VOA instrumentation as they possess strong, clearly identifiable signals.[37,38] We have already examined ECD of similar polycyclic nonplanar tertiary amides using a twistane-related lactam,[15,16] some of our polycyclic dilactams[39−41] and cyclic di- or tripeptides containing Pro or Aze residues.[42]

For the present vibrational optical activity (VOA) study we selected model compounds I and its tetradeuterio derivative II (Scheme 1), belonging to a larger group of polycyclic spirodilactams (Scheme 2).[39] Racemic I has been known since 1973,[43] but sufficient quantities of optically pure enantiomers were prepared only recently. As models simulating properties of nonplanar amide groups, I and II offer significant advantages. Due to their polycyclic frameworks, these compounds are entirely rigid, but because they are composed of five- and six-membered rings only, the overall angular strain is not excessive and the distribution of forces may stay representative even when compared with other, less constrained lactam molecules. When not further substituted, these compounds are of C_2 symmetry. This fact has two important consequences. Symmetry properties aid with assignment of molecular vibrations (see below). The crystals of compounds having higher symmetry are generally easier to prepare and analyze. The dilactams under study possess well-defined geometries which represent fixed points in our studies and are mostly known from crystallographic results.[40,44−47] It is therefore not necessary to investigate complex conformational equilibria and theoretical calculations of vibrational properties become easier. In several cases it was even possible to determine absolute configuration using Bijvoet method of anomalous X-ray diffraction.[40,47] Furthermore, the dilactams contain pairs of interacting homoconjugated amide groups, which allow us to compare and analyze the relative significance of local effects within one nonplanar amide group vs coupling between two amide groups under C_2 symmetry of the molecule. Although in these compounds the interacting amide groups are connected in a "head-to-head" manner, which is different from the usual "head-to-tail" connections within the peptide chain, we can still judge upon the ability of the used theoretical procedure to provide well balanced calculated vibrational properties of oligo- or even poly-amides. Rigidity of our spirodilactams facilitates getting accurate knowledge of their geometries but, on the other hand, complicates transferability of force field because it influences values of force constants, vibrational, and VOA spectra. Our analysis must take into account that spirodilactams containing tertiary amide groups exhibit somewhat different vibrational properties from those typical for the more frequent (and biologically relevant) secondary amides. Tertiary amides do not include N−H bonds, which hence cannot take part in vibrational motion. The changes show particularly in 400−1500 cm^{-1} region. Composition of amide vibrational modes has been thoroughly investigated in secondary amides, resulting in a classification into amide I−amide VI vibrations.[48] The data on tertiary amides are less detailed, being essentially limited to models like *N*,*N*-dimethylacetamide[49] or peptidic compounds containing proline residue.[50] The structural differences influence mainly the important amide II and amide III vibrational modes. In secondary amides these modes are typically described as the respective symmetric and antisymmetric combinations of mutually coupled C′−N stretching and N−H in-plane deformation modes. There is no such coupling in tertiary amides and C′−N stretching vibration is red-shifted about 100

Scheme 1. Structures of Spirodilactams I and II

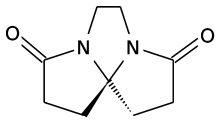

(−)-(1R)-I

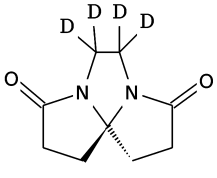

(−)-(1R)-II

Scheme 2. Polycyclic Spirodilactams III-IX

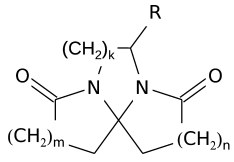

III: k=1; m=n=2; R=H
IV: k=m=1; n=2; R=H
V: k=m=n=1; R=isobutyl
VI: k=m=n=1; R=methyl
VII: k=1; m=n=2; R=methyl

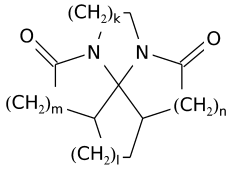

VIII:k=l=m=n=1
IX: k=2; l=m=n=1

dx.doi.org/10.1021/jp405226k | J. Phys. Chem. B 2013, 117, 9626−9642

cm^{-1} from the usual amide II position in secondary amides.[48] It also exhibits altered mode composition. Consequently, the other component in the combination (showing itself as the strongly Raman active amide III band in secondary amides typically at ∼1300 cm^{-1}) is not present. In the corresponding region we sometimes observe weak residual coupling of skeletal N−C stretching vibrations with CH_2 deformations or other skeletal stretches. In summary, our spirodilactams exhibit some specific structural features (rigidity and possibly complicated internal vibrational coupling within the tricyclic skeleton) which should be analyzed before generalization.

In the present paper we investigate vibrational and VOA properties of compounds I and II, while electronic and ECD spectra will be analyzed separately. These dilactams represent the simplest possible case with only five-membered rings. They are easy to synthesize from available precursors (a condensation of 4-oxoheptanedioic acid ester with ethylene diamine), and their geometries and absolute configurations are known. The absolute configuration assignment is based on a correlation of ECD spectrum of I with that of its methyl- and isobutyl derivatives V and VI (Scheme 2).[13] Absolute configurations of V and VI were previously determined by anomalous X-ray diffraction and by a correlation to known compounds.[40,47] We supplement spectra of I with data of the tetradeuterio derivative II in order to aid the assignment of vibrational modes. The latter compound also offers a possibility to record ROA due to C-D stretching vibrations.

In our dilactams we intend to identify effects of amide nonplanarity on vibrational and VOA spectra which can be separated from manifestation of the tricyclic framework. We will complement the already partially described experimental VCD spectra of I with those of II[40,47] and with the still unknown ROA data and correlate them with DFT calculations. In addition, we will try to identify vibrations of the tricyclic frame and to evaluate their sensitivity toward modifications and interactions with amides. A successful band-to-band comparison of calculated and experimental vibrational and VOA spectra should help us with interpretation of related data of flexible molecules involving trans-like secondary amides, which are more difficult to analyze. Results of these investigations should then provide means of detecting nonplanar amide groups in less extreme situations, e.g., in peptides/proteins.

MATERIALS AND METHODS

Melting points were determined on a Kofler block and are uncorrected. The reagents needed for the synthesis were purchased from Sigma Aldrich and Merck (spectral grade solvents) and used without further purification. Enantioselective HPLC analyses were carried out using a Knauer Smartline instrument assembly (pump model 1000, UV detector model 2500 followed by the polarimetric detector, Chiralyser). HPLC preparative separations of enantiomers were done using an Agilent 1100 Series instrument. Chiral stationary phase Eurocel 01 (Knauer, particle size 5 μm) was used for both analytical (250 × 4.6 mm) and preparative (250 × 20.0 mm) columns employing a heptane −2-propanol (70: 30) mixture as the mobile phase (flow rates: analytical 1 mL/min, preparative 20 mL/min). In the preparative runs the solution of a racemate (20−25 mg) in ethanol was repeatedly injected on the column. The separated peaks were detected by the absorption at 210 nm and in the analytical mode also polarimetrically. In all cases the enantiomers completely separated with at least 3 min eluting time between the peaks, and the enantiomer eluting from the column first was laevorotatory. Fractions containing the same enantiomers were combined and evaporated. The enantiomers were prepared in milligram quantities and in optically pure state. High resolution electrospray mass spectra were measured using LTQ Orbitrap XL (Thermo Fisher Scientific hybrid FT mass spectrometer combining a linear ion trap MS with the Orbitrap mass analyzer). The samples were dissolved in MeOH. The mobile phase was a MeOH/H_2O mixture (80:20), and the flow rate was 100 μL/min. The following conditions were optimized for suitable ionization in the ESI source: sheath gas flow rate 35 au, aux gas flow rate 10 au of nitrogen, source voltage 4.3 kV, capillary voltage 40 V, capillary temperature 275 °C, and tube lens voltage 155 V. Structures of compounds I and II were confirmed by ^1H and ^{13}C NMR spectra which were measured on a Bruker AVANCE 600 instrument (^1H at 600.13 MHz; ^{13}C at 150.9 MHz) in $CDCl_3$ and C_6D_6 at 300 K. Structural assignment of signals was achieved using the 2D-H,H-COSY and 2D-H,C-HSQC spectra. The use of C_6D_6 removed the overlap of protons H_8, $H_{8'}$ with H_{11}, $H_{11'}$. The presence of the C_2 axis results in the observation of a reduced number of signals due to symmetry equivalence. In compound II the deuteration at C_6 and $C_{6'}$ resulted in disappearance of H_{12}, $H_{12'}$, H_{13}, and $H_{13'}$ signals in ^1H NMR spectra. The presence of CD_2 groups manifests itself by triplets of carbon atoms C_6 and $C_{6'}$ with $^1J(C, D) \approx 19$ Hz and line broadening caused by two $^2J(C, D)$ couplings and by the high-field isotopic shifts of other carbon signals. ECD measurements were carried out using Jasco J-815 dichrograph in acetonitrile and 2,2,2-trifluoroethanol. We employed concentrations of ∼2.10^{-3} mol L^{-1} and a quartz cell with the optical path length of 0.5 mm. The ECD and absorption values were expressed as the respective values of $\Delta\varepsilon$ and ε [L mol^{-1} cm^{-1}].

5,8-Diazatricyclo[6,3,0,$0^{1,5}$]undecane-4,9-dione (I). Equimolar amounts of diethyl 4-oxoheptanedioate[43] (25.1 g, 109 mmol) and ethylene diamine (7.3 mL, 109 mmol) were heated at 120 °C for 3 days. The solidified reaction mixture was washed with ether/acetone (3:1) and ethyl acetate (3 × 4 mL) and further crystallized first from ethanol and then from water. Yield 5.45 g (30 mmol, 28%) of white crystalline racemic solid, mp 192−193 °C (literature[43] gives mp 190 °C). ^1H NMR: For $C_9H_{12}N_2O_2$ (180.2) calculated 59.99% C, 6.71% H, 15.55% N; found 59.72% C, 6.76% H, 15.53% N. ESI-HRMS: m/z $[M+H]^+$ 181.09715 corresponds to the formula $C_9H_{12}N_2O_2$+H (181.09715) with the error of −0.021 ppm. ^1H NMR (600.1 MHz; $CDCl_3$): 2.04 (m, H_{10} and $H_{10'}$); 2.45 (m, H_{11} and $H_{11'}$); 2.46 (m, H_8 and $H_{8'}$); 2.79 (m, H_9 and $H_{9'}$); 2.88 (m, H_{13} and $H_{13'}$); 4.04 (m, H_{12} and $H_{12'}$). ^1H NMR (600.1 MHz; C_6D_6): 1.17 (m, H_{10} and $H_{10'}$); 1.38 (m, H_{11} and $H_{11'}$); 1.88 (m, H_8 and $H_{8'}$); 2.01 (m, H_9 and $H_{9'}$); 2.09 (m, H_{13} and $H_{13'}$); 3.60 (m, H_{12} and $H_{12'}$). ^{13}C NMR (150.9 MHz; $CDCl_3$): 177.06 (C_3 and $C_{3'}$); 87.85 (C_1); 43.76 (C_6 and $C_{6'}$); 35.81 (C_5 and $C_{5'}$); 32.63 (C_4 and $C_{4'}$). ^{13}C NMR (150.9 MHz; C_6D_6): 175.73 (C_3 and $C_{3'}$); 86.85 (C_1); 43.27 (C_6 and $C_{6'}$); 35.31 (C_5 and $C_{5'}$); 32.28 (C_4 and $C_{4'}$).

(−)-(1R)-I. 64 mg, mp 115−117 °C; found 59.96% C, 6.68% H, 15.51% N; $[\alpha]_D^{20} = -28.5°$ (c = 0.6, ethanol). ECD (water) ($\lambda/\Delta\varepsilon$): 220/−9.5, shoulder; 210/−12.5, maximum; 190/0, zero crossing.

(+)-(1S)-I. 58 mg, mp 115−118 °C; found 60.17% C, 6.72% H, 15.52% N; $[\alpha]_D^{20} = +28.7°$ (c = 0.3, ethanol). ECD (water) ($\lambda/\Delta\varepsilon$): 220/+9.5, shoulder; 210/+13, maximum, 190/0, zero crossing.

dx.doi.org/10.1021/jp405226k | J. Phys. Chem. B 2013, 117, 9626−9642

6,6,7,7-Tetradeuterio-5,8-diazatricyclo[6,3,0,$0^{1,5}$]-undecane-4,9-dione (II). Prepared analogously from diethyl 4-oxoheptanedioate (1.048 g, 4.55 mmol) and 1,1,2,2-tetradeuterio-1,2-diaminoethane (0.276 g, 4.31 mmol, Isotech 426245). The sealed reaction mixture was heated at 93−95 °C for 4 days. The crude product was crystallized from water yielding 90 mg (0.50 mmol, 11%) of the racemate, mp 188−190 °C. For $C_9H_8D_4N_2O_2$ (184.2) calculated 58.68% C, 6.57% H, 15.21% N (% H corrected for deuterium content). Neither NMR nor mass spectrometry revealed presence of detectable amounts of other isotopomers. ESI-HRMS: m/z $[M+H]^+$ 185.12213 corresponds to the formula $C_9H_8D_4N_2O_2$ +H (185.12226) with the error of −0.684 ppm. ^{1}H NMR (600.1 MHz; $CDCl_3$): 2.04 (m, H_{10} and $H_{10'}$); 2.45 (m, H_{11}, $H_{11'}$); 2.46 (m, H_8 and $H_{8'}$); 2.78 (m, H_9 and $H_{9'}$). ^{1}H NMR (600.1 MHz; C_6D_6): 1.16 (m, H_{10} and $H_{10'}$); 1.39 (m, H_{11} and $H_{11'}$); 1.87 (m, H_8 and $H_{8'}$); 2.01 (m, H_9 and $H_{9'}$). ^{13}C NMR (150.9 MHz; $CDCl_3$): 177.21 (C_3 and $C_{3'}$); 87.86 (C_1); 43.23 (t, J(C,D) = 19 Hz, C_6 and $C_{6'}$); 35.96 (C_5 and $C_{5'}$); 32.75 (C_4 and $C_{4'}$). ^{13}C NMR (150.9 MHz; C_6D_6): 175.71 (C_3 and $C_{3'}$); 86.73 (C_1); 42.42 (t, J(C,D) = 19 Hz, C_6 and $C_{6'}$); 35.14 (C_5 and $C_{5'}$); 32.11 (C_4 and $C_{4'}$).

(−)-(1R)-II. 35 mg, mp 118−120 °C; found 58.65% C, 6.75% H, 14.66% N; $[\alpha]_D^{20}$ = −28.9° (c = 0.2, ethanol). ECD (water) ($\lambda/\Delta\varepsilon$): 220/−10, shoulder; 208/−14, maximum; 190/0, zero crossing.

(+)-(1S)-II. 34 mg, mp 118−119 °C; found 58.39% C, 6.67% H, 14.74% N; $[\alpha]_D^{20}$ = +29.3° (c = 0.2, ethanol). ECD (water) ($\lambda/\Delta\varepsilon$): 220/+10, shoulder; 208/+14, maximum, 190/0, zero crossing.

Vibrational Spectroscopy. We measured vibrational spectra throughout complete available spectral ranges. IR absorption was measured on Bruker Equinox 55 in $CHCl_3$/$CDCl_3$ pellets or in KBr solutions using a cell with KBr windows and a fixed path length of 0.118 mm. The spectra (see the Supporting Information) were recorded with the resolution of 2 cm^{-1} and are presented as transmittance vs wavenumbers. Vibrational circular dichroism was measured alternately on two Bruker FTIR spectrometers, both of them equipped with VCD/IRRAS modules. Each of these instruments was optimized for one particular spectral region. The setup used for amide I and mid-IR measurements (1000−1800 cm^{-1}) was based on IFS-66/S FTIR and included VCD/IRRAS PMA 37 attachment, BaF_2 polarizer, ZnSe photoelastic modulator (Hinds), MCT detector (InfraRed Associates), and a lock-in amplifier SR830 (Stanford Instruments). For the higher wavenumber region (2600−3200 cm^{-1}) we utilized different instrumentation, components and materials: Tensor 27 FTIR, VCD/IRRAS PMA 50 attachment, and the InSb detector D4143/6 (InfraRed Associates). The spectra were recorded at a resolution of 4 cm^{-1} in $CDCl_3$ at the concentrations of either 0.027 mol L^{-1} (mid-IR) or 0.109 mol L^{-1} (2600−3200 cm^{-1} region). We used a demountable sample cell (path length 0.21 mm) with the windows from either KBr (mid-IR) or Infrasil quartz (near IR). Our standard measurement protocol involved averaging of 20 min scanning blocks of interferograms (7−10 blocks of 2260 scans for mid-IR experiments and 9−18 blocks for near IR). As background we subtracted corresponding solvent scans. At least in the case of I the availability of the racemate would allow to use its solution for the background scans in order to mimic exactly the absorption of optically active sample. In practice resorting to such a procedure was not necessary as rather favorable signal-to-noise ratio and low level of artifacts allowed us to utilize just solvent scans. The spectra of enantiomers were plotted against each other in order to check for consistency and final optimal VCD data were obtained by subtracting them and dividing the result by the factor of 2. Final data were plotted as the respective ε (absorption) or $\Delta\varepsilon$ (VCD) values.

Raman scattering and Raman optical activity spectra were measured using the ICP Raman/ROA spectrometer working in backscattering mode. The instrument was built at the Institute of Physics, Charles University in Prague and has already been detailed elsewhere.[51] New development used in this study involved use of interchangeable gratings (Kaiser Optical Systems, HSG-514.5-LF, HSG-514.5-HF and HSG-532-LF) allowing us to extend the useful spectral range to 200−4000 cm^{-1}. Samples for Raman and ROA measurements were dissolved in distilled water and filtered through a 0.22 μm Millipore filter into quartz ROA microcells (~60 μL, 4 × 3 mm, Starna Scientific Ltd.). The experimental conditions were set as follows: excitation wavelength 514.5 nm, laser power at the sample 550−650 mW, and spectral resolution 6.5 cm^{-1}. The concentrations were chosen according to solubility of particular samples (0.5−0.7 M) and the acquisition time was optimized in order to get reasonable S/N ratio in ROA spectra (20−40 h). Experimental intensities of Raman and ROA spectra were corrected using a certified spectroscopic standard, National Institute of Standards and Technology, Standard Reference Material 2243.[52] This treatment allowed us to eliminate the instrument-related artifacts and to obtain spectra which do not depend on the choice of diffraction grating. Raman spectra were processed by subtracting the solvent signal and by further correcting the baseline using polynomial fitting (the fifth order polynomial). Raw ROA spectra were treated by mutually subtracting spectra of both enantiomers followed by dividing them with a factor of 2. The use of both enantiomers helped to eliminate artifacts and to increase confidence even in weak ROA signals. The final ICP ROA spectra are presented as ($I^R - I^L$) and the parent Raman spectra as ($I^R + I^L$) where I^R and I^L are the respective Raman intensities recorded in right and left circularly polarized incident laser light. Numerical data treatment was done using GRAMS/AI software (Thermo Electron Corporation). In order to further check for consistency, we have remeasured the ROA of (−)-(1R)-I in the region of 200−2000 cm^{-1} on a commercial SCP ROA instrument (Chiral*RAMAN*-2X, BioTools Inc., U.S.A.), based on the innovative concept of Hug.[53] Although the used spectrometers employ different modulation schemes, the resulting traces are almost identical (see Figure S1 in the Supporting Information).[35] Subtle differences in resolution and S/N ratio can be ascribed to different construction details of both instruments.

Although chiroptical spectra were measured utilizing both enantiomers, the final data presented in this paper refer to (−)-(1R) enantiomers (with the exception of data shown in Figure S2 in the Supporting Information), where spectra of both enantiomers are plotted against each other.

Calculations. Geometries and vibrational spectral data were calculated using standard DFT procedure[54] utilizing Gaussian 09 (AM64L-G09RevA.02)[55] computer program. We employed the B3LYP functional[56,57] and 6-311++G** basis set,[58] i.e., the balanced middle level of ab initio calculation. We have checked stability of the results toward particular details of computational procedure using other functionals (e.g., BPW91[59]), basis sets (up to aug-cc-pVTZ[60]) and methods (MP2[61]) (see Figure S3

and Table S1 in the Supporting Information). The results are not very sensitive toward the form of the functional or the basis set size. We did not find major benefits related to increased level of computation. Even simpler procedures can be used, provided that at least polarization functions on non-hydrogen atoms are included (6-31G* level and up). We have chosen identical level of calculations for the geometry optimization, calculation of the force field and vibrational intensities. The methods and procedures were utilized in their standard form as included in the Gaussian 09 package. We report results achieved with the B3LYP/6-311++G** combination, which is currently used rather frequently for the theoretical interpretation of vibrational optical activity data. We include empirical dispersion correction,[62−64] which leads to the best correspondence between experimental and simulated spectra. We have consistently used the implicit solvent model COSMO-PCM.[65,66] The used atom numbering is shown in Figure 3. It

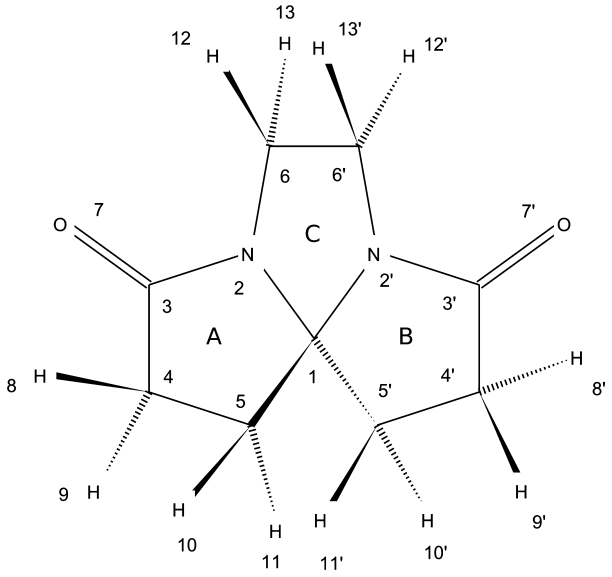

Figure 3. Numbering of atoms in the spirocyclic dilactam (−)-(1R)-I.

is common to both molecules I and II (in the latter case just the atoms $H_{12,\ 13,\ 12',\ 13'}$ need to be replaced by deuteriums). The numbering respects C_2 symmetry of the molecules and allows us to present spectral and structural data of these moderately complicated (69 vibrational modes) structures in a sufficiently transparent fashion. The assignment of experimental bands to particular vibrational modes was done in two stages. In the first step we utilized the freely available computer program Facio[67] which provided animations of nuclear motions along the computed normal modes. Visual inspection of the depicted vibrational motion resulted in the approximate understanding, which was further quantified in the second step utilizing potential energy distribution (PED) values[68] (after a conversion to internal coordinates, see below). The final assignment shown in graphical and tabular data was then based on agreement of experimental/calculated positional and intensity parameters.

Choice of Internal Coordinates. It is not trivial to select a useful set of nonredundant internal coordinates for tricyclic spirodilactams, because each of them contains three annelated (i.e., welded together) rings A, B, and C. Standard definitions of internal coordinates (e.g., refs 67, 69, and 70) and application of recommended definitions of five-membered rings to this rather special case of two or three atoms common to more than one ring system result in serious redundancy-related problems. To further complicate the matter, the compounds are strictly of C_2 symmetry while containing odd number of atoms (25).

While bisecting the $C_6-C_{6'}$ bond, the C_2 axis also intersects the central spiroatom C_1. As a consequence, only one-half of the $C_6-C_{6'}$ bond is uniquely defined. Deformations within the ring C are heavily coupled to (a) deformations within rings A and B and (b) to rocking, wagging and twisting motions of A and B rings with respect to each other. Moreover, in order to interpret vibrational spectra of I and II in chemically meaningful terms, it is necessary to define internal coordinates in a more general fashion. It would be advantageous to treat consistently not only dilactams I and II, but also the substituted dilactams V−VII and the bicyclic dilactam X (Scheme 3)[71,72] with secondary amide groups and no C ring.

Scheme 3. Bicyclic Spirodilactam X[71,72]

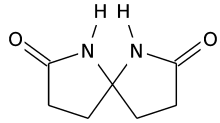

Having analyzed these complex requirements, we have chosen a set of nonredundant internal coordinates that conform to the above listed conditions. In the course of internal coordinates selection and B matrix formulation, we adhere to the following rules:

(a) We use standard definitions of stretching, deformation, and torsional modes as recommended by Fogarasi and Pulay[67,69,70] wherever possible. This includes deformation and torsional modes at the separately treated five-membered rings A, B, deformation modes at six CH_2 groups, and in-plane and out-of-plane deformations of both C═O groups. Deformations at tertiary amide nitrogens N_2, $N_{2'}$ are treated as $\delta_{ip}(N-C)$, $\delta_{oop}(N-C)$ (see below).

(b) We include explicitly all bond stretching coordinates except $\nu(C_6-C_{6'})$. This bond and the relevant force constant are not explicitly considered and the corresponding stretching potential is included implicitly as a significant contributor to $\delta(N_2-C_6)$ and $\delta(N_{2'}-C_{6'})$ in-plane and out-of-plane deformations (coordinates $S_{35}-S_{38}$ in Table S2). This choice has dual consequences. It solves part of the redundancy problem and the annelations of the rings A to C and B to C. The compounds I and II formally become bicyclic only, because closure of the ring C is realized implicitly. As a disadvantage, this cannot be separated from bending motions at N_2, $N_{2'}$ and C_6, $C_{6'}$. Although it is a definite limitation, it brings a possibility to treat compounds I−VII and X using common scheme.

(c) The special tetra-substituted spiroatom C_1 is formally modeled after a CH_2 group. The two scissoring coordinates (α_1, $\alpha_{1'}$) at C_1 are included implicitly (they form parts of the respective deformations of the rings A and B) and are not explicitly listed again, as it would introduce a redundancy. Their mutual coupling is not explicitly defined as it follows from molecular symmetry considerations. The remaining three deformations describe rocking (S_{39}), wagging (S_{40}), and torsional (S_{41}) motions of the rings A and B with respect to each other.

(d) Neither ab initio calculations of Cartesian force constants nor conversions into internal coordinate bases make use of the C_2 symmetry of these molecules. We let our procedures

dx.doi.org/10.1021/jp405226k | J. Phys. Chem. B 2013, 117, 9626−9642

perform the calculations as if the molecules were of C_1 symmetry and the calculated symmetry of vibrational motion serves to classify them.

The resulting nonsingular B matrix allows us to express vibrational motions of I and II in chemically meaningful terms. The final list of internal coordinates is given in Table S2 in the Supporting Information. (We do not include normalization factors as our procedures automatically normalize.) The conversions between alternative Cartesian and internal coordinate representations were done using a set of computer programs kindly provided by Professor T. A. Keiderling, U.I.C., Chicago, U.S.A.

RESULTS

The molecular geometry of I is known from crystallographic data;[44] however, calculation of vibrational properties requires internal consistency of geometry, force field, and property tensors with respect to the method used. Although our geometry optimization is based on a simple procedure designed to mimic the aqueous environment,[65] it reproduces the X-ray geometry with remarkable accuracy. Differences between observed and calculated bond lengths for skeletal atoms amount to approximately 0.01 Å, while the bonds involving hydrogens are calculated to be systematically longer by ~0.09 Å mainly due to systematic errors in X-ray determination of C−H bond lengths.[73] The bond angles are reproduced within 0.5° for skeletal angles and within 2° for those involving hydrogens. If we carry out a rigorous comparison of computed and experimental geometries then the only parameters which deviate a little more are those describing nonplanar deformations of amide groups. Experimentally, the amide groups (both identical under C_2 symmetry) adopt nonplanar geometries characterized by twisted (τ) pyramidal arrangements at amide nitrogens N_2, $N_{2'}$ (Θ_N) ($\Delta\omega \approx -11°$, $\Theta_N \approx +42°$, $\Theta_{C'} \approx -0.3°$, and $\tau \approx +21°$ for the (−)-(1R) enantiomer), while arrangements of bonds to carbonyl carbon atoms C'_3, $C'_{3'}$ ($\Theta_{C'}$) remain nearly planar. The twist parameter τ is quite large, making the pyramid of bonds to N significantly irregular. In computed structures the amide groups are slightly flattened ($\Delta\omega \approx -10°$), less pyramidal on N ($\Theta_N \approx +40°$), somewhat more rotationally twisted ($\tau \sim +23°$) and the pyramidal deformation on C′, though still negligible, changes sign ($\Theta_{C'} \approx +1°$). Although these differences exceed error margins of X-ray data, they are still small and do not significantly alter spatial character of amide nonplanar deviations. More importantly, these changes have little effect on the calculated spectra. The two lactam rings A and B adopt identical slightly twisted envelope conformations with apexes at the less constrained atoms C_5, $C_{5'}$, while the pseudoplanes of the envelopes are formed by C_4−C_3-N_2−C_1 and $C_{4'}$-$C_{3'}$-$N_{2'}$-C_1, i.e., they are centered on the amide groups. The structures are considerably rigid − even flipping of envelope apexes cannot be realized. The amide endocyclic torsion angles, despite corresponding to discernibly nonplanar situations, still describe flat bases of the envelopes in question. On the contrary, the central ring C reflecting the fact that this ring is bisected by C_2 axis of the molecule features a strongly puckered regular boat conformation. The pseudodihedral angle O_7═C_3···$C_{3'}$═$O_{7'}$, which is important for the estimate of amide−amide coupling, amounts to ~16° (experimental, the calculated value ~14°). The pseudobond angle O_7═C_3···$C_{3'}$ amounts to ~140°; that is, the O_7═C_3···$C_{3'}$═$O_{7'}$ grouping is not collinear. As expected, the computed geometry of the tetradeuterio derivative II is the same as that of I.

Vibrational Properties. The medium-sized molecules I and II exhibit well resolved vibrational spectra showing narrow spectral bands (see Figures 4 and 5 for the IR absorption/VCD

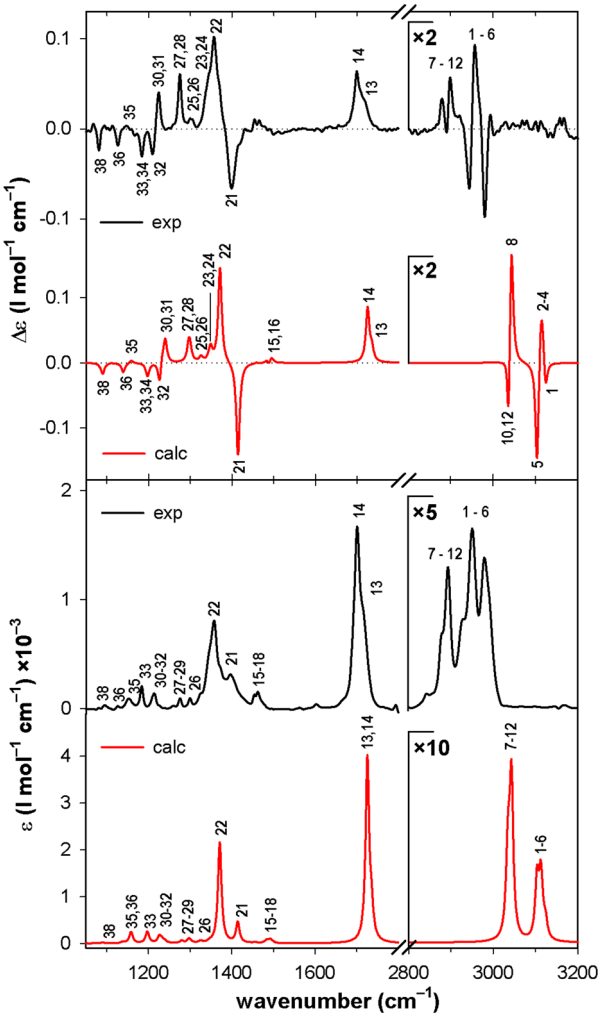

Figure 4. Experimental (black traces) and calculated (red traces) IR (bottom) and VCD (top) spectra of the dilactam I in $CDCl_3$.

combination and Figures 6 and 7 for Raman/ROA). Even small VOA features are recorded with confidence because both enantiomers of I and II were available and their spectra could have been plotted against each other (see Figure S2 in the Supporting Information). The molecules I and II possess 69 fundamental vibrational modes each. For I, we were able to resolve 39/17 bands in IR/VCD and 40/43 in Raman/ROA. With the aid of calculations it is possible to assign most of the experimental bands (see Figures 4−7 and Table S3 and S4 in the Supporting Information). The clearly identifiable spectral features include C−H and C−D stretching vibrations (~2100−3000 cm^{-1}), carbonyl group related signals (~1700 cm^{-1}), CH_2 scissoring modes (~1450 cm^{-1}) and amide C′−N stretching signals at about 1400 cm^{-1}. Below ~1350 cm^{-1} the assigment requires computational support (for the calculated PED values see the Supporting Information, Table S3 and S4).

C−H and C-D stretching vibrations in I and II correspond to $-CH_2-$ and $-CD_2-$ groups. VCD in this region has been known for a long time;[74−76] however, the ROA has yet to be

dx.doi.org/10.1021/jp405226k | J. Phys. Chem. B 2013, 117, 9626−9642

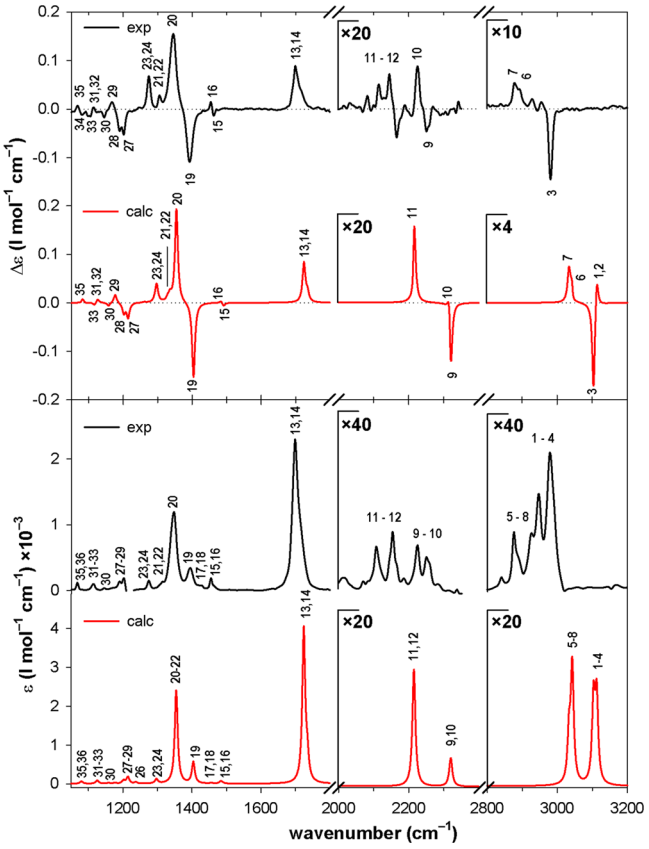

Figure 5. Experimental (black traces) and calculated (red traces) IR (bottom) and VCD (top) spectra of the dilactam II in $CDCl_3$.

evaluated in detail. The data (Figures 4–7) show that ROA is stronger than VCD if signals in C–H and C–D stretching regions are compared with the rest of the spectrum. These vibrational signals are crammed into narrow spectral regions and not very well individually resolved; hence we attempted to get more understanding using a comparison with calculations (Figures 4–7 and Tables S3 and S4 in the Supporting Information). Energies of C–H stretching modes are calculated systematically too high by about 150 cm^{-1}, though this error does not seriously influence the assignment. Detailed separations within the C–H stretching group are not correct (Figures 4–7 and Tables S3 and S4 in the Supporting Information). While basic positional differences between CH_{2s} and CH_{2as} subgroups (~60 cm^{-1}) are calculated realistically (~70 cm^{-1}), the differences within these subgroups are too small (~ 5 cm^{-1} cf. the experimental estimate of ~20 cm^{-1}) and it is not possible to distinguish between signals of $C_{4,4'}$, $C_{5,5'}$, and $C_{6,6'}$. Mutual interactions between pairs of CH_2 groups related by C_2 symmetry (i.e., splitting of modes at C_4, C_5, and C_6 vs those at $C_{4'}$, $C_{5'}$, and $C_{6'}$) are underestimated as well. Although simulated VOA spectra (based on the empirical bandwidth of 10 cm^{-1}) indicate further structure, the assignment of particular components is tentative only. Experimentally, we can detect further splitting of asymmetric components. The spectra of II are simplified compared to I by the absence of hydrogen atoms at $C_{6,6'}$. In ROA, a negative band at ~3000 cm^{-1} (~3010 cm^{-1} for II) and a positive one at ~2935 cm^{-1} (for both I and II) are present regardless of the alternative presence of deuterium or hydrogen atoms at $C_{6,6'}$, while the bands at ~3020 cm^{-1} (+) and ~2900 cm^{-1} (−) are present only in the spectra of I (see Figures 6 and 7 and Tables S3 and S4 in the Supporting Information). Although agreement between ROA calculation and experiment is not perfect because band positions are inaccurate (even mutual switching is possible) and there is a substantial band overlap, the overall shape is comparable. Further support to this general picture follows from the parallel VCD data (two observable couplets in I, one at ~2900 cm^{-1} the other at ~2950 cm^{-1}, which are not present in the spectra of II; see Figures 4 and 5 and Tables S3 and S4 in the Supporting Information).

The compound II exhibits also VOA due to C-D stretching vibrations (2050–2300 cm^{-1}, Figures 5 and 7 and Table S4 in the Supporting Information). Although VCD of C-D stretching modes has already been reported even in compounds with five-membered rings,[77,78] the corresponding Raman/ROA manifestation has not been studied yet. For II the C-D stretching signals appear stronger in Raman/ROA than in IR/VCD. In ROA we can distinguish four features corresponding to symmetric (2117 and 2165 cm^{-1} (−)) and asymmetric (~2221–2238 cm^{-1} (−) and 2268 cm^{-1} (+)) components. In Raman spectra we identify analogous signals at the same positions (bands at 2117, 2165, and 2268 cm^{-1} and a poorly resolved smaller signal between 2221 and 2238 cm^{-1}). The prominent signals are also found in IR (2108, 2155, 2225, 2253, and 2259 cm^{-1}) and VCD (2116 (+), 2145 (+), 2166 (−), 2226 (+), 2251 (−), and 2270 cm^{-1} (+)). The absorption bands at 2155 and 2259 cm^{-1} correspond to midpoints of two couplets in VCD. The basic pattern of C-D stretching signals is reasonably reproduced by calculations; however, there are several drawbacks. Analogously to C–H stretching vibrations the harmonic model fails to reproduce the experimentally observed splitting (nearly 50 cm^{-1}) caused by mutual interaction between symmetry-related features at $C_{6,6'}$. Experimental Raman data show several smaller additional features (at 2050, 2078, and 2194 cm^{-1}) which have no counterparts in ROA and cannot be satisfactorily explained. Additional lower intensity signals have been analogously found in VCD at ~2071, 2085, 2187, and 2270 cm^{-1}. In contrast to Raman/ROA, not only are these features visible in IR spectra but they have signatures even in VCD, where some of them are quite prominent (Figure 5). Therefore we limit the analysis to three discernible features comprising an IR band at 2155 cm^{-1} (corresponding to a ±VCD couplet within CH_{2s}) and a single positive band at 2226 cm^{-1} within $\nu_{as}(CH_2)$. The most probable explanation for the additional signals consists in anharmonicity of C–H and C–D stretching vibrations and the presence of overtone, combination bands. We can probably exclude other reasons such as existence of several conformers or insufficient deuterium content in II as our samples are rigid and were thoroughly tested for chemical, isotopic, and enantiomeric purity.

In the spectra of I and II, the most discernible vibrations are amide related, and among them particularly the modified amide I signals. Amide I (υ(C′═O)) vibrations exhibit a single high intensity band with a shoulder on its high (IR) or low (Raman) frequency side. This band is strong both in IR absorption and Raman scattering. Its frequency is sensitive to solvent polarity (at ~1699 cm^{-1} in $CDCl_3$, IR/VCD and ~1681 cm^{-1} in H_2O, Raman/ROA). Calculations (Tables S3 and S4 in the Supporting Information and Figures 4–7) report a pair of coupled bands in this region, a weaker feature at higher frequency (mode 13, the *A* symmetry species) and a stronger band at lower (by ~10 − 15 cm^{-1}) frequency (mode 14, *B* symmetry species). The red shifts of these bands on going from

dx.doi.org/10.1021/jp405226k | J. Phys. Chem. B 2013, 117, 9626–9642

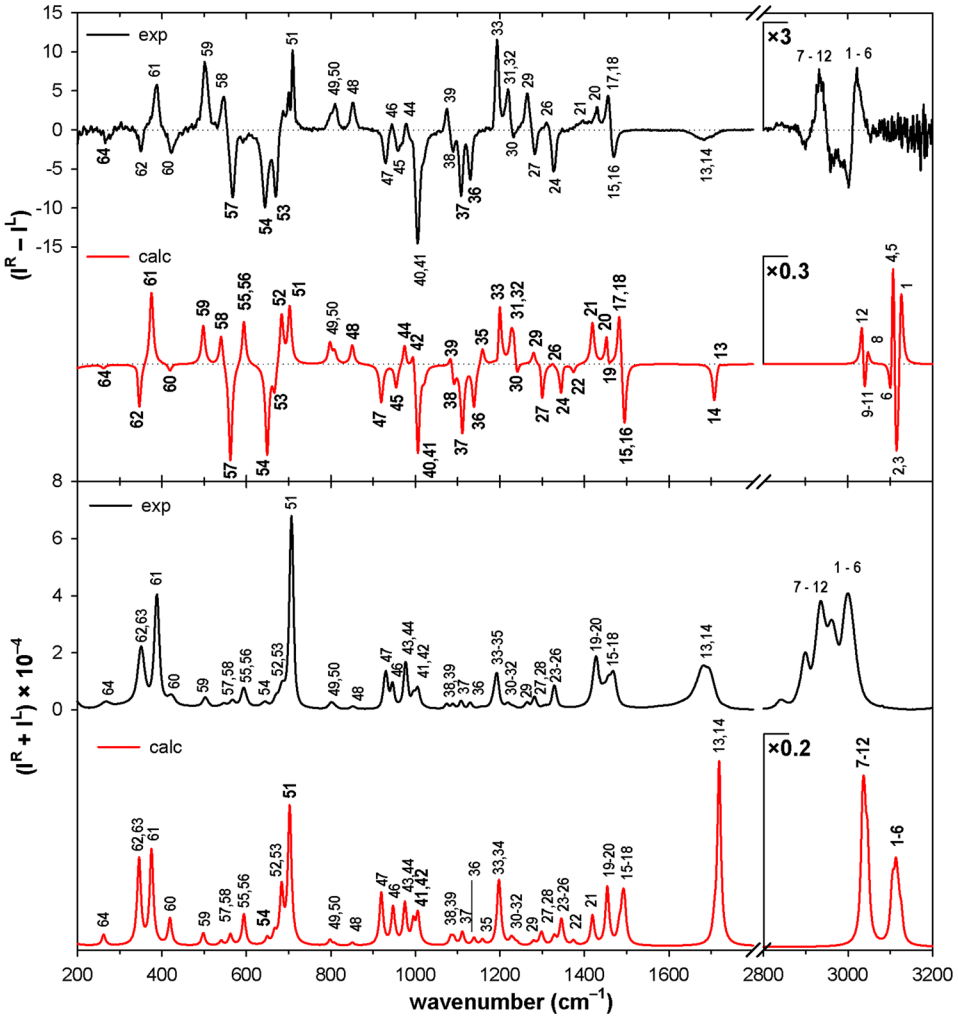

Figure 6. Experimental (black traces) and calculated (red traces) Raman (bottom) and ROA (top) spectra of the dilactam I in water.

chloroform to aqueous solutions are computed (with the polarizable continuum model, PCM or COSMO-PCM)[65] reasonably well, but absolute band positions in chloroform (1735 and 1725 cm^{-1}) or water (1719 and 1707 cm^{-1}) are calculated with ∼30 cm^{-1} erroneous blue shift. However, this error does not interfere with the assignment because amide I bands are separated from other vibrations. According to PED (Tables S3 and S4 in the Supporting Information), amide I bands in these tertiary amides are dominated by C′═O stretching modes (∼75%) supplemented by minor contributions of ring (A, B) deformations and C′−N stretches. Amide I vibrations in I and II are active both in VCD and ROA. In VCD the R enantiomer exhibits a broad asymmetrical positive feature of medium intensity with a shoulder on its high frequency side, similarly to the absorption trace. Its positions in absorption and VCD approximately correspond. The course of VCD suggests as the most probable explanation a superposition of the small couplet (positive at the low frequency side) with a broader positive feature, spanning through the whole carbonyl region. The single-signed component indicates a source of chirality that is local to each amide group, while the moderate, slightly interfering couplet probably originates from dipole−dipole interaction between two C′═O oscillators (see further analysis in the Discussion section). However, the overall situation can be more complex, because even the IR absorption intensity is concentrated in the lower energy B component, i.e. the amide I band retains its asymmetrical shape also in absorption. As expected, amide I VCD of II is nearly identical to that of I. Full ab initio theoretical calculations describe the single-signed amide I absorption and VCD features of I and II reasonably well (Tables S3 and S4 in the Supporting Information and Figures 4 and 5), including asymmetry of IR/VCD bands. The Raman scattering in amide I is generally similar to IR absorption but there are significant differences. Relative to spectral intensities in other parts of the spectrum the amide I Raman band is weaker (in IR absorption the amide I band dominates the spectrum), but still remains quite intense. Amide I band in calculated Raman spectra also consists of two components with the less intensive one at lower frequency. Experimental amide I signals appear to be more symmetrical in the Raman spectra, probably due to effects of aqueous solution which cannot be described properly by simple PCM or CPCM models.[65] Raman optical activity signals are generally similar to VCD (we observe a single-signed rather broad ROA feature), but with the negative sign, however we should keep in mind that sign convention is opposite for ROA and VCD.[35] ROA calculation hints on possible presence of weakly double-featured chiral scattering. Although the dominant calculated feature is, in agreement with experiment, a negative lower energy component at 1707 cm^{-1}, it is in this time accompanied by a weak but discernible positive one at higher frequency (1719 cm^{-1}). The calculation then results in a very asym-

dx.doi.org/10.1021/jp405226k | J. Phys. Chem. B 2013, 117, 9626−9642

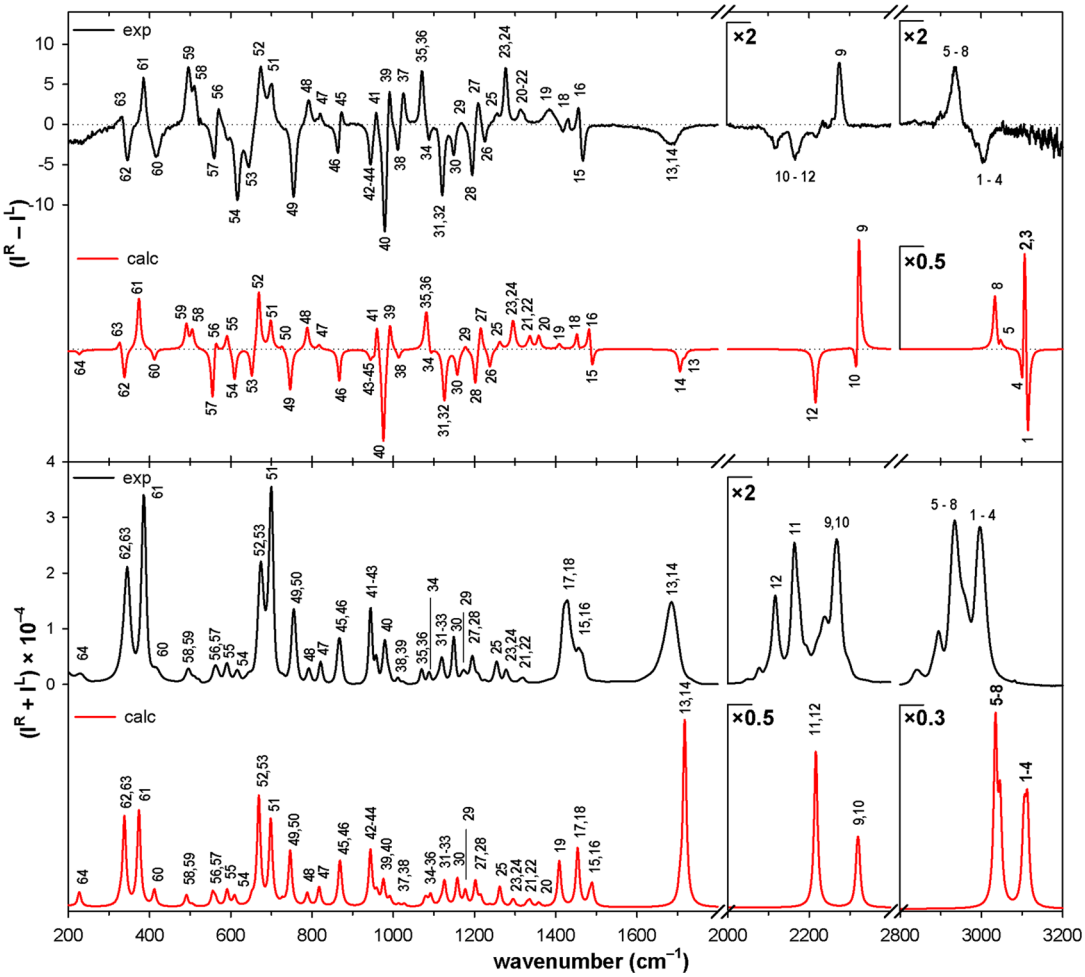

Figure 7. Experimental (black traces) and calculated (red traces) Raman (bottom) and ROA (top) spectra of the dilactam II in water.

metrical couplet, where only the low energy component agrees with experimental data. However, this small additional positive component is calculated only with larger basis sets (6-311++G**, aug-cc-pVDZ, and aug-cc-pVTZ), while simpler calculations lead solely to the above-mentioned single-signed negative ROA feature.

The next group of vibrations, characteristic for compounds containing numerous CH_2 groups, comprises CH_2 scissoring modes in a narrow, well-defined region of ~1450 − 1500 cm^{-1}. Experimental data of I provide a pair of very low-intensity absorption features at 1453 and 1461 cm^{-1} (for II a single low intensity band at 1455 cm^{-1}). They are better resolved in VCD, where they form a pair of positive bands for I or a low-intensity ± couplet for II. In the spectra of II there are just two pairs of symmetry related CH_2 groups within rings A and B, while for I there are yet CH_2 groups at C_6 and $C_{6'}$ (ring C). In II the corresponding CD_2 scissorings shift to ~1100 cm^{-1}, where they mix with other deformation modes and are generally difficult to identify without a calculation (modes 30−36, Table S4 in the Supporting Information). CH_2 scissoring vibrations are more intense and better resolved in Raman/ROA. In I we observe a pair of Raman bands and three well discernible sharp peaks in ROA. Raman/ROA calculations (Figures 6 and 7 and Tables S3 and S4 in the Supporting Information) indicate that CH_2 scissorings in I (modes 15−20) manifest themselves as two distinct bands with more underlying components, symmetric and antisymmetric with respect to C_2 axis of the molecule. It appears that localization of particular modes to C_4, C_5, or C_6 influences band positions more efficiently than coupling across C_2 axis of the molecule. The three observed ROA peaks at 1469 (−), 1455 (+), and 1429 (+) cm^{-1} correspond to the scissoring vibrations at $C_{6,6'}$, $C_{5,5'}$, and $C_{4,4'}$ respectively. According to PEDs, scissoring vibrations in I are nearly completely isolated from vibrations of the rest of the molecule. Within II the simplified CH_2 scissoring (modes 15−18) enables resolving 3−4 CH_2 scissoring modes as also shown by the calculation (Figure 7 and Table S4 in the Supporting Information).

The following signals at lower energies (~1400 cm^{-1}) correspond to amide II (modified in tertiary amides). These are prominent (although weaker than amide I) in IR absorption, strong in VCD (Figures 4 and 5) but very weak or nearly undetectable in Raman/ROA (Figures 6 and 7). In secondary amides, these bands are assigned to a combination of C′−N stretching and N−H in-plane bending modes. However, such a combination can only be realized in primary/secondary amides (there is no N−H bond in tertiary amides). In I (II) the corresponding bands are exhibited in IR absorption ($CDCl_3$) as a distinct two-component absorption feature at 1396 (1394, II) and 1356 (1347, II) cm^{-1} that is just shifted toward lower energies by ~100 cm^{-1} compared to secondary amides with planar amide groups (~1515 cm^{-1}).[21] The splitting into two components is visible already in IR absorption (the maxima observed for both components are separated in $CDCl_3$ by ~40 cm^{-1}, cf. a calculated value of ~43 cm^{-1} in $CHCl_3$). According

dx.doi.org/10.1021/jp405226k | J. Phys. Chem. B 2013, 117, 9626−9642

to PED (Tables S3 and S4 in the Supporting Information), the symmetric (*A*) and antisymmetric (*B*) components at the respective 1414 (1404, II) cm^{-1} and 1371 (1354, II) cm^{-1} (modes 21, 22 (I); 19, 20 (II)) involve combinations of C′−N stretching motions (∼33−40%) with a mixture of ∼40−50% skeletal (N−C, C−C′) stretching, A, B ring deformation, skeletal and C′═O in-plane deformation modes. In contrast to secondary amides the dilactams I and II present these modified amide II vibrations as rather variegated mixtures of interconnected skeletal atom motions. Still, the bands maintain their spectroscopic identity including intense IR absorption, low intensity Raman scattering and a significant proportion of C′−N stretching. Similarly to amide I, the calculated amide II features are nearly independent of the alternative presence of hydrogen or deuterium atoms at C_6 and $C_{6'}$ (i.e., the spectra of I and II in this region are nearly identical). The bands are prominent in VCD where they exhibit a high intensity, almost symmetrical couplet with the positive lower energy *B* component which dominates the whole VCD spectrum (Figures 4 and 5). If we analyze its details then particularly this lower energy *B* component (in I) is slightly wider than other VCD bands and its shape is not exactly Gaussian or Lorentzian, probably due to the presence of an additional positive signal indicated by the calculations ($\delta(CH_2)$ modes 23 and 24). The exact positions of both components of the VCD couplet match quite closely those of the relevant absorption features. In accord with expectations, amide II bands are almost undetectable in experimental Raman/ROA spectra (Figures 6 and 7), although ROA calculations indicate a pair of signals with the signs opposite to those displayed in VCD (low-intensity lower energy band and middle-intensity higher energy band). In experimental ROA spectra we can see only a tiny positive component in place of the high energy feature which is exhibited in VCD. The negative lower energy component is not experimentally detected at all. An additional negative ROA feature in this region at ∼1327 cm^{-1} in I is of a different origin (mode 24, CH_2 wagging). The modified amide II VCD pattern is computationally reproduced rather well and the calculation offers a possibility to cross compare VCD in amide I and II region and to discuss local effects vs amide−amide coupling.

Vibrational transitions below 1350 cm^{-1} usually contain several coupled components of different origin. Despite the extensive mode mixing, a direct comparison of experimental vs calculated traces achieves a very good agreement (Figures 4−7 and Tables S3 and S4 in the Supporting Information). The agreement is even better for VOA than for nonchiroptical vibrational spectra. The assignment benefits from PED values (Tables S3 and S4 in the Supporting Information) and a visualization of vibrational motions. Within this region, experimental bands are mostly weak in IR/VCD and strong and rather prominent in Raman/ROA. Data on IR absorption are available down to 400 cm^{-1}, but experimental VOA below 1000 cm^{-1} relies on ROA in water (experimental VCD does not reach below ∼900 cm^{-1}). We observe predominantly CH_2 deformation modes: wagging (between modes 23−47 (I)), twisting (between 24 and 47 (I)), and rocking (lower in energy, between 34 and 56 (I)), together with skeletal stretching vibrations of the tricyclic system (the coupled C−C and N−C motions between modes 23−61 (I)). In II, there are additional contributions from CD_2 scissoring vibrations (between modes 30−36). Because of the absence of N−H bonds there is no substantial amide manifestation around 1300 cm^{-1} (the typical position of amide III in secondary amides). On the other hand, at lower wavenumbers (below ∼1250 cm^{-1}) we observe amide-related contributions to vibrations given by the tightly bound tricyclic system. These involve first alicyclic N−C (−C_1 and -$C_{6,6'}$) stretching vibrations (between modes 29−44) and minor contributions from δ_{ip}, δ_{oop} deformations centered around amide nitrogen atoms (contributing mainly to modes between 33 and 41, 47−48) and deformation motions around the spiroatom C_1 (i.e., wagging, rocking and twisting motions of A, B rings with respect to each other). The bonds to amide nitrogens participate additionally in the implicit definition of C_6−$C_{6'}$ stretching coordinate. This follows quite clearly from visualization of mode 47, although this mode is described as a combination of δ_{ip} and δ_{oop} vibrations around amide nitrogen, according to mode visualization it results in a nearly pure C_6−$C_{6'}$ stretching motion. The above-mentioned involvement of N−C stretching has been already observed and calculated by Krimm and Bandekar[48] in the spectra of acetyl-*N*′-methyl-amide, so this phenomenon is not specific for these rigid tertiary amides. The most intense negative ROA signal in this region is observed at 1005 cm^{-1} (979 cm^{-1} for II). The corresponding calculated ROA agrees with experiment (mode 41 (I), 40 (II), Tables S3 and S4 in the Supporting Information and Figures 6 and 7), while PED exhibits rather complex mixing: ∼20% of N−C stretching motion, besides skeletal stretching (18%) and $\delta(CH_2)$ rocking (15%) together with minor portions of in plane amide N and C′═O deformations (13%). The data between ∼900 and 1350 cm^{-1} are difficult to utilize analytically because of extensive mixing of modes having very different origins. Any chemical modification could influence the extent and character of this mode mixing and, consequently, it is difficult to transfer vibrational information relevant to this region from our models to other molecules. It is of advantage that a replacement of hydrogen atoms (I) with deuteriums (II) causes in this region just minor band shifting to lower wavenumbers (∼10 cm^{-1}) and the calculations including Raman and ROA intensities hold even in this dense part of the spectrum (Figures 6 and 7 and Tables S3 and S4 in the Supporting Information). Although the deformations involving amide groups generally contribute to a wide range of transitions, their contributions to vibrations between 900 and 1300 cm^{-1} amount only to 5−10%, and at the same time they extensively mix mainly with CH_2 deformations. Below 900 cm^{-1} the situation simplifies and the low frequency modes become more characteristic. In Raman/ROA spectra we observe an approximately separated group of discernible bands at 200−900 cm^{-1}. In this case the composition of vibrational transitions can be better characterized, because the closely related CH_2 deformations no longer participate (see Tables S3 and S4 in the Supporting Information). The modes active in this region belong to three categories: (a) δ_{ip}, δ_{oop} vibrations involving bonds to amide nitrogens $N_{2,2'}$; contributions due to these modes are rather widespread (ip modes 47, 55, 63−65, oop modes 47, 49, 52, 54−60, 62, 65, 66, 68, 69), because $N_{2,2'}$ atoms are located at the branching points of the multiconnected tricyclic structure and the relevant vibrational motion can influence other parts of the molecule through bonds; (b) δ_{ip}, δ_{oop} vibrations of the $C'_{7,7'}$═O bond (amide VI in secondary amides); these vibrations are restricted to a narrower spectral range (ip mode 63, oop modes 51, 52, 54, 55, 59); and (c) the vibrations describing ring system deformations (τ ring), spirosystem rocking, wagging, twisting, and additional stretching υ (C_1−$N_{2,2'}$) (modes 52−69). These vibrational modes describe numerous variants of not very specific skelet-

dx.doi.org/10.1021/jp405226k | J. Phys. Chem. B 2013, 117, 9626−9642

distorting vibrational motions. Amide related modes are generally superimposed on this skeleton-related basis, forming minor, but visible contributions. However, there are several such Raman/ROA features, where amide contributions are important if not numerically dominant (modes 52−60). Quite interestingly, particular vibrational transitions are frequently contributed by both δ(C−N) and δ(C═O) components (see modes 52, 54, 55, and 59). The in-plane and out-of-plane deformations mutually mix (i.e, within one vibrational transition) only exceptionally (modes 55 and 65) despite the fact that their distinguishing plane is defined only vaguely in nonplanar amides. Classification of these low-energy vibrational modes according to extent and form of their participation within amide vibrations, as they are known from other studies,[48] is not straightforward in tertiary amides. Even more importantly, the rigid nonplanar structures tend to obscure simple symmetry-related criteria and, consequently, this classification is not apparent at first glance. However, in analogy with simpler cases we can separate the following groups of vibrational modes, which contribute consistently in I and II to these characteristic although modified amide vibrations: amide IV (δ_{ip}(C═O), δ_{ip}(N−C), mode 63); amide V (δ_{oop}(N−C), modes 52, 56, 57, and 60); amide VI (δ_{oop}(C═O), modes 51, 54, and 55). The pattern of calculated Raman/ROA intensities in this region agrees with experiment (Figures 6 and 7 and Tables S3 and S4 in the Supporting Information) with two exceptions. Mode 55 is calculated with the wrong sign; however, this problem is resolved only in the spectra of II; for I modes 55 and 56 superimpose and we observe no ROA at all. According to visual inspection, the concerned mode 55 involves skeletal stretching, $\delta(CH_2)$ torsion involving all three rings A, B, and C, and the already complex vibrational motion is further mixed with out-of-plane deformations of amide groups. It is interesting that this disagreement (which is a unique one within our spectra) between calculated and observed ROA does not depend on details of a computational procedure. The other problem concerns experimental bands corresponding to calculated modes 51 and 52. In I, these signals are influenced by the strongly polarized Raman band at 707 cm^{-1} (mode 51), which probably causes some line-shape distortions. In this region the well observable ROA features are shown even for rather low intensity Raman bands. Despite the fact that recognized amide vibrations contribute each to several experimental bands, we can still identify experimental Raman/ROA features which represent the amide V and VI vibrations quite closely (amide IV mode at 342 cm^{-1} is not detectable on the basis of its very low calculated and experimental intensity). Thus amide V vibration (δ_{oop}(N−C)) seems to project best into the intense negative ROA band at 568 cm^{-1} (mode 57). Amide VI (δ_{oop}(C═O)) contributes to a positive ROA band at 707 cm^{-1} (mode 51) and a negative ROA band at 649 cm^{-1} (mode 54).

At lower wavenumbers most ROA bands are connected with skeletal deformations. PED-based analysis combined with visual inspection reveals that skeletal deformations often involve spiro-system deformations around C_1 atom describing relative motions of A, B and C rings. Many of these vibrations involve complex mode mixing with participation of amide vibrations and involving only minor portions of the above identified deformations. These are particularly modes 31, 33, 34, 39, 44−46, 49, 55, 57, 60, 63, 64, 66, and 69, but there are two modes (61 and 62) where spirosystem deformations appear to dominate and which seem well separated from other vibrations. These modes correspond to middle-intensity ROA signals (for I positive at 375 cm^{-1} (61), negative at 367 cm^{-1} (62)) which is in accord with calculations.

DISCUSSION

We investigate spectroscopic properties of the nonplanar amide group at very specific and well-defined conditions represented by rigid chiral model compounds I and II that serve as standards of fixed and known geometry. These special properties are achieved by incorporating amide groups into a complicated tricyclic framework, where we must expect complex interconnections and mutual interactions of vibrational modes. If we wish to use amides in these and similar bonding situations as more general models, we have to understand the relative roles of rigid skeletons and embedded functional groups in the spectra of these tailor-made compounds. Their structural complexity is a distinct disadvantage; however it is partially balanced by the rigid structure (in I and II the rigidity is maximized at the branching points, spiroatom C_1 and amide nitrogens $N_{2,2'}$) and rather extreme nonplanarity. These molecules contain two amide groups fixed with respect to one another and mutually related by molecular C_2 symmetry axis. We can thus evaluate the relative importance of mutual distance and orientation against local effects within each of these amide groups. In order to verify our theoretical relations[28] between the sense of nonplanar amide deformations and parameters of vibrational optical activity we present a set of vibrational spectral data including IR/Raman and their chiral variants VCD/ROA. We expand our previous, limited (ECD/VCD) studies of methyl- and/or isobutyl derivatives of I and related spirodilactams.[40,47] New data include Raman/ROA spectra recorded in water and extend both below 1000 and above 2000 cm^{-1}. The compound II, a derivative of I, aids the assignment and provides VOA of C-D vibrations. As shown in the Results section these data provide good agreement with calculation, but a detailed understanding requires us to perform experiments with higher resolution and to incorporate anharmonicity into our theoretical interpretation. At the current level, although general experimental features are properly described, the harmonic-level calculation fails to assign unambiguously particular signals to individual CH_2/CD_2 groups. We intend to tackle this problem in a future computational study.

Characteristic vibrations of I and II related to amide I and amide II modes can be analyzed separately. The amide I signal that is widely used for amide characterization is found at ∼1710 cm^{-1} (in I). It is based on the C′═O stretching vibrations (∼75% according to Tables S3 and S4 in the Supporting Information) with minor proportions of C′−N stretching and ring A, B deformations. In both VCD and ROA we observe single-signed, although broad, amide I features, which are composed of two components, symmetric and antisymmetric. Single-signed VOA spectra appear unexpectedly as compounds with multiple amide groups (e.g., peptides/proteins) usually exhibiting VCD couplets describing dipole−dipole interactions, which vary in sign pattern according to different types of secondary structures. This coupling is certainly present, because both components of the amide I band are simultaneously (50/50) contributed by vibrations within both symmetry-related rings A and B. However, the appearance of observed single-signed VCD bands indicates a different origin, perhaps a local effect. We attempted to evaluate the relative importance of dipole−dipole coupling vs local effects by calculating rotational

dx.doi.org/10.1021/jp405226k | J. Phys. Chem. B 2013, 117, 9626−9642

strengths arising from the coupled oscillator mechanism. The dipole-coupling contribution can be estimated because we know absorption intensities (i.e., transition dipole moments) and molecular geometries. The previously suggested interpretation[47] assumes that C′═O bonds in I (and II) are nearly collinear. Consequently, the dipole−dipole coupling should be weak and the resulting couplet not visible. However, according to X-ray analysis (see above) the C′═O bonds are not collinear and their calculated coupling including rotational strength is not small. Using experimental values we calculated coupled oscillator contributions to amide I bands as $\mp 1.5 \times 10^{-42}$ esu^2 cm^2 at 1710/1700 cm^{-1} (the calculated component splitting of ∼10 cm^{-1} falls in the range of experimental values). This result indicates that, although the coupled oscillator contribution is comparable in magnitude to other bands in VCD spectra of dilactams, it definitely fails to describe the observed amide I VCD. Complete DFT calculation gives the correct result (a single-signed positive broad smaller band with two components in agreement with the experimental data); thus, we can conclude that some kind of local mechanism in this case largely prevails. Hence the sizable local effect overrides the coupling. In our spirocyclic dilactams, the reversed (head-to-head) connection of both amide groups weakens the interamide interactions because both C′═O groups are more distant (5.5 Å) than in a regularly arranged peptide chain (∼4 Å). Therefore the course of VOA can be dominated by local interactions originating independently from each amide group. The most probable candidate for such efficient local effect in I and II is the amide nonplanarity. Although within this artificial model situation the nonplanarity effect is probably overestimated, we can expect that its manifestation would be detectable even in less extreme situations (e.g., more flexible peptide chains containing secondary amide groups). The analogous phenomenon is exhibited also in ROA, although calculations hint at a low intensity couplet-like signal. This couplet is however strongly biased toward a single-signed amide I signal in agreement with experiment (Figures 6 and 7 and Tables S3 and S4 in the Supporting Information). It is interesting to note that tertiary amide groups exhibit similar nonsymmetrical single-signed ROA band in amide I region for structures showing a significant proportion of polyproline II conformation.[50] However, compared to spectra of the dilactams, this band appears some ∼40 cm^{-1} red-shifted.

Modified amide II vibration at ∼1400 cm^{-1} (modes 21 and 22 (I); 19 and 20 (II); see Figures 4−7 and Tables S3 and S4 in the Supporting Information) is more specific. The tricyclic structure influences these modes via several mechanisms. The nitrogen atoms are even more fixed than the remaining parts of these molecules and their vibrational motion senses limitations imposed by two rings at once. At the same time, the absence of N−H bonds (in secondary amides δ_{ip}(N−H) supplies nearly 50% of amide II mode)[48] seriously influences mode composition. Additional effects consist in amide nonplanarity and proximity of the two nitrogens within the whole structure of the molecule which in this case may favor amide−amide coupling against local effects. The observed transition wavenumber is lower than usually observed for secondary amides (∼1570 cm^{-1}).[48] In our dilactams, the modified amide II modes contain ∼35% of C′−N stretching vibrations, correlating well with the analogous contribution in secondary amides (33%). The missing contribution of the N−H in-plane bending is replaced by combined skeletal stretching (N−C including) vibrations together with spiro-system and in-plane deformations (30−35%) within the rings. The close proximity of both amide nitrogen atoms (∼2.3 Å), resulting from reversed orientation of amide groups clearly means that the associated LP can easily interact. At the same time, the distance between C′−N bonds remains approximately equal to that in peptides. In summary, this situation favors interamide coupling vs potential local effects of amide nonplanarity, contrary to above-mentioned findings for amide I mode. Accordingly, in VCD we observe a very strong couplet with the sign pattern conforming to simple coupled oscillator calculation based again on experimental data (the large splitting of ∼25 cm^{-1} and rotational strength of $\mp 1.1 \times 10^{-42}$ esu^2 cm^2). Calculated couplet intensities for amide I and II transitions are comparable. As a consequence, the simplified calculation on amide II does not quantitatively balance local vs coupling effects (according to experiment, the amide II couplets dominate VCD spectra). This is not surprising because this mode exhibits a more complicated composition than amide I besides uncertain knowledge of local transition moments. On the contrary, the balance of coupling and local effects is properly described by complete ab initio calculation (the coupling is favored). As follows from the above discussion, the detailed results on amide II vibrations and the connected VOA of our spirodilactams are not exactly transferable to more flexible molecules. Interestingly, calculations indicate an existence of analogous, though weak couplet also in ROA spectra, but this phenomenon is not experimentally detected (Figures 6 and 7).

Excluding amide II bands, the region between 700 and 1500 cm^{-1} contains mostly skeletal stretches and CH_2 deformations. These include CH_2 scissoring (1450−1500 cm^{-1}), wagging, rocking, and twisting deformations (700−1350 cm^{-1}) and skeletal system stretching (700−1350 cm^{-1}, but mainly below 1000 cm^{-1}). Among them we identify a dominant skeletal breathing vibration at ∼700 cm^{-1} which is a high-intensity Raman band with a positive counterpart in ROA spectra. According to PED data this Raman signal represents the most characteristic manifestation of the entire rigid polycyclic skeleton. Interestingly, bands analogous to this feature keep appearing in spectra of other compounds having rigid polycyclic hydrocarbon skeletons, e.g., α-pinene (at ∼660 cm^{-1}), pinane, camphor, and other terpenic compounds.[35,38,79] The vibrations in this region often involve minor mixing with amide modes (this is conditioned by specific geometries of I and II, which lack any symmetry plane); however, the corresponding contributions generally amount to less than 10% (according to PED data).

Further characteristic amide-related features are located below 900 cm^{-1}. Within spectra of I and II we observe well resolved Raman/ROA of relatively high intensity. Raman and ROA spectra of the available topologically similar systems like terpenes exhibit in this region generally less intense signals, particularly in the absence of functional groups. The well resolved bands in the spectra of I and II provide therefore an adequate material for the assignment and analysis of additional amide related modes. This procedure leads to a group of Raman/ROA features associated with δ_{ip}, δ_{oop} bonds to amide nitrogen atoms. As shown above, these modes contribute significantly to several vibrations. In several cases (e.g., modes 41 and 55−57), the in-plane and out-of-plane deformations tend to act together probably because of nonplanar amide geometries, which obscure differences between in-plane and out-of-plane bending motions. Comparison of calculations to experiment enables us to identify the most promising

dx.doi.org/10.1021/jp405226k | J. Phys. Chem. B 2013, 117, 9626−9642

candidates for amide nonplanarity detection and evaluation of their spectral manifestation. Among them the most characteristic vibration, describing the out-of-plane bending motion around nitrogen atoms, seems to be associated with the strong ROA feature at 568 cm^{-1}. Intensity of this signal definitely indicates that the associated vibration is connected with a considerable polarizability change. Similar character is displayed by other features at 707 and 649 cm^{-1}, but these are connected with bending motions involving C′═O grouping. Connection of these low wavenumber signals with vibrational motion involving nonplanar amides seems to be firmly established. The Raman/ROA features probably possess the potential for quantitative evaluation of nonplanar amide characteristics (e.g., sense and magnitude of amide distortion). However, for such analysis we need additional model compounds having desirable properties, like varying degree and detailed nature of amide nonplanarity (e.g., regular or twisted pyramid of bonds to amide nitrogen), varying flexibility, nature of amides (secondary vs tertiary), and a change of mutual orientation of amide groups. In this respect we have already selected several compounds for further studies. Similarly, it is possible to observe separate manifestation of skeletal deformations as shown in our spectra within modes 61 and 62. Signals corresponding to these modes are well observable, but their assignment to either amide or skeletal deformations needs further computational support. Consequently, it seems difficult to utilize ROA in this low wavenumber region as the direct means for detecting and/or evaluating amide nonplanarity manifestation.

The next step in the studies of the possible role amide nonplanarity plays in peptide structures should include further model molecules designed more toward real peptides. Examples of such an approach might be dipeptide units (e.g., acetylalanine methylamide). Such structures may potentially exhibit a minor degree of amide nonplanarity within very flexible molecules. Vibrational and chiroptical properties of amide group in nonplanar conformations of dipeptide units have been already investigated by Polavarapu and Jalkanen[80,81] although particular attention to amide nonplanarity has yet to be paid. The use of suitable models with somewhat limited conformational freedom, e.g., acetyl-L-tert-leucine methylamide,[82] might provide amide nonplanarity detection in the less special situation than represented by polycyclic dilactams. It is yet possible to tentatively compare VOA data of our spirodilactams to the results of our previous computational study of conformations of NMA,[28] which possess nonplanar amide groups. Unfortunately, NMA contains only a secondary amide group, and a comparison of its calculated VOA with the spectra of tertiary amides in I and II is difficult even to justify. The NMA calculations assume only fixed values of the ω angle (probably affecting the force field) and the pyramid of bonds to N remains calculated approximately regular, i.e. $\tau \approx 0°$, while the corresponding arrangement in I (or II) is seriously twisted ($\tau \approx +20°$ for R-I or II). For these reasons we limit the comparison to amide I vibrations only. These nearly linear vibrations might be least influenced by the above approximations. Experimental dilactam geometries exhibit $\omega \approx -10°$ (R-I, R-II), for which the approximate calculation predicts a positive amide I band in VCD and a negative one in ROA (see Figures 7 and 8 of ref 28) in agreement with our experiment. Although significance of this finding cannot be overrated, it is still remarkable. Unfortunately, this correlation could not be extended to lower-energy amide vibrations, because the corresponding modes are either very seriously affected by the above approximations, or not existent in tertiary amides at all (amide III). This result would have to be verified by studies on more model situations to have a real value for amide nonplanarity detection.

CONCLUSIONS

In the spectra of selected model dilactams I and II, which bear a resemblance to peptidic molecules, we located VOA signals reflecting selectively the amide nonplanarity manifestation. We can detect amide nonplanarity mainly on the basis of the classical amide I and pseudoamide II vibrations. Rigid tricyclic structure allowed us to utilize the advantage of fixed geometries. According to our findings, amide I and amide II vibrations are decisively influenced by nonplanar deformations. Dilactam structures allowed us to compare amide nonplanarity (a local effect) with amide−amide coupling acting over a distance of several bonds. In the tricyclic dilactams the relative distances between carbonyls are bigger than those between amide nitrogens. Accordingly, VOA (VCD and ROA) signals of the farther apart C′═O groups (amide I vibrations) are probably governed by the amide nonplanarity resulting in single signed VOA features, while the close together N−C′ bonds show a couplet (in C′−N stretching vibrations) due to interamide coupling (detectable in VCD only). We have located further nonplanarity related to VOA features within amide V and amide VI vibrations, which can be accessed only by Raman/ROA spectroscopy. As a distinct advantage, the Raman/ROA experiments can be done in water. DFT calculations done at the nowadays standard level (B3LYP functional with long-range dispersion correction, 6-311++G** basis set, CPCM solvent model) achieve within harmonic model a successful band-to-band spectral interpretation. In summary our study demonstrates that amide nonplanarity can be investigated in solution using methods of vibrational optical activity, especially when the experiments are complemented with ab initio calculations. Our model studies indicate that the computations can be extended to more flexible structures, e.g., peptides and proteins. However, there is still a need for further studies using less rigid models containing amides of varying degrees of nonplanarity and, preferentially, the secondary amide groups. The measurement of VOA within C−H and C−D stretching vibrations cannot be thoroughly interpreted within just a harmonic level calculation. On the other hand, our high-quality experimental data can be used as a test for anharmonicity corrections.

ASSOCIATED CONTENT

Supporting Information

(a) Comparison of experimental ROA spectra of I as measured on two different instruments; (b) ROA spectra comparison of both enantiomers of I; (c) a comparison of VOA data obtained with different theoretical methods and basis sets; (d) a definition of internal coordinates used for force field calculation; and (e) vibrational data of I and II in a tabular form. This material is available free of charge via the Internet at http://pubs.acs.org.

AUTHOR INFORMATION

Corresponding Author

*Phone: 00420-221-911-346. E-mail: malonp@karlov.mff.cuni.cz.

Notes

The authors declare no competing financial interest.

■ ACKNOWLEDGMENTS

This work has been supported by the Grant Agency of the Czech Republic (P205-10-1276), by MSMT (21/2011), by the Grant Agency of Charles University in Prague (Project No. 578212), and by Research Projects RVO 61388963 and MSM6046137301. The VCD part of this work has been started in the laboratory of Professor T. A. Keiderling, University of Illinois, Chicago, U.S.A. Elemental analyses and optical rotation measurements of the compounds I and II were carried out at Analytical Laboratories of the IOCB (Mgr. S. Matějková, Head). IR absorption spectra were measured by P. Fiedler and Vašíčková, Department of Molecular Spectroscopy. We thank A. Březinová and Dr. J. Cvačka of the Mass Spectrometry Department for the measurement and help with the presentation of high resolution mass spectra.

■ REFERENCES

(1) Dasgupta, A. K.; Majumdar, R.; Bhattacharyya, D. Characterization of Non-Planar Peptide Groups in Protein Crystal Structures. *Indian J. Biochem. Biophys.* **2004**, *41* (5), 233−240.

(2) MacArthur, M. W.; Thornton, J. M. Deviations from Planarity of the Peptide Bond in Peptides and Proteins. *J. Mol. Biol.* **1996**, *264* (5), 1180−95.

(3) Pauling, L.; Corey, R. B.; Branson, H. R. The Structure of Proteins; Two Hydrogen-Bonded Helical Configurations of the Polypeptide Chain. *Proc. Natl. Acad. Sci. U.S.A.* **1951**, *37* (4), 205−211.

(4) Edison, A. S. Linus Pauling and the Planar Amide Bond. *Nat. Struct. Biol.* **2001**, *8* (3), 201−202.

(5) Ramachandran, G. N.; Lakshminarayanan, A. V.; Kolaskar, A. S. Theory of the Non-Planar Peptide Unit. *Biochim. Biophys. Acta* **1973**, *303* (1), 8−13.

(6) Kolaskar, A. S.; Lakshminarayanan, A. V.; Sarathy, K. P.; Sasisekharan, V. The Non-Planar Peptide Unit III. Quantum Chemical Calculations for Related Compounds and Experimental X-Ray Diffraction Data. *Biopolymers* **1975**, *14*, 1081−1094.

(7) Renugopalakrishnan, V.; Rein, R. Energetics of Deformation of a Peptide Unit - Semiempirical Molecular-Orbital and Ab-Initio Study of *N*-Methyl Acetamide and *N*-Acetyl-L-Alanine *N*-Methyl Amide. *Biochim. Biophys. Acta* **1976**, *434* (1), 164−168.

(8) Ramachandran, G. N.; Kolaskar, A. S. The Non-Planar Peptide Unit. II. Comparison of Theory with Crystal Structure Data. *Biochim. Biophys. Acta* **1973**, *303* (2), 385−388.

(9) Winkler, F. K.; Dunitz, J. D. Non-Planar Amide Group. *J. Mol. Biol.* **1971**, *59* (1), 169−182.

(10) Berkholz, D. S.; Driggers, C. M.; Shapovalov, M. P.; Dunbrack, R. L. J.; Karplus, P. A. Nonplanar Peptide Bonds in Proteins Are Common and Conserved but Not Biased toward Active Sites. *Proc. Natl. Acad. Sci. U.S.A.* **2012**, *109*, 449−453.

(11) Improta, R.; Vitagliano, L.; Esposito, L. Peptide Bond Distortions from Planarity: New Insights from Quantum Mechanical Calculations and Peptide/Protein Crystal Structures. *PLOS One* **2011**, *e24553*, 1−10.

(12) Tichý, M.; Dušková, E.; Bláha, K. Optically Active 4-Azatricyclo[4,4,0,$0^{3,8}$]Decan-5-One: Model of a Non-Planar Amide Bond. *Tetrahedron Lett.* **1974**, *15*, 237−240.

(13) Bláha, K.; Maloň, P.; Tichý, M.; Frič, I.; Usha, R.; Ramakumar, S.; Venkatesan, K. Crystal Structure and Chiroptical Properties of (+)-(3S)-4-Azatricyclo[4,3,1,$0^{3,7}$]Decan-5-One. *Collect. Czech. Chem. Commun.* **1978**, *43*, 3241−3251.

(14) Frič, I.; Maloň, P.; Tichý, M.; Bláha, K. Chiroptical Properties of 4-Azatricyclo[4,4,0,0,^{3,8}]Decan-5-One - Lactam with a Non-Planar Cis-Amide Group. *Collect. Czech. Chem. Commun.* **1977**, *42* (2), 678−686.

(15) Maloň, P.; Bláha, K. Quantum Chemical Calculations on 4-Azatricyclo[4,4,0,$0^{3,8}$]Decan-5-One - Lactam with a Non-Planar Cis-Amide Group. *Collect. Czech. Chem. Commun.* **1977**, *42* (2), 687−696.

(16) Maloň, P.; Frič, I.; Tichý, M.; Bláha, K. Chiroptical Properties of (-)-4-Methyl-4-Azatricyclo[4,4,0,$0^{3,8}$]Decan-5-One - Lactam with a Non-Planar Tertiary Cis-Amide Group. *Collect. Czech. Chem. Commun.* **1977**, *42* (10), 3104−3110.

(17) Tichý, M.; Farag, A. M.; Maloň, P.; Kálal, P.; Bláha, K. (3R)-5-Azatricyclo[4.3.1.$0^{3,8}$]Decan-4-One, a Lactam with a Non-Planar Cis-Amide Group - Synthesis, Geometry and Chiroptical Properties. *Collect. Czech. Chem. Commun.* **1984**, *49* (4), 834−839.

(18) Tichý, M.; Maloň, P.; Frič, I.; Bláha, K. Synthesis and Chiroptical Properties of (−)-(1R)-3-Azatricyclo[5,4,0,$0^{4,9}$]Undecan-2-One − Lactam with Non-Planar Cis-Amide Group. *Collect. Czech. Chem. Commun.* **1979**, *44* (9), 2653−2659.

(19) Bláha, K.; Maloň, P. Non-Planarity of the Amide Group and Its Manifestation. *Acta Univ. Palacki Olomuc.* **1980**, *93*, 81−96.

(20) Maloň, P.; Bystrický, S.; Bláha, K. Non-Planar Amide Group and Its Chiroptical Manifestation. In *Peptides 1978, Proc. 15th European Peptide Symposium*, Wroclaw University Press: Wroclaw, 1979; pp 269−272.

(21) Smolíková, J.; Bláha, K. Structure of Amide Group. *Chem. Listy* **1975**, *69* (10), 1009−1055.

(22) Klyne, W.; Kirk, D. N.; Tilley, J.; Suginome, H. Chiroptical Studies 99. Circular Dichroism of 7-Membered Lactams and Lactones. *Tetrahedron* **1980**, *36*, 543−553.

(23) Shustov, G. V.; Kadorkina, G. K.; Varlamov, S. V.; Kachanov, A. V.; Kostyanovsky, R. G.; Rauk, A. The Nonplanar Amide Group in *N*-Acylaziridines - Conformational Behavior and Chiroptical Properties. *J. Am. Chem. Soc.* **1992**, *114* (5), 1616−1623.

(24) Shustov, G. V.; Kachanov, A. V.; Chervin, I. I.; Kostyanovsky, R. G.; Rauk, A. Stereochemistry and Chiroptical Properties of 1,3-Dialkylaziridinones (α-Lactams) - Chiral Rules for the Nonplanar Amide Chromophore. *Can. J. Chem.* **1994**, *72* (2), 279−286.

(25) Shustov, G. V.; Polyak, F. D.; Kadorkina, G. K.; Vosekalna, I. A.; Shokhen, M. A.; Alekperov, R. K.; Eremeev, A. V.; Kostyanovsky, R. G. Chiroptical Properties of the Nonplanar Amide Chromophore in N-Acylaziridines. *Chem. Heterocycl. Compd.* **1989**, *25*, 32−39.

(26) Boyd, D. B.; Riehl, J. P.; Richardson, F. S. Chiroptical Properties of 1-Carbapenam and Orbital Mixing in Nonplanar Amides. *Tetrahedron* **1979**, *35*, 1499−1506.

(27) Frelek, J.; Lysek, R.; Borsuk, K.; Jagodzinski, J.; Furman, B.; Klimek, A.; Chmielewski, M. Structure-Chiroptical Properties Relationship in Oxabicyclic Beta-Lactam Derivatives. *Enantiomer* **2002**, *7*, 107−114.

(28) Bednárová, L.; Maloň, P.; Bouř, P. Spectroscopic Properties of the Nonplanar Amide Group: A Computational Study. *Chirality* **2007**, *19* (10), 775−786.

(29) Maloň, P.; Bystrický, S.; Bláha, K. Semi-Empirical Calculation of Optical-Rotatory Strength of Non-Planar Conformations of Formamide. *Collect. Czech. Chem. Commun.* **1978**, *43* (3), 781−790.

(30) Woody, R. W. A Simple-Model for the Optical-Properties of Chiral Amides. *Biopolymers* **1983**, *22* (1), 189−203.

(31) Andrushchenko, V.; Matějka, P.; Anderson, D. T.; Kaminský, J.; Horníček, J.; Paulson, L. O.; Bouř, P. Solvent Dependence of the *N*-Methylacetamide Structure and Force Field. *J. Phys. Chem. A* **2009**, *113* (35), 9727−9736.

(32) Chalupský, J.; Vondrášek, J.; Špirko, V. Quasiplanarity of the Peptide Bond. *J. Phys. Chem. A* **2008**, *112* (4), 693−699.

(33) Tvaroška, I.; Bystrický, S.; Maloň, P.; Bláha, K. Nonplanar Conformations of Methylacetamide - Solvent Effect and Chiroptical Properties. *Collect. Czech. Chem. Commun.* **1982**, *47* (1), 17−28.

(34) Maloň, P.; Bouř, P. In *Amide Group Non-Planarity in Helical Peptide Segments: Vibrational Optical Activity Implications*; 23rd European Peptide symposium; Maia, H. L. S., Ed.; Escom Science Publishers, Leiden: Bragga, 1995.

(35) Barron, L. D., *Molecular Light Scattering and Optical Activity*. 2 ed.; Cambridge University Press: Cambridge, 2004.

(36) Berova, N.; Nakanishi, K.; Woody, R. W., *Circular Dichroism Principles and Applications*. 2 ed.; Wiley-VCH, New York,: 2000.
(37) Nafie, L. A. *Vibrational Optical Activity Principles and Applications*; Wiley: Chichester, U.K., 2011.
(38) Bouř, P.; Baumruk, V.; Hanzlíková, J. Measurement and Calculation of the Raman Optical Activity of a-Pinene and Trans-Pinane. *Collect. Czech. Chem. Commun.* **1997**, *62*, 1384−1395.
(39) Bláha, K.; Buděšínský, M.; Frič, I.; Koblicová, Z.; Maloň, P.; Tichý, M. Polycyclic Dilactams with Inherently Chiral Amide Chromophores. *Tetrahedron Lett.* **1978**, *41*, 3949−3952.
(40) Bláha, K.; Buděšínský, M.; Koblicová, Z.; Maloň, P.; Tichý, M.; Baker, J. R.; Hossain, M. B.; van der Helm, D. Optically-Active Tricyclic Dilactams with Nonplanar Cis-Amide Groups - Synthesis, X-Ray, NMR and CD Studies. *Collect. Czech. Chem. Commun.* **1982**, *47* (3), 1000−1019.
(41) Bláha, K.; Farag, A. M.; van der Helm, D.; Hossain, M. B.; Buděšínský, M.; Maloň, P.; Smolíková, J.; Tichý, M. Stereoisomeric Chiral 2,9-Diazabicyclo[4.4.0]Decane-3,10-Diones as Models of Dipeptide Grouping − Synthesis, X-Ray, IR, NMR and CD Studies. *Collect. Czech. Chem. Commun.* **1984**, *49*, 712−742.
(42) Vičar, J.; Maloň, P.; Trka, A.; Smolíková, J.; Frič, I.; Bláha, K. Synthesis and Spectral Properties of Cyclotripeptides Containing 2-Azetidinecarboxylic Acid or Proline. *Collect. Czech. Chem. Commun.* **1977**, *42*, 2701−2717.
(43) Smoliková, J.; Koblicová, Z.; Bláha, K. Amino-Acids and Peptides 110. Infrared-Spectra of Polycyclic Spiro-Dilactams with Non-Planar Amide Bonds. *Collect. Czech. Chem. Commun.* **1973**, *38* (2), 532−547.
(44) Ealick, S. E.; van der Helm, D. The Crystal and Molecular Structure of 5,8-Diaza-4,9-Dioxotricyclo[6,3,0,0,^{1,5}]Undecane, a Non-Planar Tertiary Amide. *Acta Crystallogr.* **1975**, *31*, 2676−2680.
(45) Ealick, S. E.; van der Helm, D. The Crystal and Molecular Structure of 6,9-Diaza-5,10-Dioxotricyclo[7.3.0.0^{1,6}]Dodecane, a Molecule Designed to Contain Non-Planar Amide Bonds. *Acta Crystallogr.* **1977**, *33*, 76−80.
(46) Ealick, S. E.; Washecheck, D. M.; van der Helm, D. The Crystal Structures of Two Tetracyclic Spirodilactams Containing Non-Planar Amide Bonds. *Acta Crystallogr.* **1976**, *32*, 895−900.
(47) Maloň, P.; Barness, C. L.; Buděšínský, M.; Dukor, R. K.; van der Helm, D.; Keiderling, T. A.; Koblicová, Z.; Pavliková, F.; Tichý, M.; Bláha, K. (1S,7S)-7-Methyl-6,9-Diazatricyclo[6,3,0,0^{1,6}]Tridecane-5,10-Dione, a Tricyclic Spirodilactam Containing Non-Planar Amide Groups - Synthesis, NMR, Crystal Structure, Absolute-Configuration, Electronic and Vibrational Circular Dichroism. *Collect. Czech. Chem. Commun.* **1988**, *53* (11A), 2447−2472.
(48) Krimm, S.; Bandekar, J. Vibrational Spectroscopy and Conformation of Peptides, Polypeptides, and Proteins. *Adv. Protein Chem.* **1986**, *38*, 181−364.
(49) Dwivedi, A. M.; Krimm, S.; Mierson, S. Vibrational Force Field and Normal Mode Analysis of N,N-Dimethylacetamide. *Spectrochim. Acta* **1989**, *45A*, 271−279.
(50) Kapitán, J.; Baumruk, V.; Bouř, P. Demonstration of the Ring Conformation in Polyproline by the Raman Optical Activity. *J. Am. Chem. Soc.* **2006**, *128*, 2438−2443.
(51) Hanzlíková, J.; Praus, P.; Baumruk, V. Raman Optical Activity Spectrometer for Peptide Studies. *J. Mol. Struct.* **1999**, *481*, 431−435.
(52) Choquette, S. J.; Etz, E. S.; Hurst, W. S.; Blackburn, D. H.; Leigh, S. D. Relative Intensity Correction of Raman Spectrometers: NIST SRMs 2241 through 2243 for 785 nm, 532 nm, and 488 nm/514.5 nm Excitation. *Appl. Spectrosc.* **2007**, *61* (2), 117−129.
(53) Hug, W.; Hangartner, G. A Novel High-Throughput Raman Spectrometer for Polarization Difference Measurements. *J. Raman Spectrosc.* **1999**, *30* (9), 841−852.
(54) Parr, R. G.; Yang, W. *Density-Functional Theory of Atoms and Molecules*; Oxford University Press: New York, 1994.
(55) Frisch, M. J.; et al. *Gaussian 09*, revision B01; Gaussian, Inc.: Wallingford, CT, 2009.
(56) Kim, K.; Jordan, K. D. Comparison of Density Functional and MP2 Calculations on the Water Monomer and Dimer. *J. Phys. Chem.* **1994**, *98* (40), 10089−10094.
(57) Stephens, P. J.; Devlin, F. J.; Chabalowski, C. F.; Frisch, M. J. Ab Initio Calculation of Vibrational Absorption and Circular Dichroism Spectra Using Density Functional Force Fields. *J. Phys. Chem.* **1994**, *98* (45), 11623−11627.
(58) Ditchfield, R.; Hehre, W. J.; Pople, J. A. Self-Consistent Molecular-Orbital Methods. IX. An Extended Gaussian-Type Basis for Molecular-Orbital Studies of Organic Molecules. *J. Chem. Phys.* **1971**, *54* (2), 724−728.
(59) Perdew, J. P.; Wang, Y. Accurate and Simple Analytic Representation of the Electron-Gas Correlation Energy. *J. Chem. Phys.* **1992**, *45* (23), 13244−13249.
(60) Dunning, T. H., Jr. Gaussian Basis Sets for Use in Correlated Molecular Calculations. I. The Atoms Boron through Neon and Hydrogen. *J. Chem. Phys.* **1989**, *90* (2), 1007−1023.
(61) Møller, C.; Plesset, M. S. Note on an Approximation Treatment for Many-Electron Systems. *Phys. Rev.* **1934**, *46* (7), 618−622.
(62) Grimme, S. Semiempirical GGA-Type Density Functional Constructed with a Long-Range Dispersion Correction. *J. Comput. Chem.* **2006**, *27*, 1787−1799.
(63) Grimme, S.; Antony, J.; Ehrlich, S.; Krieg, H. A Consistent and Accurate Ab Initio Parametrization of Density Functional Dispersion Correction (DFT-D) for the 94 Elements H-Pu. *J. Chem. Phys.* **2010**, *132* (15), 154104.
(64) Schwabe, T.; Grimme, S. Double-Hybrid Density Functionals with Long-Range Dispersion Corrections: Higher Accuracy and Extended Applicability. *Phys. Chem. Chem. Phys.* **2007**, *9* (26), 3397−3406.
(65) Klamt, A.; Schuurman, G. Cosmo: A New Approach to Dielectric Screening in Solvents with Explicit Expressions for the Screening Energy and Its Gradient. *J. Chem. Soc., Perkin Trans. 2* **1993**, *2* (5), 799−805.
(66) Klamt, A. Cosmo and Cosmo-Rs. In *Encyclopedia of Computational Chemistry*; Schleyer, P. R., Allinger, N. L., Clark, T., Gasteiger, J., Kollman, P. A., Schaefer, H. F., III, Schreiner, P. R., Eds.; John Wiley & Sons: Chichester, U.K., 1998; Vol. *1*, pp 604−615.
(67) Suenaga, M. Facio: New Computational Chemistry Environment for PC Gamess. *J. Comput. Chem. Jpn.* **2005**, *4* (4), 25−32.
(68) Califano, S. *Vibrational States*; Wiley: New York, 1976; pp 235−236.
(69) Fogarasi, G.; Pulay, P. *Ab Initio Vibrational Force Fields*; Elsevier: Amsterdam, 1985; Vol. *14*, pp 125−150.
(70) Fogarasi, G.; Pulay, P. *Vibrational Spectra and Structure*; Elsevier: Amsterdam, 1984.
(71) Kajtár, M.; Hollósi, M.; Kinsky, K.; Majer, Z. Spiro-Bis(2-Pyrrolidinones) 0.1. Synthesis and Absolute-Configuration of 3 Isomeric Spiro-Bis(2-Pyrrolidinones). *Collect. Czech. Chem. Commun.* **1982**, *47* (3), 936−949.
(72) Scipioni, A. Sulla Preparazione Dell'acido Γ-Chetopimelico E Di Alcuni Suoi Derivati. *Ann. Chim. (Rome)* **1952**, *42*, 53−61.
(73) Jones, P. G. Crystal Structure Determination: A Critical View. *Chem. Soc. Rev.* **1984**, *13* (2), 157−172.
(74) Maloň, P.; Keiderling, T. A.; Uang, J.; Chickos, J. S. Vibrational Circular-Dichroism Study of [3R,4R]-Dideuteriocyclobutane-1,2,-Dione − Preliminary Comparison of Experiment and Calculations. *Chem. Phys. Lett.* **1991**, *179*, 282−290.
(75) Keiderling, T. A.; Stephens, P. J. Vibrational Circular Dichroism of Spirononadiene. Fixed Partial Charge Calculations. *J. Am. Chem. Soc.* **1979**, *101*, 1396−1400.
(76) Nafie, L. A.; Keiderling, T. A.; Stephens, P. J. Vibrational Circular Dichroism. *J. Am. Chem. Soc.* **1976**, *98*, 2715−2723.
(77) Bouř, P.; Tam, C. N.; Shaharuzzaman, M.; Chickos, J. S.; Keiderling, T. A. Vibrational Optical Activity Study of Trans-D2-Succinic Anhydride. *J. Phys. Chem.* **1996**, *100*, 15041−15048.
(78) Maloň, P.; Mickley, L. J.; Sluis, K. M.; Tam, C. N.; Keiderling, T. A.; Kamath, S.; Uang, J.; Chickos, J. S. Vibrational Circular Dichroism Study of (2S,3S)-Dideuteriobutyrolactone − Synthesis, Normal Mode

Analysis and Comparison of Experimental and Calculated Spectra. *J. Phys. Chem.* **1992**, *96*, 10139−10149.
(79) Brocki, T.; Moskovits, M.; Bosnich, B. Vibrational Optical Activity. Circular Differential Raman Scattering from a Series of Chiral Terpenes. *J. Am. Chem. Soc.* **1980**, *102*, 495−500.
(80) Deng, Z.; Polavarapu, P.; Ford, S. J.; Hecht, L.; Barron, L. D.; Ewig, C. S.; Jalkanen, K. Solution-Phase Conformations of *N*-Acetyl-*N*′-Methyl-L-Alaninamide from Vibrational Raman Optical Activity. *J. Phys. Chem.* **1996**, *100*, 2025−2034.
(81) Wen-Ge, H.; Jalkanen, K. J.; Elstner, M. S. S. Theoretical Study of Aqueous *N*-Acetyl-L-Alanine *N*′-Methylamide: Structures and Raman, VCD and ROA Spectra. *J. Phys. Chem. B* **1998**, *102*, 2587−2602.
(82) Maloň, P.; Pančoška, P.; Buděšínský, M.; Hlaváček, J.; Pospíšek, J.; Bláha, K. Amino-Acids and Peptides.181. Chiroptical Properties and Conformation of *N*-Acetyl-L-Amino Acids *N*′-Methylamides with Aliphatic Side Chains, Amino Acids and Peptides 181. *Collect. Czech. Chem. Commun.* **1983**, *48*, 2488−2861.

Supporting Information

Non-Planar Tertiary Amides in Rigid Chiral Tricyclic Dilactams. Peptide Group Distortions and Vibrational Optical Activity

Markéta Pazderková[1,2], Václav Profant[2], Jana Hodačová[3], Jaroslav Šebestík[1], Tomáš Pazderka[2], Pavlína Novotná[3], Marie Urbanová[3], Martin Šafařík[1], Miloš Buděšínský[1], Miloš Tichý[1], Lucie Bednárová[1], Vladimír Baumruk[2] and Petr Maloň[1,2]

[1]*Institute of Organic Chemistry and Biochemistry AS CR, 166 10 Prague 6, Czech Republic*
[2]*Charles University in Prague, 121 16 Prague 2, Czech Republic*
[3]*Institute of Chemical Technology, 166 28 Prague 6, Czech Republic*

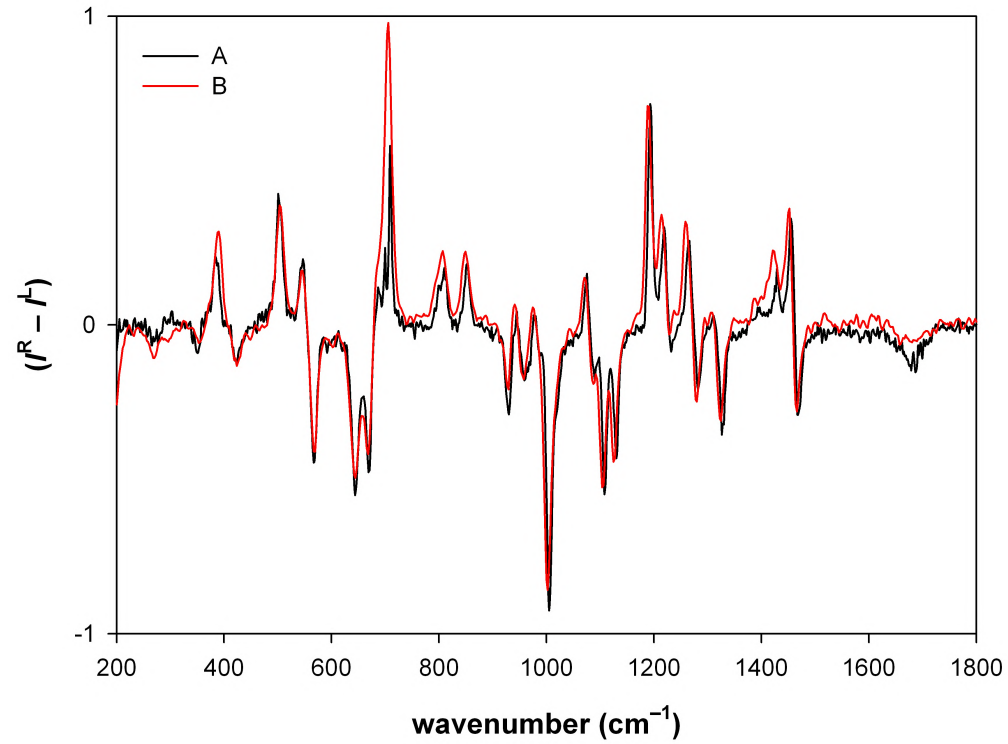

Figure S1. Comparison of ROA spectra of (–)-(1R)-I measured on two different instruments: A – ICP ROA instrument built at Charles University in Prague; B – commercial SCP ROA instrument Chiral*RAMAN*-2X™ (BioTools Inc., USA)

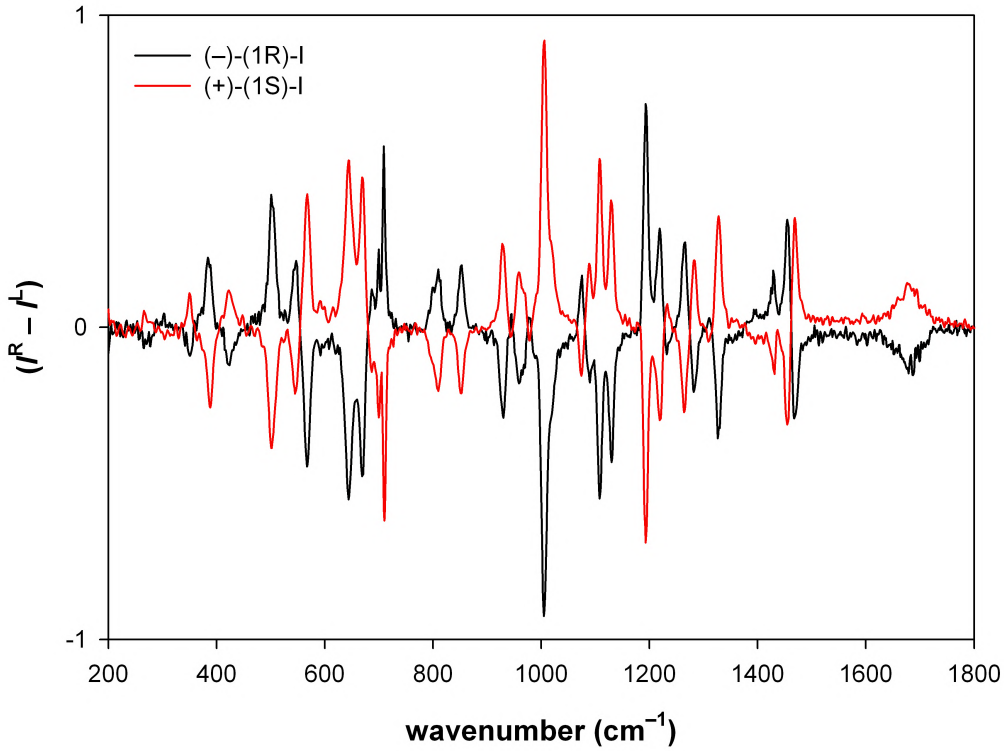

Figure S2. Uncorrected ROA spectra of both enantiomers of I measured in H_2O

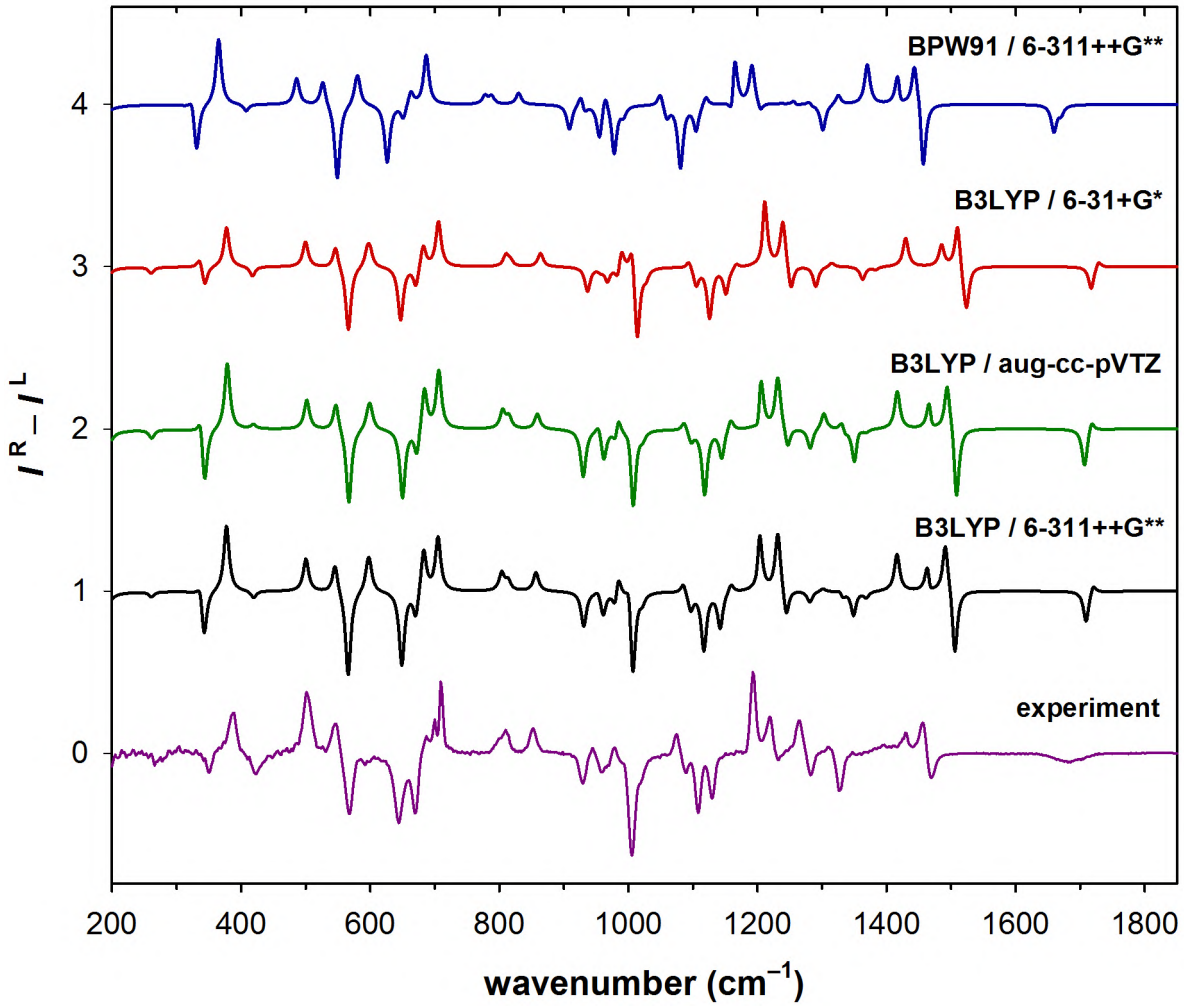

Figure S3. ROA spectra of (–)-(1R)-I calculated by different variants of DFT procedures. All DFT calculations were performed using implicit water solvation model.

Table S1. Energy and cost effectivity of Raman/ROA calculations of I related to computational methodology

method / functional	basis set	number of basis functions	energy [Ha]	time cost of opt [h]	time cost of spec [h]
	3-21G	141	-606.83	0.51	0.89
	3-21+G	193	-606.93	1.1	2.3
	4-31G	141	-609.36	0.66	1.24
	4-31G**	255	-609.61	1.21	4.1
	6-21G	141	-609.47	0.41	1.15
	6-21G**	255	-609.71	1.35	3.63
	6-31G	141	-609.99	0.64	0.74
B3LYP	6-31+G	193	-610.02	1.2	1.84
	6-31++G	205	-610.02	1.75	2.36
	6-31G*	219	-610.18	1.02	2.05
	6-31G**	255	-610.2	1.21	2.86
	6-31+G*	271	-610.21	1.91	6.37
	6-31++G**	319	-610.22	2.75	6.44
	6-311++G**	370	-610.35	4.43	11.06
	6-311++G** (6d 10f)	383	-610.36	4.52	11.08
	cc-pVDZ	242	-610.21	2.11	
B3LYP	aug-cc-pVDZ	407	-610.26	10.28	22.72
	aug-cc-pVDZ (6d 10f)	433	-610.27	10.32	29.73
	aug-cc-pVTZ	1015	-610.41	198.48	520.12
BPW91	6-311++G** (6d 10f)	383	-610.29	3.08	12.45
MP2	6-311++G** (6d 10f)	383	-608.68	18.54	

opt – optimization; spec – spectral calculation

Table S2. Internal coordinate definitions

S	description	S	description
1	$\nu(C_1\text{-}C_5)$	35	$\delta_{ip}\ C_6(C_1, N_2, C_3)$
2	$\nu(C_4\text{-}C_5)$	36	$\delta_{ip}\ C_{6'}(C_1, N_{2'}, C_{3'})$
3	$\nu(C_3\text{-}C_4)$	37	$\delta_{oop}\ C_6(C_1, N_2, C_3)$
4	$\nu(N_2\text{-}C_3)$	38	$\delta_{oop}\ C_{6'}(C_1, N_{2'}, C_{3'})$
5	$\nu(C_1\text{-}N_2)$	39	$\rho\ C_1, \beta_1 - \beta_2 + \beta_3 - \beta_4$
6	$\nu(C_1\text{-}C_{5'})$	40	$\omega\ C_1, \beta_1 + \beta_2 - \beta_3 - \beta_4$
7	$\nu(C_{4'}\text{-}C_{5'})$	41	$\tau\ C_1, \beta_1 - \beta_2 - \beta_3 + \beta_4$
8	$\nu(C_{3'}\text{-}C_{4'})$	42	$\delta_{ip}\ O_7(N_2, C_3, C_4)$
9	$\nu(N_{2'}\text{-}C_3)$	43	$\delta_{oop}\ O_7(N_2, C_3, C_4)$
10	$\nu(C_1\text{-}N_{2'})$	44	$\delta_{ip}\ O_{7'}(N_{2'}, C_{3'}, C_{4'})$
11	$\nu(N_2\text{-}C_6)$	45	$\delta_{oop}\ O_{7'}(N_{2'}, C_{3'}, C_{4'})$
12	$\nu(N_{2'}\text{-}C_{6'})$	46	$\delta_s\ C_5(H_{10}, H_{11})$
13	$\nu(C_3\text{=}O_7)$	47	$\rho\ C_5(H_{10}, H_{11})$
14	$\nu(C_{3'}\text{=}O_{7'})$	48	$\omega\ C_5(H_{10}, H_{11})$
15	$\nu(C_5\text{-}H_{10})$	49	$\tau\ C_5(H_{10}, H_{11})$
16	$\nu(C_5\text{-}H_{11})$	50	$\delta_s\ C_4\ (H_8, H_9)$
17	$\nu(C_4\text{-}H_9)$	51	$\rho\ C_4\ (H_8, H_9)$
18	$\nu(C_4\text{-}H_8)$	52	$\omega\ C_4\ (H_8, H_9)$
19	$\nu(C_{5'}\text{-}H_{11})$	53	$\tau\ C_4\ (H_8, H_9)$
20	$\nu(C_{5'}\text{-}H_{10'})$	54	$\delta_s\ C_{5'}\ (H_{10'}, H_{11'})$
21	$\nu(C_{4'}\text{-}H_{9''})$	55	$\rho\ C_{5'}\ (H_{10'}, H_{11'})$
22	$\nu(C_{4'}\text{-}H_{8'})$	56	$\omega\ C_{5'}\ (H_{10'}, H_{11'})$
23	$\nu(C_6\text{-}H_{12})$	57	$\tau\ C_{5'}\ (H_{10'}, H_{11'})$
24	$\nu(C_6\text{-}H_{13})$	58	$\delta_s\ C_{4'}\ (H_{8'}, H_{9'})$
25	$\nu(C_{6'}\text{-}H_{12'})$	59	$\rho\ C_{4'}\ (H_{8'}, H_{9'})$
26	$\nu(C_{6'}\text{-}H_{13'})$	60	$\omega\ C_{4'}\ (H_{8'}, H_{9'})$
27	δ ring A, $\alpha_1 + a(\alpha_2 + \alpha_5) + b(\alpha_3 + \alpha_4)$	61	$\tau\ C_{4'}\ (H_{8'}, H_{9'})$
28	δ'ring A, $(a - b)(\alpha_2 - \alpha_5) + (1 - a)(\alpha_3 - \alpha_4)$	62	$\delta_s\ C_6\ (H_{12}, H_{13})$
29	τ ring A, $b(\tau_1 + \tau_5) + a(\tau_2 + \tau_4) + \tau_3$	63	$\rho\ C_6\ (H_{12}, H_{13})$
30	τ' ring A, $(a - b)(\tau_4 - \tau_2)+(1 - a)(\tau_5 - \tau_1)$	64	$\omega\ C_6\ (H_{12}, H_{13})$
31	δ ring B, $\alpha_{1'} + a(\alpha_{2'} + \alpha_{5'}) + b(\alpha_{3'} + \alpha_{4'})$	65	$\tau\ C_6\ (H_{12}, H_{13})$
32	δ'ring B, $(a - b)(\alpha_{2'} - \alpha_{5'}) + (1 - a)(\alpha_{3'} - \alpha_{4'})$	66	$\delta_s\ C_{6'}\ (H_{12'}, H_{13'})$
33	τ ring B, $b(\tau_{1'} + \tau_{5'}) + a(\tau_{2'} + \tau_{4'}) + \tau_{3'}$	67	$\rho\ C_{6'}\ (H_{12'}, H_{13'})$
34	τ' ring B, $(a - b)(\tau_{4'} - \tau_{2'}) + (1 - a)(\tau_{5'} - \tau_{1'})$	68	$\omega\ C_{6'}\ (H_{12'}, H_{13'})$
		69	$\tau\ C_{6'}\ (H_{12'}, H_{13'})$

For definitions of the parameters α_i, β_i, τ_i, a, b, see [61-63]

ν – stretching, δ – deformation, τ – torsion, ρ – rocking, ω – wagging, δ_s – scissoring

Table S3. Vibrational data of the spirodilactam (–)-(1R)-I

mode	sym	PED	frequency (cm^{-1}), intensity								remark
			IR ($CHCl_3$)		Raman (H_2O)		VCD ($CDCl_3$)		ROA (H_2O)		
			calc.	exp.	calc.	exp.	calc.[b]	exp.	calc.	exp.	
1	B	S_{23},S_{25}	3124,vw	2980,m	3126,vs	3000,s	–3124,vw	–2980,m	+3126,vs	+3020,m	
2	A	S_{25},S_{23}	3117,vw	2951,m	3119,vs		+3117,vw		–3119,vs	–3000,m	
3	A	S_{22},S_{19}	3113,vw	2927,w	3114,vs		+3113,w	+2957,m	–3114,vs	–2962,m	
4	B	S_{18},S_{22}	3112,w		3112,s		+3112,vw		+3112,vs		
5	A	S_{19},S_{22},S_{16},S_{18}	3104,w		3106,vs		–3104,m	–2944,m	+3106,vs		
6	B	S_{16},S_{19},S_{15}	3100,vw		3103,vs		+3100,vw		–3103,vs		
7	A	S_{15},S_{20},S_{16},S_{19}	3044,vw	2894,m	3046,vs	2962,s	–3044,vw		–3046,s		
8	B	S_{24},S_{26}	3043,w	2879,w	3046,vs	2936,s	+3043,m	+2899,m	+3046,vs	+2936,m	
9	B	S_{15},S_{20},S_{24},S_{16},S_{19}	3043,w		3044,s	2900,m	–3043,w		–3044,vs	–2900,w	
10	A	S_{26},S_{24}	3036,w		3039,vs		–3036,m		–3039,vs		
11	A	S_{21},S_{17}	3034,vw		3035,vs		+3034,w	+2879,w	–3035,vs		
12	B	S_{17},S_{21}	3034,vw		3034,vs		–3034,vw		+3034,vs		
13	A	S_{14},S_{13}	1735,m	1718,sh	1719,vs	1694,m	+1735,w	+1718,sh	+1719,vw	–1681,w	amide I'
14	B	S_{13},S_{14}	1725,vs	1700,vs	1707,m	1681,m	+1725,s	+1699,m	–1707,s		amide I'
15	A	S_{62},S_{66}	1497,vw		1495,s	1467,m	+1497,vw	+1465,vw	–1495,s	–1469,m	
16	B	S_{66},S_{62},S_{46}	1493,w	1462,m	1491,m		+1493,w		–1491,m		
17	A	S_{54},S_{46},S_{66}	1490,vw		1489,m		–1490,vw		+1489,w	+1455,m	
18	B	S_{54},S_{46}	1484,w	1453,w	1482,m	1457,m	+1484,vw	+1454,vw	+1482,s		
19	A	S_{50},S_{58}	1457,vw		1455,m	1428,m	+1457,vw		–1455,s		
20	B	S_{58},S_{50}	1456,vw		1454,s		–1456,vw		+1454,s	+1429,m	
21	A	S_9,S_4	1414,m	1399,m	1419,s		–1414,vs	–1399,s	+1419,s	+1425,vw	amide II'
22	B	S_4,S_9	1371,s	1357,s	1374,vw		+1371,vs	+1357,s	–1374,w		amide II'
23	B	S_{64},S_{68},S_{56},S_{48}	1349,vw	1345,sh	1349,vw		+1349,m	+1345,sh	+1349,w		
24	A	S_{68},S_{64}	1345,vw		1345,m	1329,m	+1345,vw		–1345,m	–1327,m	
25	A	S_{56},S_{48}	1329,vw	1326,w	1329,w		+1329,vw	+1299,w	–1329,vw		
26	B	S_{68},S_{64},S_{48},S_{56}	1325,w	1299,w	1326,vw		+1325,vw		+1326,vw	+1310,vw	
27	A	S_{60},S_{57}	1299,w	1276,w	1299,w	1282,w	+1299,m	+1275,m	–1299,s	–1282,m	
28	B	S_{52},S_{49},S_{60}	1296,w		1296,vw		+1296,m		+1296,m		
29	A	S_{52},S_{60}	1280,w	1259,vw	1280,vw	1264,w	+1280,vw	+1260,vw	+1280,w	+1265,m	
30	B	S_{10}	1240,w		1240,vw	1232,w	+1240,m	+1224,m	–1240,w	–1233,w	
31	B	S_{49}	1233,w	1212,w[a]	1232,vw	1219,w	+1233,w		+1232,m	+1219,m	
32	A	S_{69},S_{65},S_{57}	1227,w		1227,vw		–1227,m	–1209,m	+1227,m		
33	B	S_{39},S_{40},S_{53},S_{61}	1198,w	1184,m	1199,s	1193,m	–1198,w	–1224,m	+1199,s	+1193,s	
34	A	S_{61},S_{53}	1196,vw		1196,m		–1196,vw		–1196,s		
35	B	S_5,S_{10}	1159,w	1153,w	1159,vw	1157,sh	+1159,vw	+1146,vw	+1159,w		
36	A	S_{63},S_{67}	1139,vw	1126,w	1139,w	1130,w	–1139,w	–1126,m	–1139,m	–1130,m	
37	A		1111,vw		1111,w	1108,w	+1111,vw		–1111,s	–1108,m	
38	B		1090,vw		1091,vw	1088,w	–1090,m	–1081,m	–1091,m	–1090,w	
39	A	S_{41}	1084,vw	1081,w	1084,w	1074,w	–1084,vw		+1084,w	+1075,w	
40	B	S_{11}	1021,w	1012,w	1021,vw		+1021,w		–1021,w	–1019,sh	
41	A	S_{10}	1005,vw		1006,m	1005,m	+1005,vw		–1006,s	–1005,s	δ_N amide
42	B		995,vw		995,m	996,m	–995,vw		+995,m		

mode	sym	PED	frequency (cm^{-1}), intensity								remark
			IR ($CHCl_3$)		Raman (H_2O)		VCD ($CDCl_3$)		ROA (H_2O)		
			calc.	exp.	calc.	exp.	calc.[b]	exp.	calc.	exp.	
43	B	S_7	977,vw	973,vw	977,vw		+977,vw		–977,vw		
44	A	S_2,S_7	975,vw		975,m	977,m	–975,vw		+975,m	+978,vw	
45	B	S_7,S_2	954,w	950,vw	954,vw		–954,vw		–954,m	–959,w	
46	A	S_2	947,vw		947,m	946,m	+947,vw		+947,vw		
47	A	S_{35},S_{36}	919,vw		919,s	930,m	+919,vw		–919,m	–929,m	
48	B	S_{67},S_{63}	850,w	846,w	851,vw	852w	–850,m		+851,w	+852,m	
49	B	S_{40},S_{39}	808,w	804,vw	809,vw	810,sh	–808,vw		+809,vw	+810,m	
50	A	S_{55},S_{47}	797,vw		798,vw	802,w	+797,vw		+798,w	+801,sh	
51	A		702,vw		702,s	707,vs	+702,vw		+702,m	+707,s	δ skelet.
52	A	S_{38},S_{37}	684,vw		683,m	687,m	+684,vw		+683,m		
53	B	S_{32},S_{28}	667,w	668,vw	667,vw	671,sh	–667,m		–667,w	–669,s	
54	B	S_{38},S_{37},S_{43},S_{45}	650,w	644,vw	649,vw	644,w	–650,s		–649,s	–644,s	$\delta_{C=O}$
55	A	S_{38},S_{35},S_{39}	595,w	594,w	594,w	594,m	–595,vw		+594,w		δ_N amide
56	B	S_{37},S_{38}	594,w		594,vw		–594,vw		+594,w		δ_N amide
57	A	S_{37},S_{38},S_{41}	562,vw		562,vw	567,w	–562,vw		–562,m	–568,s	δ_N amide
58	B	S_{40},S_{39},S_{38}	540,w	542,vw	540,vw	547,w	+540,m		+540,w	+547,m	
59	B	S_{39},S_{40}	497,w	498,vw	498,vw	503,w	+497,w		+498,w	+501,s	
60	A	S_{37},S_{38},S_{41}	420,w		419,w	422,w	–420,w		–419,vw	–423,m	
61	A	S_{41},S_{27},S_{31}	375,vw		375,m	389,s	+375,vw		+375,m	+389,m	
62	A	S_{41}	347,vw		346,m	351,s	–347,vw		–346,w	–350,m	
63	B	S_{36},S_{39},S_{35}	344,w		342,vw		+344,w		+342,vw		
64	A	S_{41},S_{35},S_{36}	264,w		262,vw	269,w	–264,w		–262,vw	–266,w	
65	B	S_{38},S_{37}	188,w		185,vw		–188,vw		–185,vw		
66	B	S_{38},S_{37},S_{30},S_{34},S_{29}	163,w		163,vw		–163,vw		–163,vw		
67	A	S_{41},S_{33},S_{29}	138,vw		138,vw		+138,vw		–138,m		
68	A	S_{37},S_{38},S_{34},S_{30}	103,w		103,vw		+103,w		+103,m		
69	B	S_{30},S_{34},S_{37}	76,m		76,vw		–76,w		–76,m		

IR absorption data measured in KBr pellets are not shown here and may be obtained from the authors on request;
PED (potential energy distribution), values lower than 10 % are not included;
vw – very weak, w – weak, m – medium sized, s – strong, vs – very strong; sh – shoulder;

[a] Measured in $CDCl_3$ due to solvent band interference;

[b] Calculated in $CHCl_3$ (COSMO model)

Table S4. Vibrational data of the spirodilactam (–)–(1R)–II

mode	sym	PED	frequency (cm^{-1}), intensity								remark
			IR ($CHCl_3$)		Raman (H_2O)		VCD ($CDCl_3$)		ROA (H_2O)		
			calc.	exp.	calc.	exp.	calc.[b]	exp.	calc.	exp.	
1	B	S_{22},S_{19}	3113,vw	2980,w	3114,vs	2998,vs	+3113,vw		–3114,vs	–3008,m	
2	A	S_{18},S_{22}	3112,w	2948,w	3112,s		+3112,vw		+3112,vs		
3	A	$S_{19},S_{22},S_{16},S_{18}$	3104,w	2927,w	3106,vs		–3104,m	–2982,m	+3106,vs		
4	B	S_{16},S_{19},S_{15}	3100,vw		3103,vs		+3100,vw		–3103,vs		
5	A	$S_{20},S_{15},S_{16},S_{19}$	3044,vw	2877,w	3046,vs	2962,sh	–3044,vw		+3046,vs	+2933,m	
6	B	$S_{15},S_{20},S_{16},S_{19}$	3043,w		3044,s	2936,vs	+3043,vw	+2881,w	–3044,vs		
7	A	S_{21},S_{17}	3034,vw		3035,vs	2896,s	+3034,w	+2879,w	–3035,vs		
8	B	S_{17},S_{21}	3034,vw		3034,vs		–3034,vw		+3034,vs		
9	B	$S_{23},S_{25},S_{24},S_{26}$	2320,vw	2252,w	2322,vs	2268,s	–2320,vw	–2250,vw[c]	+2322,vs	+2274,m	
10	A	$S_{25},S_{23},S_{26},S_{24}$	2316,vw	2225,w	2318,vs	2238,m	+2316,vw	+2225,vw[c]	–2318,vs	–2221,w	
11	A	S_{24},S_{23}	2215,w	2155,w	2217,vs	2164,s	+2215,w	+2145,vw[c]	+2217,s	–2165,m	
12	B	S_{26},S_{25}	2214,w	2109,w	2216,vs	2117,m	–2214,w		–2216,vs	–2117,w	
13	A	S_{14},S_{13}	1734,m	1718,sh	1718,vs	1685,s	+1734,w	+1715,sh	–1718,w	–1685,m	amide I'
14	B	S_{13},S_{14}	1724,vs	1699,vs	1706,m		+1724,s	+1699,s	–1706,s		amide I'
15	A	S_{46},S_{54}	1491,vw	1454,w	1490,m	1465,m	–1491,vw	–1465,w	–1490,s	–1467,w	
16	B	S_{54},S_{46}	1484,w		1483,w	1457,m	+1484,vw	+1454,w	+1483,s	+1456,m	
17	A	S_{50},S_{58}	1457,vw	1428,vw	1455,m	1430,s	+1457,vw		–1455,s		
18	B	S_{58},S_{50}	1456,vw		1454,s	1419,s	–1456,vw		+1454,s	+1429,w	
19	A	S_9,S_4	1404,m	1394,m	1409,s		–1404,vs	–1392,vs	+1409,vw	+1387,w	amide II'
20	B	S_4,S_9	1354,vs	1347,s	1358,vw		+1354,vs	+1346,vs	+1358,m	+1319,sh	amide II'
21	A	S_{56},S_{48}	1336,vw	1313,vw	1336,vw	1318,vw	+1336,w	+1305,w	+1336,m	+1314,w	
22	B	S_{48},S_{56}	1329,vw		1330,vw		+1329,vw		+1330,vw		
23	B	S_{60},S_{52},S_{57}	1297,w	1274w	1297,vw	1277,w	+1297,m	+1274,m	+1297,m	+1277,m	
24	A	S_{52},S_{49},S_{60}	1293,vw		1294,vw		+1293,vw		+1294,m		
25	A	S_5,S_{10},S_{40},S_{39}	1261,vw		1262,m	1254,m	+1261,vw	+1246,vw	+1262,w	+1256,vw	
26	B	$S_{57},S_{60},S_{49},S_{52}$	1238,w	1219,w[a]	1238,vw	1225,vw	+1238,vw		–1238,m	–1225,w	
27	B	S_{40},S_{39}	1214,w	1203,w	1215,w	1209,sh	–1214,m	–1201,m	+1215,m	+1209,w	
28	A	S_{53},S_{61}	1202,w	1190,w	1202,m	1194,m	–1202,m	–1190,m	–1202,s	–1194,m	
29	A	S_5,S_{10}	1177,vw	1171,w	1177,m	1173,w	+1177,m	+1169,w	+1177,vw	+1169,vw	
30	B	S_{36},S_{35}	1158,vw	1145,vw	1158,m	1148,m	–1158,vw	–1146,w	–1158,m	–1149,m	
31	B	S_{62},S_{68},S_5,S_{12}	1127,w	1114,w	1127,w	1118,w	+1127,vw	+1114,vw	–1127,m	–1120,m	
32	A	S_{66},S_{64},S_{10}	1125,w		1125,w		+1125,vw		–1125,m		
33	B	$S_{66},S_{62},S_{12},S_{11}$	1117,vw	1081,vw	1117,vw	1105,sh	–1117,vw	–1105,w	+1117,vw		
34	A		1091,vw		1092,w	1087,w	–1091,vw	–1080,w	–1092,w	–1088,w	
35	B	S_{41}	1082,vw	1067,w	1082,vw	1069,w	+1082,w	+1068,vw	+1082,m	+1070,m	
36	A	$S_{66},S_{62},S_{68},S_{64}$	1079,w		1078,vw		–1079,vw		+1078,w		
37	A	S_8	1027,w	1019,vw	1027,vw	1024,vw	–1027,w		+1027,vw	+1025,m	
38	B	S_3	1013,w	1006,vw	1013,vw	1010,vw	–1013,vw		–1013,w	–1011,m	
39	A		992,vw		992,vw	991,sh	–992,vw		+992,m	+991,m	
40	B	S_7,S_2	976,vw	978,vw	976,m	978,m	–976,vw		–976,vs	–979,s	
41	A	$S_{63},S_{67},S_{69},S_{65}$	960,vw		960,w	957,m	+960,vw		+960,m	+958,w	
42	B	S_2,S_7	954,w	954,vw	954,vw		–954,vw		–954,w	–944,m	

mode	sym	PED	frequency (cm^{-1}), intensity								remark
			IR ($CHCl_3$)		Raman (H_2O)		VCD ($CDCl_3$)		ROA (H_2O)		
			calc.	exp.	calc.	exp.	calc.[b]	exp.	calc.	exp.	
43	A		944,vw	941,vw	944,s	943,s	+944,vw		–944,w		
44	B	S_{31},S_{27}	937,vw		938,vw		+937,vw		–938,vw		
45	B	S_{65},S_{37},S_{69}	870,w	863,w	870,w	866,m	–870,m		+870,w	+872,w	
46	A	S_{69},S_{38}	868,vw		868,m		–868,vw		–868,s	–864,m	
47	A		817,vw	814,vw	817,w	820,m	–817,w		+817,vw	+820,w	
48	B	S_{55},S_{47}	787,vw	785,vw[a]	788,w	792,w	+787,vw		+788,m	+791,w	
49	B	S_{68},S_{64},S_{69},S_{65}	747,vw		746,m	755,s	+747,vw		–746,m	–754,s	
50	A	S_{63},S_{67}	728,w	723,vw	727,vw	726,vw	–728,vw		+727,vw		
51	A	S_{28}	699,vw		698,s	699,vs	+699,vw		+698,m	+699,m	
52	A	S_{38},S_{37}	670,vw		669,s	674,s	+670,vw		+669,s	+674,m	
53	B	S_{43},S_{45},S_{38},S_{37}	654,w	646,w	652,vw	645,vw	–654,s		–652,m	–644,m	
54	B	S_8,S_3	610,w	612,vw	609,vw	615,w	+610,vw		–609,m	–616,s	
55	B	S_{39},S_{40}	591,vw	590,vw	591,w	590,w	–591,vw		+591,w	–592,w	
56	A	S_{38},S_{37}	562,w	563,vw	562,vw	562,w	+562,vw		+562,w	+570,w	
57	A	S_{37},S_{38},S_{41}	555,vw	554,vw	555,vw		–555,vw		–555,m	–562,m	
58	B	S_{40},S_{39}	505,vw	508,vw	505,vw	510,vw	+505,vw		+505,w	+510,m	
59	B	S_{37},S_{38},S_{39},S_{40}	490,w	491,vw	491,vw	495,w	+490,m		+491,w	+495,m	
60	A	S_{37},S_{38},S_{41}	413,w	413,vw	412,vw	417,w	–413,w		–412,vw	–419,m	
61	A	S_{41},S_{27},S_{31},S_{39},S_{40}	374,vw		374,m	386,vs	+374,vw		+374,m	+385,m	
62	A	S_{41}	338,vw		338,m	345,s	+338,vw		–338,w	–345,m	
63	B	S_{36},S_{39},S_{35},S_{40}	328,w		327,vw		+328,vw		+327,vw	+329,w	
64	A	S_{35},S_{36},S_{41},S_{37}	229,w		227,vw	229,w	–229,w		–227,vw		
65	B	S_{38},S_{37}	176,w		174,vw		–176,vw		+174,vw		
66	B	S_{38},S_{37},S_{30}	162,w		161,vw		–162,vw		–161,w		
67	A	S_{41},S_{33},S_{29}	137,w		137,vw		+137,w		–137,m		
68	A	S_{37},S_{38},S_{34},S_{30}	99,w		99,vw		+99,w		+99,m		
69	B	S_{30},S_{34}	74,m		74,vw		–74,w		–74,w		

IR absorption data measured in KBr pellets are not shown here and may be obtained from the authors on request;
PED (potential energy distribution), values lower than 10 % are not included;
vw – very weak, w – weak, m – medium sized, s – strong, vs – very strong;

[a] Measured in $CDCl_3$ due to solvent band interference;

[b] Calculated in $CHCl_3$ (COSMO model);

[c] Measured in $CHCl_3$

Appendix 3

Relative Intensity Correction of Raman Optical Activity Spectra Facilitates Extending the Spectral Region

J. Raman Spectrosc. 2014, 45, 603–609

Profant, V., Pazderková, M., Pazderka, T., Maloň, P., Baumruk, V.

Charles University in Prague, Faculty of Mathematics and Physics, Ke Karlovu 5, 121 16 Prague 2, Czech Republic

Research article

Journal of RAMAN SPECTROSCOPY

Received: 14 January 2014 Revised: 29 April 2014 Accepted: 30 April 2014 Published online in Wiley Online Library: 2 June 2014

(wileyonlinelibrary.com) DOI 10.1002/jrs.4503

Relative intensity correction of Raman optical activity spectra facilitates extending the spectral region

Václav Profant, Markéta Pazderková, Tomáš Pazderka, Petr Maloň and Vladimír Baumruk*

Using home-built Raman optical activity (ROA) spectrometer and a relative intensity correction for different instrument responses, we report ROA spectra beyond the traditionally utilized spectral region of 200–2500 cm^{-1}. With three different interchangeable gratings covering partially overlapping spectral regions, we can study ROA in the whole region of fundamental molecular vibrations (150–4000 cm^{-1}). Complete panoramic spectra are assembled from subparts collected with different gratings after a relative intensity correction based on the National Institute of Science and Technology standards known from the analogous application in Raman and fluorescence spectroscopy. Using this setup, we report the still little known ROA from C–H and C–D stretching region of the testing substances α-pinene and a tricyclic spirodilactam. The intensity-corrected experimental data were compared with calculated ROA and Raman spectra of these substances both with and without anharmonic corrections. A comparison revealed that above 1200 cm^{-1}, the anharmonic correction provides a clear improvement of the agreement. While the calculation of Raman spectra achieves already good accuracy, the analogous ROA calculations still need further development. Copyright © 2014 John Wiley & Sons, Ltd.

Additional supporting information may be found in the online version of this article at the publisher's web site.

Keywords: ROA; C–H stretching region; relative intensity correction; instrument response function; Standard Reference Materials (SRMs); luminescence standards

Introduction

Raman optical activity (ROA)[1–3] is a relatively novel chiroptical variant of vibrational spectroscopy that is rich in structural information but experimentally rather difficult. The advances both in experimental techniques [multichannel charge-coupled device (CCD) detectors, holographic edge and notch filters, simultaneous acquisition of signals at both circular polarizations and fiber optics] and theoretical calculations [density functional theory (DFT) procedures, advances in electron correlation description and anharmonic corrections[4]] have made ROA applicable to a wide range of chemistry, biochemistry and biophysics-related problems. On the basis of the increased quality of experimental ROA data, it becomes interesting to pay closer attention to numerical intensities. A suitable intensity correction of spectra can bring data to common numerical basis along the wavenumber range. It can also make experimental data easier to compare when they are recorded at different experimental conditions, e.g. measured on several distinct instruments. Relative intensity correction (RIC) was already suggested[5] and introduced[6–9] for Raman spectra,[10–14] but its potential for ROA has yet to be determined. This application is promising because the information content of ROA is fundamentally based on signs and intensities. Moreover, if we evaluate uncorrected ROA intensities over wider wavenumber range or data from different instrumental setups, we can encounter significant numerical inconsistencies.

Internal RIC enables comparison of data obtained at widely varying instrumental conditions (different optical and experimental details – instrument, optical setup, excitation wavelength, etc.). In addition, it facilitates creation of panoramic spectra over extended spectral ranges. Current experimental ROA usually covers a region of ~200–2500 cm^{-1}. The data outside this spectral range, particularly at higher wavenumbers (fundamental X–H stretching vibrations, overtones and combination vibrations), but also in the low-wavenumber range (~100–600 cm^{-1}, signals of C–S and S–S stretching vibrations,[15] polyproline II delocalized vibrations,[16,17] carbohydrates glycosidic linkages,[18] etc.), are valuable, but the attempts to experimentally record them are scarce. Up to now, ROA measurements covering the whole range of fundamental vibrations (~0–3500 cm^{-1}) were only reported by Hug *et al.*[19] in 1975 using an instrument recording one spectral point at a time. There are also recent ROA data on C–H and C–D vibrations.[4,20] With current multichannel spectrometers, measurements in the extended spectral range can be realized by either compressing the spectrum along the CCD detector or by combining data from several shorter spectral subregions, each of them measured separately with a region-optimized arrangement, particularly grating.[21] Even though the latter approach may be more difficult to implement, it seems more advantageous because it

* *Correspondence to: Vladimír Baumruk, Charles University in Prague, Faculty of Mathematics and Physics, Institute of Physics, Ke Karlovu 5, 12116, Prague 2, Czech Republic.*
E-mail: baumruk@karlov.mff.cuni.cz

Institute of Physics, Faculty of Mathematics and Physics, Charles University in Prague, Ke Karlovu 5, 12116, Prague 2, Czech Republic

does not sacrifice the already limited spectral resolution of ROA experiment (usually ~8 cm^{-1}).

RIC can be implemented in several ways (using blackbody emitter,[22] calibrated tungsten lamp,[23] etc.). So far, the most practical procedure has been described and analyzed in Etz *et al.*[24] It is based on the use of luminescent glass standards developed by the National Institute of Science and Technology (NIST). Custom-designed luminescent glass standards have been developed for correcting Raman spectra excited by various lasers, and the whole procedure has been thoroughly tested.[25,26] It is yet necessary to examine the effect of placing the standard into the sample position in a reproducible way. We intend to apply the RIC procedure to the specific case of ROA spectra. Although correcting the ROA is numerically identical to that of the Raman spectra, the information content of ROA spectra is more given by intensities and sign variations. Therefore, ROA requires even better determination of the corrective curve including its local variations.

Systematic application of RIC to Raman and ROA spectra could improve data independence on the experimental specifics including instrumentation and optical setup. Such well-defined data having higher numerical accuracy could provide suitable material for testing quality of methods used for simulation of vibrational spectra. In relation to our previous study,[4] we report comparison between corrected and uncorrected experimental spectra and theoretical simulations. This is easier for the Raman spectra, as their calculations are considerably less complicated. Simulations of ROA spectra require theory beyond the dipole approximation and have to include, additionally, the electric dipole–magnetic dipole and electric dipole–electric quadrupole interactions. Not long ago, quality of a match between experimental and calculated ROA spectra was evaluated on the basis of sign agreements only. In addition, the commonly used simulation methods operate within the harmonic approximation. Although it results in a substantial decrease of computational requirements, it also negatively affects calculation of vibrations that are of anharmonic nature (mostly C–H stretching and deformation vibrations). Therefore, we report also calculations that include anharmonic corrections.

Experimental methods

Both enantiomers of α-pinene (I) were purchased from Sigma-Aldrich (product nos. 305715 and 268070) and used without further purification. Synthesis of both enantiomers of the tricyclic spirodilactam 6,6′,7,7′-tetradeuterioderivative of 5,8-diazatricyclo [6,3,0,$0^{[1,5]}$]undecane-4,9-dione (II) was described in Smolikova *et al.*[27] Compound I was measured as a neat liquid. Compound II was dissolved in distilled water (0.5–0.7 M) and filtered through 0.22-μm Millipore filter.

The luminescence standards, Standard Reference Material (SRM) 2242 (for the RIC of Raman spectra obtained with instruments employing 532-nm laser excitation) and SRM 2243 (488/514-nm laser excitation), were purchased from NIST.[26] The certified polynomials describing ideal fluorescence response of the SRMs to the illumination and their uncertainty curves are shown in Fig. S1 (Supporting Information). Polynomials are certified for the use between 150 and 4000 cm^{-1} for SRM 2242 (or 200 and 4800 cm^{-1} for SRM 2243). SRMs were used in their original optical mounts. Laser power used for SRM illumination was 50 mW (~30 mW at the sample).

ROA measurements were mainly performed on the home-built instrument at the Institute of Physics of Charles University in Prague employing incident circular polarization (ICP) strategy and backscattering geometry (ICP-P).[28] Experimental layout follows the original design by L. D. Baron and co-workers.[29] Single-line continuous-wave argon laser (Coherent, Innova 305, 514.5 nm) serves as an excitation source. The spectrograph is equipped with three interchangeable holographic transmission gratings covering partly overlapping spectral regions: HSG-514.5-LF (−250–2370 cm^{-1}; ICP-P low), HSG-532-LF (580–3070 cm^{-1}; ICP-P medium) and HSG-514.5-HF (2270–4510 cm^{-1}; ICP-P high). Nitrogen-cooled CCD detector (Roper Scientific) contains 1340 × 100 pixels. Spectral resolution of the spectrometer combining the previously described gratings with the used CCD array is nearly uniform (~7 cm^{-1}).

ROA data were further compared with those recorded on conceptually different commercial ROA spectrometers (BioTools, Inc.) of two subsequent generations – ChiralRAMAN™ and μ-ChiralRAMAN-2X™ – which use scattered circular polarization (SCP) modulation scheme and 532-nm laser excitation. Both use fiber optics elements for simultaneous collection of left-circularly and right-circularly polarized scattered light. μ-ChiralRAMAN-2X™ uses a slightly modified layout. The ChiralRAMAN™ instrument at the Manchester Institute of Biotechnology (SCP-M) currently uses both notch and edge holographic filters to suppress the Rayleigh line and records data within −20–2510 cm^{-1}. The second generation instrument μ-ChiralRAMAN-2X™ at the Institute of Organic Chemistry and Biochemistry in Prague (SCP-P A) covers the spectral range −10–2430 cm^{-1}. Recently, the original notch filter (SuperNotch-Plus™, Kaiser Optical Systems, Inc.) was replaced by the edge filter (532-nm RazorEdge, LP03-532RE-25, Semrock, Inc.; SCP-P B) enabling more accurate measurements down to 100 cm^{-1}. These spectrometers achieve a resolution of ~8 cm^{-1}.

ROA measurements were performed in quartz thin-wall microcells (Starna Scientific Ltd; ~60 μl, 4 × 3 mm) with antireflectively coated windows. The acquisition time varied depending on the instrument, spectral range and the sample (4–20 h). Raw data were wavenumber calibrated. With ICP-P instrument, the conversion employs neon-lamp standard, while data from both commercial SCP spectrometers are converted using toluene signals. To obtain the required regular 1 cm^{-1} per data point spacing, the data are linearly interpolated. The wavenumber-corrected raw spectra (Raman and ROA) were at this point either subjected to RIC (refer to the succeeding texts) or left uncorrected for comparison. After this step, the Raman and ROA spectra were treated differently. The Raman spectra of II (measured in water) were corrected by a solvent signal subtraction. Final correction of all Raman spectra included a baseline correction by subtracting a first-order polynomial (our data referring to high-purity compounds needed only marginal correction). The final ROA spectra were obtained by subtracting spectra of enantiomers from one another (R–S, in this particular case) and dividing the result by two. This is the ultimate procedure helping us to get rid of the remaining optical artifacts, particularly in the high-wavenumber region.

The RIC follows the method elaborated and described in McCreery[6,8] for the correction of Raman spectra. The ROA corrective procedure is an extension of Raman spectra correction and uses the identical correction curve. The corrected spectrum $S_{CORR}(\Delta\nu)$ is created by multiplying the measured spectrum $S_{MEAS}(\Delta\nu)$ by the correction curve $C(\Delta\nu)$, which can be obtained by dividing the certified relative spectral intensity polynomial

Journal of RAMAN SPECTROSCOPY

$P_{SRM}(\Delta\nu)$ by the measured glass luminescence spectrum $S_{SRM}(\Delta\nu)$. The latter part is a characteristic for the particular instrumental arrangement and has to be experimentally determined.

$$S_{CORR}(\Delta\nu) = S_{MEAS}(\Delta\nu)\cdot C(\Delta\nu) = S_{MEAS}(\Delta\nu)\cdot P_{SRM}(\Delta\nu)/S_{SRM}(\Delta\nu). \quad (1)$$

For the quantitative evaluation of similarity (correlation) between spectra obtained with differently arranged experiments, we use the hit-quality index (HQI),[30,31] defined as

$$HQI = \frac{(S_{INS}\cdot S_{REF})^2}{(S_{INS}\cdot S_{INS})(S_{REF}\cdot S_{REF})}, \quad (2)$$

where S_{REF} and S_{INS} stand for the respective reference and inspected spectra (expressed as vectors with a common *x*-dimension). HQI spans from 0 (totally different spectra) to 1 (the exact match). As it is just a single number that cannot depict changes of relative intensities within individual spectral bands, we supplement it using a comparison of integral intensities of selected spectral bands.

We quantified variations among SRM glass fluorescence profiles ($S_{SRM}(\Delta\nu)$) when experimental conditions were changed. In the case of measurements with various laser power and from different spots of SRM glass, the final fluorescence response was calculated as a mean value, and variations in every point were calculated as relative standard deviations. In the case of focus shift and angular deflection, the deviations were calculated *versus* corresponding unperturbed values. The uncertainty of fluorescence curves is then expressed by means of their maximum value.

For the comparison with experimental data, we calculated theoretical Raman and ROA spectra of compound I. Molecular geometries were optimized using the Gaussian 09 program[32] by energy minimization, and the same computational level was used for the calculation of spectral properties within the harmonic approximation. The calculations were performed using a moderate level of DFT theory (B3PW91[33] functional, 6-311++G** basis set). Molecular environment was simulated by the Conductor-like Screening Model (COSMO)[34] dielectric model ($\varepsilon_r = 2.69$ for neat α-pinene, using Gaussian parameters for pentanoic acid). Theoretical spectral profiles were generated by a convolution of calculated intensities with a Lorentzian function (full-width half-maximum value, 10 cm^{-1}). Raman and ROA spectral profiles were adjusted by a Boltzmann factor to 298 K and expressed as intensity sums ($I^R + I^L$, Raman) and differences ($I^R - I^L$, ROA) of the right-circularly and left-circularly polarized light.

Anharmonic corrections were calculated using limited vibrational configurational interaction described in Hudecova *et al*[4]. The original harmonic vibrational potential was extended by cubic and quartic parts (*W*), and the new vibrational wavefunction was expressed as a linear combination of harmonic oscillator (HO) wavefunctions, $\Phi_\varepsilon = \sum_f C_f^\varepsilon \psi_f$. As shown in the previous studies,[35,36] several criteria were employed in order to limit the number of HO basis functions. The process involved two stages. (i) Only states (*f*) obliging $W_{fn} > c_1|E_n - E_f|$ were included, where c_1 is the interaction parameter and *n* is a ground state. (ii) A second set of HO basis functions (*f'*) was added (interacting with the already chosen basis) based on the coefficient c_2 ($W_{f'f} > c_2|E_{f'} - E_f|$). The lowest-frequency normal modes were not excited, and Hamiltonian elements with extensively energy-separated states ($|H_{ij}| < 10^{-4}|E_i - E_j|$) were excluded as well. In our case, the parameters were set as follows (36 modes fixed, $c_1 = 0.002$, $c_2 = 0.1$, 749398 HO states), which led to a high but still affordable calculation time (~10^3 CPU hours).

Note that experimental Raman and ROA intensities are not measured as absolute values. Therefore, computed and experimental intensities were normalized to integral intensities of selected spectral intervals. For the normalization of Raman spectra, we used the interval 1200–1500 cm^{-1}. Integral intensities of experimental and calculated anharmonic spectra were normalized to unity, and the intensity of the harmonic spectrum was adjusted to maintain the original integral intensity ratio of the calculated spectra. Normalization factors were then transferred to corresponding ROA spectra.

Calculated harmonic frequencies were scaled by a factor 0.967. No scaling was applied to computed anharmonic frequencies. This work is focused on the effect of the intensity correction, and we compare mainly experimental and calculated spectral shapes and intensities. We do not extensively analyze the calculated frequencies but rely on our previous results instead.[4]

Results and discussion

As follows from Fig. S1 (Supporting Information), fluorescence levels of NIST standards as measured on ROA spectrometers are considerably lower than the original data reported by NIST, particularly at high-wavenumber ends of the spectral subranges. This is a consequence of response functions of the particular setups, which generally depend on several factors such as experimental geometry, excitation wavelength, efficiency of Rayleigh cutoff filter, detector quantum efficiency, grating efficiency, etc.[8] Dividing the standard-describing polynomial $P_{SRM}(\Delta\nu)$ with the instrument response function $S_{SRM}(\Delta\nu)$ gives the real correction curve $C(\Delta\nu)$ as shown in Fig. 1. For each grating covering ~2500 cm^{-1}, the central part of its spectral usability involves ~800 cm^{-1} where the correction curve values are close to unity ($C(\Delta\nu) < 1.1$, i.e. error lower than 10%; refer to Table 1 for the accurate spectral intervals), and the correction is merely marginal. Toward ends of the useful range, the correction usually gets more serious (>2), particularly for the SCP-M (>4 below 270 cm^{-1}, steeply rises up to 200 at 200 cm^{-1}) and SCP-P (>4 above

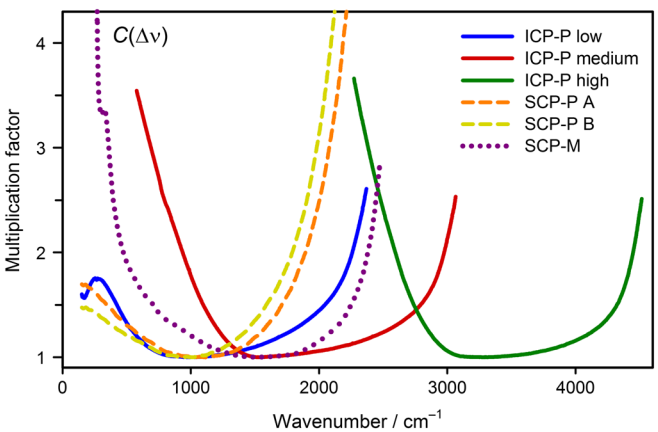

Figure 1. Correction curves $C(\Delta\nu)$ for the ICP-P, SCP-P and SCP-M instruments and different setups. The low-wavenumber edge of the curves is cut off at 150 cm^{-1} (the lower limit of certified luminescence spectrum).

Table 1. Experimental arrangements

Instrument setup	Recorded spectral region (cm^{-1})	Intensity reliable* region (cm^{-1})
ICP-P low	−250–2370	660–1510
ICP-P medium	580–3060	1330–2170
ICP-P high	2270–4510	2960–3870
SCP-P A	−10–2430	740–1410
SCP-P B	40–2470	660–1270
SCP-M	−20–2470	1150–1930

* Correction curve multiplication factor $C(\Delta\nu) < 1.1$.

2100 cm^{-1}, maximum of 11 at 2450 cm^{-1}). Generally, it seems better to preferably utilize central parts of particular subranges because in this way, we obtain data having the highest possible signal-to-noise (S/N) ratio. At the edges of the accessible range, there are narrow regions where the errors are too large. In our case, it applies to the low-wavenumber edge of the SCP-M instrument.

The actual measurement of luminescence spectra of the SRM glass ($S_{SRM}(\Delta\nu)$) is an important step for accurate determination of correction curves $C(\Delta\nu)$ and also a potential source of errors. The intensity and shape of the luminescence spectrum both depend on the fine positioning inside the sample holder. Fluorescence spectra measured at different spots show that the glass surface is not perfectly homogenous, and fluorescence intensity varies up to 30%. However, spectral shape remains similar with differences lower than 2% (data not shown). The orientation of the SRM with respect to the incident laser beam needs not to be strictly perpendicular. Thanks to the frosted surface of the glass, rotations up to 20° do not cause loss of fluorescence intensity, and differences of its shape are lower than 4%, which is still within the certification uncertainty (data not shown). A further rotation (~40°) results in higher divergence (up to 15%); however, such rotations are larger than usual errors caused by inaccurate sample positioning. Fluorescence profiles were also found to be independent on the laser power within the interval 4–100 mW with differences of <1% (data not shown). On the other hand, luminescence spectra of the SRM glass were found considerably sensitive to a position of the glass with respect to laser focus (Fig. 2). Out of focus, fluorescence intensity rapidly drops. When focused in front of the glass (+), the shape remains similar within 5% uncertainty (and slightly more at the very edges of corrected interval); however, when focused inside or behind the SRM glass (−), the reabsorption causes a substantial change of the fluorescence profile (15–20%). The apparent peak shift results from two effects: minor gradual effect of focus shifting and the much more important effect of fluorescence reabsorption inside the SRM glass. There is a big (and not gradual) difference whether the focus point is right at the surface of the glass or inside.

To evaluate the effect of the RIC on spectra measured at varying conditions, we compared corrected and uncorrected ROA of I (the compound showing large, low-noise signals, commonly used for testing of vibrational optical activity) measured at five different setups (ICP-P with three different gratings, SCP-P and SCP-M with one grating each). The analogous comparison was carried out at four different setups (ICP-P with three different gratings and SCP-P with one grating) for compound II (the rigid model compound with intense ROA and including C–D stretching signals). We used integral intensities for the comparison of corrected *versus* uncorrected (and experimental *vs* calculated) spectra. This approach should be independent on particular spectral resolution. The overall effect of the RIC on ROA spectra of I and II is shown in Fig. S2 (Supporting Information). Within central 800 cm^{-1}, the correction is nearly negligible for each of the gratings, and the spectra can be used without any correction. However, the border 400 cm^{-1} get comparable only when the correction is made. As depicted in Fig. 3, the correction makes comparable even the data from border regions measured on three different instruments. Comparing integral intensities below ~700 cm^{-1} (Table S1 in Supporting Information), the uncorrected data exhibit relative standard deviations up to ~25%. After the correction is applied, standard deviations drop to ~5%. However, the HQI improves by a factor of 0.02 only (Table S2 in Supporting Information). The RIC is even more necessary for ROA signals at higher wavenumbers (e.g. C–D, C–H, O–H and N–H stretching vibrations). This follows from Fig. S3 (Supporting Information) showing C–D stretching vibrations of compound II recorded on two different

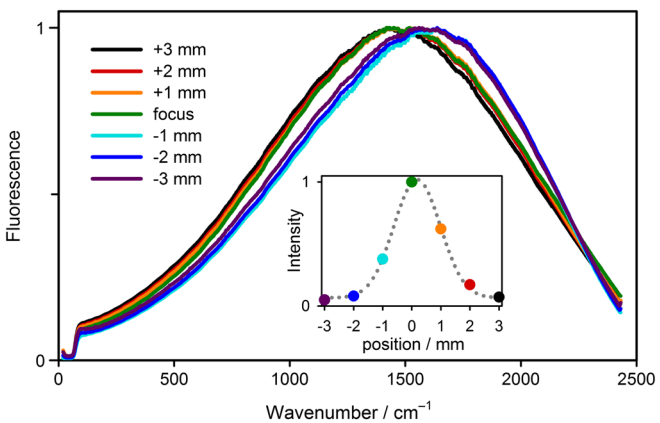

Figure 2. The effect of fine positioning of the SRM standard 2242 within the sample holder. The symbols + and − denote the respective SRM positions in front or behind of focus.

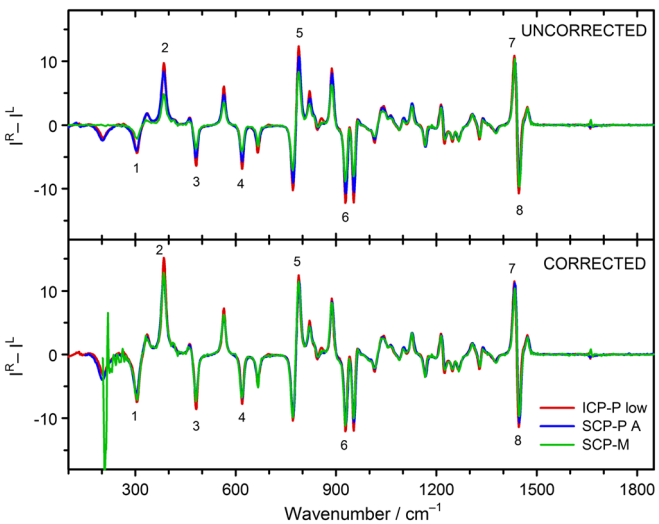

Figure 3. Uncorrected and corrected ROA spectra of (1*R*)-(+)-α-pinene (I) measured on three different instruments and normalized to integral intensity within 1100–1400 cm^{-1}, where the effect of correction is minimal. The spectra are shown in the 100–1850 cm^{-1} interval where data from all three instruments are available. For integral intensities of the labeled bands, refer to Table S1.

Journal of RAMAN SPECTROSCOPY

instruments. In the C–D stretching region (~2100–2300 cm^{-1}), the integral intensities differ by a factor of 5, and the respective relative standard deviations reach up to 60% (Table S3 in Supporting Information). After the correction, the errors diminish to less than 8%. The HQI changes notably by a factor of ~0.1. Circular intensity difference, i.e. ratio between ROA and Raman signal, remains unaffected by the RIC as both Raman and ROA spectra are multiplied by the same correction curve.

The effect of a replacement of notch to edge filter (i.e. SCP-P A to SCP-P B) has been measured for compound II in the interval 150–2425 cm^{-1} (refer to Fig. S4 in Supporting Information for spectral profiles and Table S4 for integral intensities of marked spectral bands). The exchange of the cutoff filter has only a week impact on spectral shape and relative intensities. Without RIC, the uncorrected spectra differ by ~8%, in average. Still, even better agreement with relative standard deviations ≤2% is achieved when RIC procedure is applied. HQI is rather insensitive with $\Delta HQI \sim 0.006$.

Corrected spectra measured on the home-built ICP-P instrument further enabled assembling the so-called panoramic spectra that cover wider spectral region. The procedure involved three simple steps: (1) measurement of the spectra covering partially overlapping subregions, (2) selection of overlapping regions where consecutive data from the two gratings would be combined and (3) unification of spectral intensities over these overlapping regions. The selection of overlapping regions is based on two considerations. The spectra within each subrange should be obtained with acceptable S/N ratio and contain significant spectroscopic features. Particular selection should be evaluated using HQI to ensure that the assembly does not lead to excessive errors. The optimization/unification process involves normalization of spectra to identical integral intensities over the whole overlapping region. Final adjustment of spectral intensities within the region of overlap was based on calculating the weighted average of signals at particular data points. The weights were determined by a linear function so that signals in the middle of the overlapping regions were contributed by 50% of signals from both gratings, while toward the ends, the signals were gradually more contributed by the data from the preceding or the following part. Our ICP data make use of three gratings with two largely overlapping spectral regions (580–2370 and 2270–3070 cm^{-1}). Although this looks excessive, it allows us to use the regions where intensity correction is low and the data are of higher quality. It is also dictated by technical parameters of our gratings. With alternate selection, it might be possible to obtain data through the whole spectral region using just two gratings. Construction of panoramic spectra is illustrated on ROA of compound I (Fig. 4). Particular selection of intervals for connecting the spectra included 1000–1750 and 2650–3070 cm^{-1} where the HQI is higher than 0.99 (0.9907 and 0.9932, respectively), which is usually considered a perfect spectral match [Fig. S5 (Supporting Information)]. At higher wavenumbers, we utilized only a narrow region, as there are no significant signals except for C–H stretches. The correction procedure has only small effect on the central part of the panoramic spectrum (~750–2000 cm^{-1}), but the differences are significant (a factor of ~2) outside this range (both in low-wavenumber and high-wavenumber regions).

Similarly to Raman spectra, the application of RIC to ROA improves the data reliability. The resulting corrected spectra are consistent over a wide spectral range and enable common utilization of spectra recorded at different instruments or conditions. In this improved form, the experimental data offer a comparison to currently available theoretical methods. This should distinguish

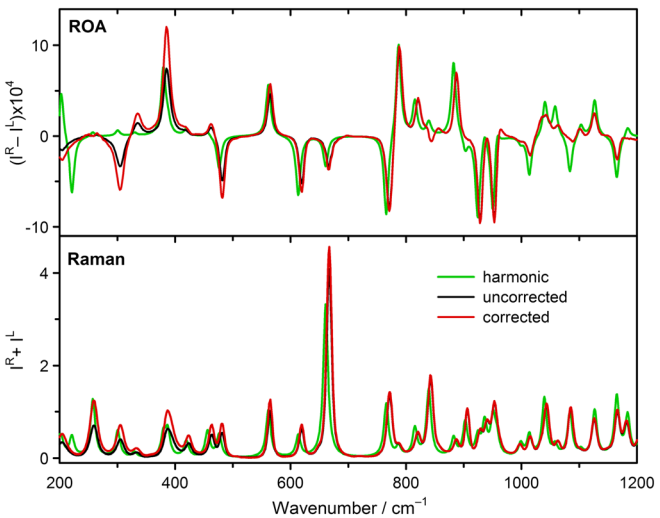

Figure 5. Experimental (corrected and uncorrected) and calculated (harmonic) ROA and Raman spectra of (1*R*)-(+)-α-pinene (I).

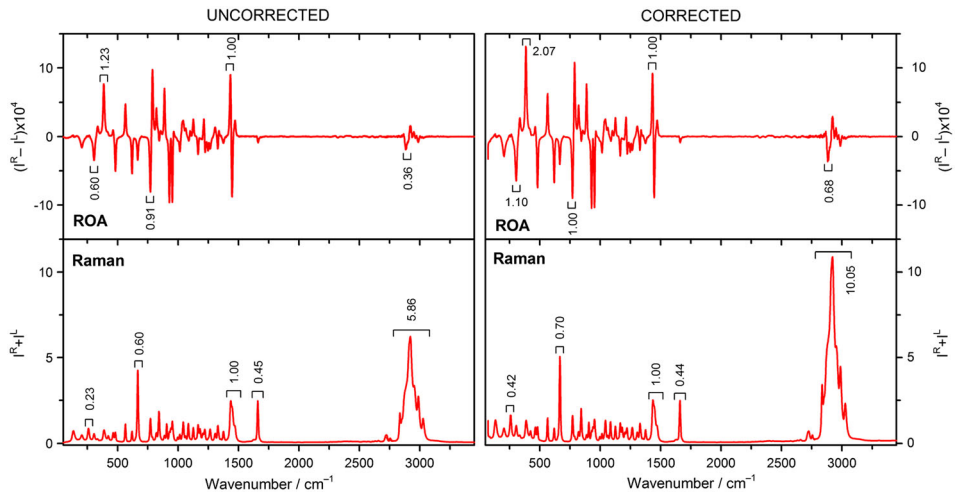

Figure 4. Panoramic spectra of (1*R*)-(+)-α-pinene (I) composed of three subregions measured with different gratings on the ICP ROA instrument.

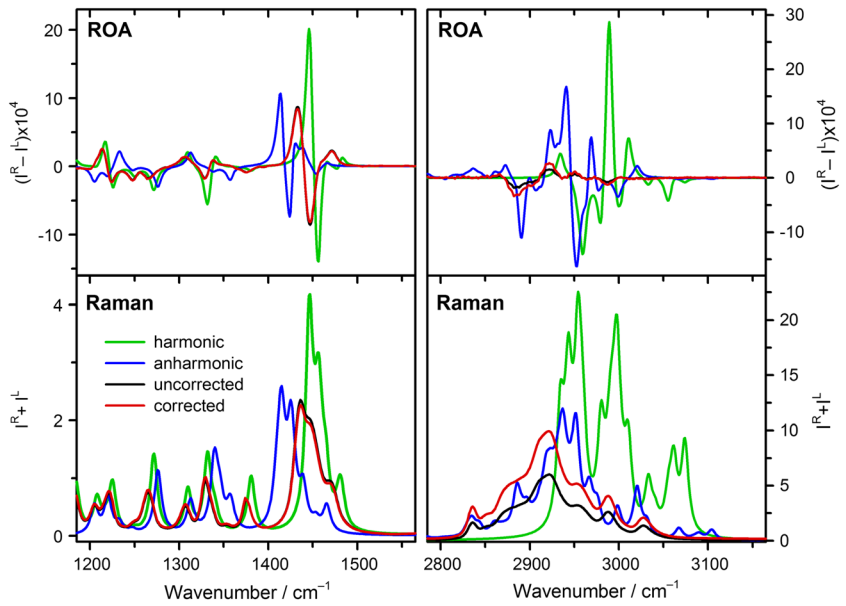

Figure 6. Experimental (corrected and uncorrected) and calculated (harmonic and anharmonic) ROA and Raman spectra of (1*R*)-(+)-α-pinene (I).

Table 2. Integral intensities of selected spectral intervals in experimental and calculated Raman and ROA spectra of (1*R*)-(+)-α-pinene (I)

	Spectral interval (cm^{-1})	Integral intensities			
		Uncorrected	Corrected	Harmonic	Anharmonic
Raman	170–635	0.62	0.90	0.80	
	720–1240	1.49	1.53	1.55	
	1240–1550	1.00	1.00	1.31	1.00
	2800–3100	3.82	6.38	11.25	6.42
ROA	170–635	1.45	2.19	1.65	
	720–1240	2.37	2.45	2.84	
	1240–1550	1.01	1.00	1.36	0.86
	2800–3100	0.27	0.48	1.94	2.13

whether theoretical data are already at the level of semiquantitative agreement allowing configurational and conformational studies utilizing complete vibrational spectral range. For this purpose, it seems ideal to employ α-pinene that is commonly used as a model compound for testing quality of experimental and theoretical data. Calculating VOA of such a molecule at the harmonic level is not too difficult. However, its hydrocarbon skeleton contains C–H bonds in different environments that are known to be strongly influenced by anharmonic contributions to vibrational potential, especially when considering vibrations above 1400 cm^{-1}. Vibrations at lower wavenumbers seem to be described well enough within the harmonic approximation. On the contrary, the vibrations occurring at higher wavenumbers (C–H stretchings and C–H scissorings) need inclusion of anharmonic terms. Considering that anharmonic corrections to vibrational potential require extensive calculations, we include them only for vibrations above 1200 cm^{-1}.

In the low-wavenumber region, the agreement between Raman/ROA calculated at the harmonic approximation and the experiment is already very good (Fig. 5). Still, the agreement between calculated and experimental intensities is notably better for Raman than for ROA (specifically, calculated bands in the interval 250–500 cm^{-1} are less intense and in the interval 1000–1200 cm^{-1} more intense than in the experiment). Intensity-corrected ROA spectra as a result of their independency on the used experimental setup can therefore serve as benchmarks for the further development and refinement of theoretical methods used for ROA simulation.

The analogous comparison above 1200 cm^{-1} is shown in Fig. 6 (refer to Table 2 for integral intensities). Within the 1200–1550 cm^{-1} interval, the difference between the overall integral intensity of Raman and ROA spectra simulated at the harmonic and anharmonic levels is ~30%. This difference is even bigger in the C–H stretching region. While the Raman spectrum calculated with anharmonic corrections resembles the intensity-corrected experimental curve, both in shape and intensity, the spectrum computed at the harmonic level exhibits nearly two times higher integral intensity and possesses a rather different shape. The shape of experimental ROA spectrum is again mimicked better by a simulation at the anharmonic level. However, integral intensities of both calculated spectra are still ~4 and ~7.5 times higher than integral intensities of the respective corrected and uncorrected spectra (Table 2). It is obvious that anharmonic corrections improve the experimental-to-calculated relation, but further development of vibrational configuration interaction methodology is still needed. The calculated intensities of Raman spectra with anharmonic correction agree with the intensity-corrected experimental data in

C–H stretching region, but the corresponding ROA intensities are overestimated. According to our opinion, these observations should further stimulate future development of ROA calculations.

Conclusions

The analysis of RIC of ROA spectra shows that such procedure is useful and needed. With continuing technical development, ROA data get more accurate, and consequently, the calibration errors become more important. Similar to Raman, ROA intensity correction is easy to use and can bring significant improvement to data quality. Therefore, where possible, it could be implemented as a general procedure.

Acknowledgements

This work has been supported by the Czech Science Foundation (P205-10-1276). Authors gratefully acknowledge the P. Bouř's group at the Institute of Organic Chemistry and Biochemistry AS CR in Prague and the E. Blanch's group at the Manchester Interdisciplinary Biocentre for the opportunity to use their instruments and provided experimental time.

References

[1] L. D. Barron, M. P. Bogaard, A. D. Buckingham, *J. Am. Chem. Soc.* **1973**, *95*, 603–605.
[2] L. D. Barron, M. P. Bogaard, A. D. Buckingham, *Nature* **1973**, *241*, 113–114.
[3] L. D. Barron, A. D. Buckingham, *Mol. Phys.* **1971**, *20*, 1111–1119.
[4] J. Hudecova, V. Profant, P. Novotna, V. Baumruk, M. Urbanova, P. Bour, *J. Chem. Theory Comput.* **2013**, *9*, 3096–3108.
[5] H. O. Hamaguchi, *Appl. Spectrosc. Rev.* **1988**, *24*, 137–174.
[6] R. L. McCreery, in Handbook of Vibrational Spectroscopy, (Eds: J. M. Chalmers, P. R. Griffiths), John Wiley & Sons Ltd, Chichester, **2002**, pp. 920–932.
[7] K. J. Frost, R. L. McCreery, *Appl. Spectrosc.* **1998**, *52*, 1614–1618.
[8] R. L. McCreery, Raman Spectroscopy for Chemical Analysis, (Ed: J. D. Winefordner), Wiley-Interscience, New York, **2000**, pp. 269–291.
[9] K. G. Ray, R. L. McCreery, *Appl. Spectrosc.* **1997**, *51*, 108–116.
[10] J. R. Beattie, J. V. Glenn, M. E. Boulton, A. W. Stitt, J. J. McGarvey, *J. Raman Spectrosc.* **2009**, 40, 429–435.
[11] F. Bonnier, A. Mehmood, P. Knief, A. D. Meade, W. Hornebeck, H. Lambkin, K. Flynn, V. McDonagh, C. Healy, T. C. Lee, F. M. Lyng, H. J. Byrne, *J. Raman Spectrosc.* **2011**, 42, 888–896.
[12] C. W. Huang, L. K. Dai, X. F. Dong, *Spectrosc. Spectr. Anal.* **2011**, *31*, 1279–1282.
[13] K. Y. Noonan, L. A. Tonge, O. S. Fenton, D. B. Damiano, K. A. Frederick, *Appl. Spectrosc.* **2009**, *63*, 742–747.
[14] J. D. Rodriguez, B. J. Westenberger, L. F. Buhse, J. F. Kauffman, *Analyst* **2011**, *136*, 4232–4240.
[15] P. Malon, L. Bednarova, M. Straka, L. Krejci, L. Kumprecht, T. Kraus, M. Kubanova, V. Baumruk, *Chirality* **2010**, *22*, E47–E55.
[16] V. Profant, V. Baumruk, X. J. Li, M. Safarik, P. Bour, *J. Phys. Chem. B* **2011**, *115*, 15079–15089.
[17] V. Profant, M. Safarik, P. Bour, V. Baumruk, *Spectr.-Int. J.* **2010**, *24*, 213–217.
[18] F. J. Zhu, N. W. Isaacs, L. Hecht, G. E. Tranter, L. D. Barron, *Chirality* **2006**, *18*, 103–115.
[19] W. Hug, S. Kint, G. F. Bailey, J. R. Scherer, *J. Am. Chem. Soc.* **1975**, *97*, 5589–5590.
[20] M. Pazderková, V. Profant, J. Hodačová, J. Šebestík, T. Pazderka, P. Novotná, M. Urbanová, M. Šafařík, M. Buděšínský, M. Tichý, L. Bednárová, V. Baumruk, P. Maloň, *J. Phys. Chem. B* **2013**, *117*, 9626–9642.
[21] W. Hug, *Appl. Spectrosc.* **1981**, *35*, 115–124.
[22] C. J. Petty, G. M. Warnes, P. J. Hendra, M. Judkins, *Spectroc. Acta Pt. A-Molec. Biomolec. Spectr.* **1991**, *47*, 1179–1187.
[23] M. Fryling, C. J. Frank, R. L. McCreery, *Appl. Spectrosc.* **1993**, *47*, 1965–1974.
[24] E. S. Etz, S. J. Choquette, W. S. Hurst, *Microchim. Acta* **2005**, *149*, 175–184.
[25] E. S. Etz, W. S. Hurst, S. J. Choquette, in Microbeam Analysis 2000, Proceedings, (Eds: D. B. Williams, R. Shimizu), Iop Publishing Ltd, Bristol, **2000**, pp. 121–122.
[26] S. J. Choquette, E. S. Etz, W. S. Hurst, D. H. Blackburn, S. D. Leigh, *Appl. Spectrosc.* **2007**, *61*, 117–129.
[27] J. Smolikova, Z. Koblicova, K. Blaha, *Collect. Czech. Chem. Commun.* **1973**, *38*, 532–547.
[28] J. Hanzlikova, P. Praus, V. Baumruk, *J. Mol. Struct.* **1999**, *481*, 431–435.
[29] L. Hecht, L. D. Barron, A. R. Gargaro, Z. Q. Wen, W. Hug, *J. Raman Spectrosc.* **1992**, 23, 401–411.
[30] J. D. Rodriguez, B. J. Westenberger, L. F. Buhse, J. F. Kauffman, *Anal. Chem.* **2011**, *83*, 4061–4067.
[31] Spectral ID Users Guide, Galactic Industries Corporation, Salem, NH, **1998**, 71.
[32] M. J. Frisch, G. W. Trucks, H. B. Schlegel, G. E. Scuseria, M. A. Robb, J. R. Cheeseman, G. Scalmani, V. Barone, B. Mennucci, G. A. Petersson, H. Nakatsuji, M. Caricato, X. Li, H. P. Hratchian, A. F. Izmaylov, J. Bloino, G. Zheng, J. L. Sonnenberg, M. Hada, M. Ehara, K. Toyota, R. Fukuda, J. Hasegawa, M. Ishida, T. Nakajima, Y. Honda, O. Kitao, H. Nakai, T. Vreven, J. A. Montgomery, Jr., J. E. Peralta, F. Ogliaro, M. Bearpark, J. J. Heyd, E. Brothers, K. N. Kudin, V. N. Staroverov, R. Kobayashi, J. Normand, K. Raghavachari, A. Rendell, J. C. Burant, S. S. Iyengar, J. Tomasi, M. Cossi, N. Rega, N. J. Millam, M. Klene, J. E. Knox, J. B. Cross, V. Bakken, C. Adamo, J. Jaramillo, R. Gomperts, R. E. Stratmann, O. Yazyev, A. J. Austin, R. Cammi, C. Pomelli, J. W. Ochterski, R. L. Martin, K. Morokuma, V. G. Zakrzewski, G. A. Voth, P. Salvador, J. J. Dannenberg, S. Dapprich, A. D. Daniels, Ö. Farkas, J. B. Foresman, J. V. Ortiz, J. Cioslowski, D. J. Fox, Gaussian 09, Revision B.01, Gaussian, Inc., Wallingford CT, **2009**.
[33] J. P. Perdew, K. Burke, Y. Wang, *Phys. Rev. B* **1996**, 54, 16533–16539.
[34] A. Klamt, in The Encyclopedia of Computational Chemistry, (Eds: P. R. Schleyer, N. L. Allinger, T. Clark, J. Gasteiger, P. A. Kollman, H. F. Schaefer, III, P. R. Schreiner), John Wiley & Sons, Chichester, **1998**, pp. 604−615.
[35] P. Danecek, P. Bour, *J. Comput. Chem.* **2007**, *28*, 1617–1624.
[36] A. Samsonyuk, C. Scheurer, *J. Comput. Chem.* **2013**, *34*, 27–37.

Supporting information

Additional supporting information may be found in the online version of this article at the publisher's web site.

Relative intensity correction of Raman optical activity spectra facilitates extending the spectral region

Václav Profant, Markéta Pazderková, Tomáš Pazderka, Petr Maloň, Vladimír Baumruk

Charles University in Prague, Faculty of Mathematics and Physics, Institute of Physics, Ke Karlovu 5, 12116, Prague 2, Czech Republic

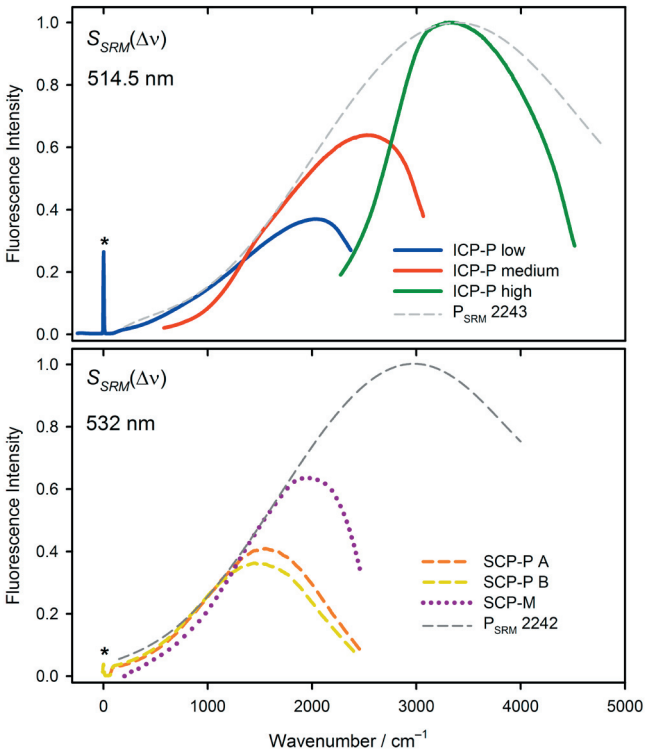

Figure S1. Fluorescence profiles $S_{SRM}(\Delta\nu)$ of SRM 2243 and 2242 (for the RIC of Raman spectra obtained with instruments employing 514.5 and 532 nm laser excitation) measured with three different gratings on the ICP-P instrument (top) and on the two SCP instruments SCP-P and SCP-M (bottom). The experimental spectra were normalized by one point alignment.

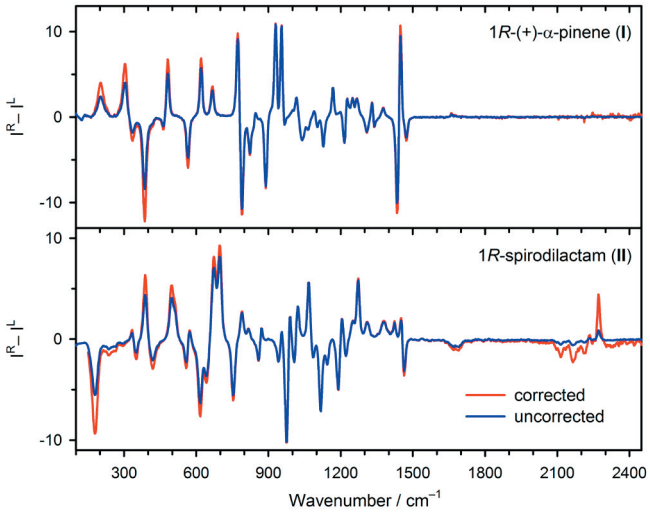

Figure S2. Effect of the RIC on the ROA spectra of (1*R*)-(+)-α-pinene (I) and 1*R*-spirodilactam (II) (shown from 150 to 2425 cm^{-1}) measured on SCP-P A.

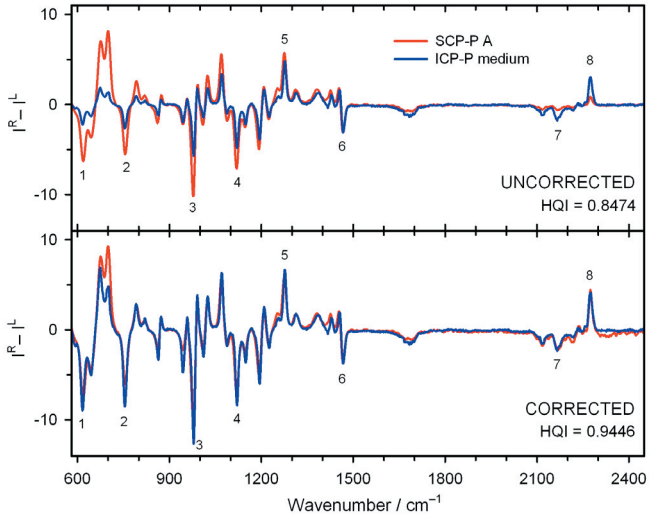

Figure S3. Uncorrected and corrected ROA spectra of the 1*R*-spirodilactam (II) recorded on two different instruments (SCP-P A and ICP-P medium). The spectra are normalized to integral intensity within 1300–1550 cm^{-1}. Only the overlapping spectral region (580–2390 cm^{-1}) is shown. Integral intensities of the labeled bands can be found in the Table S3.

Table S1. Integral intensities of selected ROA bands of (1*R*)-(+)-α-pinene (I) in Fig. 3. Variations among the values are expressed as relative standard deviations η.

Band (No.)	Wavenumber (cm^{-1})	Uncorrected				Corrected			
		ICP-P low	SCP-P A	SCP-M	η (%)	ICP-P low	SCP-P A	SCP-M	η (%)
1	304	0.85	0.91	0.45	27	1.45	1.41	1.53	3
2	386	1.94	1.94	1.06	25	3.03	2.80	2.77	4
3	482	0.80	0.73	0.51	18	1.08	0.97	1.00	4
4	618	0.85	0.86	0.62	14	0.96	1.03	1.02	3
5	788	1.49	1.40	1.12	12	1.50	1.49	1.53	1
6	928	1.46	1.53	1.23	9	1.44	1.55	1.56	4
7	1433	1.32	1.27	1.23	3	1.39	1.42	1.24	6
8	1447	0.96	0.86	0.97	5	1.02	0.98	0.97	2

Table S2. HQI values of uncorrected and corrected spectra of (1*R*)-(+)-α-pinene (I) measured on different instruments (plain – Raman, bold – ROA).

	Uncorrected				Corrected		
	ICP-P low	SCP-P A	SCP-M		ICP-P low	SCP-P A	SCP-M
ICP-P low	—	0.989	0.972	ICP-P low	—	0.994	0.996
SCP-P A	**0.979**	—	0.975	SCP-P A	**0.980**	—	0.994
SCP-M	**0.973**	**0.975**	—	SCP-M	**0.987**	**0.990**	—

Table S3. Integral intensities of selected ROA bands of 1*R*-spirodilactam (II) in Fig. S3. Variations between values are expressed as relative standard deviations η.

Band (No.)	Wavenumber (cm^{-1})	Uncorrected			Corrected		
		SCP-P A	ICP-P med	η (%)	SCP-P A	ICP-P med	η (%)
1	619	2.99	0.92	53	3.61	3.57	1
2	757	2.28	0.93	42	2.49	2.89	7
3	979	3.16	1.48	36	3.18	3.17	0
4	1121	2.90	1.56	30	2.90	2.59	6
5	1278	2.25	1.52	19	2.33	2.03	7
6	1472	0.87	0.85	1	1.01	0.99	1
7	2165	0.43	1.16	46	1.65	1.48	5
8	2273	0.24	1.02	61	1.24	1.33	3

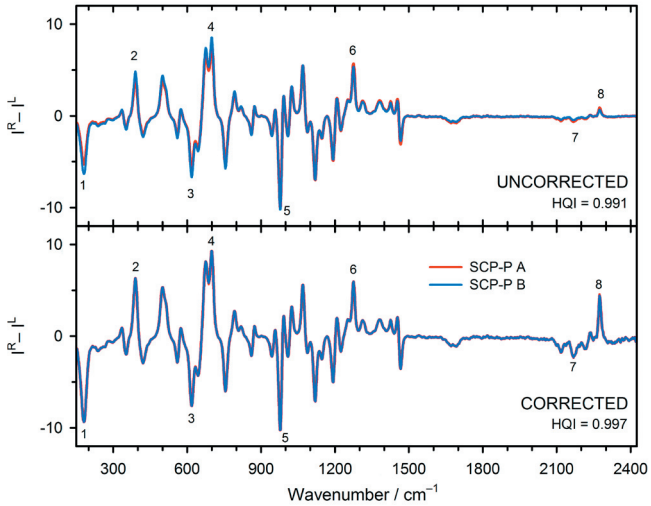

Figure S4. The effect of alternative notch or edge filters on ROA spectra of 1*R*-spirodilactam (II) (measured on SCP-P instrument).

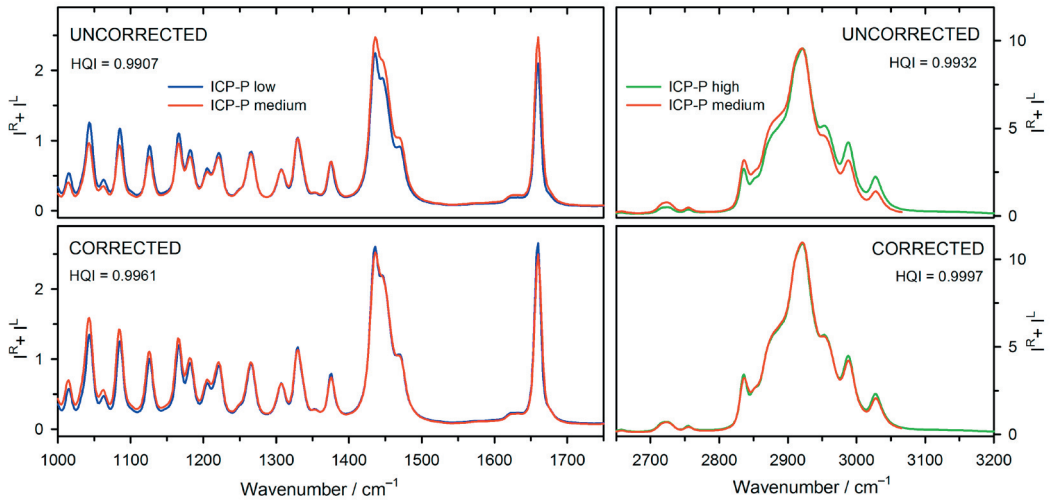

Figure S5. Effect of the RIC on normalized Raman spectra of (1*R*)-(+)-α-pinene (I) in overlaying spectral regions when used for the assembly of panoramic spectra.

Table S4. Integral intensities of selected ROA bands of 1*R*-spirodilactam (II) in Fig. S4. Variations between the values are expressed as relative standard deviations η.

Band (No.)	Wavenumber (cm^{-1})	Uncorrected			Corrected		
		SCP-P A	SCP-P B	η (%)	SCP-P A	SCP-P B	η (%)
1	181	2.95	3.53	9	4.97	5.19	2
2	389	1.28	1.48	7	1.86	1.93	2
3	618	2.56	2.80	4	3.09	3.19	1
4	699	2.84	3.06	4	3.22	3.31	1
5	978	2.43	2.50	1	2.46	2.51	1
6	1275	1.74	1.64	3	1.80	1.82	0
7	2167	0.35	0.26	15	1.35	1.31	1
8	2274	0.20	0.14	16	1.01	0.98	2

Appendix 4

Electronic and Vibrational Optical Activity of Several Peptides Related to Neurohypophyseal Hormones: Disulfide Group Conformation

Biopolymers 2012, 97, 923–932

Pazderková, M.,[1,2] Bednárová, L.,[1] Dlouhá, H.,[1] Flegel, M.,[1,3] Lebl, M.,[4] Hlaváček, J.,[1] Setnička, V.,[5] Urbanová, M.,[5] Hynie, S.,[3] Klenerová, V.,[3] Baumruk, V.,[2] Maloň, P.[1]

[1]*Institute of Organic Chemistry and Biochemistry, AS CR, Fleming square 2, 166 10 Prague 6, Czech Republic*
[2]*Charles University in Prague, Faculty of Mathematics and Physics, Ke Karlovu 5, 121 16 Prague 2, Czech Republic*
[3]*Charles University in Prague, 1st Faculty of Medicine, Institute of Medical Biochemistry, Albertov 4, 128 00 Prague 2, Czech Republic*
[4]*Spyder Institut Praha s. r. o., Nad Safinou II c. 365, Vestec, 252 42 Jesenice u Prahy, Czech Republic*
[5]*Institute of Chemical Technology Prague, Department of Physics, Technická 190, 166 28 Prague 6, Czech Republic*

Electronic and Vibrational Optical Activity of Several Peptides Related to Neurohypophyseal Hormones: Disulfide Group Conformation

Markéta Pazderková,[1,2] Lucie Bednárová,[1] Helena Dlouhá,[1] Martin Flegel,[1,3] Michal Lebl,[4] Jan Hlaváček,[1] Vladimír Setnička,[5] Marie Urbanová,[5] Sixtus Hynie,[3] Věra Klenerová,[3] Vladimír Baumruk,[2] Petr Maloň[1]

[1] *Institute of Organic Chemistry and Biochemistry, Academy of Sciences of the Czech Republic, Fleming sq. 2, 166 10 Prague 6, Czech Republic*

[2] *Charles University in Prague, Faculty of Mathematics and Physics, Ke Karlovu 5, 121 16 Prague 2, Czech Republic*

[3] *Charles University in Prague, 1st Faculty of Medicine, Institute of Medical Biochemistry, Albertov 4, 128 00 Prague 2, Czech Republic*

[4] *Spyder Institut Praha s. r. o., Nad Safinou II c. 365, Vestec, 252 42 Jesenice u Prahy, Czech Republic*

[5] *Institute of Chemical Technology Prague, Department of Physics, Technická 190, 166 28 Prague 6, Czech Republic*

Received 24 February 2012; revised 1 June 2012; accepted 9 June 2012
Published online 21 June 2012 in Wiley Online Library (wileyonlinelibrary.com). DOI 10.1002/bip.22105

ABSTRACT:

Electronic and vibrational optical activity of the set of neurohypophyseal hormones and their analogs was investigated to clarify the S—S bond solution conformation. The selected compounds include oxytocin (I), lysine vasopressin (II), arginine vasopressin (III), and their analogs (IV–IX), differing widely in their pharmacological properties. We have extended the already known electronic circular dichroism data by new information provided by vibrational circular dichroism (VCD) and Raman optical activity (ROA). The use of VCD brought additional details on three-dimensional structure of the chain reversal in the ring moiety and on its left handedness. Furthermore, Raman scattering and ROA allowed us to deduce the sense of the disulfide bond torsion. © *2012 Wiley Periodicals, Inc. Biopolymers 97: 923–932, 2012.*

Keywords: neurohypophyseal hormones; disulfide bridge; chiroptical spectroscopy; circular dichroism; Raman optical activity; vibrational circular dichroism; oxytocin; vasopressin; analogs; conformation

This article was originally published online as an accepted preprint. The "Published Online" date corresponds to the preprint version. You can request a copy of the preprint by emailing the Biopolymers editorial office at biopolymers@wiley. com

INTRODUCTION

Neurohypophyseal hormones (NHHs) are among the longest recognized biologically active peptides. Oxytocin (OT) and arginine vasopressin (AVP—human hormone) are structurally related nonapeptides, synthesized in hypothalamic neurons, stored in the posterior pituitary gland (neurohypophysis, NH), and released into the circulation as NHHs with very different physiological roles (Gimpl and Fahrenholz[1]). The primary physiological role of OT is milk ejection and contraction of the uterus, whereas AVP is involved in regulation of cardiovascular functions and acts as a hormone with antidiuretic

Additional Supporting Information may be found in the online version of this article.

Correspondence to: Markéta Pazderková; e-mail: pazderkova@karlov.mff.cuni.cz

Contract grant sponsor: Grant Agency of the Czech Republic (project no. P205/10/1276)
Contract grant sponsor: Grant Agency of Charles University (project no. 578212)
Contract grant sponsor: Ministry of Education, Youth and Sports (MSM 0021620806)

Table I List of Samples

Compound	Accepted Title	Structure[a]	Basic Pharmacological Effects (Peripheral)
Neurohypophyseal hormones			
I	Oxytocin	**C** Y I Q N **C** P L G-NH_2	Uterotonic (UTT), milk ejecting (ME)
II	Arginine vasopressin Natural human hormone	**C** Y F Q N **C** P R G-NH_2	Antidiuretic (AD), pressoric (PR)
III	Lysine vasopressin Hog hormone	**C** Y F Q N **C** P K G-NH_2	Antidiuretic (AD), pressoric (PR)
Analogs produced as bulk pharmaceutical chemicals for remedies			
IV	Methyloxytocin[b]	**C** Y(OMe) I Q N **C** P L G-NH_2	UTT (lower activity and protracted effect)
V	Atosiban[c]	**Mpr** y(OEt) I T N **C** P Orn G-NH_2	UTT, inhibitor OTR, V1 a V2 receptors
VI	Desmopressin[b]	**Mpr** Y F Q N **C** P r G-NH_2	AD (DDAVP) (V2 agonist in diabetes insipidus)
VII	Terlipressin[c]	G G G **C** Y F Q N **C** P K G-NH_2	PR low and very protracted effect—used for esophageal bleeding
Analogs			
VIII	NHH inhibitor	cpm**C** y I T N **C** P Orn-NH_2	UTT, strong OTR inhibitor
IX	Ring model	**C** G G G N **C**-NH_2	Not known, for conformational studies only

[a] In all structures, the Cys (or Mpr) residues are connected via the disulfide bridge and form a heterodetic ring closure (indicated in Bold type); Mpr, mercaptopropionic acid; cmpC, β-cyclopentamethylene-cysteine. Lower case letters are used to denote D-amino acid residues.

[b] Methyloxytocin was used as the safe uterotonic stimulator (later replaced by even safer Carbetocin (deamino-carba[1]-Tyr(OMe)[2]-oxytocin)).

[c] Atosiban is able to antagonize uterotonic effect of oxytocin and is used for the suppression of the development of unwanted uterotonic activity.

[d] Desmopressin (also known as DDAVP) is still considered as one of the most successful very powerful antidiuretic drugs.

[e] Terlipressin (also known as glypressin) is hormonogen-like peptide with very protracted pressoric activity which is used in the various bleedings disorders and during vascular surgery.

function. New experimental approaches disclosed the role of OT and AVP as important regulatory factors in the brain (maternal and social behavior, learning and memory, stress, etc.). At present, it is well recognized that NHHs act in central nervous system and this role seems to be perhaps equally important in comparison with the peripheral effects already described in detail.[2] Central activities of NHHs are currently studied from various aspects. Both hormones act through G-protein-coupled receptors, OT through OT receptor, whereas AVP by activation receptors V1a, V1b (or V3), and V2.[1] However, the receptor selectivity is not absolute and there exists some crosstalk between vasopressin (VP) and OT receptors. Amino acid sequence of OT including its disulfide bridge was elucidated in 1953 by Du Vigneaud et al.[3] OT was the first peptidic hormone that was successfully synthesized, shortly after its discovery.[3,4] Syntheses of OT and AVP analogs with agonistic and antagonistic properties, based on the modulation of their receptor activity, followed soon; some of these drugs have important therapeutic use (Table I). V2 agonists are used for the treatment of diabetes insipidus and its antagonists may be used in the case of congestive heart failure; terlipressin is used against esophageal bleeding. OT antagonist atosiban was approved for the treatment of preterm labor. Nowadays, many (i.e. hundreds of) synthetic analogs and structural descendants of NHHs exist. Analogs of NHHs were utilized as drugs in both human and veterinary medicine and their investigation significantly contributed to knowledge of general methodics of QSAR studies, inhibitor, and receptor investigation.[2,5]

Structural studies of NHHs are numerous as well. The molecules display considerable conformational constraints and limited conformational mobility. Their spatial arrangement has been thoroughly investigated. There are numerous nuclear magnetic resonance (NMR) (^{1}H, ^{13}C, relaxation times, and Overhauser effect)[6–22] (for a review, see Hruby and Lebl[23]) and molecular spectroscopy (CD,[24–28] Raman,[27–31] and fluorescence[32–34]) studies. Several analogs were crystallized and the X-ray studies of them[35,36] or of the complex with neurophysin[37,38] and trypsin[39] provide a conception of their three-dimensional structure. Structural studies in solution are mainly based on NMR and electronic CD spectroscopies. The results indicate that NHH molecules—at least the ring parts—are remarkably consistent in their spatial arrangements. It is difficult to relate quite variant biological properties, which respond sensitively to even minor changes in structure of NHH analogs, with the fact that three-dimensional structures of these molecules vary little. NMR studies have provided considerable information about NHH structural arrangement in solution, but it has not been useful for investigating conformation around the disulfide bridge. Disulfide group is a characteristic and important structural element of NHH molecules because it closes the 20-membered ring which is essential for

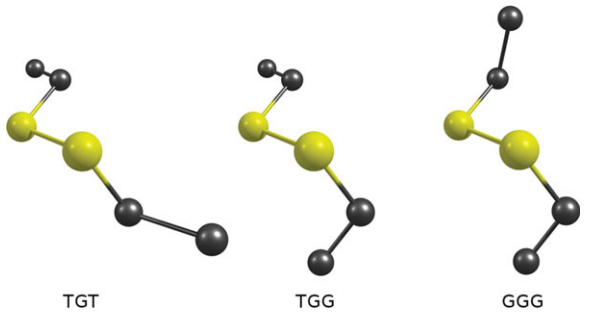

FIGURE 1 Frequent conformations of the disulfide bridge, C—C—S—S—C—C. Left: TGT; middle: TGG; right: GGG (G, *gauche*; T, *trans*). Sulfur atoms are shown in yellow.

the manifestation of pharmacological activities. However, the ring can be modified, leading often to analogs more stable toward cleaving enzymes. In addition, some studies indicate that NHH conformation might react sensitively to the interaction of disulfide group with the aromatic side chain at position 2.[40] This interaction was also confirmed by data from high-performance liquid chromatography (HPLC)[41,42] and NMR and fluorescence[43] studies of OT analogs modified with replacement of sulfur atoms by methylene groups or S—O groups.

Many spectroscopic studies of disulfide conformation in NHHs and their analogs have been already made.[24–31,44–50] Generally, disulfide bridge in peptides is quite flexible and can adopt various geometries. However, statistical treatment of known protein structures reveals preferences for several conformational types. There are three general conformations of the disulfide group (Figure 1), all with the central dihedral angle (C—S—S—C, i.e. around the S—S bond) nearly $\pm 90^{\circ}$ denoted as GGG, GGT, and TGT (in this three-letter symbolics the initial and final G or T designates *gauche*- or *trans*-conformation of the C—C—S—S or S—S—C—C termini; the central G is a standard designation of the S—S conformation with χ_{S-S} nearly $\pm 90^{\circ}$). These conformations can be distinguished by standard Raman spectroscopy which allows detecting individual C—S and S—S stretching modes and identifying corresponding disulfide conformations. It is generally accepted that GGG, TGG, and TGT conformations give rise to the respective S—S stretching signals nearly 510, 525, and 540 cm^{-1} (Refs. [51–53]). Conformations of the disulfide bond with prevailing GGG arrangement were found in the spectra of most agonistic OT and VP analogs.[27–31] On the other hand, different disulfide bond conformations can be found in some OT antagonists, for example molecules having penicillamine in position 1−.[45] Although the information obtained mainly by Raman spectroscopy is valuable, it cannot distinguish between right- and left-handed arrangements of the system. However, nonplanar disulfide group is chiral and this makes its handedness approachable by chiroptical methods involving electronic and vibrational circular dichroism (VCD) and Raman optical activity (ROA). There are some difficulties with investigation of disulfide groups by electronic circular dichroism (ECD) owing to group symmetry, orbital degeneracy, and strong overlap of disulfide bands with the amide transitions at 190–250 nm and with π–π^* transitions of aromatic residues at 250–300 nm (see, e.g. Refs. [27,54]). We have shown earlier that useful information about the disulfide conformation might be obtained using methods of vibrational optical activity (VOA), particularly ROA which is a chiral variant of Raman spectroscopy. Our earlier experimental and theoretical results indicate that ROA might represent a long sought-after solution of disulfide group conformation and might be capable of distinguishing between its right- and left-handed chirality.[55,56]

For the present study, we take advantage of the fact that NHHs are used as drugs in various indications for the treatment of disorders in both human and veterinary medicine and for this purpose they are manufactured under the rules of current good manufacturing practice (cGMP) in large quantities and in high purity as described in the Pharmacopeia. We selected a set of such compounds (Table I), including hormones themselves (OT I, arginine, and lysine vasopressins II, III), their pharmaceutically used analogs (methyloxytocin IV, atosiban V, desmopressin VI, and terlipressin VII) and related models (VIII, IX). Although the selected compounds differ widely in their pharmacological properties, these are achieved just by little changes of their primary and perhaps secondary structures. Our list forms a suitable basis for a more detailed structural scrutiny which could provide us the still missing view. We intend to investigate these compounds with a combination of several optical and chiroptical spectroscopies including ECD, VCD, Raman spectroscopy, and ROA. The use of vibrational chiroptical methods (VCD and ROA) might provide additional information because neither amide (VCD and ROA) nor disulfide (ROA) signals overlap with the π–π^* bands of aromatic side chains as they unfortunately do in ECD spectra. In addition, these methods, in particular the ROA, provide insight even into small-scale structural changes. Comparison of new chiroptical data with already known results of conformational studies should further elucidate the role of disulfides in NHHs structure and function.

MATERIALS AND METHODS

The hormones I–III and their analogs IV–VII were bulk-synthesized pharmaceutical chemicals prepared under cGMP (Polypeptide Group). They were fully analytically characterized and used without further purification. The sample of inhibitor VIII was provided by Prof. Manning (Medical College of Ohio) and used without further purification. The simplified ring model IX was prepared using

standard procedures of solid-phase peptide synthesis employing Fmoc/*tert*-butyl strategy, TFA reagent cleavage from the resin, oxidation, and standard HPLC purification. The synthesized peptide was at least 95% pure (based on HPLC).

Electronic absorption and ECD spectra were measured in solutions on Jasco J-815 spectrometer equipped with a Peltier-based temperature control module. The solvents included 0.01*M* phosphate buffer (pH = 7.5), 0.01*M* HCl (pH = 2) and, for compound II, 2,2,2-trifluoroethanol. Concentrations were in the approximate range of 5–20 $\times \cdot 10^{-4}$ mol L^{-1}. We used quartz cells with the optical path length of 1 cm. The spectra were recorded in the spectral region 255–360 nm mostly at room temperature but we also measured the dependence on temperature in the range of 5–75°C. Each spectrum was obtained as an average of three subsequent computer-controlled scans taken at the scanning speed of 50 nm/min and the time constant of 4 s. The final ECD and absorption spectra are expressed as the respective values of $\Delta\varepsilon$ and ε (L mol^{-1} cm^{-1}) (Figure. 2). ECD and absorption of compound VIII in low pH was not measured because of too low quantity which was available.

VCD was measured on Bruker FTIR spectrometer equipped with the VCD/IRRAS module. The setup used for amide I and mid IR measurements (1800–1200 cm^{-1}) was based on IFS-66/S FTIR and included: VCD/IRRAS PMA 37 attachment, BaF_2 polarizer, ZnSe photoelastic modulator (Hinds), MCT detector (InfraRed Associates), and a lock-in amplifier (SR830 Stanford Instruments). The spectra were recorded at the resolution of 8 cm^{-1} in D_2O at the concentration range of 4–9 $\cdot 10^{-2}$ mol L^{-1}. We used a demountable sample cell (path length, 0.025 mm) with CaF_2 windows. Our standard measurement protocol involved averaging of four 30 min blocks of interferograms. Corresponding solvent scans were subtracted as background. The compounds II, VIII, and IX showed the presence of TFA as an absorption signal at 1671 cm^{-1} which has been subtracted. Final data were plotted as the respective ε((absorption) and $\Delta(\varepsilon$((VCD) values normalized to number of amino acid residues. Second derivatives of absorption spectra were calculated using GRAMS/AI software (Thermo Electron Corporation) to enable decomposition and detailed interpretation of overlapping amide I band components according to a procedure described elsewhere.[57]

Raman scattering and ROA spectra were measured on the commercial scattered circular polarization (SCP) ROA spectrometer (Chiral Raman, Bio Tools, USA)[58] and on the incident circular polarization (ICP) Raman/ROA instrument built at the Institute of Physics, Charles University in Prague working in backscattering.[59] The latter spectrometer is based on a fast stigmatic spectrograph HoloSpec HS-f/1.4 (Kaiser Optical Systems) with an interchangeable holographic transmission grating and a back-illuminated CCD detection system (Roper Scientific, 1340 × 100 pixels). The compounds I–VII and IX for Raman and ROA measurements were dissolved in distilled water at ambient temperature (20°C) and filtered through a 0.22-μm Millipore filter into quartz ROA micro-cells (~60 μL, 4 × 3 mm, Starna Scientific) with antireflectively coated windows. The pH of aqueous solutions was adjusted with 0.2*M* HCl to a value of ~3. For the compound VIII, we were not able to obtain Raman and ROA spectra because of its low quantity which allowed only the measurement of ECD (in neutral buffer) and VCD. The conditions for ROA experiments were set on the two instruments as follows: Chiral Raman: excitation wavelength 532 nm, laser power at the sample 250–300 mW, spectral resolution 7 cm^{-1}; noncommercial spectrometer: excitation wavelength 514.5 nm, laser power at the sample 550–650 mW, spectral resolution 6.5 cm^{-1}. We used concentrations in the range of 6–10 $\times \cdot 10^{-2}$ mol L^{-1}. Acquisition time was optimized to get reasonable *S*/*N* ratio in ROA spectra (3–4 days). Spectra were processed by subtracting the solvent signal and correcting the baseline by polynomial fitting (5th order polynomial). The final ROA spectra are presented as ($I^R - I^L$) and the Raman spectra as ($I^R + I^L$) where I^R and I^L are Raman intensities in right- and left- circularly polarized ICP or SCP laser light. Numerical data treatment was done using GRAMS/AI software (Thermo Electron). Decomposition of Raman spectra into single bands was made using second derivatives.

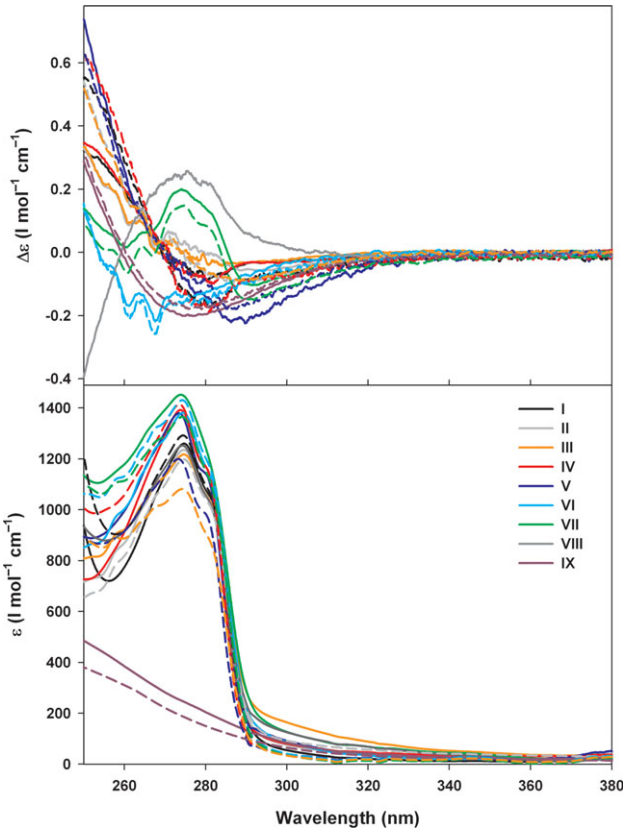

FIGURE 2 ECD (top) and UV absorption (bottom) of compound I (OT), II (AVP), III (lysine vasopressin), IV (methyloxytocin), V (atosiban), VI (desmopressin), VII (terlipressin), VIII (NHH inhibitor), and IX (ring model) measured in phosphate buffer (solid) and 0.01*M* HCl (dashed).

RESULTS AND DISCUSSION

We have measured ECD and electronic absorption of the whole series of compounds I–IX at neutral (pH 7.5, phosphate buffer) and acidic (pH 2, 0.01*M* HCl) conditions in the disulfide transition range (250–380 nm). Even in the case of compounds I–III, VI, IX, which have been previously measured,[25,26,28,48] we have collected the new data to have all spectra measured under comparable conditions. The results are shown in Figure 2. Below 280 nm, the disulfide bands

unfortunately overlap with the long-wavelength π–π^* bands of aromatic chromophores (Tyr in OT analogs, Tyr and Phe in VP analogs) and consequently pure disulfide signal can be observed only in the ECD spectra of IX which possesses no aromatic side chains. The interfering π–π^* bands show typical vibronic structure (tyrosine in absorption, phenylalanine in ECD—at 255, 261, and 268 nm). This phenomenon complicates spectra and makes isolation of disulfide contributions more difficult. In the presence of aromatic residues, we can thus safely ascribe disulfide origin to just the long wavelength tail in the 300–340 nm region as has been also recommended earlier.[60] On the basis of this long-wavelength disulfide CD band, we can classify our compounds I–IX into three categories: The first category (a) includes compounds with a negative band of low intensity; this is by far the most numerous category including all mainstream agonists I–IV, desmopressin VI and terlipressin VII. Although differences between their spectra are definitely over the error bars, the general course of these curves remains similar. A significant difference is observed only with OT I and methyloxytocin IV in low pH. In these latter cases, intensity of the negative disulfide band markedly increases on acidification. The second category (b) includes atosiban V with the disulfide band of clearly higher intensity. The spectra of the ring model IX form the transition between the first two categories. Although the differences between spectra belonging to classes (a) and (b) are quantitative and rather subtle, the category (c) shows disulfide band of the opposite sign. There is only one compound in this category—the inhibitor VIII. At shorter wavelengths, it is sometimes possible to observe a second disulfide band as predicted by the theory. With our compounds, it is observable only in the ECD spectrum of IX having no aromatic residues. This compound represents a simplified model of the OT ring with Gly residues replacing tyrosine and isoleucine. In neutral buffer, it exhibits a negative ECD band at 275 nm which can be considered a pure disulfide manifestation. In the early studies,[24] there were attempts to correlate the analogous 280 nm negative ECD band in I (also in IV, see above) and its pH dependence with the effect of possible protonation of the neighboring α-NH_2 group on the disulfide chromophore. However, no effect of protonation on disulfide conformation can be seen in ECD spectra of the ring model IX with Gly at position 2. This might indicate that the disulfide chromophore is influenced by neighboring Tyr (or Ile—Ref. [24]) residue. Much smaller changes can be observed in the spectra of NHH analogs lacking the α-NH_2 group (V, VI). The long-wavelength spectral tail which we used above for the classification of our compounds/spectra into (a, b, c) classes can be observed in spectra of all compounds I–IX. Its sign does not correlate with either the presence or the absence of α-NH_2 group (V, VI) and the correlation with configuration of the amino acid at the position 2 (V, VIII) is uncertain. However, it is interesting but hardly causally significant that this band somehow correlates with pharmacological properties: the agonists all belong to class (a) with small and similar disulfide bands, whereas the inactive IX and antagonists V, VIII display spectral differences and fall into categories (b, c). Consequences and importance of the D-configuration of aromatic amino acid for biological activities of OT analogs and their spectral properties were studied earlier in detail with both conformationally relaxed and constrained amino acids.[61] Analogs with D-amino acid clearly belong to different structural classes.

There have been many attempts to correlate experimental signs and magnitudes of disulfide bands with sense and magnitude of the disulfide twist on the basis of theoretical considerations and calculations.[54,62,63] Although nowadays it is not difficult to execute such a calculation at a very good theoretical level[55,64] (TD DFT calculation using B3LYP functional and at least the 6-31G* basis set may be considered a reasonable level of calculation), the results of such a calculation suffer numerous problems. The low-energy conformation of the C—S—S—C grouping is a perpendicular conformation with $\chi_{S-S} = \pm 90^\circ$. It would seem advantageous that this conformation represents simultaneously the arrangement having topologically maximal possible chirality. However, it is most unfortunate that the two lowest energy electronic transitions of the disulfide group are exactly degenerate in this conformation and consequently the sign of predicted CD sharply changes at $\chi_{S-S} = \pm 90^\circ$, where the two bands cancel and no CD is predicted. This situation has been known for some time[54,62,63] and it is usually generalized in a requirement that for the theoretical interpretation not only the sign but also some measure of the magnitude of the χ_{S-S} angle is needed (with values of χ_{S-S} close to $\pm 90^\circ$ this information needs to be rather precise). Applied to our case of NHH analogs, we may only say that similar course of disulfide-related ECD as shown in Figure 2 may mean similar S—S bridge conformation, but such a finding is not certain and there is a need for additional unambiguous information.

Vibrational and particularly chiral vibrational spectra should provide some still-missing structural details of NHHs, which are inaccessible by other spectroscopies. In addition, VOA promises to enrich significantly the current understanding of NHH's structure–function relationship. VCD and IR absorption spectra in the mid IR region (1300–1800 cm^{-1}) include signals owing to amide I (in D_2O amide I′) and amide II (II′) vibrations. In its current state of development, VCD cannot provide direct information on disulfide arrangement as vibrational bands owing to C—S—S—C

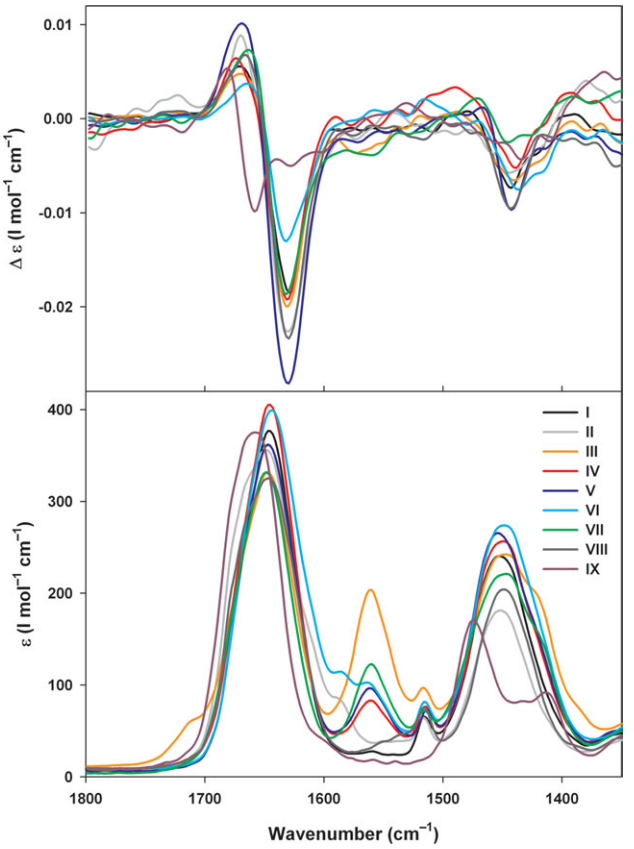

FIGURE 3 VCD (top) and IR absorption (bottom) of compound I (OT), II (AVP), III (lysine vasopressin), IV (methyloxytocin), V (atosiban), VI (desmopressin), VII (terlipressin), VIII (NHH inhibitor), and IX (ring model) measured in D_2O (spectra are normalized to the number of amino acid residues). The less compressed spectra are shown in Supporting Information material.

grouping lie outside the experimentally accessible region. The relevant region (~250–800 cm^{-1}) can be accessed by IR absorption spectroscopy, but the bands related to C—S and S—S bonds are usually invisible or of very low intensity. Vibrational transitions related to disulfide group are more conveniently accessed by Raman/ROA spectroscopy. On the other hand, VCD combined with IR spectroscopy can provide detailed information on peptide backbone and strengthen the knowledge given by other techniques. In our case, this means resolving information provided by ECD and NMR into detailed conformationally defined fragments. The spectra of compounds I–IX in D_2O are shown in Figure 3. The bands observed in absorption in amide I spectral region indicate the presence of the random coil/PPII structure (these two structures cannot be distinguished solely by IR spectroscopy) or of an α-helix (at ~1645 cm^{-1}, however α-helix can be excluded owing to VCD and Raman spectra—see below) together with the β-turn structure (shoulder at ~1665 cm^{-1}). VCD pattern owing to these signals has been described earlier[65] and its sensitive response to changes and types of secondary structures in peptides/proteins is well understood.[66] Our NHHs and their derivatives exhibit remarkably constant VCD spectral pattern consisting of a rather intense negative couplet corresponding to amide I′ at ~1650 cm^{-1} (a positive VCD band at ~1670 cm^{-1} together with a negative band at ~1630 cm^{-1}) and a smaller negative band at ~1440 cm^{-1} (amide II′). The positions of particular bands in I–VIII do not appear to be dependent on particular structures, only in the analog IX the position of amide I′ VCD bands is shifted to higher wavenumbers by about 25 cm^{-1}. The observed VCD patterns resemble very closely polyproline II (PPII) type secondary structures with a positive/negative couplet in the amide I (I′) region and a negative band in the amide II (II′) region. This type of conformation and associated VCD spectra has been extensively studied by Dukor and Keiderling.[67] Although it is generally difficult to distinguish between the left-handed helical PPII-like conformation and the truly unordered state of a peptide/protein, we can rather safely derive that the general three-dimensional ring pattern of NHHs includes a PPII-type left helical turn. For the extent of PPII turn, we can get an indication from the corresponding VCD intensities. If we calculate $\Delta A/A$ or alternately $\Delta\varepsilon/\varepsilon$ values for our compounds and compare these with intensities measured for real polyprolines,[67] we find our spectra approximately three times less intense. This indicates that a direction reversal of NHH ring probably involves just two to three amino acid residues. VCD intensities in the amide I′ and amide II′ region allow also some differentiation between compounds I and IX. The lowest intensity is shown by the compound IX in accordance with its assumed bigger flexibility.

Raman and ROA spectra provide a different point of view. Although there is also a significant manifestation of backbone conformation (it is shown in Raman/ROA mainly via extended amide III at 1240–1310 cm^{-1} [Ref. 68] and amide I bands), the most useful information follows from the low-wavenumber region (<800 cm^{-1}) with the prominent bands owing to disulfide vibrations. The spectra of compounds I–VII and IX in H_2O are shown in Figure 4 and the extracted Raman frequencies (amide I, amide III, ν_{C-S} and ν_{S-S}) obtained from the spectral decomposition using second derivatives are listed in Table II. Conformational analysis and band assignment was proposed with respect to the previous Raman investigations of OT (I), AVP (II), and their analogs.[27–31,45]

Raman bands of compounds I–VII in amide I and amide III region agree with the already expected presence of both random coil and β-sheet/β-turn structures[53,68] (Table II). Amide I and amide III bands in compound IX (the simplified

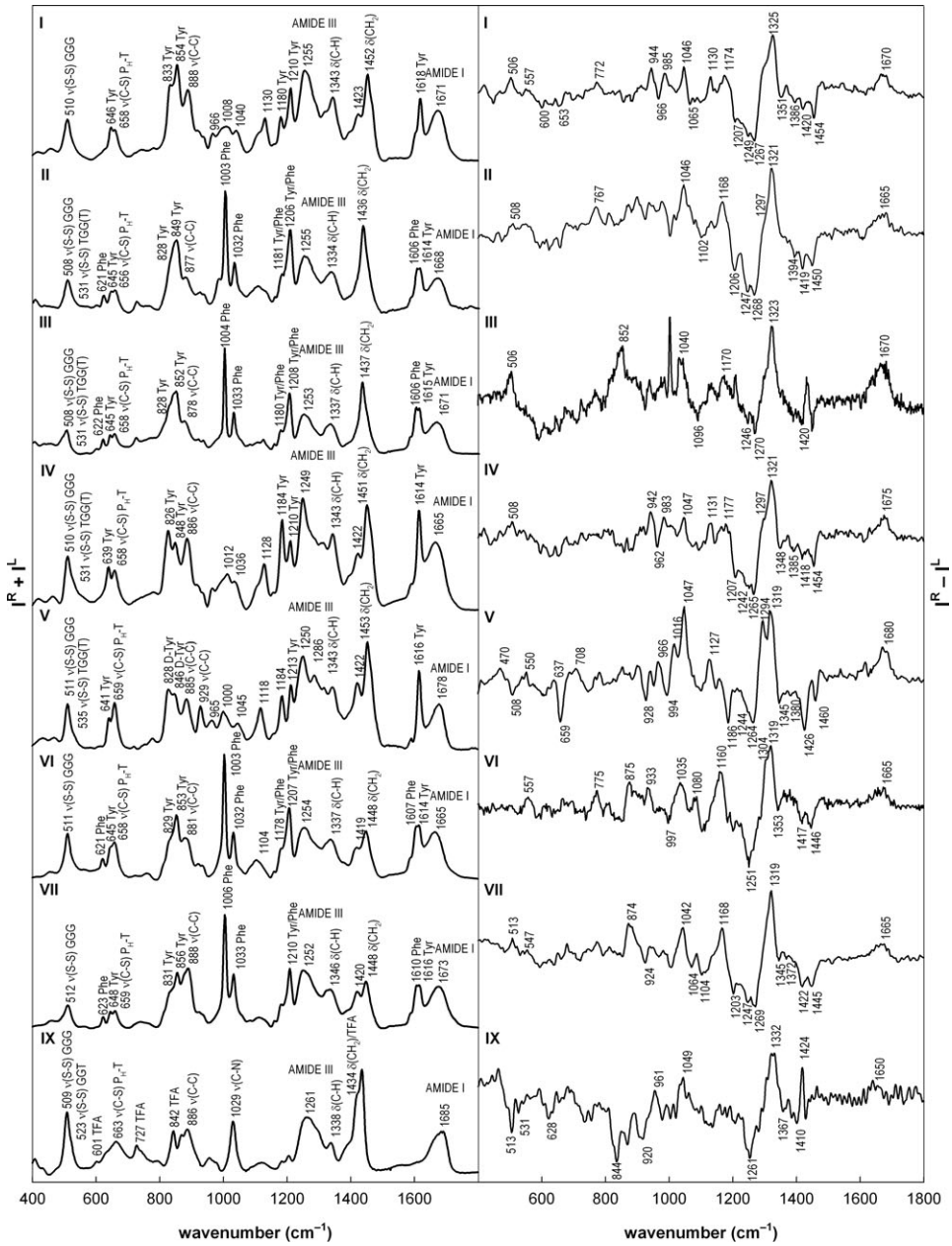

FIGURE 4 Raman scattering (left) and ROA (right) spectra of compounds I (OT), II (AVP), III (lysine vasopressin), IV (methyloxytocin), V (atosiban), VI (desmopressin), VII (terlipressin), and IX (ring model) measured at acidic pH. These spectra are shown at higher resolution in Supporting Information material.

model of the OT ring moiety) are shifted to higher wavenumbers and indicate the presence of β-sheet/β-turn structure. Raman bands at 850 and 830 cm^{-1} correspond to tyrosine side chain and their relative intensities are related to its environment.[69] The I_{850}/I_{830} intensity ratio exceeds 1 for compounds I–III, VI, VII, and IX, indicating that the Tyr residue is probably exposed to solvent. On the other hand, the ratio lower than 1 is observed for compounds IV and V where Tyr (2) OH group is alkylated and therefore no suitable partner for hydrogen bonding to the solvent is available. ROA spectra in this region show for compounds I–VII a sharp positive band at ~1320 cm^{-1} (extended amide III) and a weak positive band with the maximum at ~1665–1680 cm^{-1} (amide I). These findings further strengthen arguments in favor of the already indicated presence of PPII type secondary structure.[70–72] The additional negative band between ~1242–1251 cm^{-1} in compounds I–VII has been previously assigned to an antiparallel β-strand.[70] The presence of a short segment of

Table II C—S, S—S, and Amide-Related Frequencies in the Raman Spectra of Compounds I–VII, IX[a]

	Frequency (cm^{-1})							
Band assignment	I	II	III	IV	V	VI	VII	IX
Amide I	1686	1691	1690	1683	1687	1684	1685	1692
	1678	1683	1681				1682	
	1668	1666	1671	1667	1667	1670	1668	1672
	1659	1658		1657		1657	1653	
Amide III	1292	1285	1291	1288	1286	1286		1274
	1267	1263	1268	1274			1268	1257
	1250	1249	1247	1247	1250		1243	1247
		1238			1235			
ν(C—S) P_H	658	656	658	658	659	658	659	663
ν(S—S) TGG(T)		531sh	533sh	533sh	531sh			
ν(S—S) TGG								523sh
ν(S—S) GGG	510	508	508	509	511	511	512	508

[a] TGG(T)—Weak bands do not allow reliable distinguishing between G and T conformation on S—C dihedral angle.
sh, Shoulder.

this type of structure is quite probable. A positive band at ~1295 cm^{-1} and negative bands at ~1350 and ~1385 cm^{-1} in ROA spectra of I, IV, V, and VI might in addition indicate the presence of a β-turn-like structure.[72,73] VCD/IR/Raman and ROA data on NHHs (OT I, AVP II, LVP III, desmopressin VI) agree with the backbone arrangement found by NMR spectroscopy in combination with molecular dynamics (MD) simulations[19,21,22,74,75] although the latter data were often obtained in a different solvent (dimethyl sulfoxide) (Table I in Ref. [76]). NMR results favor β-turn (over the residues 2,3 or 3,4) or γ-turn conformations (desmopressin). However, NMR spectroscopy is not sensitive to disulfide group conformation.

Unlike in ECD spectra where Tyr and disulfide-related bands overlap and obscure each other, signals owing to the disulfide bridge (ν_{S-S} and ν_{C-S} vibrations) can be distinguished clearly in Raman and ROA spectra. Although a broad water band at 400–520 cm^{-1} overlaps just slightly with the S—S stretching band, it usually does not obscure the ν_{S-S} signal. The strong S—S stretching band in Raman spectra of all the measured compounds (I–VII and IX) at ~510 cm^{-1} is an indicator of prevailing GGG conformation of C—C—S—S—C—C grouping.[52] Second derivative spectra reveal a shoulder at ~523 cm^{-1} (IX) or ~530 cm^{-1} (I, II, IV), and ~535 cm^{-1} (V) which indicates a small fraction of the respective GGT and TGT conformation.[52,53] Raman signal of C—S stretching vibrations can be found in the region of 655–663 cm^{-1} for all studied compounds, indicating prevailing P_H conformation of the X—CH—CH_2—CH moiety (X=H, C, or N) with H_α atom in trans-position to the sulfur atom.[77] Theoretical analysis of ROA in S—S stretching region (490–550 cm^{-1}) indicates that the corresponding signals reflect rather sensitively differences in the absolute configuration/conformation of the disulfide group and that there is an unequivocal relationship of ROA sign and handedness of the C—S—S—C group.[55,56] A positive ROA signal of S—S stretching in I, III (~506 cm^{-1}), II, IV (~508 cm^{-1}), and VII (~513 cm^{-1}) indicates right-handed chirality of the disulfide group in all these compounds. On the contrary, a negative signal in ROA spectra of V (sharp negative band at 508 cm^{-1}) and IX (sharp negative band at 513 cm^{-1}) might indicate left-handed chirality of disulfide group. No ROA signal of the S—S stretching vibration can be clearly distinguished in VI. This may be owing to higher flexibility of the disulfide bridge in this compound (no N-terminus in this compound) with both negative and positive disulfide conformations possible or by the presence of D-arginine in position 8. The compound VI exhibits positive ROA signal at ~550 cm^{-1} which can also be found in ROA spectra of I, II, IV, V, and VII; however, its origin is probably not related to disulfide vibrations. As already noted, the above ROA data of our set of NHH agonists I–IV, VII indicate right-handed disulfide chirality. This finding conforms to ECD at least in the sense that these compounds all consistently exhibit very similar ECD. On the other hand, the inhibitor V and the inactive model IX behave differently. Sometimes, inhibitor-like properties relate to modifications in the position 1. The incorporation of β-mercaptopropionic acid leads to compounds lacking α-amino group (1-deamino analogs V, VI, VIII). Such modification may quite logically change disulfide conformation as documented most clearly by ROA. At the same time, it brings a different behavior toward a pH change. This

has been already noted in the past.[49] It is further noteworthy that a right-handed disulfide arrangement has been detected in most existing X-ray studies of agonistic NHH analogs[35,36] and of their complexes with carrier proteins.[37–39] HPLC[41,42] and NMR and fluorescence[43] studies of OT analogs support the existence of an interaction of sulfur in position 6 with the aromatic ring of tyrosine. The fact that right-handed helicity of the disulfide bridge in the crystal structure of deamino OT shows the possible proximity of aromatic side chain and the sulfur in position 6 as well, speaks in favor of the conclusion that the conformation in solution is close to the conformation found in the crystal, including the helicity of the disulfide bridge. We have shown that VOA can provide similar knowledge also for samples in solution.

CONCLUSIONS

We have collected the basic series of vibrational optical activity data related to NHHs and some of their analogs. The data show remarkable conformational consistency within most compounds. VCD and particularly ROA agree with the previously found and/or suggested structural data based mainly on NMR and MD simulations together with X-ray studies of NHH–neurophysin complexes. VOA extends the already existing knowledge in several significant details. The main-chain reversal of the ring moiety is undoubtedly left-handed. This follows from VCD pattern in amide I region, which quite closely resembles polyproline II type helix or maybe a certain type of β-turn. This finding is further supported by ROA because NHH spectra contain a prominent marker band of the PPII structure at 1320 cm^{-1}. Furthermore, ROA spectra contain information about arrangement of the disulfide group, which is otherwise difficult to obtain. Interestingly, the investigated NHH agonists seem to possess identical right handedness of the disulfide, whereas the inactive or inhibitory compounds show a tendency to opposite arrangement. This will be a matter of further investigation. Vibrational optical activity proved its ability to provide useful data on peptide conformation even in the presence of aromatic side chains, unlike ECD.

The authors thank Professor M. Manning (Medical College of Ohio) for kindly providing them with the sample of compound VIII. Spectroscopic part of this work has been initiated in the laboratory of Prof. T.A. Keiderling, University of Illinois, Chicago.

REFERENCES

1. Gimpl, G.; Fahrenholz, F. Physiol Rev 2001, 81, 629–683.
2. Jost, K.; Lebl, M.; Brtnik, F.CRC Handbook of Neurohypophyseal Hormone Analogs, Vol. 2; CRC Press: Boca Raton, FL, 1987.
3. Du Vigneaud, V.; Ressler, C.; Swan, J. M.; Roberts, C. W.; Katsoyannis, P. G.; Gordon, S. J Am Chem Soc 1953, 75, 4879–4880.
4. Du Vigneaud, V.; Ressler, C.; Swan, J. M.; Roberts, C. W.; Katsoyannis, P. G. J Am Chem Soc 1954, 76, 3115–3121.
5. Manning, M.; Stoev, S.; Chini, B.; Durroux, T.; Mouillac, B.; Guillon, G. Prog Brain Res 2008, 170, 473–512.
6. Urry, D. W.; Ohnishi, M.; Walter, R. Proc Natl Acad Sci USA 1970, 66, 111–116.
7. Urry, D. W.; Walter, R. Proc Natl Acad Sci USA 1971, 68, 956–958.
8. Von Dreele, P. H.; Brewster, A. I.; Scheraga, H. A.; Ferger, M. F.; Du Vigneaud, V. Proc Natl Acad Sci USA 1971, 68, 1028–1031.
9. Walter, R.; Glickson, J. D.; Schwartz, I. L.; Havran, R. T.; Meienhofer, J.; Urry, D. W. Proc Natl Acad Sci USA 1972, 69, 1920–1924.
10. Walter, R.; Prasad, K. U.; Deslauriers, R.; Smith, I. C. Proc Natl Acad Sci USA 1973, 70, 2086–2090.
11. Walter, R.; Ballardin, A.; Schwartz, I. L.; Gibbons, W. A.; Wyssbrod, H. R. Proc Natl Acad Sci USA 1974, 71, 4528–4532.
12. Glickson, J. D.; Urry, D. W.; Havran, R. T.; Walter, R. Proc Natl Acad Sci USA 1972, 69, 2136–2140.
13. Glickson, J. D.; Rowan, R.; Pitner, T. P.; Dadok, J.; Bothner-By, A. A.; Walter, R. Biochemistry 1976, 15, 1111–1119.
14. Brewster, A. I.; Hruby, V. J.; Spatola, A. F.; Bovey, F. A. Biochemistry 1973, 12, 1643–1649.
15. Brewster, A. I.; Hruby, V. J. Proc Natl Acad Sci USA 1973, 70, 3806–3809.
16. Deslauriers, R.; Smith, C. P.; Walter, R. J Am Chem Soc 1974, 96, 2289–2291.
17. Live, D. H.; Wyssbrod, H. R.; Fischman, A. J.; Agosta, W. C.; Bradley, C. H.; Cowburn, D. J Am Chem Soc 1979, 101, 474–479.
18. Cowburn, D.; Live, D. H.; Fischman, A. J.; Agosta, W. C. J Am Chem Soc 1983, 105, 7435–7442.
19. Yu, C.; Yang, T. H.; Yeh, C. J.; Chuang, L. C. Can J Chem 1992, 70, 1950–1955.
20. Wang, J. J.; Hodges, R. S.; Sykes, B. D. J Am Chem Soc 1995, 117, 8627–8634.
21. Walse, B.; Kihlberg, J.; Drakenberg, T. Eur J Biochem 1998, 252, 428–440.
22. Ohno, A.; Kawasaki, N.; Fukuhara, K.; Okuda, H.; Yamaguchi, T. Magn Reson Chem 2010, 48, 168–172.
23. Hruby, V. J.; Lebl, M. In CRC Handbook of Neurohypophyseal Hormone Analogs; Jost, K.; Lebl, M.; Brtnik, F., Eds.; CRC Press: Boca Raton, 1987, pp 105–155.
24. Beychok, S.; Breslow, E. J Biol Chem 1968, 243, 151–154.
25. Urry, D. W.; Quadrifo F; Walter, R.; Schwartz, I. L. Proc Natl Acad Sci USA 1968, 60, 967–974.
26. Fric, I.; Kodicek, M.; Flegel, M.; Zaoral, M. Eur J Biochem 1975, 56, 493–502.
27. Hruby, V. J.; Deb, K. K.; Fox, J.; Bjarnason, J.; Tu, A. T. J Biol Chem 1978, 253, 6060–6067.
28. Tu, A. T.; Lee, J.; Deb, K. K.; Hruby, V. J. J Biol Chem 1979, 254, 3272–3278.
29. Maxfield, F. R.; Scheraga, H. A. Biochemistry 1977, 16, 4443–4449.
30. Tu, A. T.; Bjarnason, J. B.; Hruby, V. J. Biochim Biophys Acta 1978, 533, 530–533.

31. Podstawka, E.; Sikorska, E.; Proniewicz, L. M.; Lammek, B. Biopolymers 2006, 83, 193–203.
32. Gryczynski, I.; Szmacinski, H.; Laczko, G.; Wiczk, W.; Johnson, M. L.; Kusba, J.; Lakowicz, J. R. J Fluoresc 1991, 1, 163–176.
33. Szmacinski, H.; Wiczk, W.; Fishman, M. N.; Eis, P. S.; Lakowicz, J. R.; Johnson, M. L. Eur Biophys J Biophy 1996, 24, 185–193.
34. Wiczk, W.; Lankiewicz, L.; Kasprzykowski, F.; Oldziej, S.; Szmacinski, H.; Lakowicz, J. R.; Grzonka, Z. Eur Biophys J 1997, 26, 183–193.
35. Wood, S. P.; Tickle, I. J.; Treharne, A. M.; Pitts, J. E.; Mascarenhas, Y.; Li, J. Y.; Husain, J.; Cooper, S.; Blundell, T. L.; Hruby, V. J.; Buku, A.; Fischman, A. J.; Wyssbrod, H. R. Science 1986, 232, 633–636.
36. Husain, J.; Blundell, T. L.; Cooper, S.; Pitts, J. E.; Tickle, I. J.; Wood, S. P.; Hruby, V. J.; Buku, A.; Fischman, A. J.; Wyssbrod, H. R.; Mascarenhas, Y. Philos Trans R Soc Lond B Biol Sci 1990, 327, 625–654.
37. Rose, J. P.; Wu, C. K.; Hsiao, C. D.; Breslow, E.; Wang, B. C. Nat Struct Biol 1996, 3, 163–169.
38. Wu, C. K.; Hu, B.; Rose, J. P.; Liu, Z. J.; Nguyen, T. L.; Zheng, C.; Breslow, E.; Wang, B. C. Protein Sci 2001, 10, 1869–1880.
39. Ibrahim, B. S.; Pattabhi, V. J Mol Biol 2005, 348, 1191–1198.
40. Fric, I.; Kodicek, M.; Jost, K.; Blaha, K. Collect Czech Chem Commun 1974, 39, 1271–1289.
41. Lebl, M.; Fric, I.; Sugg, E. E.; Cody, W. L.; Hruby, V. J. In Peptides 1986, Proc 19 EPS; Theodoropoulos, D., Ed.; Walter de Gruyter & Co.: Berlin, 1987, pp 341–344.
42. Lebl, M. In Handbook of the Use of High Performance Liquid Chromatography for the Analytical and Preparative Separation of Amino Acids, Peptides and Proteins; Hancock, W. S., Ed.; CRC Press: Boca Raton, 1985, pp 169–178.
43. Lebl, M.; Sugg, E. E.; Hruby, V. J. Int J Pept Protein Res 1987, 29, 40–45.
44. Fric, I.; Leonteva, L. I.; Malon, P.; Jost, K.; Blaha, K. Collect Czech Chem Commun 1980, 45, 1109–1131.
45. Hruby, V. J.; Mosberg, H. I.; Fox, J. W.; Tu, A. T. J Biol Chem 1982, 257, 4916–4924.
46. Gwizdala, E.; Lammek, B.; Grzonka, Z. Pol J Chem 1985, 59, 1153–1160.
47. Hlavacek, J.; Konvalinka, J.; Slaninova, J.; Fric, I. In Peptides; Walter de Gruyter & Co.: Berlin, New York, 1986, pp 497–500.
48. Hlavacek, J.; Fric, I.; Malon, P.; Jost, K.; Blaha, K. Collect Czech Chem Commun 1987, 52, 1841–1856.
49. Fric, I.; Malon, P.; Jost, K.; Blaha, K. In Proceedings of the 1st International Conference on Circular Dichroism; Kurtev, B., Ed.; VCH Publishers: Sofia, 1987, pp 332–337.
50. Belec, L.; Blankenship, J. W.; Lubell, W. D. J Pept Sci 2005, 11, 365–378.
51. Sugeta, H.; Go, A.; Miyazawa, T. Bull Chem Soc Jpn 1973, 46, 3407–3411.
52. Van Wart, H. E.; Scheraga, H. A. Proc Natl Acad Sci USA 1986, 83, 3064–3067.
53. Havel, H. A. Spectroscopic Methods for Determining Protein Structure in Solution; VCH Publishers, Inc.: New York, 1996.
54. Linderberg, J.; Michl, J. J Am Chem Soc 1970, 92, 2619–2625.
55. Bednarova, L.; Bour, P.; Malon, P. Chirality 2010, 22, 514–526.
56. Malon, P.; Bednarova, L.; Straka, M.; Krejci, L.; Kumprecht, L.; Kraus, T.; Kubanova, M.; Baumruk, V. Chirality 2010, 22, E47–E55.
57. Barth, A.; Haris, P. I. Biological and Biomedical Infrared Spectroscopy; IOS Press: Amsterdam, Berlin, Tokyo, Washington, DC, 2009.
58. Hug, W.; Hangartner, G. J Raman Spectrosc 1999, 30, 841–852.
59. Hanzlikova, J.; Praus, P.; Baumruk, V. J Mol Struct 1999, 481, 431–435.
60. Fric, I.; Malon, P.; Jost, K.; Blaha, K. In Peptides 1982, Proceedings of the 17th European Peptide Symposium; Blaha, K.; Malon, P., Eds.; W. de Gruyter: Berlin, New York, 1983, pp 103–116.
61. Lebl, M.; Hill, P.; Kazmierski, W.; Karaszova, L.; Slaninova, J.; Fric, I.; Hruby, V. J. Int J Pept Protein Res 1990, 36, 321–330.
62. Bergson, G. Ark Kemi 1958, 12, 233–237.
63. Bergson, G. Ark Kemi 1962, 18, 409–434.
64. Skomorowski, W.; Pecul, M.; Salek, P.; Helgaker, T. J Chem Phys 2007, 127, 085102.
65. Keiderling, T. A. In Circular Dichroism: Principles and Applications; Berova, N.; Nakanishi, K.; Woody, R. W., Eds.; Wiley-VCH: New York, 2000, pp 621–666.
66. Keiderling, T. A.; Kubelka, J.; Hilario, J. Vibrational Circular Dichroism of Biopolymers: Summary of Methods and Applications; CRC Press: Boca Raton, FL, 2006.
67. Dukor, R. K.; Keiderling, T. A. Biopolymers 1991, 31, 1747–1761.
68. Diem, M. Introduction to Modern Vibrational Spectroscopy; Willey: New York, 1993.
69. Siamwiza, M. N.; Lord, R. C.; Chen, M. C.; Takamatsu, T.; Harada, I.; Matsuura, H.; Shimanouchi, T. Biochemistry 1975, 14, 4870–4876.
70. Barron, L. D.; Hecht, L.; Blanch, E. W.; Bell, A. F. Prog Biophys Mol Biol 2000, 73, 1–49.
71. Shi, Z.; Woody, R. W.; Kallenbach, N. R. Adv Protein Chem 2002, 62, 163–240.
72. Zhu, F. J.; Isaacs, N. W.; Hecht, L.; Barron, L. D. Structure 2005, 13, 1409–1419.
73. McColl, I. H.; Blanch, E. W.; Gill, A. C.; Rhie, A. G.; Ritchie, M. A.; Hecht, L.; Nielsen, K.; Barron, L. D. J Am Chem Soc 2003, 125, 10019–10026.
74. Bhaskaran, R.; Chuang, L. C.; Yu, C. Biopolymers 1992, 32, 1599–1608.
75. Schmidt, J. M.; Ohlenschlager, O.; Ruterjans, H.; Grzonka, Z.; Kojro, E.; Pavo, I.; Fahrenholz, F. Eur J Biochem 1991, 201, 355–371.
76. Sikorska, E.; Rodziewicz-Motowidlo, S. J Pept Sci 2008, 14, 76–84.
77. Sugeta, H.; Go, A.; Miyazawa, T. Chem Lett 1972, 1, 83–86.

Reviewing Editor: Robert Glaeser

Supplementary material

Vibrational optical activity data of compounds I-IX are shown in Figures 1-6 of this supplementary material. Compared to the main body of the text these figures contain two or three curves each, making it easier to follow their individual characteristics. Figures 1, 4 show spectra of the hormones themselves, similarly Figures 2, 5 the curves of their agonistic analogs and Figures 3, 6 the remaining spectra of compounds V, VIII and IX.

FIGURE 5 Vibrational circular dichroism (top) and IR absorption (bottom) of compound I (oxytocin), II (arginine vasopressin) and III (lysine vasopressin) measured in D_2O (normalized to the number of amino acid residues).

FIGURE 6 Vibrational circular dichroism (top) and IR absorption (bottom) of compound IV (methyloxytocin), VI (desmopressin) and VII (terlipressin) measured in D_2O (normalized to the number of amino acid residues).

FIGURE 7 Vibrational circular dichroism (top) and IR absorption (bottom) of compound V (atosiban), VIII (NHH inhibitor) and IX (ring model) measured in D_2O (normalized to the number of amino acid residues).

FIGURE 8 Raman scattering (left) and Raman optical activity (right) spectra of compounds I (oxytocin), II (arginine vasopressin) and III (lysine vasopressin) measured in acidic pH.

FIGURE 9 Raman scattering (left) and Raman optical activity (right) spectra of compounds IV (methyloxytocin), VI (desmopressin) and VII (terlipressin) measured in acidic pH.

FIGURE 10 Raman scattering (left) and Raman optical activity (right) spectra of compounds V (atosiban) and IX (ring model) measured in acidic pH.

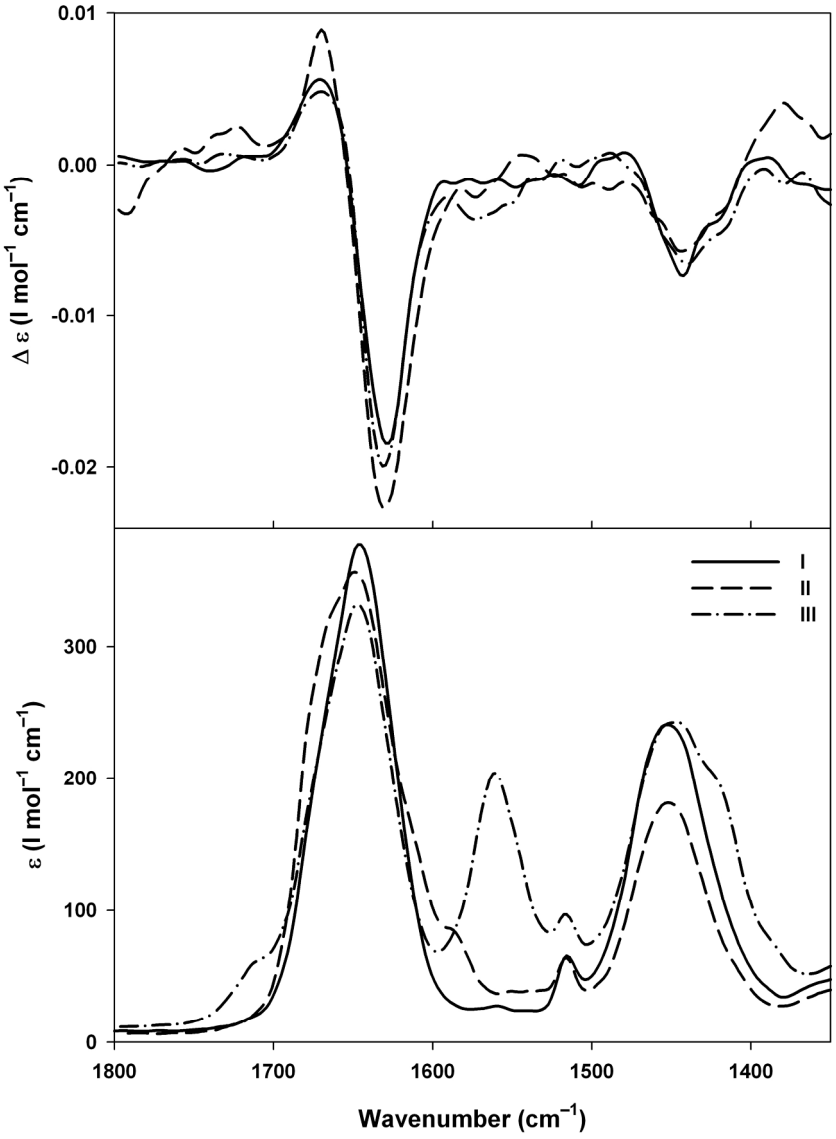

FIGURE 5: Vibrational circular dichroism (top) and IR absorption (bottom) of compound I (oxytocin), II (arginine vasopressin) and III (lysine vasopressin) measured in D_2O (normalized to the number of amino acid residues).
206x283mm (300 x 300 DPI)

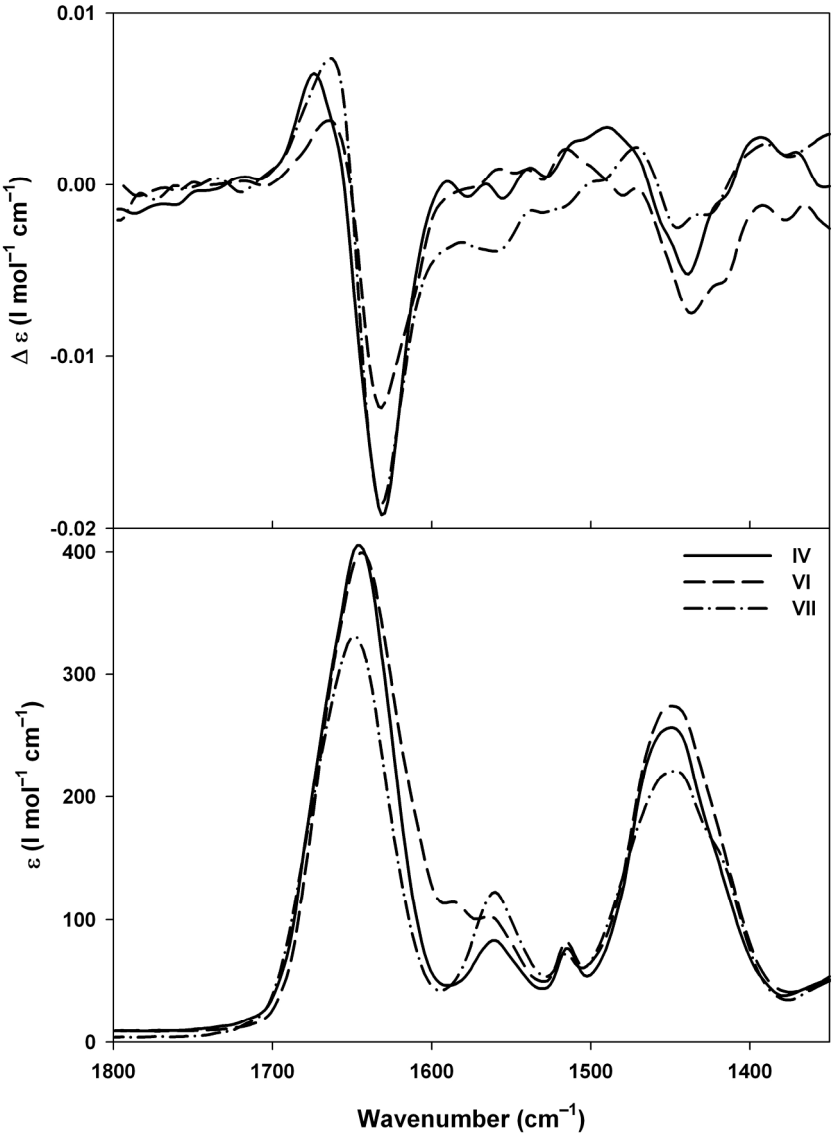

FIGURE 6: Vibrational circular dichroism (top) and IR absorption (bottom) of compound IV (methyloxytocin), VI (desmopressin) and VII (terlipressin) measured in D_2O (normalized to the number of amino acid residues).
206x283mm (300 x 300 DPI)

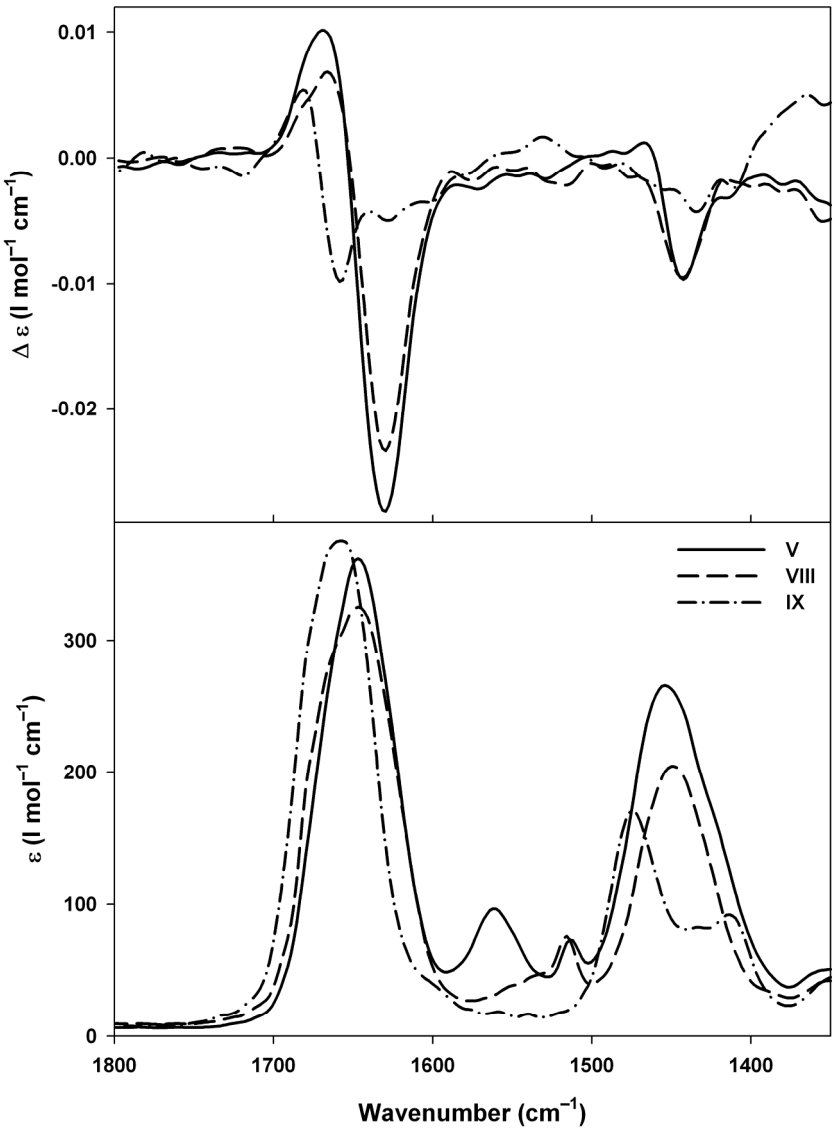

FIGURE 7: Vibrational circular dichroism (top) and IR absorption (bottom) of compound V (atosiban), VIII (NHH inhibitor) and IX (ring model) measured in D_2O (normalized to the number of amino acid residues).
206x283mm (300 x 300 DPI)

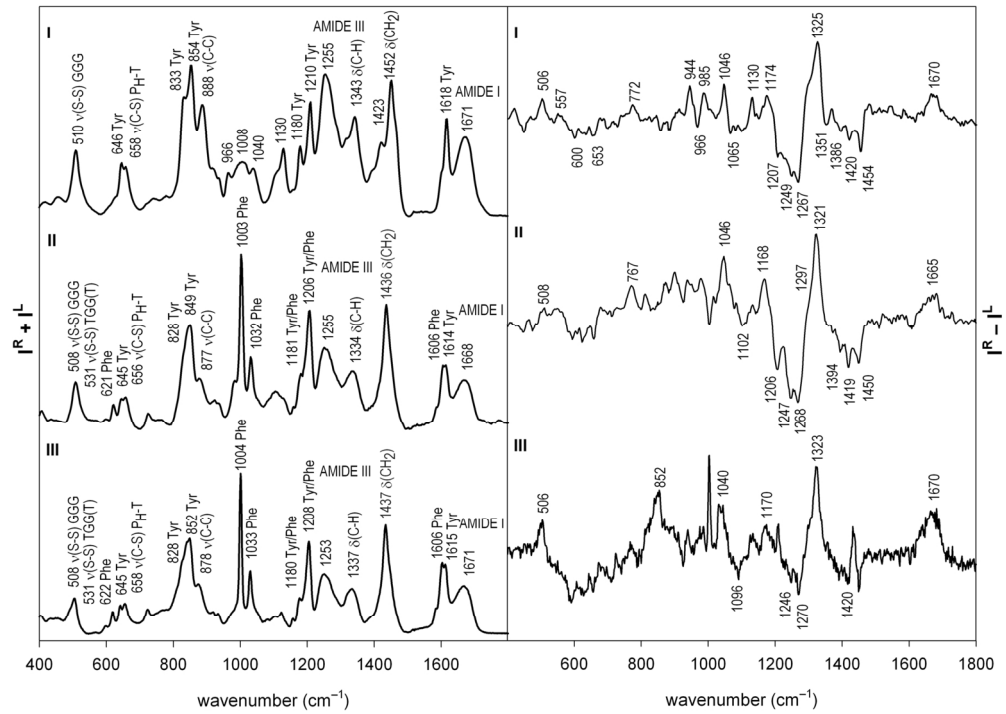

FIGURE 8: Raman scattering (left) and Raman optical activity (right) spectra of compounds I (oxytocin), II (arginine vasopressin) and III (lysine vasopressin) measured in acidic pH.
154x119mm (300 x 300 DPI)

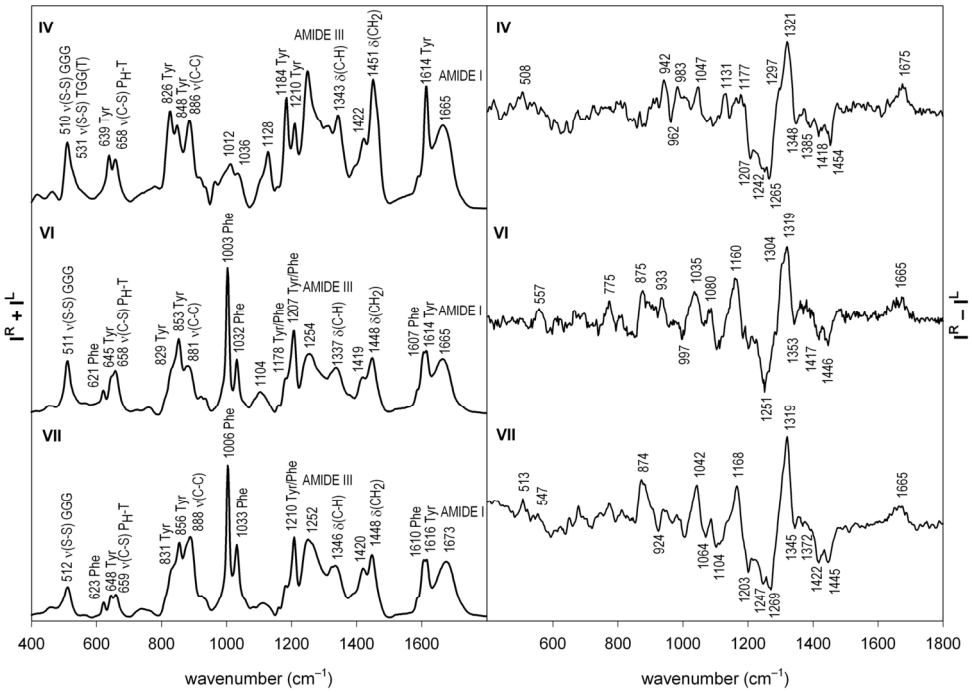

FIGURE 9: Raman scattering (left) and Raman optical activity (right) spectra of compounds IV (methyloxytocin), VI (desmopressin) and VII (terlipressin) measured in acidic pH.
152x115mm (300 x 300 DPI)

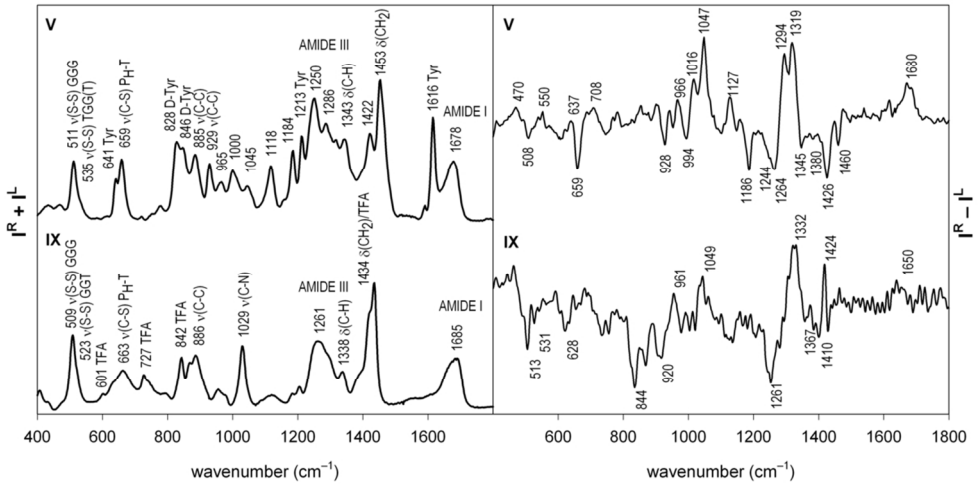

FIGURE 10: Raman scattering (left) and Raman optical activity (right) spectra of compounds V (atosiban) and IX (ring model) measured in acidic pH.
104x54mm (300 x 300 DPI)